Distribution Network Modelling and Analysis of the Application of HTS Transformer

Muhammad Azizi Abdul Rahman

A thesis submitted to

Auckland University of Technology

in fulfilment of the requirements for the degree of

Doctor of Philosophy (PhD)

2012

School of Engineering

TABLE OF CONTENTS

LIST OF FIGURES

LIST OF TABLES

ATTESTATION OF AUTHORSHIP

"I hereby declare that this submission is my own work and that, to the best of my knowledge and belief, it contains no material previously published or written by another person (except where explicitly defined in the acknowledgements), nor material which to substantial extent has been submitted for the award of any other degree or diploma of a university or other institution of higher learning".

Muhammad Azizi Abdul Rahman:_____

Date:_____

ACKNOWLEDGEMENTS

I would like to take this opportunity to thank many wonderful people who have contributed to the successful completion of this study. First and foremost, I would like to express my gratitude and appreciation to my principal supervisor, Prof. Tek Tjing Lie for his patience, guidance, advice and continuous support throughout the completion of this thesis. Thank you for keeping me focus and on track through these years. I am also thankful for my secondary supervisor, Prof. Krishnamachar Prasad for his fruitful advice, encouragement and suggestions to complete this thesis.

This thesis would not have been completed without the tolerance and understanding of my beloved wife, Sarina. Thank you for your love and encouragement, you have served as an important source of strength for me. To my dearest son and daughters, Syahir, Syasya and Syafia, thank you for the happiness you have brought into my life. I pray that you will be more successful in your future. I dedicate this thesis to my dear parents, Abdul Rahman and Zaliah, who have always been there to support me in my journey in every way possible. My deepest thank also to my grandparents, father and mother-in-laws, sisters and brothers for their ongoing encouragement.

This work was supported in part by Industrial Research Limited (IRL), New Zealand through the Foundation for Research, Science and Technology (FRST) High Temperature Superconductors (HTS) Accelerated Development Transformational Research, Science and Technology (TRST) funding. The FRST is now acknowledged as the Ministry of Science and Innovation (MSI). My respect and gratitude particularly for Neil Glasson from IRL who sparked a number of ideas reported in this thesis.

ABSTRACT

Advancement of High Temperature Superconductor (HTS) materials has increased interest in research and development of superconducting transformers. One of the challenges in the design and development of HTS transformer is the modelling of load flow, system losses and over current phenomena to be experienced by the transformer. Even though HTS technology is claimed to offer better power system and other packaging benefits, the performance and reliability need to be proven and verified through the proper modelling of power system network.

The study set up the electrical characteristics of a HTS transformer. The parameters need to be validated before any effort is to carry out to model the behaviour of a distribution network under a range of conditions. The characteristics is then adapted into existing network models and analysed under various system loading and over current conditions. The modelling is carried out on a three phase distribution feeder which is inherently unbalanced. The technical information on the HTS transformer is based on a preliminary baseline design. The exploration is intended to establish the performance of HTS transformers in comparison with that of conventional transformers.

The short circuit design of a transformer is one of the most significant and challenging criteria. Additional generating capacity and interconnections due to the growth of electrical power demand have contributed to an increase in short circuit capacity of power networks. One of the consequences is that the short circuit duty to be undertaken by transformers becomes more severe. The short circuit strength of a transformer is designed to withstand through fault currents due to external short circuit. Any weakness in the strength may result in a mechanical collapse of windings and deformation to

clamping structures. The internal faults initiated by the external short circuits may lead to bushing blowouts, tank bursting, fire hazard, etc.

Meanwhile, the inrush current of a transformer can be as high as seven to ten times the rated current. Inrush current events are more frequent compared to short circuits. They also last for much longer time (few seconds) compared to short circuits (tens of milliseconds). The users are very anxious about the repeated switching of a transformer. Even though the inrush currents are usually not seriously looked into in the mechanical design considerations, the forces generated due to an extensive number of switching in a day may weaken the winding over a period of time. The continuous occurrences may lead to winding looseness and subsequent failure.

The active development of HTS materials has led to extensive research and development studies of superconducting transformers worldwide. Considerable benefits have been accomplished with the introduction of HTS transformer such as reduced power loss, size and transformer weight. This study focuses on modelling the effects of various distribution network conditions towards a distribution HTS transformer and looks comprehensively into the thermal effects of short circuit current on various architectural designs and fault current limiting properties of HTS transformer winding conductor. Recent advancement in the design technology has looked into the HTS transformer's ability to also perform as Fault Current Limiter (FCL). This study presents the computation of the thermal effects of short circuit currents on a non-FCL HTS transformer and demonstrates how it will behave with a HTS-FCL winding conductor.

CHAPTER 1

INTRODUCTION

1.1 Introduction

Rapid changes and developments are being witnessed in the transformer design technologies. The phenomenal growth of power systems has put tremendous responsibilities on the industry to supply reliable and cost effective transformers. Advent of high temperature superconductor (HTS) materials has increased the interest in research and development of superconducting transformers with major projects being carried out worldwide. Among the major challenges in the design and development of HTS transformers is the modelling of power flow and short circuit current phenomena the transformer will experience. The performance and reliability need to be proven both to the users and the customers. Even though the HTS technology is believed to be more efficient, reliable and eco-friendly, efforts must be appropriately verified through the proper modelling of power system network (McConnell, 2000; Reis, Mehta, McConnell, & Jones, 2002). Consequently, it is important to develop an understanding of the fundamental HTS transformer design issues that can provide guidance for

developing practical devices of interest to the electric utility industry. The parameters of HTS transformer need to be validated before any attempts are made to model the behaviour of a distribution network under a range of conditions. The predicted performance and reliability of HTS transformers can then be verified through network modelling and analysis. The ultimate purpose is to furnish electric utilities precise information as to which HTS transformers work under various conditions with greater technical efficiency and proven reliability.

1.2 Background

The introduction of high temperature superconductors (HTS) in 1986 by Georg Bednorz and Alex Muller (Bednorz & Muller, 1986) has created many new prospects for the practical application of superconductivity in utility power equipment such as transformers, cables, current limiters, *etc*.. The feasibility of HTS transformers has been weighted from perspectives of high performance of the windings and lower cost of refrigeration on the basis of advanced HTS wires with high critical current and low AC loss. The load loss generated mostly in the windings is expected to reduce drastically in comparison with copper windings. Meanwhile, the coolant, liquid nitrogen, has the function of providing electrical insulation as good as the insulation oil in the case of conventional transformers (McConnell, 2000). The HTS properties of higher refrigeration reliability and lower refrigeration cost make it achievable to overcome the limitations experienced in the low temperature semiconductor (LTS) transformer designs of the 1970s and 1980s (Mehta, Aversa, & Walker, 1997).

Superconducting coils for utility power transformers are attractive because they require a smaller amount of conductor for the same transformer capacity compared to

conventional transformers. In the United States, conventional transformers account for about 25% of the losses in the power transmission and distribution system and resistive heating is a great portion of these losses (Mehta, *et al.*, 1997). Thus, the use of HTS transformers can produce substantial energy savings and reduce lifetime ownership costs. Other projected benefits include the ability to limit and withstand high currents without loss of lifetime due to thermal damage. They are also able to reduce potential fire and environmental hazards because liquid nitrogen replaces oil, which is used for the cooling and insulation in conventional transformers. HTS transformers with very low internal impedance and self-protecting capability against short-circuit current will help improve the voltage regulation. The network system will exhibit better voltage consistency over a wide range of load conditions (McConnell, Mehta, & Walker, 2000; Reis, *et al.*, 2002). Furthermore, the weight and volume of HTS transformers can be very much reduced compared to that of conventional transformers.

Transformers utilizing high temperature superconductors are considered as a timely invention. The number of power transformers, aged more than 30 years old and nearing retirement, is increasing. If this window of opportunity is not grabbed, there would be great reluctance to replace any recently installed highly priced capital assets. Major projects of developing HTS transformers are making good progress in the United States, Europe, Japan, Korea and China, which clearly indicates the interest by international community (Hawsey & Christen, 2006; Liye & Liangzhen, 2007; Manuel *et al.*, 2002; Minwon, Young-Sik, & Kang-Sik, 2007; Tsukamoto & Akita, 2002). The efforts must be appropriately verified through the economic interest of the discounted losses. Consequently, it is very important to develop an understanding of the fundamental HTS transformer design issues that can provide guidance for developing practical devices of interest to the electric utility industry.

1.3 Rationale

Progressive changes and developments are being made in the transformer design technologies (Amoiralis, Tsili, & Kladas, 2009). The exceptional expansion of power systems has put enormous responsibilities on the transformer industry to supply reliable and cost effective transformers. The introduction of HTS materials has enhanced interest in research and development of superconducting transformers with major projects being carried out around the world. The major challenges in design and development of HTS transformers are short circuit withstand, through fault recovery and withstand against high voltage tests. The high voltage tests on distribution transformers should be applied in accordance with IEC 60076-3 standard to specify the insulation requirements. The tests include induced AC voltage test and lightning impulse test (IEC60076-3, 2000). The performance and reliability need to be proven to the users and manufacturers not only through analysis calculation and experimental measurement, but also through site demonstration for ensuring a trouble-free performance during service.

Power distribution networks, which can be distinguished from that of transmission system with their unbalanced loading characteristics, are getting more and more attention. However, these evaluations employ conventional transformers in the modelling and analysis. The research work presented in this thesis will apply a baseline design parameters of an HTS transformer. The adaptation of electrical characteristics of the HTS transformer into the evaluation will determine the performance as compared to that of a conventional transformer. As the project evolves, more and more HTS transformer designs will be experimented. Investigations will be carried out further to observe the performance of the HTS transformer for greater loading capacity, higher efficiency and better over current endurance.

1.4 Significance

Several significant issues have been identified for this study. The first is to develop an understanding of the fundamental HTS transformer design issue that can provide guidance for developing practical devices of interest to the electric utility industry. At the same time, it will provide transformer manufacturers powerful knowledge of the design technology subject to their customers, who will appreciate the value added services. The study will validate the parameters of HTS transformers and model the behaviour of a distribution network under a range of conditions. The broad understanding of HTS transformer capabilities that will evolve will benefit power network designers so that they will be able to refine the network accordingly. The study will then verify the predicted performance and reliability of HTS transformers through the network modelling and analysis calculation. Finally, the study is intended to furnish electric utilities precise information as to which HTS transformers work under various conditions with greater technical efficiency and proven reliability. The major original contribution of the research work presented in this thesis is to use HTS transformers in distribution network and to verify the validity of their use, through suitable simulation studies, taking into account various system operating conditions.

The research foundation will be based upon the development of HTS transformer by High Temperature Superconductor New Zealand (HTSNZ) transformer project group led by Industrial Research Limited (IRL). The study will also look into Vector Limited (Vector) power distribution network where the transformer will be installed. Auckland University of Technology and Vector are members of the project group to look into the existing power distribution network availability, suitability, modelling and analysis. Other members include HTS-110, Wilson Transformer, ETEL, Fabrum Solution, General Cable Superconductor, Weltec, *etc*., which are looking into other areas of the

projects such as HTS technological development, transformer design and manufacture, cooling system design and manufacture, winding cable design and manufacture and technical training. The study will also be based on literature and findings on the development of HTS transformers in other countries as well as the advancement of power distribution network modelling and analysis. From ongoing technological development of HTS transformer and current improvement of power distribution network modelling and analysis, a model of power distribution modelling and analysis with the application of HTS transformer will be developed.

1.5 Structure of the thesis

This thesis is constructed in 7 chapters. The first chapter is the introduction which presents the background of the study; describes the rational and the significance of conducting the research; and finally, provides an overview of the structure of this thesis.

Chapter 2 is a literature review that provides a brief overview of the historical development of superconductor from the early recorded discovery in 1911 until recent progresses. The chapter also presents the advancement of high temperature superconductor materials with the main focus on the Yttrium Barium Copper Oxide (YBCO) compound. The literature review continues with the applications of superconductor in general before exploring deeper into its utilization in electric power industry. The literature is extended into the development of superconducting transformer and the comparison with the conventional transformer. Finally, the chapter explores the potential benefits of the application of superconducting transformers in the power industry. Recent developments in superconducting fault current limiting transformers are also briefly discussed in this literature review.

Chapter 3 starts with an overview of distribution power network. The chapter presents the methodology to model the distribution power equipment and network system. The description of analytical approach begins with the modelling of conventional and superconducting transformers. The elaboration is stretched out into the modelling of other distribution power equipment related to this research such as underground cable and overhead line. The chapter concludes with an outline on the approach to model a distribution network using the phase frame method.

Chapter 4 and 5 present the analysis of the application of superconducting transformer in a distribution power network. Chapter 4 begins with the description on the setting up of the simulated distribution network. The analysis continues with a preliminary data processing for the constructed circuit. The investigation then proceeds with the description on the analysis techniques and the accomplished results for power flow study. Meanwhile, Chapter 5 moves ahead with the analysis of short circuit and inrush current phenomena on the superconducting transformer. The two chapters conclude with a discussion on the simulation carried out.

Chapter 6 investigates the thermal effects of short circuit currents on the transformer windings. The chapter starts with some background on the technology development for the transformer winding and continues with the explanation on how the analysis will be approached. The calculation method is demonstrated on a conventional transformer and adapted for the HTS transformer. The architectural design of the HTS and HTS-FCL conductor windings are presented. The chapter highlights the thermal effects of short circuit forces on the superconducting transformer evaluated based on the preliminary design by Industrial Research Limited. The research navigates further with an analysis of a present design of superconducting transformer winding with fault current limiting properties. The chapter concludes with a discussion on the investigation conducted.

Chapter 7, the last chapter, briefly summarizes the research study carried out and draws relevant conclusions. Finally, the chapter proposes the recommendations for further research and future works.

CHAPTER 2

SUPERCONDUCTOR

Superconductivity of a material is defined as the phenomenon in which the material loses its resistance on cooling to a temperature lower than the transition temperature of the material (Khare, 2003). The quest for new superconducting materials has been very extensive with the discovery of superconductivity behaviour at temperatures higher than the boiling point of liquid nitrogen (77 K), which is a cheap and widely available cryogen, in certain composite materials. High temperature superconductors are prepared in various forms for different applications. For high-current applications, the manufacturing of the superconductors are in the forms of wires and tapes. They are usually fabricated in thick and thin film forms for most electronic applications.

This chapter reviews several key developments in superconducting materials starting from the first discovery in 1911 (Golubov, 1998a). The advancement of the technology from type I to type II and the second generation superconducting materials are also deliberated. Type I superconductors have a sharp transition from the superconducting state to the normal state. The superconductivity is destroyed when the strength of the

applied magnetic field rises above a critical value. This characteristic is normally shown by pure metal such as lead and mercury. Type II superconductors exhibit two critical magnetic fields, lower critical field (H_{c1}) and upper critical field (H_{c2}). The material is in completely superconducting state when the applied magnetic field is lower than H_{c1}. When the applied field slowly and continuously penetrates the superconductor, the transformation to the normal state takes place. It is also known as voltex or mixed state. The superconductivity is completely destroyed when the applied field surpasses H_{c2}, and the material is in completely normal state. Type II superconductors are usually made of metal alloys. HTS materials are in this category (Khare, 2003). Subsequently, the applications of superconducting technology in general are discussed before finally highlighting the utilization and benefits of the technology in distribution power transformers.

2.1 Historical development

This section explores the history of superconductivity by looking into a series of crucial events in the field. For a couple of decades from the first recorded discovery in 1911, the pursuance was limited to the area of Leiden, Berlin and Toronto, which were located the only available laboratories with liquid helium. After World War II, the journey for exploration has become more exciting with the participation of the United States as one of the leading participants with exceptional government funding (Pippard, 2003).

The revelation of Bardeen Cooper Schrieffer (BCS) theory on low temperature superconductor in 1957 breathed new life into the era of superconductivity. Meanwhile, strong interest in the Asia-Pacific region was observed only after several decades particularly following the 1986 discovery of high temperature superconductor.

Government funded projects have been carried out in certain countries such as China, Japan and Korea (Liye & Liangzhen, 2007; Minwon *et al.*, 2007; Tsukamoto & Akita, 2002).

2.1.1 Early discovery

A Dutch scientist, H. Kamerlingh Onnes, accidentally encountered superconductivity in mercury just below the normal boiling point of helium while observing the relationship between electrical resistance and temperature of the material in 1911. Previously in 1908, he liquefied helium which was used in the experiment in his laboratory in Leiden. He discovered the resistivity of mercury unexpectedly dropped to zero at temperatures below 4.2 K (Golubov, 1998a; Pippard, 2003; Sykulski, 1997). However, the resistance drop was not continuous. A new state of the material with zero resistance was established. This transition phase was described as the superconducting state. The temperature at which the phenomenon occurred was called the transition temperature.

Within a couple of years, superconductivity was also detected in other metals such as lead and tin (Sykulski, 1997). As a result, erratic speculation arose from this sensational phenomenon that large field magnets and heavy electric machinery could be operated without loss. However, this anticipation was met by disappointment and frustration. The superconductivity behaviour of the metals was discovered to be disappearing above a certain critical temperature. In addition, the characteristic could also be wiped out by relatively small currents and magnetic fields.

By 1913, Onnes had already tested a Nickel (Ni) alloy coated with Lead (Pb)-rich superconducting solder. Unfortunately, the material lost its superconductivity at magnetic fields of less than 50 milli-Tesla (mT) (David, Alex, Feldmann, & Anatoly,

2001). Meissner and Ochsenfeld found in 1933 (Meissner & Ochsenfeld, 1933) that the magnetic field reduced to zero when a superconductor was cooled below the critical temperature (T_c) in a weak magnetic field of a value less than the critical value (H_c). This is the basic principal of a superconductor which is known as Meissner effect.

Physicists then found that in order to maintain the superconductivity, not only temperature and magnetic field, but also electrical current density need to be remain below critical values (Smith, Alexander, Buyrn, & Alic, 1989). The critical values for each field depend on the material. Recently, high temperature superconducting equipment has been developed to operate in liquid nitrogen temperature regime of 77 K. Meanwhile, the current density values have also been raised to useful levels of 10^5 to 10^6 A/cm^2. Figure 2.1 shows the temperature-magnetic field-current density phase diagram of an ideal superconductor. *S* represents the area for an ideal superconductivity state and *N* corresponds to normal state area. Meanwhile, T_c, H_c, and J_c are the critical values for the temperature, magnetic field, and current density, respectively.

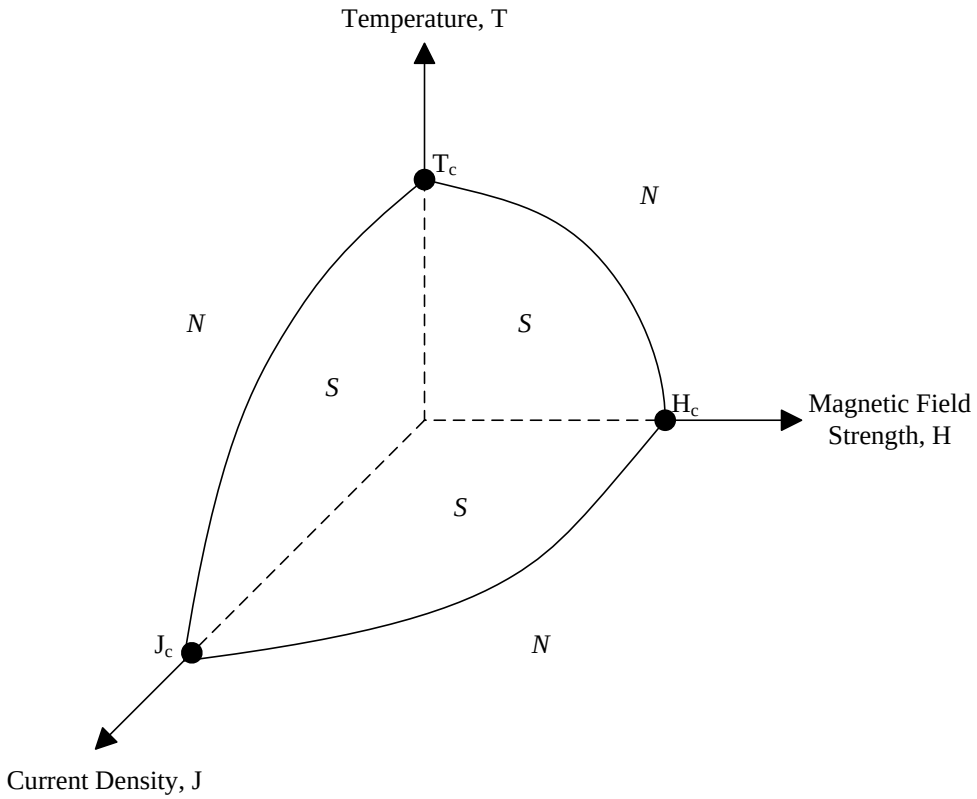

Figure 2.1: T-H-J phase diagram of an ideal superconductor

Numerous superconducting materials were brought to light in the next half century from 1911 with many inspiring theories being proposed and forgotten. Extensive research was carried out on electromagnetic properties of these materials. However, moderate accomplishment in terms of critical currents and magnetic fields discouraged researchers to follow through in their applications. Nevertheless, Bardeen, Cooper and Schrieffer (Bardeen, Cooper, & Schrieffer, 1957) disclosed their findings in 1957 on the microscopic theory of superconductivity which is also known as the BCS theory of superconductivity. The theory among others provided a description of the microscopic behaviour of low temperature superconductors that clarified many ambiguities and uncertainties of the superconductivity nature.

During the same period, Kunzler (Kunzler, 1961) found a new category of superconducting alloys that could withstand very high magnetic fields and large current

densities. High performance superconducting wires were commercially available in the mid 1970s from the advancement of these composite wires. The wires were formed by embedding fine superconducting filaments in a normal metal such as aluminium or copper. The invention permitted the building up of high direct current (d.c.) and pulsed field magnets. Consequently, the applications on high power alternating current (a.c.) could be seriously looked into.

2.1.2 Types of superconductor

Superconductivity is categorized into two types (Larbalestier, Gurevich, Feldmann, & Polyanski, 2001; Sykulski, 1997). The first type which was discovered by H. Kamerlingh Onnes is also classified as Type I. These superconductors appeared to be found in many pure metals such as tin, lead and mercury. However, their superconductivity characteristics were discovered to be destroyed in the presence of magnetic field of about 0.1 T or at temperatures slightly above 7 K. This type of low temperature superconductors was the first to come into picture. However, the extent of industrial applications of Type I superconductors has been hampered by the complicated and expensive cryogenic technology required. The operation of superconducting devices required cooling by liquid helium to about 4 K. Besides the requirement for extremely good containers, refrigeration at these low temperatures is very expensive. Approximately 500 W of power is required at room temperature to produce 1 W of cooling power at 4 K.

Type II superconductors were found by the end of 1950s mostly in Niobium-based alloys such as Niobium-Titanium (NbTi), Niobium-Tin (Nb_3Sn), Niobium-Germanium (Nb_3Ge) and Niobium-Aluminide (Nb_3Al). They were also later found in other

intermetallic compounds such as Vanadium-Gallium (V_3Ga) and Magnesium-diBoride (MgB_2). The superconductivity characteristic of this type is diminished by relatively higher magnetic field or temperatures than Type I superconductors. For examples, the superconductivity of Nb_3Ge, MgB_2 and NbTi disappear at a magnetic field of 40, 20 and 10 T, respectively, or at temperatures above 23, 39 and 9 K, respectively. These superconductors are also known as low-temperature or low-T_c metallic Type II superconductors.

2.1.3 Recent progress

The pursuit for superconductivity with high transition temperature, particularly above the liquid nitrogen temperature of 77 K, since the first discovery of superconductivity in 1911 has been very challenging to material scientists. Prior to 1986, the highest transition temperature obtained was only 23.2 K for Niobium-Germanium (Nb_3Ge) (Smith *et al.*, 1989). It was found to be a superconductor in 1973 and held the record for over 12 years until the discovery of the cuprate superconductors. The research was only through practical or empirical study since there are no theoretical or definitive guidelines to predict any new materials with higher transition temperatures. One of the approaches was to search for new superconducting oxides. This led to the discovery of superconductivity in perovskite solid solutions of $BaPb_{1-x}Bi_xO_3$ with 13 K critical temperature in 1975 (Golubov, 1998b). The superconducting ceramic is the predecessor of the existing high temperature superconductors.

Swiss physicists from the IBM research laboratory in Zurich announced in April 1986 the discovery of high temperature superconductor in the perovskite structure Lanthanum-Barium-Copper at 30 K (Bednorz & Muller, 1986). The discovery has

opened up interest in research and development for the technology and many superconductors have been found since then (Oomen, 2000; Pan *et al.*, 2000). Several of these superconductors which have been discovered show superconductivity at temperatures higher than liquid-nitrogen temperature of 77 K. The most common high temperature superconductors are Yttrium Barium Copper Oxide $YBa_2Cu_3O_x$ (Y-123 or YBCO) and Bismuth Strontium Calcium Copper Oxides $Bi_2Sr_2Ca_2Cu_3O_x$ (Bi-2223) and $Bi_2Sr_2Ca_1Cu_2O_x$ (Bi-2212). These materials have exhibited a superconducting behaviour at the temperature below 92, 110, and 85 K, respectively, which allow them to be operated in liquid nitrogen.

However, the search for superconductivity at higher temperatures is still continuing (Djurek, Medunić, Tonejc, & Paljević, 2001). The technical properties of high temperature superconductors are subject to ongoing research (Sheahen, 1994; Sheahen, McConnell, & Mulholland, 2002; Wesche, 1998). The basic advantages of high temperature superconductors are relatively high operating temperature and heat capacity. These characteristics allow simple cooling and high stability against disturbances. However, a major shortcoming of high temperature superconductors is still the substantially higher conductor cost compared to that of copper.

2.2 High temperature superconductors

The intermetallic superconductor, Niobium-Germanium (Nb_3Ge), with the critical temperature of 23.2 K is used as the benchmark between low and high temperature superconductors (Shaw, 2003). In other words, high temperature superconductors (HTS) are a group of materials with the transition temperature above that of Nb_3Ge. The first HTS material was discovered in 1986 by Bednorz and Muller (Bednorz & Muller,

1986). It was a ceramic oxide compound $(La,Ba)_2CuO_4$ with a critical temperature of approximately 30 K. The compound is usually used as insulator and was not anticipated to be suitable as a superconductor.

The discovery of superconductivity in ceramic materials by the 1987 Nobel Prize winners in Physics, J. Georg Bednorz and K. Alexander Muller, sparked a turbulence of excitement to search for new HTS materials. Subsequently, materials such as Yttrium Barium Copper Oxide (YBCO), Bismuth Strontium Calcium Copper Oxide (BSCCO) and Thallium Barium Calcium Copper Oxide (TBCCO) with critical temperatures of 92, 115 and 125 K, respectively, were discovered. More than 50 cuprate compounds were established by interchanging exotic and sometimes toxic elements into the basic Y-based, Bi-based and Ti-based HTS systems.

2.2.1 Basic properties

The high temperature superconductors are produced in the form of either bulk or thick films (10-100μm) or thin films (<1μm) or wires and tapes in single or multifilament composites (Sykulski, 1997). The materials exhibit superconductivity behaviour of zero resistance on cooling below the transition temperature of the conductor. These composite materials have copper oxides which are insulators and therefore, require dopants such as barium to build up carriers along the copper oxide planes. Besides the main characteristic, the superconductors are also highly anisotropic with the resistivity perpendicular to the copper oxide planes being very much higher than that of parallel to the planes. The perpendicular resistivity increases with increasing temperature while the parallel resistivity decreases.

Other superconductor properties such as penetration depth (λ), coherence length (ξ) and energy gap (Δ) are also highly anisotropic (Khare, 2003). The penetration depth of a high temperature superconductor is defined as the distance over which an applied magnetic field decays to 1/*e* of its value at the surface of the conductor. The value of penetration depth along the *z*-axis is not the same as that of along the *x*-*y* plane. The coherence length is the measurement of the correlation distance of the superconducting charge carriers. It represents the size of the Cooper pair in the superconductor and is inversely proportional to the values of the transition temperature. The existence of energy gap in superconductors is very important in low energy excitation for pairing of electrons.

Another characteristic of superconducting materials is the critical magnetic field (H_c) (Khare, 2003). The boundary for changing of state from normal to superconductive or otherwise is not only dependent on the transition temperature, but also the magnetic field strength. The superconductivity is destroyed above certain critical value of magnetic field. The magnetic lines of force will penetrate through the superconductor if a paramagnetic material is placed in the magnetic field. However, the lines of force are completely expelled from the interior of the superconductor when cooling below the transition temperature. This is called the Meissner effect which is the basis for classification of superconducting materials into type I and type II. A sharp transition from the superconducting state to the normal state is the behaviour of type I superconductors, which is normally shown by pure metals. Type II superconductors exhibit two critical fields, *i.e.*, lower critical field (H_{c1}) and upper critical field (H_{c2}). The effects of the magnetic field strength on superconducting materials are shown in Table 2.1.

Table 2.1: The effects of magnetic field on superconducting materials

Magnetic Field Strength	Effects on the Materials
$H < H_{c1}$	The magnetic field is completely expelled from the superconductor. Completely superconducting state.
$H_{c1} < H < H_{c2}$	The magnetic field slowly and continuously penetrates the superconductor. The transformation from the superconducting state to the normal state. Also known as vortex or mixed state.
$H > H_{c2}$	The superconductivity of the material is completely destroyed. Completely normal state.

Similar to the critical magnetic field (H_c) and critical temperature (T_c) as described previously in Figure 2.1, the critical current density (J_c) is also an important parameter that determines the superconducting state of a material (Khare, 2003). The critical current density is restricted by the grain-boundary weak links in a superconductor material. The weak links are localized regions in a superconducting material in which various superconducting properties degraded.

2.2.2 Common materials

The first superconductor was discovered by Onnes in 1911. Following the discovery, superconductivity was found later in many other metals, alloys and intermetallic compounds. Bednorz and Muller (Bednorz & Muller, 1986) discovered high temperature superconductivity in ceramic cuprate oxides La-Ba-Cu-O at transition temperature 30 K in 1986. Subsequent to this major breakthrough, groups at the

University of Alabama and the University of Houston found in 1987 (Wu *et al.*, 1987) that by replacing Lanthanum (La) with Yttrium (Y) for the composition of Y-Ba-Cu-O, a significant Yttrium compound (YBCO) composition with transition temperature of 92 K which is well above the boiling point of liquid nitrogen at 77 K was achieved.

Meanwhile, in 1988, a group at the National Research Institute for Metals in Tsukuba, Japan (Maeda *et al.*, 1988), reported the discovery of Bismuth compound (BSCCO) with transition temperature of 105 K through the composition of Bi-Sr-Ca-Cu-O compound. The compound later achieved a better transition temperature of 110 K through a different composition. In the same year, another group at the University of Arkansas (Sheng & Hermann, 1988) substituted the non-magnetic trivalent Thallium (TI) for a rare-earth element (R), and partially substituted Calcium (Ca) for Barium (Ba) to produce the Thallium compounds (TBCCO). The TI-Ba-Ca-Cu-O composition was found to have the transition temperature of around 120 K. Meanwhile, Schilling of Zurich, Switzerland (Schilling, Cantoni, Guo, & Ott, 1993), detected the superconductivity in Mercury compounds (HBCCO) with the composition of Hg-Ba-Ca-Cu-O that can reach a transition temperature of up to 133 K. Table 2.2 lists some of the most promising high temperature superconductor materials for high current applications with their formula, notation and transition temperature.

Table 2.2: Examples of high temperature superconducting materials

Compound	Formula	Notation	Transition Temperature (K)
Yttrium	$Y_1Ba_2Cu_3O_7$	YBCO 123	92
	$Y_2Ba_4Cu_7O_{15}$	YBCO 247	95
Bismuth	$Bi_2Sr_2Ca_1Cu_2O_8$	Bi 2212	85
	$Bi_2Sr_2Ca_2Cu_3O_{10}$	Bi 2223	110
Thallium	$TI_1Ba_2Ca_2Cu_3O_9$	TI 1223	110
	$TI_2Ba_2Ca_2Cu_3O_{10}$	TI 2223	125
Mercury	$Hg_1Ba_2Ca_2Cu_3O_{10}$	Hg 1223	134

2.2.3 YBCO coated conductor

There are several alternatives for HTS coated conductors (Blaugher, Bhattacharya, Chen, & Padmanabhan, 2002). This research study focuses on the Yttrium based compound (YBCO) since the HTS distribution transformer currently being developed at the Industrial Research Limited in Wellington, New Zealand, uses the YBCO wires for the windings. $YBa_2Cu_3O_{7-x}$ can be considered the most commonly investigated high temperature superconductor in recent years. The compound was first discovered by Wu (Wu *et al.*, 1987) and is a superconductor with the critical temperature of 92 K, far exceeding the boiling point of liquid nitrogen at 77 K. It is also labelled as YBCO-123.

Even though there are many other high temperature superconductors with higher critical temperatures that have been discovered in the recent years, YBCO is still the most promising candidate or material for current applications which are intended to perform at 77 K. The high current density, high current carrying capability and high magnetic field tolerance (Chen, Donzel, Lakner, & Paul, 2004; Koblischka-Veneva, Sakai, Tajima, & Murakami, 2003) of YBCO are the critical advantages compared with other superconducting materials. Meanwhile, the expected low cost potential of YBCO coated

conductor (Chen *et al.*, 2004; Tsukamoto, 2005) has also significantly attracted the research into its applications.

YBCO has also been chosen as the preferred superconducting materials to be developed and deployed for the second generation (2G) HTS wires. One of the areas that has been concentrated on is the process of textured template (Chen *et al.*, 2004). Ion-Beam Assisted Deposition (IBAD) is one of the processes and it was established by Los Alamos National Lab in the United States. The process makes use of a second ion beam to mill away out-of-plane growth of Yttria-Stabilized Zirconia (YSZ) so that an excellent textured of YSZ template layer on substrate can be accomplished. Later on, a better quality of Magnesium Oxide (MgO) template layer has also been obtained through the process. Subsequently, the other layers of materials, *i.e.*, a buffer layer, YBCO, and a shunt can be deposited into the wire. Another common process is Rolling-Assisted Biaxially Textured Substrate (RABiTS) which was developed at Oak Ridge National Lab, also in the United States. The process is based on cold rolling texture of Ni-based alloys.

Another area that has been focused on is the deposition of HTS layer (Chen *et al.*, 2004). Several techniques have been developed such as Pulsed Laser Deposition (PLD), Metal-Organic Chemical Vapour Deposition (MOCVD), Electron-Beam BaF_2 Deposition, Metal-Organic Deposition – chemically derived (MOD), and Liquid Phase Epitaxy (LPE). Intense research has been conducted to establish lower cost of manufacturing process with the targets to achieve better wire texture and higher current carrying capacity. Consequently, substantial benefits in electrical power industry such as better energy efficiency, increased power density, and improved power-to-weight ratio can be achieved if the length of the coated superconducting wire can be scaled up from a few hundred metres to several kilometres.

2.3 Applications of HTS

Low temperature superconductors (LTS) have been developed for adoption in applications that require large magnetic fields such as Magnetic Resonance Imaging (MRI). However, after the discovery of high temperature superconductors (HTS), the range of potential applications has widened into both electronics and electric power industries (Masur, Kellers, Pegrum, & Cardwell, 2003). High temperature superconductors are available in three different forms - wires or tapes, thick and thin films, and bulk. For wires or tapes, the superconducting materials such as YBCO-123 are deposited on long and flexible substrates. The focus is in electric power applications such as cables and transformers. Electronics and microwave applications utilize thin film HTS. This technology has excellent potential to be applied in high speed electronics, logic, and microwave circuits which require sharp bandwidth characteristics. Meanwhile, bulk materials have the capability to produce magnetic fields that are much larger than those generated by conventional permanent magnets.

2.3.1 General applications

Two bismuth-based HTS compounds $(BiPb)_2Sr_2Ca_2Cu_3O_x$ (BSCCO-2223) and $Bi_2Sr_2Ca_1Cu_2O_x$ (BSCCO-2212) have been developed into wires and utilized in several applications. BSCCO-2223 is more suitable for electric power applications because of its higher critical temperature (110 K) which makes it possible to operate in liquid nitrogen compared with that of BSCCO-2212 (80 K). However, for operation below 20 K such as high-field magnets, the latter is a better alternative. In the mean time, YBCO coated conductor wire is more promising for applications at high current and magnetic fields in the 77 K range than the BSCCO compounds because it possesses higher

irreversibility field. The irreversibility field at a given temperature is defined as the field at which the magnetic behaviour of the material becomes reversible. In other words, it is still superconducting but unable to support a useful current density (Masur *et al.*, 2003). However, the selection of materials for applications in liquid nitrogen regime should also look into the overall cost; especially the manufacturing cost over the performance provided.

HTS have also been utilized in thin film devices and applications; especially in high frequency microwave devices such as resonators, filters, and mixers (Masur *et al.*, 2003). The Josephson junction based device, HTS superconducting quantum interference device (SQUID), is one of the main interests. SQUID is a very sensitive detector for magnetic flux and has been employed in many applications such as biomagnetism or non-destructive evaluation. Another favourable application field for HTS thin films is in passive microwave filters that possess lower insertion loss and greater sharply-defined passbands compared with their conventional metal-based counterparts. A notable example in their application is for cellular radio based-stations. Also, HTS thin films have been used in nuclear magnetic resonance (NMR) or magnetic resonance imaging (MRI) detector coils. The lower losses of the superconductor are very significant in order to increase the signal-to-noise ratio and as a result, the data acquisition times can be reduced.

Bulk HTS materials are able to handle large induced currents. The materials can be utilized to generate large magnetic field for permanent magnet type applications such as magnetic bearing, flywheel energy storage, and clamps. One of the categories in which bulk materials are employed in engineering devices is for motors and generators. The bulk HTS materials are able to increase the current and raise the power, density, and trapped fields in the operation of rotating machines. The operation of rotating machines

is based on the torque produced by the interaction between magnetic fields and currents. The magnitude of this torque is limited by the saturation magnetic flux density of iron. The increased current associated with bulk HTS materials has the potential to enhance the performance of permanent magnet and reluctance electrical machines by increasing the available torque and by reducing the amount of iron required to contain the magnetic flux. This translates to smaller, lighter, more efficient machine designs (Masur *et al.*, 2003).

2.3.2 Power applications

High temperature superconductivity is still an on-going area of research worldwide (Appleton, 1994; Chen *et al.*, 2004; Garlick, 1997; Giese, Sheahen, Wolsky, & Sharma, 1992; Hornfeldt, 2000; Jones, 2008). The characteristics of higher transition temperature and economical cryogenic cooling have increased the potentials for the applications in the electrical power industry. The advancement of high temperature superconducting technologies has spurred on the demonstration of various prototypes such as power cables, transformers, motors and fault current limiters.

In the initial stage, the currents at which the superconducting occurred for the available metals such as mercury were too low to permit any effective experimentation, and as the current increased, the produced magnetic field would destroy the superconducting state of the metals. The specific heats of the metals are very low. A small amount of heat would be enough for the metals to reach their transition temperatures and to move beyond their superconducting region. Furthermore, the refrigeration at these temperatures is very expensive and it is estimated that 1 W of cooling power at 4 K requires more than 1 kW at room temperature (Appleton & Prothero, 1998). This

situation had restrained the development of superconducting transformer in the early stage of superconductivity era. However, the advancement of composite superconducting materials has significantly reduced the magnitude of the losses and boosted the interest in pursuing the research on the high power rating equipment. In addition, the progress in liquid nitrogen technology in superconductivity has further enhanced the development of superconducting transformers. Further elaboration on HTS transformers will be discussed in the next section.

Fault current limiters have been developed to protect other power equipment in expanding electrical power networks. The growth of power networks brings about the increase in fault current level. The device should be able to operate with low impedance under normal operating conditions and with high impedance under fault conditions. Several designs have been promoted which are categorized into resistive and inductive types (Appleton & Prothero, 1998). The resistive type utilizes the change in resistance between the superconducting and normal state for the switching. Meanwhile, the inductive type employs the change in inductance by flux exclusion in magnetic circuit during the transition. The fault current limiting properties in superconductors have been proposed in recent development of superconducting transformers.

Prior to the discovery of HTS in 1980s, the research on LTS power transmission were only focused on economically viable superconducting underground cable of higher rating at between 1000 MVA and 3000 MVA (Appleton & Prothero, 1998). However, the interests have been revived with the potential of HTS cables which offer small impedance for loss reduction and low thermal heating for current carrying capacity amplification. The power that can be transmitted by an underground cable is limited by the amount of heat generated. Superconducting cable operates at liquid nitrogen temperatures. The current carrying capacity of the cable can be improved due to the low

thermal heating effects. The technology has also offered the feasibility for applications in lower voltage levels. Several HTS power transmission cable projects have been carried out in the United States, European and Asian countries since 1992 (Jones, 2008).

Synchronous machines have been developed with HTS rotor and copper stator winding. The rotor winding would be subjected to a constant magnetic field and superconducting a.c. losses would therefore be zero. By contrast, the stator winding would see significant current and magnetic field variations, and therefore would be subjected to large a.c. losses if the winding were superconducting. Many existing research work had look into extremely fine superconducting filaments which have extremely low losses to make it possible for an all superconducting machine (Appleton & Prothero, 1998). The challenge for the industry would be to develop all-superconducting machines with both superconducting rotor and stator windings that are able to increase the efficiency in addition to the reduction in weight and volume.

Significant acceleration programmes have been carried out in the USA, Europe and Asia in the hope for larger scale applications. The US Department of Energy (DOE) and Electricite de France (EDF) lead the programmes related to the electric power sector in the USA and France, respectively (Hawsey & Christen, 2006; Manuel *et al.*, 2002). In Japan, several national projects on superconducting apparatuses have been conducted by NEDO (New Energy and Industrial Technology Development Organization) since 2000 with the objective of real applications in the years of 2011-2015 (Iwakuma *et al.*, 2009; Tsukamoto & Akita, 2002). A 10-year DAPAS (Development of the Advance Power system by Applied Superconductivity technologies) programme in Korea has entered the final phase with several significant achievements (Minwon *et al.*, 2007). Meanwhile, the State "863" Programme (High Technology Research & Development Programme) by the Ministry of Science and Technology of China, Chinese Academy of

Sciences (CAS) and the power equipment industries, which has supported the power application research of superconductor in China since the year 2000, has successfully made, tested and demonstrated several superconducting power equipment on the field (Liye & Liangzhen, 2007). Amongst the critical factors that are being looked into for full commercialization of the application are stability and reliability, robustness, energy efficiency and cost-effectiveness of the superconductors (Chen *et al.*, 2004; Garlick, 1997; Smith *et al.*, 1989).

2.3.3 Potential benefits

The prospects for the application of the superconductor technology have been recognized in the early stage of the material development. The ability to transmit electricity without resistance and the associated magnetic characteristics of the superconductors has opened up a new vision, particularly in revolutionizing the electricity supply industry (McGowan, 1988). The applications would offer numerous benefits such as increase in energy efficiency due to low losses and high current carrying capability characteristic of the materials. HTS technology also offers environmental advantages such as oil-free transformers and devices with low magnetic field leakage. Superconducting equipment must be designed with low magnetic field leakage in order to maintain the high critical current and to reduce the a.c. losses in the tapes (Chen *et al.*, 2004). Other potential benefits include reduction in equipment size, deferment in expansion, increase in reliability and flexibility in transmission and distribution of power system (Garlick, 1997).

However, all the possible advantages from the superconductor technology development mentioned above require realistic analysis in order to quantify them. The markets are

targeted at the power industry. Power utilities and industrial manufacturers are frequently questioned on the adequacy, reliability and cost of the conventional equipment. These factors are able to create ambiguities to assist in the exploitation of superconductor technology. The performance and reliability of conventional equipment are always being questioned. The suspicions or lacks of faith are providing additional incentives or motivations in the development of the superconducting technology (Garlick, 1997). Finally, the ultimate focus for the new technology will be on lower electricity costs, improved environmental quality and competitive products for global competition. Environmental quality can be expressed through the replacement of conventional oil with liquid nitrogen as the electrical insulation and the cooling media. The application should be able to avoid potential fire hazard and environmental impact. It is safe, non-flammable, and environmental friendly. It will eliminate a potential source of explosions. It will also take out the possibility of soil contamination from any leakage oil from the transformers (Reis *et al.*, 2002).

2.4 Superconducting transformer

Strong international interest in the development and commercialization of the HTS transformer can be observed (Donnier-Valentin, Tixador, & Vinot, 2001; Formisano *et al.*, 2006; Funaki *et al.*, 2001; Liye & Liangzhen, 2007; Minwon *et al.*, 2007; Sissimatos, Harms, & Oswald, 2001b; Weber *et al.*, 2005). Some have estimated that in the year 2020 up to 80% of new power transformers will be using high temperature superconductors instead of copper (Sheahen *et al.*, 2002). The expectations are rather high in the power engineering sector. Several studies have been carried out to compare conventional and HTS power transformers (McConnell *et al.*, 2000; Nagasawa, Yamaguchi, & Fukui, 2003). The viability of a superconducting transformer is dealt not

only with technical points of view but also economical aspects. For the use of superconducting transformers, the end users will be looking at the lifecycle costing or total ownership cost of both conventional and superconducting transformers. The superconducting transformers must be available at a competitive price as compared to that of conventional transformers. The cooling system and conductor cost will be the determinant element. The conventional copper transformers have been produced for almost a century and have reached their physical and technological limits in many aspects. The crucial expectation will be at what cost-effective conditions the overall efficiency of a high temperature superconducting transformer can be made higher than that of a conventional copper transformer. Moreover, the application will have to start slowly to gain experience and customer acceptance.

2.4.1 Design approach of HTS transformers

Power transformers have evolved little in the last fifty years with the exception of core steel and improvements in insulation. While the fundamental design principles and overall construction techniques have changed little, today's utility power transformer has losses that are less than 0.4% of total rating. Modern power transformers are very reliable, robust equipment which operate under less than perfect environmental conditions from near zero loads to greater than 125% of nameplate for over thirty years under limited human surveillance. Even though protected externally by voltage surge arresters, the transformers are designed to withstand high voltage tests which include induced a.c. voltage test and lightning impulse test. A transformer is normally protected against high voltage amplitudes and high time-rates of voltage changes. The surge arrestor is normally in high impedance state under nominal supply voltage conditions. However, under transient conditions, the arrestor rapidly moves into a lower impedance

state, diverting the excess transient energy (current) to the ground or source and thus limiting the transient voltage to a safe level. The arrestor will automatically resets after the transient. While current limiting relaying systems and fuses protect transformers against high currents induced by short circuit faults, transformer windings must be designed to survive significant current overloads of 10-20 times the normal full load for 1-2 seconds. This requirement insures the mechanical integrity of both the windings and the insulation system. The superconducting transformers must be designed and developed to meet these or similar strenuous specifications.

There are two basic design approaches that have been practiced worldwide (Reis *et al.*, 2002). Both approaches adopt a one-for-one substitution of HTS transformer for conventional transformer. The first approach is a liquid nitrogen (LN_2) bath cooled transformer. In the design, the winding coils are positioned in a bath of LN_2 which provides the thermal and electrical insulation. The operating temperature range of the transformer is limited to between the LN_2 boiling point of 77 K and the LN_2 freezing point of 64K. The current carrying capacity of the superconductor is heavily dependent on the operating temperature. As a consequence, more of the superconductor is required for operation at this high temperature compared to that of a lower temperature range. Cryocooler is used to re-condense the LN_2 for cooling the system. Another technique for the cooling purposes is by periodically filling up the boiled-off LN_2. The enclosures for the liquid nitrogen insulation surround each of the core leg. Because of that, they cannot be from a completely metallic material which can contribute to a shorted turn configuration. They are donut-shaped vacuum fitted enclosures and usually are double-walled with ring-shaped vacuum space in between for thermal insulation. This design has the possibility of air cooling the transformer core. This design approach has been practiced by Fuji (Japan), ABB (France), Siemens (Germany) and RTRI (Japan) for their projects.

In the other basic design approach, the overall tank acts as vacuum enclosure to take away the bath cooling and directly cool the windings. This design arrangement allows the superconductor to operate at lower temperature range. The beneficial gains are reduction in the amount of superconductor required and also reduction in the cost of winding conductor. However, there is a disadvantage for operating at the lower temperature. The energy that is required to get rid of 1 W of losses will increase greatly as the operating temperature decreases. It is found that 25, 30 and 50 W of cryocooler compressor power are required to remove 1 W of losses at the temperatures of 77, 64 and 40 K, respectively. Therefore, the lower the operating temperature, the more difficult it will be to get a very low alternating current loss winding design and a more efficient cryocooler.

2.4.2 Comparison with conventional transformer

A three phase power transformer system consists mainly of core, windings, insulation, tank and bushing. The windings transmit alternating current and they are exposed to alternating magnetic field. The current and magnetic fields are sinusoidal that alternate in phase at the same frequency. The amplitudes of the current and magnetic fields are coupled via the magnetic field constant.

In a conventional transformer, the operating temperature of the core is almost the room temperature. Oil is normally employed for electrical insulation and at maximum ambient temperature of 40°C, a limit on top oil temperature rise of 60°C is normally specified (Kulkarni & Khaparde, 2004). The mineral oil is also used for cooling both the iron core and the conductor windings. The size of a transformer which has to include the oil and cooling radiator is essentially determined by the core and windings.

The core of an HTS transformer is also operated at room temperature. However, the superconductor windings operate at a very much lower temperature. These windings are put in cryostats. They are connected to the bushings by current leads at the room temperature. A refrigerator is installed to provide the cooling for the windings.

One of the most important enemies for the conventional power transformer is heat. The transformer is designed to meet a target lifetime of typically 30 or more years. Therefore, it is important for the capacity ratings of the transformer to be able to hold the temperature of the hottest portion of the insulation below 110°C or even 90°C for older transformer design (Mehta *et al.*, 1997). Thermal damage for paper-oil electrical insulation system is cumulative with time. For example, continuous operation at 20°C above the design limit for 100 days, which is less than 1 percent of 30 years, will reduce the transformer life by 25%.

Consequently, thermal management of conventional transformers has become very significant. Such example can be observed on the usage of air-conditioning systems during several very hot days of the year. Customers tend to apply heavier usage, which results in peak loading conditions for durations of 10 hours or more. Without proper management by the utilities, the transformers will suffer significant loss of insulation life. Some utilities have opted for purchasing transformers with excess capacity in order to meet the maximum temperature limits that may occur only for a few days in the year. And, these transformers operate well below the optimal level in most of their operational life.

The windings and insulations of HTS transformers are designed to operate in the ultra-cold temperature range of between 20 K and 77 K (Mehta *et al.*, 1997). The insulation used for the HTS transformer is liquid nitrogen (LN_2). There will be no thermal degradation on the insulations. Therefore, HTS transformers can operate at rated power

continuously and efficiently. As a matter of fact, the transformers can operate up to two times their rated power continuously without loss of operating life. However, the efficiency will be significantly reduced because of disproportionately increased use of liquid nitrogen or increased refrigeration load. Most importantly, one HTS transformer is able to carry twice the rated loads in emergencies, which is normally handled by two conventional transformers, and its lifetime can be greatly extended.

HTS transformers are designed to serve as direct replacement for conventional transformers. They have the ability to run through a fault current of 10-12 times their rated current, which is limited only by their own internal impedance. Meanwhile, conventional transformers are efficient. For example, 30 MVA class transformers are 99.3 to 99.7% efficient depending on the loading. However, there is still room for improvement. In the US, a quarter of the 7 to 10% losses in transmission and distribution systems come from power transformers. These transformer losses cost more than USD2 billion per year (Mehta *et al.*, 1997).

The characteristic of low impedance makes transformer better. It maintains output voltage levels over a wide range of operating power levels. It also produces better transmission of power down-stream through the power system. Most of conventional transformer losses come from resistive heating in the windings. And, HTS transformers have "zero" winding resistance with some alternating current losses that require refrigeration power. This characteristic makes the HTS transformers considerably more efficient than the conventional transformers. HTS transformers still have a.c. losses in the iron core that are comparable with that of conventional transformers. There will also be low levels of a.c. losses in the windings. The load losses generated in the HTS transformers are only on the order of hundreds of Watts at cryogenic temperature. However, the cryocooler compressor power needed to remove these Watts at low

temperature is on the order of tens or hundreds of Watts per Watt of loss (Reis, Mehta, McConnell, & Jones, 2001).

2.4.3 Demonstrators and prototypes

Superconducting transformers have the potential to reduce up to 30% losses, 50% size, and 70% weight compared with conventional transformers (Chen *et al.*, 2004). The HTS transformer would require less winding conductor as compared to the conventional transformer of the same capacity due to the increase in current density. The thickness of the winding pack can therefore be reduced. The HTS transformer also would not require large cooling fins. Meanwhile, the HTS transformers are oil-free. The region occupied by the oil has been replaced by either vacuum or liquid nitrogen, making the HTS transformer much lighter than conventional oil-filled transformers (Reis *et al.*, 2001). The transformers also offer overloading capability without accelerated aging. The most recent interest is the feasibility to integrate the function of fault current limiter in the superconducting transformer windings. The attractions have developed interest in several countries to construct prototypes of the transformer and carry out demonstrations on the applications. Several demonstration projects on HTS power transformers executed worldwide are shown in Table 2.3.

Table 2.3: Demonstration projects on HTS transformers

GROUP	YEAR	PHASE	KVA	KV	HTS	TEST	REFERENCE
ABB, EDF, ASC, Services Industriels de Geneve (SIG)	1994	3	630	18.7/0.4	Bi-2223	Field	(Mehta *et al.*, 1997; Zueger, 1998)
Kyushu University, Fuji Electric, Sumitomo Electric Industries	1996	1	800 (500)	6.6/3.3	Bi-2223	Lab	(Funaki *et al.*, 2001; Mehta *et al.*, 1997)
WES, IGC-SP, ORNL, RG&E, RPI	1998	1	1000	13.8/6.9	Bi-2212	Lab	(Schwenterly *et al.*, 1999; Schwenterly Mehta, Walker, & Jones, 2002; Weber *et al.*, 2005)
Kyushu University, KEPCO, Fuji Electric, Kyushu Transformer, Taiyo-Toyo Sanso	2000	1	1000	22/6.9	Bi-2223	Field	(Funaki *et al.*, 2001; Kimura *et al.*, 2002)
Tebian Electric Company (TBEA)	2001	3	630	10.5/0.4	Bi-2223	Field	(Jianxun & Xiaoyuan, 2008; Liye & Liangzhen, 2007; Yinshun *et al.*, 2007)
WES, IGC-SP, ORNL, Energy East	2002	3	5000 / 10,000	24.9/4.2	Bi-2212	Field	(Schwenterly *et al.*, 1999; Schwenterly *et al.*, 2002; Weber *et al.*, 2005)
Siemens AG	2002	1	1000	25/1.5	Bi-2223	Lab	(Leghissa *et al.*, 2002)
Seoul National University, Korea Polytechnic University, HICO	2004	1	1000	22.9/6.6	Bi-2223	Lab	(Minwon *et al.*, 2007)
Korea Polytechnic University, LS Industry, Cheongju, KESRI, Seoul, Woosuk University, Korea University.	2007	1	5000	89.1/56.2	YBCO	Lab	(Jeehoon *et al.*, 2008)

The projects involve interested parties from various research groups and also companies in the industry. The prototypes involve the designs for single and three phase transformers for various capacities and voltage levels. Some of the transformers were evaluated in laboratories while others were tested in existing network systems.

2.4.4 Technical benefits

The HTS transformers run at very low temperatures. If the network system experiences overload condition, the amount of heat generated in the transformers should be very little (Reis *et al.*, 2001). Therefore, the thermal degradation on the insulations of the transformers is not expected to take place as in conventional transformers. With regards to this, the emergency overload capability of HTS transformers can be double the normal rating by putting extra superconductor in the windings, taking into account they are also designed to manage the additional overload mechanical forces. However, operation for extended duration under overload conditions would not be efficient because ac losses and refrigeration costs will increase as the square or even cube of the operating current (Reis *et al.*, 2001). The utilities, above all, will find it very attractive to have economically feasible and technically viable HTS transformers that can operate up to twice the rating under emergency overload conditions and have longer life at full rated current.

The HTS transformers are targeted at the reduction of size and weight compared to the conventional transformers. The HTS superconductors with high current densities will make it possible to produce smaller and lighter transformers. The elimination of oil as an insulator and coolant will provide further weight and volume reductions. The design of associated large external heat exchangers that are required to transfer the heat from major load losses could also be done away with. However, further reduction in size and weight is limited by the required space for insulation and dielectric design to handle the operating voltages and BIL levels. The benefits of high power density which enable more compact transformers will be most effective in areas where substation space is at a premium (McConnell, 2000; Reis *et al.*, 2001).

Eddy current losses together with hysteresis losses constitute the no-load losses (Kulkarni & Khaparde, 2004). Both losses arise due to successive reversal of magnetization in the iron core. The eddy current loss is due to the eddy current formed in the body of the magnetic core. Whenever the iron core is exposed to a changing magnetic field, a magnetic field is produced in the magnetic core and that induces a circulating current or eddy current in it. The load loss of a transformer consists of I^2R losses and stray losses. The stray losses occur due to leakage field of the windings and field of high current carrying leads. The stray losses in the windings are further classified as eddy loss and circulating current loss. The stray flux impinge on conducting parts such as winding conductors give rise to eddy currents in them. Stray losses also occur in structural steel parts. The stray losses in windings can be substantially high in large transformers if conductor dimensions and transposition methods are not chosen properly (Kulkarni & Khaparde, 2004). The stray losses in conventional transformers are more or less equal to the power required for cooling or refrigeration in HTS transformers. Also, the core losses are comparable in similarly rated HTS and conventional transformers (McConnell, 2000; Reis *et al.*, 2001). Therefore, superconducting transformers offer very much lower operating losses by "eliminating" resistive losses in the windings.

The material properties and the current-voltage characteristics of a HTS provide inherent capabilities as a fault current limiter (McConnell, 2000; Reis *et al.*, 2001). For a transformer, the possibility is relied on the mode of transition of the entire length of superconductors to the resistive state. However, the transformation would not be easy for low level faults. The advantage to the power system which would be able to limit current under severe transient fault conditions is to reduce the current interruption ratings of circuit breakers. The other advantage is to also act as current limiting devices

which would eliminate the requirement for additional devices such as fault current limiters.

2.4.5 Non-technical benefits

The HTS transformers are oil-free equipment. The weight is very much reduced with the use of liquid nitrogen as the replacement. In addition, the large oil-filled heat exchangers are also replaced by much smaller cryocoolers. The size is also reduced with the application of the high power density of high temperature superconductors (Reis *et al.*, 2001).

Both the weight and size are expected to reduce between 50 to 70% smaller than those of conventional transformers of the same power rating (Chen *et al.*, 2004). Consequently, manufacturing, shipping and installation costs can be reduced. In addition, the space requirement to locate the transformers can also be reduced especially in overcrowded urban substations.

Liquid nitrogen replaces the conventional oil as the electrical insulation and the cooling media. The application should be able to avoid potential fire hazard and environmental impact in accordance with European Union guidelines (Morandi *et al.*, 2008). It is safe, non-flammable and environmental friendly. Therefore, it will eliminate a potential source of explosions. Furthermore, it will also take out the possibility of soil contamination from oil leaks.

2.5 HTS transformer for this work

A demonstration HTS transformer is currently being developed by Industrial Research Limited with its partners. The principal criteria of the transformer are the utilization of the second generation YBCO superconducting wire and the locally developed continuously transposed Roebel cable. The design is for a distribution transformer. The transformer is to be installed in a potential electricity distribution network site to be identified by one of the project partners, Vector Limited. This study uses the baseline design of the transformer and several typical power distribution equipments in a distribution network for the analysis.

The transformer is designed for a three phase distribution network application. The rating capacity is 1 MVA. The primary voltage is 11 kV and the secondary voltage is 0.415 kV. The winding connection type is Dyn11 in which the high voltage winding is delta connected and the low voltage winding is star connected with neutral brought out. The phase displacement between the winding is 30° leading, or the low voltage leads the high voltage with 30°.

The transformer utilises a three legged iron core which is similar to that of a conventional transformer. The core is outside of the cryogenic region. The core or no-load losses can therefore be dissipated into the air and this set up considerably reduces the cryogenic load. The Roebel cable makes up the LV winding in the form of a single layer solenoid. Meanwhile, the HV winding is in the form of a stack of double pancake coils positioned outside of the LV winding (Glasson, Staines, Buckley, Pannu, & Kalsi, 2010). The HV and LV windings are immersed in liquid nitrogen enclosed in a composite cryostat. In order to minimize the heat from leaking into the cryogenic zone, the cryostat is vacuum insulated.

Conventional transformers normally use insulation papers and pressboard for the insulation. For the HTS transformer, glass-fibre composite materials are utilized for insulation barriers and also supporting structures. One of the advantages of glass-fibre composite materials is to provide the required stiffness without conducting too much heat into the cold part. They also have a very low thermal conductivity and good mechanical properties (Cheon *et al.*, 2008). Conventional transformers employ a highly refined mineral oil as a dielectric and a suppressor for corona and arcing. The oil also serves as a coolant. The cooling of the HTS transformer is by liquid nitrogen which is designed to operate in the cryogenic temperature range of 70-77 K (Staines *et al.*, 2012). The distinguish characteristics of a HTS transformer are the design of safe composite pressure vessel and the development of cheap and efficient cooling system. A sketch of the HTS transformer is shown in Figure 2.2.

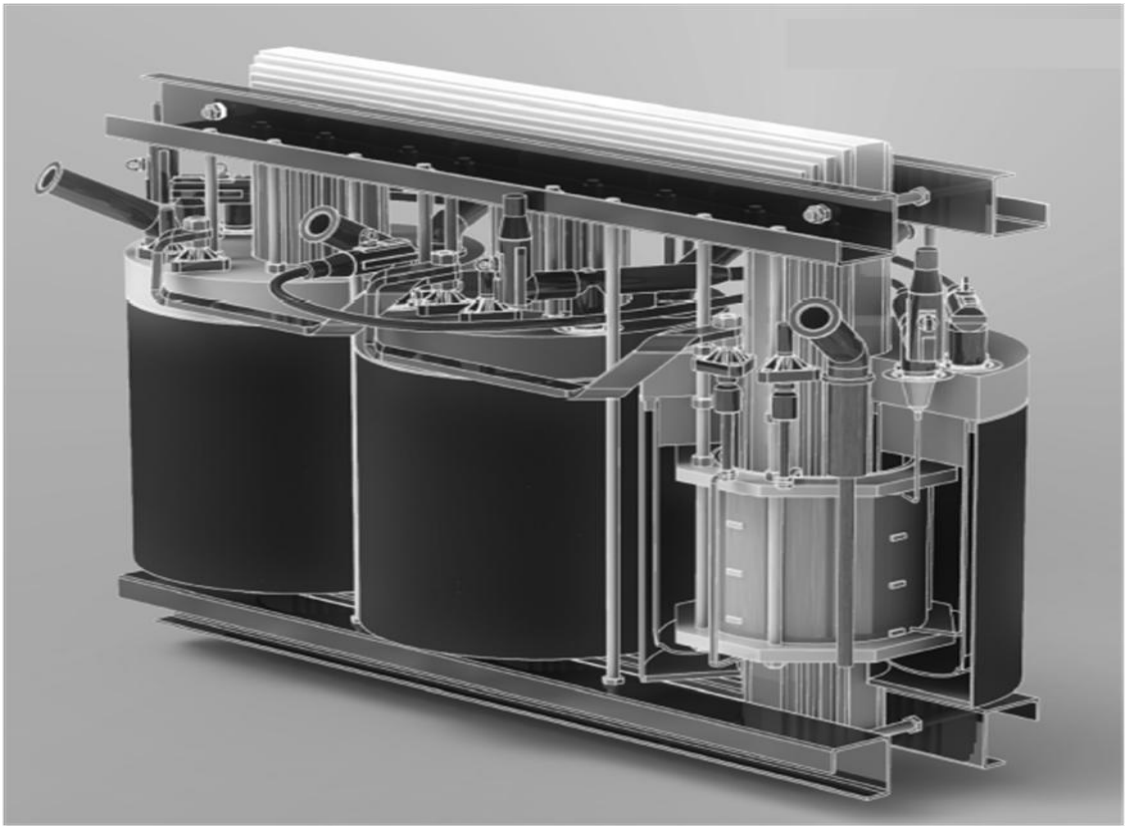

Figure 2.2: A graphical illustration of the HTS transformer (courtesy of Neil Glasson from Industrial Research Limited, New Zealand)

2.6 HTS-FCL transformer

Numerous benefits of superconducting transformers for the application in electric power network have been discussed in the previous section. However, recent development in the technology is the integration of fault current limiting properties into the superconducting transformer. The additional benefits of high temperature superconducting fault current limiting (FCL-HTS) transformers for the entire power system network design and operation should be far greater and exceptional.

Typical values of the voltage impedance of conventional distribution transformers are between 3% and 6%. Further reduction to the impedance values will increase the limit of maximal short-circuit current during a fault (Short, 2004). A previous study (Sissimatos, Harms, & Oswald, 2001a) showed the possibility to design HTS transformers with an impedance voltage of less than 3%. The low impedance value will reduce the network system impedance under normal operating conditions, but will increase the short-circuit current on the grid under fault conditions. Superconducting windings with fault current limiting properties should be able to provide the high impedance necessary during the short-circuit conditions.

The HTS-FCL transformers should be designed with specific winding parameters in order to meet power system requirements. The winding should not limit during inrush current conditions such as the switching on of the transformers. The resistance value of the winding during fault current conditions should not affect the response of the relay equipments. Also, the insulation of the winding should be able to withstand the over-voltage situations and the structure of the winding should be able to withstand the mechanical stresses from the over-current forces.

HTS-FCL transformers have been developed and the prototypes have been constructed in several countries (Janowski *et al.*, 2011; Kotari *et al.*, 2010; Rey, Duckworth, Schwenterly, & Pleva, 2011; Vajda *et al.*, 2011). The short circuit current ratings of other power equipment in the network such as circuit breakers can be reduced substantially with the introduction of HTS-FCL transformers. The transformers would also be able to protect power transmission cables in the same network in case of a fault. Furthermore, the neutral of the HTS-FCL transformers can be connected directly to the ground without the use of additional reactors and this arrangement would increase the human safety against step voltage.

CHAPTER 3

POWER EQUIPMENT & NETWORK MODELLING

The research project is associated with the Foundation for Research, Science and Technology (FRST) High Temperature Superconductors (HTS) Accelerated Development Transformational Research, Science and Technology (TRST), New Zealand. The FRST is now acknowledged as the Ministry of Science and Innovation (MSI). The main focus of the study is on the modelling and analysis of power distribution network with the application of an HTS transformer currently being developed by a transformer project group led by Industrial Research Limited (IRL). The HTS transformer will eventually be installed in a power distribution network owned by one of the project group members, Vector Limited (Vector). However, in this study, the modelling and analysis are carried out on a sample network with the proposed HTS transformer.

The research was established from the development of an HTS transformer by the transformer project group coordinated by IRL. This study was working on a preliminary baseline design that was set up for the transformer. During the progression of the

project, several improved design criteria of the HTS transformer may have been brought forward (Glasson *et al.*, 2010; Staines *et al.*, 2012). The exploration prepared the analysis for the suitability of any other possible HTS distribution transformer configurations proposed by the group.

The project group has also decided to install the first prototype HTS transformer in one of Vector's power distribution network. The location for the installation of the HTS transformer will be decided by the project group based on the technical and physical suitability. The analyses were carried out on a feasible distribution network design the transformer could be set up. A combination of overhead line and underground cable arrangement was investigated with different loading criteria.

Finally, the data analysis was utilised to set up a distribution network model with the application of an HTS transformer. The network model was investigated under various circuit conditions to scrutinise and discover the performances of the proposed HTS transformer toward loading capacity, power transmission efficiency and over current durability. These performances were also examined for the effects they could bring on to the overall power distribution network.

The study had subsequently been developed into several measures starting with the review and assessment of the state-of-the-art of HTS transformer designs and technologies as presented Chapter 2. The next step would be to develop a set of parameters representing the HTS transformer that can be correlated with existing distribution network designs and modelled accordingly under various network conditions. The parameters of other common and essential power network components would also be established in this chapter. A sample distribution network, which is inherently unbalanced, would be presented while taking into account the three phase models of all the other relevant network components. Further analyses would then be

carried out and presented in the next three chapters to validate the parameters of a preliminary baseline design of the HTS transformer. The main purpose would be to exhibit that the HTS transformer should be performing as anticipated under various conditions of the power distribution network.

3.1 Distribution power network

More and more people have dedicated themselves for the development of modelling and analysis on distribution network (Kersting & Dugan, 2006; Makram & Girgis, 1988; Tsai-Hsiang & Wen-Chih, 2001). Previously, most advancement had been devoted to large transmission networks and synchronous generators. Various tools are now available for distribution engineers to run power flow studies and simulate loading conditions on the network (Chen, Chen, Hwang, Kotas, & Chebli, 1991; Ciric, Fadilha-Feltrin, & Ochoa, 2003). Such progression on the analysing tools allows for in-depth studies in short circuit, switching scenarios, losses, *etc.* (Chen, Chen, Lee, Kotas, & Van Olinda, 1992; Kersting, 2004; Kersting & Phillips, 1990; Makram, Bou-Rabee, & Girgis, 1987; Makram & Girgis, 1989; Ochoa, Ciric, Feltrin, & Harrison, 2005).

A distribution network typically starts with a distribution substation which is supplied by one or more sub transmission or transmission lines. The substation serves one or more feeders and most of these feeders are radially operated (Kersting, 2002). The major network components are overhead lines, underground cables, transformers and loads. The study was looking especially into the transformer, overhead lines and underground cables in the modelling and analysis.

The evaluation of distribution power network can be well distinguished from that of transmission for its unbalanced loading characteristic (Kersting & Phillips, 1992). The

main contributing features for the analysis are the unequal single-phase loads and conductor spacing either for overhead lines or underground cables. The conventional power flow and short circuit programs which are implemented in the transmission network studies would not be adequate because they are limited to modeling and analysis of balanced three-phase systems. The three phase transmission network is assumed to be balance and thus it can be represented by a single phase equivalent circuit in the model as well as in the analysis. However, it is not sufficient for the modeling and analysis of a distribution system. A distribution system is inherently imbalance, and therefore three-phase models of all the components must be employed. Furthermore, the data requirements for the distribution system models are more extensive (Kersting, 2002).

3.2 Modelling of transformer

Distribution transformers transform transmission or sub-transmission voltage to low voltage from the capacity rating of a few kVA to a few MVA which will be connected to the customer's load. The modelling of distribution transformer must take into account the connections with other power equipment and must satisfy the Kirchhoff's Current Laws (KCL) and Kirchhoff's Voltage Laws (KVL) (Chen, Chen, Inoue, Kotas, & Chebli, 1991; Kersting, Phillips, & Carr, 1999). The transformers can either be of a combination of single-phase components or a three-phase unit with normally a no-load tap changer on the high voltage winding. Several types of phase connection are available from the combinations of delta, grounded wye, ungrounded wye, open wye and open delta (Chen, Chen, Inoue *et al.*, 1991; Kersting & Phillips, 1996). The most common connection for a four-wire feeder is the delta-grounded wye. The transformers

come in different styles such as pole mounted, ground mounted and cubicle depend on the required rating and field application.

3.2.1 Three-phase impedance

Conventional distribution transformer impedances are normally between the range of 3% and 6% (Short, 2004). These low impedances serve better voltage regulation and less voltage flicker for motor starting or the fluctuating loads. However, they raise fault currents on the secondary which result in deeper voltage sags and higher fault current on the primary. The percent impedance of the transformer (Z_t) can be derived from the triangle with the percentage values of the resistance (R_t) and inductance (X_t) as

$$\%Z_t^2 = \%R_t^2 + \%X_t^2 . \tag{3.1}$$

However, prior to that, a simplified distribution transformer model can be created by removing the magnetizing impedance, but still acknowledging that the no-load loss is still generated and the magnetizing current, which is so small compares to the rated current, still flows (Galloway & Mulkey, 2004; Short, 2004). The ohmic values of R_t (Ω_R) and X_t (Ω_L) can be converted to the percentage values by

$$\%R_t = \frac{load\ loss}{10 \cdot kVA} = \frac{\Omega_R \cdot kVA}{kV^2} \tag{3.2}$$

$$\%X_t = \frac{apparent\ watts}{10 \cdot kVA} = \frac{\Omega_L \cdot kVA}{kV^2} \tag{3.3}$$

where apparent watts is the scalar product of applied voltage and exciting current in units of amperes. In the analysis, since percentage impedance (Z) was already known and the percentage of real impedance was calculated based on the given load loss value,

the percentage of reactive impedance was acquired from triangle of the percentage values as in equation (3.1) (Galloway & Mulkey, 2004). Hence, the phase impedance for a three-phase delta-grounded wye step-down transformer in a matrix form (Kersting, 2002) can be presented as

$$[Zt_{abc}] = \begin{bmatrix} \Omega_R + j\Omega_L & 0 & 0 \\ 0 & \Omega_R + j\Omega_L & 0 \\ 0 & 0 & \Omega_R + j\Omega_L \end{bmatrix}. \quad (3.4)$$

3.2.2 Delta-grounded wye connection

The research study was focusing on a three-phase step-down distribution transformer model with delta-grounded wye connection. This is a popular connection to serve a four-wire feeder system and to provide service to loads which are primarily single phase (Kersting, 2002). The transformer models are generalized for the connection with other series components of the network such as line segments and voltage regulators. The matrix equations to calculate the voltages and currents at the input point as a function of the voltages and currents at the output point are

$$[VLN_{abc}]_{in} = [a] \cdot [VLN_{abc}]_{out} + [b] \cdot [I_{abc}]_{out} \quad (3.5)$$

$$[I_{abc}]_{in} = [c] \cdot [VLN_{abc}]_{out} + [d] \cdot [I_{abc}]_{out} \quad (3.6)$$

where $[VLN_{abc}]_{in}$ is the input or source voltage matrix, $[VLN_{abc}]_{out}$ is the output or load voltage matrix, $[I_{abc}]_{in}$ is the input or source current matrix, $[I_{abc}]_{out}$ is the output or load current matrix, and $[a]$, $[b]$, $[c]$ and $[d]$ are the generalized matrices. The subscripts '*in*' represents input or source side, and '*out*' represents output or load side. The equation

for the voltages at the output point as a function of voltages at the input point and the currents at the output point is

$$[VLN_{abc}]_{out} = [A] \cdot [VLN_{abc}]_{in} - [B] \cdot [I_{abc}]_{out} \tag{3.7}$$

where [*A*] and [*B*] are also the generalized matrices. The voltages are equivalent to line-to-neutral voltages for a delta connection. Meanwhile, for a grounded wye connection, the voltages are the line-to-ground voltages. The currents are the line currents regardless of the types of connection (Kersting, 2002). The connection with relation to voltages is shown in Figure 3.1.

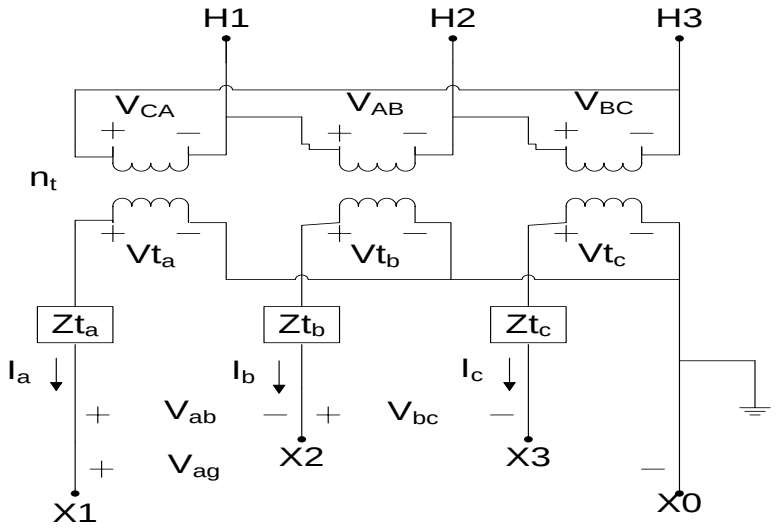

Figure 3.1: Delta-grounded wye connection with reference to voltages

The equations derived from Figure 3.1 as shown in Appendix B1 provide the generalized matrices of [*a*], [*b*], [*A*] and [*B*] for the transformer as per equations (3.5) and (3.7). Meanwhile, Figure 3.2 shows the delta-grounded wye connection with the currents. The polarity marks on the transformer windings are indicated in the figure. The derived equations from Figure 3.2 also presented in Appendix B1 provide the generalized matrices of [*c*] and [*d*] for the transformer as per equation (3.6) (Kersting, 2002).

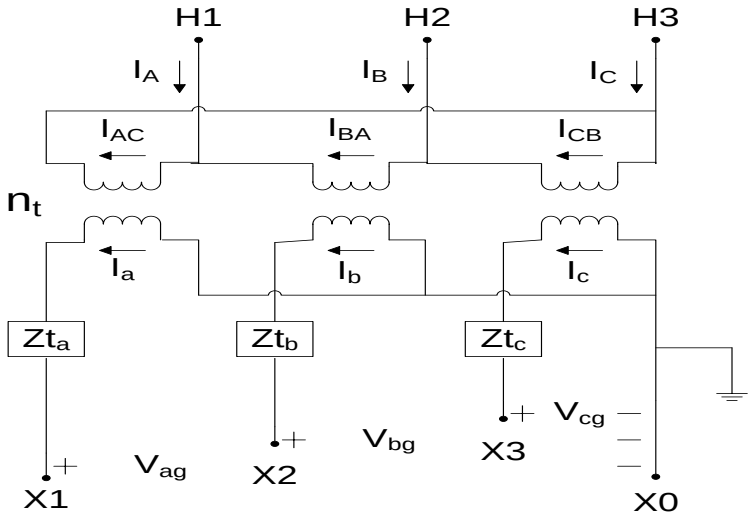

Figure 3.2: Delta-grounded wye connection with reference to currents

3.2.3 Generalized matrices

In summary, the generalized matrices for a delta-grounded wye step-down transformer to be applied for connection with other network components are

$$[a_t] = \frac{-n_t}{3}\begin{bmatrix} 0 & 2 & 1 \\ 1 & 0 & 2 \\ 2 & 1 & 0 \end{bmatrix} \tag{3.8}$$

$$[b_t] = \frac{-n_t}{3}\begin{bmatrix} 0 & 2Z_{tb} & Z_{tc} \\ Z_{ta} & 0 & 2Z_{tc} \\ 2Z_{ta} & Z_{tb} & 0 \end{bmatrix} \tag{3.9}$$

$$[c_t] = \begin{bmatrix} 0 & 0 & 0 \\ 0 & 0 & 0 \\ 0 & 0 & 0 \end{bmatrix} \tag{3.10}$$

$$[d_t] = \frac{1}{n_t}\begin{bmatrix} 1 & -1 & 0 \\ 0 & 1 & -1 \\ -1 & 0 & 1 \end{bmatrix} \tag{3.11}$$

$$[A_t] = \frac{1}{n_t}\begin{bmatrix} 1 & 0 & -1 \\ -1 & 1 & 0 \\ 0 & -1 & 1 \end{bmatrix} \tag{3.12}$$

$$[B_t] = \begin{bmatrix} Z_{ta} & 0 & 0 \\ 0 & Z_{tb} & 0 \\ 0 & 0 & Z_{tc} \end{bmatrix}. \tag{3.13}$$

Several electrical characteristics of a distribution transformer are required to develop the model. These parameters are significant especially to observe the operational differences between the conventional transformers and the HTS transformers. Those parameters are voltage ratings at the high voltage and low voltage sides, capacity rating of the transformers in kVA, impedance (*Z*), resistance (*R*) and reactance (*X*) in ohms, and load loss at rated load in Watt. The parameters will be used to calculate the generalized matrices for the modelling of the transformers.

3.3 Modelling of overhead line and underground cable

Power distribution lines that provide electricity supply to customers are either in the overhead structures or underground installations (Short, 2004). The overhead distribution circuits are physically accessible and their reliability can be influenced by factors such as trees, animals, weather and many others. Meanwhile, the underground distribution segments can be directly buried or in the trench which are not easily accessible but are better protected.

The line models are also generalized for the connection with other series components of a distribution network (Ciric *et al.*, 2003; Kersting, 2006; Kersting & Phillips, 1995). The matrix equations are basically the same as equations (3.5), (3.6), and (3.7). The

voltages and currents in terms of the types of connection are also similar as explained in section 3.2 (Kersting, 2002). The major parameters for modelling of lines segments will be the series impedance and shunt admittance. The accurate measurements are significant prior to carrying out the analysis of a distribution feeder. The actual phasing of each conductor needs to be clarified and the correct spacing between each conductor needs to be confirmed.

Several factors must be taken into the measurements for the series impedance (Kersting, 2002). These factors are the resistance of each conductor and the magnetic fields, *i.e.*, self inductive reactance and mutual inductive reactance which surrounding each conductor. The self and mutual inductive reactances are functions of total magnetic fields surround a conductor. Figure 3.3 shows the magnetic flux lines produced by currents flowing in the conductors. Two assumptions are made, *i.e.*, the currents are flowing out and the sum of the currents is zero.

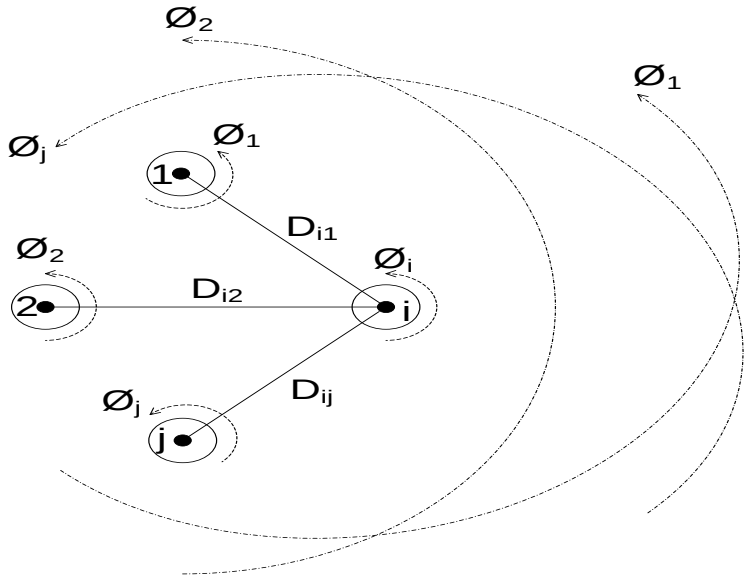

Figure 3.3: Magnetic fields on live conductors

The total flux for conductor i is

$$\lambda_i = 2\cdot 10^{-7}\cdot\left(I_1\cdot In\frac{1}{D_{i1}} + I_2\cdot In\frac{1}{D_{i2}} + ..I_i\cdot In\frac{1}{GMR_i} + ..I_j\cdot In\frac{1}{D_{ij}}\right) \tag{3.14}$$

where D_{ij} is the distance between conductor i and conductor j and GMR_i is the Geometric Mean Radius of conductor i. We then have the self inductance as

$$L_{ii} = \frac{\lambda_{ii}}{I_i} = 2\cdot 10^{-7}\cdot In\frac{1}{GMR_i} \tag{3.15}$$

and mutual inductance as

$$L_{ij} = \frac{\lambda_{ij}}{I_j} = 2\cdot 10^{-7}\cdot In\frac{1}{D_{ij}}. \tag{3.16}$$

For a transposed line in which each phase occupies the same physical position on the structure for one-third of the length of the line and balanced line in which each phase is equally loaded, the self and mutual impedances can be combined into one phase inductance as

$$L_i = 2\cdot 10^{-7}\cdot In\frac{\sqrt[3]{D_{ab}\cdot D_{bc}\cdot D_{ca}}}{GMR_i} \tag{3.17}$$

where D_{ab}, D_{bc} and D_{ca} are the distances between phases a and b, b and c and c and a, respectively.

Therefore, the phase impedance for each phase of a transposed line can be determined as

$$\bar{z}_i = r_i + j\omega L_i = r_i + j2\pi f\cdot 2\cdot 10^{-7}\cdot In\frac{\sqrt[3]{D_{ab}\cdot D_{bc}\cdot D_{ca}}}{GMR_i} \tag{3.18}$$

where r_i is the resistance of conductor i and f is the system frequency.

Meanwhile, the untransposed distribution network comprises of single-phase, two-phase and three-phase lines to supply electricity for unbalanced loads. The self and mutual impedance for the line can then be determined. We have the self impedance as

$$\bar{z}_{ii} = r_i + j\omega L_{ii} = r_i + j2\pi f \cdot 2 \cdot 10^{-7} \cdot In\frac{1}{GMR_i} \tag{3.19}$$

and mutual impedance as

$$\bar{z}_{ij} = j\omega L_{ij} = j2\pi f \cdot 2 \cdot 10^{-7} \cdot In\frac{1}{D_{ij}}. \tag{3.20}$$

In 1926, John Carson developed a set of equations to calculate the self and mutual impedances of power lines which took ground as the return path of the currents (Carson, 1926; Kersting, 2002). The equations utilize conductor images. Every conductor above ground has an image conductor with the same distance below ground as shown in Figure 3.4.

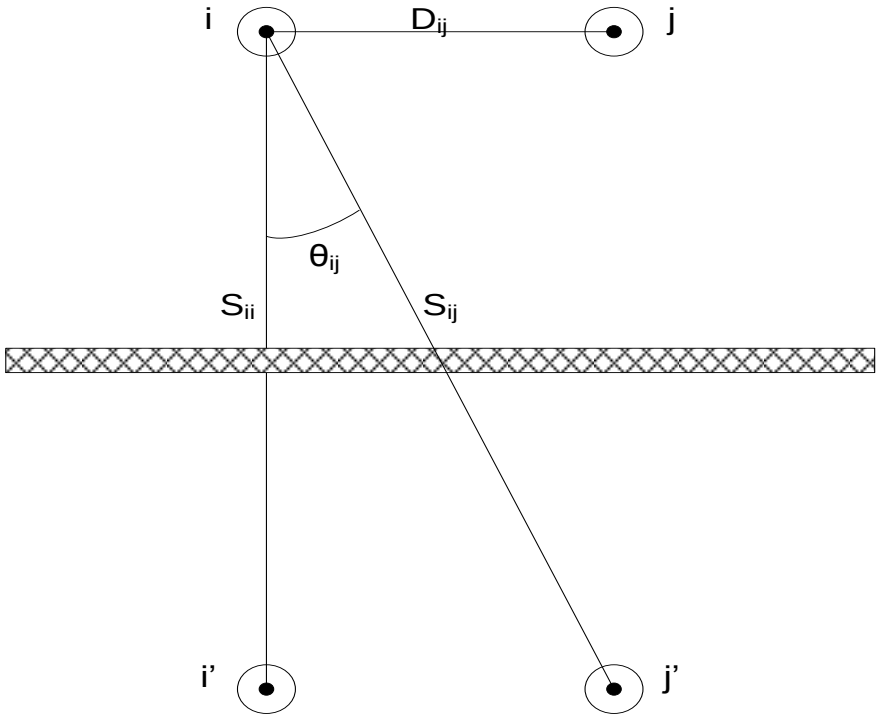

Figure 3.4: Conductors and their images

The original Carson's equations for self and mutual impedances are

$$\hat{z}_{ii} = r_i + 4\omega P_{ii} G + j\left(X_i + 2\omega G \cdot In\frac{S_{ii}}{RD_i} + 4\omega Q_{ii} G \right) \tag{3.21}$$

$$\hat{z}_{ij} = 4\omega P_{ij} G + j\left(2\omega G \cdot In\frac{S_{ij}}{D_{ij}} + 4\omega Q_{ij} G \right) \tag{3.22}$$

and they are further defined by

$$X_i = 2\omega G \cdot In\frac{RD_i}{GMR_i} \tag{3.23}$$

$$P_{ij} = \frac{\pi}{8} - \frac{1}{3\sqrt{2}} k_{ij} \cos(\theta_{ij}) + \frac{k_{ij}^2}{16}\cos(2\theta_{ij}) \cdot \left(0.6728 + In\frac{2}{k_{ij}} \right) \tag{3.24}$$

$$Q_{ij} = -0.0386 + \frac{1}{2} \cdot In\frac{2}{k_{ij}} + \frac{1}{3\sqrt{2}} k_{ij} \cos(\theta_{ij}) \tag{3.25}$$

$$k_{ij} = 8.565x10^{-4} \cdot S_{ij} \cdot \sqrt{\frac{f}{\rho}} \tag{3.26}$$

where $\hat{z}_{ii}$ is the self impedance of conductor i, $\hat{z}_{ij}$ is the mutual impedance between conductor i and j, r_i is the resistance of conductance i, $\omega = 2\pi f$ is the system angular frequency, $G = 0.1 \times 10^{-3}$ ohm/km, RD_i is the radius of conductor i, GMR_i is the Geometric Mean Radius of conductor i, f is the system frequency, ρ is the resistivity of earth, D_{ij} is the distance between conductors i and j, S_{ij} is the distance between conductor i and image j, and θ_{ij} is the angle between a pair of lines drawn from conductor i to its own image and to the image of conductor j.

At this stage, several unknown values have been identified. They are resistance of the dirt, GMR of dirt and distances from conductors to dirt. Carson's equations have made

two assumptions, *i.e.*, the earth has a constant resistivity and it is also an infinite, uniform solid with a flat uniform upper surface. The Carson's equations were modified to solve the problem regarding the identified unknown values (Ciric, Ochoa, & Padilha-Feltrin, 2004; Kersting, 2002, 2004). Approximations are made in deriving the modified equations and therefore, we have the self and mutual impedances of

$$\hat{z}_{ii} = r_i + \pi^2 fG + j4\pi fG\left(In\frac{1}{GMR_i} + 7.6786 + \frac{1}{2}In\frac{\rho}{f} \right) \tag{3.27}$$

$$\hat{z}_{ij} = \pi^2 fG + j4\pi fG\left(In\frac{1}{D_{ij}} + 7.6786 + \frac{1}{2}In\frac{\rho}{f} \right) \tag{3.28}$$

where f is the system frequency, ρ is the resistivity of earth, G = 0.1609344×10^{-3} ohm/mile, r_i is the resistance of conductor i, GMR_i is the Geometric Mean Radius of conductor i and D_{ij} is the distance between conductor i and j.

3.3.1 Overhead line

The modified Carson's equations are used to compute the primitive self and mutual impedances of overhead lines (Ciric, Ochoa *et al.*, 2004; Kersting, 2004). Figure 3.5 shows a typical bare overhead line structure where D_{ab}, D_{ac} and D_{bc} are the distances between phases and D_{an}, D_{bn} and D_{cn} are the distances between the neutral and the three phases. The distance between the phases or the neutral and the ground is labelled as D_{ng}.

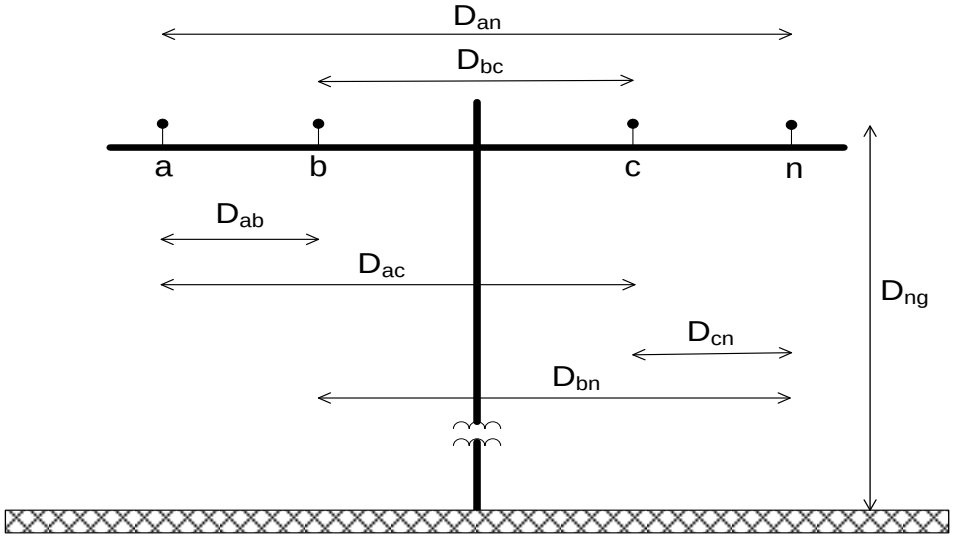

Figure 3.5: Typical three phase overhead line structure

The modified Carson's equations are used to compute the primitive self and mutual impedances of overhead lines. The four-wire grounded wye overhead lines will result in a 4×4 primitive impedance matrix. However, the matrix can be partitioned into

$$\left[\hat{z}_{primitive}\right]=\begin{bmatrix}\left[\hat{z}_{ij}\right] & \left[\hat{z}_{in}\right]\\ \left[\hat{z}_{nj}\right] & \left[\hat{z}_{nn}\right]\end{bmatrix}. \tag{3.29}$$

For the phase frame analytical method, the primitive impedance matrix needs to be converted to a 3×3 phase impedance matrix for connection with other components. Kron reduction method can be applied to achieve the required matrix size (Kersting, 2004; Makram *et al.*, 1987). Applying KVL, we get

$$\begin{bmatrix}V_{ag}\\ V_{bg}\\ V_{cg}\\ V_{ng}\end{bmatrix}_{input}=\begin{bmatrix}V_{ag}\\ V_{bg}\\ V_{cg}\\ V_{ng}\end{bmatrix}_{output}+\begin{bmatrix}\hat{z}_{aa} & \hat{z}_{ab} & \hat{z}_{ac} & \hat{z}_{an}\\ \hat{z}_{ba} & \hat{z}_{bb} & \hat{z}_{bc} & \hat{z}_{bn}\\ \hat{z}_{ca} & \hat{z}_{cb} & \hat{z}_{cc} & \hat{z}_{cn}\\ \hat{z}_{na} & \hat{z}_{nb} & \hat{z}_{nc} & \hat{z}_{nn}\end{bmatrix}.\begin{bmatrix}I_a\\ I_b\\ I_c\\ I_n\end{bmatrix} \tag{3.30}$$

or, in partition form as

$$\begin{bmatrix}\left[V_{abc}\right]\\ \left[V_{ng}\right]\end{bmatrix}_{in}=\begin{bmatrix}\left[V_{abc}\right]\\ \left[V_{ng}\right]\end{bmatrix}_{out}+\begin{bmatrix}\left[\hat{z}_{ij}\right] & \left[\hat{z}_{in}\right]\\ \left[\hat{z}_{nj}\right] & \left[\hat{z}_{nn}\right]\end{bmatrix}.\begin{bmatrix}\left[I_{abc}\right]\\ \left[I_n\right]\end{bmatrix}. \tag{3.31}$$

Since the neutrals are grounded, V_{ng} values will be zero. Solving the equation will provide the phase impedance matrix as

$$[z_{abc}] = [\hat{z}_{ij}] - [\hat{z}_{in}] \cdot [\hat{z}_{nn}]^{-1} \cdot [\hat{z}_{nj}]. \tag{3.32}$$

Hence, the final phase impedance matrix takes the form

$$[z_{abc}] = \begin{bmatrix} z_{aa} & z_{ab} & z_{ac} \\ z_{ba} & z_{bb} & z_{bc} \\ z_{ca} & z_{cb} & z_{cc} \end{bmatrix}. \tag{3.33}$$

On the other hand, the shunt admittance calculation will include the conductance and capacitive susceptance of the line. However, the conductance is normally very small and ignored (Kersting, 2002). The voltage drop between two conductors (i and j) as a result of all the surround charged conductors is

$$V_{ij} = \frac{1}{2\pi\varepsilon} \sum_{n=1}^{N} q_n In \frac{D_{nj}}{D_{ni}} \tag{3.34}$$

where $\varepsilon = \varepsilon_o \varepsilon_r$ is the permittivity of the medium, ε_o is the permittivity of free space, ε_r is the relative permittivity of the medium, q_n is the charge density on conductor n, D_{ni} is the distance between conductor n and conductor i, D_{nj} is the distance between conductor n and conductor j, and RD_n is the radius of conductor n.

The method of conductors and their images applied in Carson's equations as per Figure 3.4 is also employed in the calculation of the shunt capacitance of overhead lines. Assuming the charge density for the image conductors to be zero, we get

$$V_{ii} = \frac{1}{2\pi\varepsilon} \left(q_i In \frac{S_{ii}}{RD_i} - q_i In \frac{RD_i}{S_{ii}} + q_j In \frac{S_{ij}}{D_{ij}} - q_j In \frac{D_{ij}}{S_{ij}} \right) \tag{3.35}$$

$$V_{ii} = \frac{1}{2\pi\varepsilon}\left(2q_i In\frac{S_{ii}}{RD_i} + 2q_j In\frac{S_{ij}}{D_{ij}}\right). \tag{3.36}$$

where S_{ii} is the distance from conductor i to its image i', S_{ij} is the distance from conductor i to the image of conductor j, D_{ij} is the distance from conductor i to conductor j, and RD_i is the radius of conductor i.

The voltage drop between conductor i and the ground will be one-half that of between conductor i and its image as given by

$$V_{ig} = \frac{1}{2\pi\varepsilon}\left(q_i In\frac{S_{ii}}{RD_i} + q_j In\frac{S_{ij}}{D_{ij}}\right) \tag{3.37}$$

$$V_{ig} = \hat{P}_{ii}\cdot q_i + \hat{P}_{ij}\cdot q_j . \tag{3.38}$$

The self and mutual potential coefficients are then acquired as

$$\hat{P}_{ii} = \frac{1}{2\pi\varepsilon} q_i In\frac{S_{ii}}{RD_i} \tag{3.39}$$

$$\hat{P}_{ij} = \frac{1}{2\pi\varepsilon} q_j In\frac{S_{ij}}{D_{ij}} \tag{3.40}$$

where ε is the permittivity of the medium, q_i and q_j are the charge densities on conductor i and j respectively, S_{ii} and S_{ij} are distance from conductor i to its own image and the image of conductor j respectively, RD_i is the radius of conductor i, and D_{ij} is the distance between conductor i and j.

The primitive potential coefficient matrix in partition form is given by

$$\left[\hat{p}_{primitive}\right] = \begin{bmatrix} \hat{P}_{ij} & \hat{P}_{in} \\ \hat{P}_{nj} & \hat{P}_{nn} \end{bmatrix}. \tag{3.41}$$

Again, since the neutral is grounded, the matrix can be reduced to acquire the 3×3 phase potential coefficient matrix by using the Kron reduction method

$$[P_{abc}] = [\hat{P}_{ij}] - [\hat{P}_{in}] \cdot [\hat{P}_{nn}]^{-1} \cdot [\hat{P}_{nj}]. \tag{3.42}$$

The capacitance matrix is the inverse of the potential coefficient matrix and is given by

$$[C_{abc}] = [P_{abc}]^{-1}. \tag{3.43}$$

And, the phase shunt admittance matrix can be presented as

$$[y_{abc}] = 0 + j\omega[C_{abc}]. \tag{3.44}$$

3.3.2 Underground cable

The research was focusing on the tape screened type for the underground cables which are very popular and common at the moment. The cable consists of a phase conductor covered by a semiconducting layer which is bonded to the insulation. The insulating material is covered by another semiconducting layer. The copper tape screen is applied helically around the second semiconducting layer. The final layer is the insulating jacket which encircles the tape screen (Short, 2004).

The modified Carson's equations can also be used to compute the primitive self and mutual impedances of the phase conductor and the tape screen for the underground cables (Ciric, Ochoa *et al.*, 2004; Kersting, 2002, 2004). The resistance and the Geometric Mean Radius of the phase conductor can be acquired from a standard table of conductor data (Short, 2004). The resistance of the tape screen is given by

$$r_t = 7.9385x10^8 \frac{\rho}{d_t \cdot T} \tag{3.45}$$

where ρ is the resistivity of the tape, d_t is the outer diameter of the tape screen, and T is the thickness of the copper tape. The GMR of the tape screen is the radius of a circle passing through the middle of the screen and is given by

$$GMR_t = \frac{d_t - \frac{T}{1000}}{24}. \tag{3.46}$$

The spacing, D_{ij}, between the tape screen and its own phase conductor is defined as the radius to the midpoint of the screen. Meanwhile, the spacing between the tape screen and an adjacent tape screen is defined as center to center distance of the phase conductors. Finally, the spacing between the tape screen and an adjacent phase conductor is defined as center to center distance between phase conductors.

Since the tape screens for all the phases touch each other and become common neutral, the three-wire underground cables will result in a 4×4 primitive impedance matrix. However, as for the overhead lines, the matrix can also be partitioned as

$$\left[\hat{z}_{primitive}\right] = \begin{bmatrix} \left[\hat{z}_{ij}\right] & \left[\hat{z}_{in}\right] \\ \left[\hat{z}_{nj}\right] & \left[\hat{z}_{nn}\right] \end{bmatrix}. \tag{3.47}$$

For the phase frame analytical method, the primitive impedance matrix needs to be reduced to a 3×3 phase impedance matrix for connection with other components. Figure 3.6 shows a three-core tape-screen underground cable.

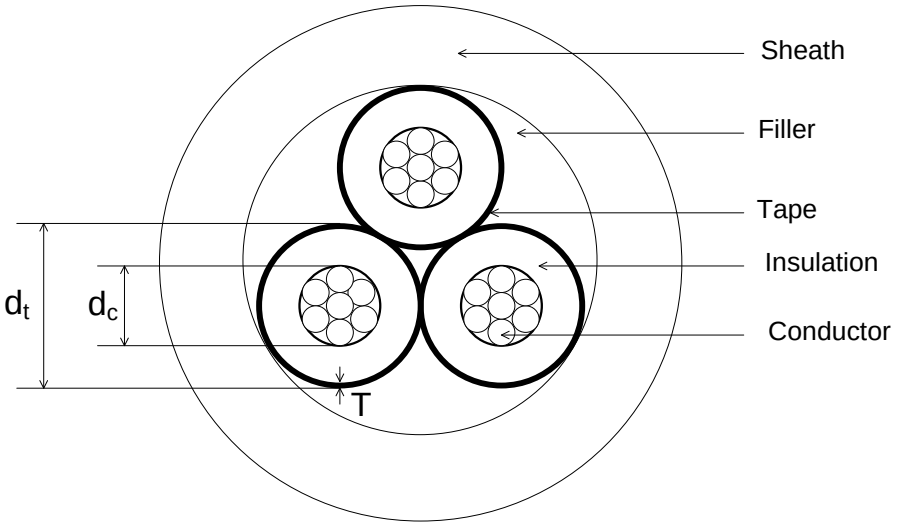

Figure 3.6: Three core tape screen cable

The tape screen is grounded so that it has the same potential at any position. Because of the screening, the electric field is assumed to be created by the charge of the phase conductor which will be confined to the surrounding tape screen. The general voltage drop equation can be applied to calculate the capacitance between the phase conductor and the tape screen. Since the surrounding tape screen has the same potential, it is only necessary to determine the potential different between phase conductor, *i*, and tape screen, *t* by

$$V_{it} = \frac{q_i}{2\pi\varepsilon}\left(In\frac{R_{it}}{RD_i}\right) \tag{3.48}$$

where R_{it} is the spacing between the centre of conductor and the centre of tape screen and RD_i is the radius of conductor *i*.

The capacitance from phase conductor to ground for a tape screened cable is given by

$$C_{it} = \frac{q_i}{V_{it}} = \frac{2\pi\varepsilon}{In\frac{R_{it}}{RD_i}} \tag{3.49}$$

where ε is the permittivity of the insulating material. Therefore, the phase shunt admittance matrix can be presented as

$$[y_{abc}] = 0 + j\omega[C_{abc}]. \tag{3.50}$$

3.3.3 Generalized matrices

Figure 3.7 shows the three phase distribution overhead and underground line model. The generalized matrices for the line are developed from the model of the phase impedance matrices and the phase admittance matrices deliberated earlier (Ciric, Ochoa *et al.*, 2004; Kersting, 2002, 2004).

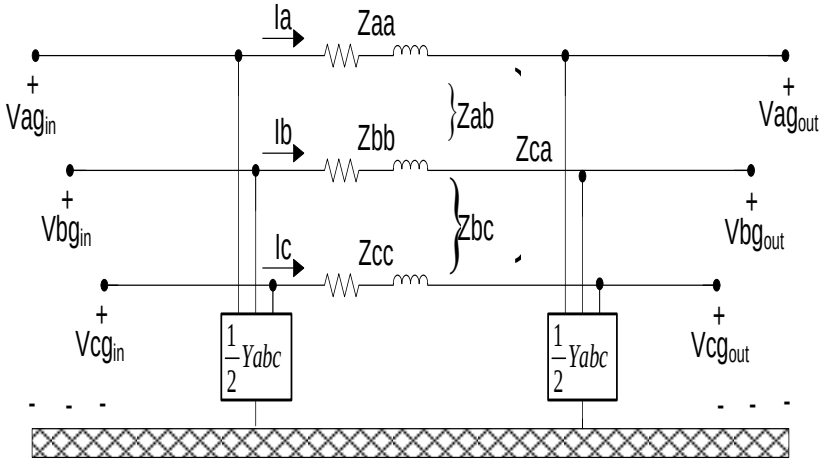

Figure 3.7: Three phase distribution line segment

Applying KCL and KVL to the line segment with reference to Figure 3.7, the generalized matrix equations can be derived as shown in Appendix B2 (Kersting, 2002). As a result, we get the condensed equations for the generalized matrices of the line segments as

$$[a_l] = [U] + \frac{1}{2}[z_{abc}] \cdot [y_{abc}] \tag{3.51}$$

$$[b_l] = [z_{abc}] \tag{3.52}$$

$$[c_l] = [y_{abc}] + \frac{1}{4}[y_{abc}] \cdot [z_{abc}] \cdot [y_{abc}] \tag{3.53}$$

$$[d_l] = [U] + \frac{1}{2}[y_{abc}] \cdot [z_{abc}] \tag{3.54}$$

$$[A_l] = [a]^{-1} \tag{3.55}$$

$$[B_l] = [a]^{-1} \cdot [b]. \tag{3.56}$$

The critical steps in the analysis are to determine the actual phasing of the lines and the correct spacing between conductors. Several parameters are significant in the calculation for the modelling of overhead lines and underground cables. They are voltage rating, type of insulation, conductor size, phase connection, spacing between conductors (including neutral conductor), distances between conductors and ground level, Geometric Mean Radius of the conductors, diameter of the conductors and resistance of the conductors. These parameters are used to calculate the generalized matrices for the modelling of the line segments.

The model applies no approximations, *i.e.*, both the phase impedance matrix and the shunt admittance matrix are taken into account in the calculation. This is important especially for long, rural and lightly loaded overhead lines and for most of underground cables. However, in many cases, the shunt admittance is very small and can be neglected in the computation with very little error (Kersting, 2002). Neglecting the shunt admittance matrix will result in the following generalised matrices

$$[a]=[U] \tag{3.57}$$

$$[b]=[z_{abc}] \tag{3.58}$$

$$[c]=[0] \tag{3.59}$$

$$[d]=[U] \tag{3.60}$$

$$[A]=[U] \tag{3.61}$$

$$[B]=[z_{abc}]. \tag{3.62}$$

3.4 Network modelling

A simulation was carried out on a sample distribution feeder. The source voltages were balanced three-phase 11 kV line-to-line. The system involved a short three-wire delta 11 kV tape screened underground cable and four four-wire wye 415 V line-to-line overhead lines with the distribution transformer in-between. The network is shown in Figure 3.8.

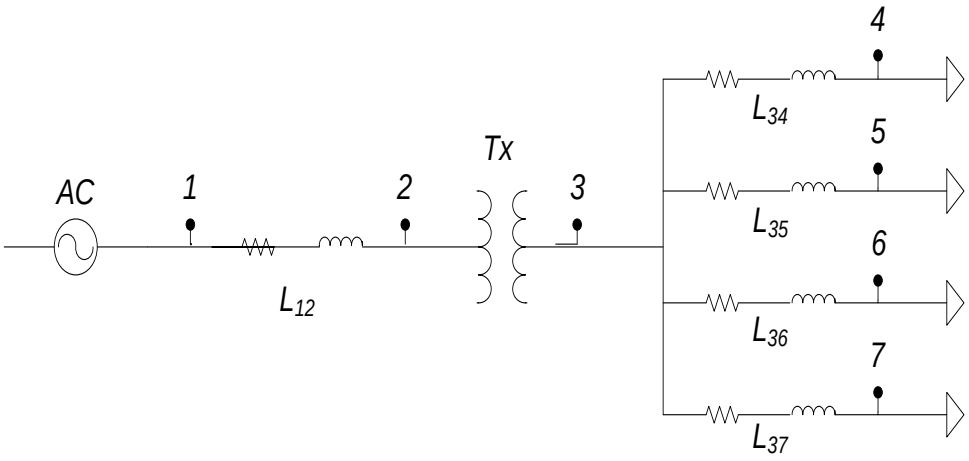

Figure 3.8: Network of a distribution feeder for the simulation

Conventional and HTS distribution transformers were employed in the network study. The electrical characteristics for a typical conventional transformer were based on those used in distribution system by an existing utility whose details are not to be identified. Meanwhile, the technical information on the HTS transformer was based on a preliminary baseline design (Abdul Rahman, Lie, & Prasad, 2010; Kalsi, 2008). The design parameters, as compared to those of a conventional transformer, are shown in Table 3.1.

Table 3.1: Transformers design parameters

Parameters	**Transformer Type**	
	HTS	***Conventional***
Rating (kVA)	1000	1000
Primary Voltage (kV)	11	11
Secondary Voltage (kV)	0.415	0.415
Frequency (Hz)	50	50
Primary Connection	Delta	Delta
Secondary Connection	Wye	Wye
HV Rated Current (A)	30	52.5
LV Rated Current (A)	1390	1333
HV Winding (no. of turns)	1098	739
LV Winding (no. of turns)	24	16
Percent Impedance (%)	5	5

The underground cable was a 300 mm^2 three-core tape-screened Cross-Linked Polyethylene (XLPE) cable and the overhead line structure used a 500 kcmil 19 strands All Aluminium Conductors (AAC) for both the phase and neutral conductors. Each line was short and assumed to be only 0.40 km for the underground cable and 0.10 km for

the overhead lines. Further details on the power equipment and network parameters for the simulation would be provided with the relevant analyses in the next three chapters.

CHAPTER 4

POWER FLOW ANALYSIS

The analysis on distribution power network can be distinguished from that of transmission for its unbalanced loading characteristic (Kersting & Phillips, 1992; Makram & Girgis, 1988). The main features for the evaluation are the unequal single-phase loads and the non-equilateral conductor. The conventional power flow and short circuit programs which are employed in the transmission network analysis would not be sufficient because they are intended to modeling and analysis of balanced three-phase systems. The three-phase transmission network is assumed to be balance and thus it can be represented by a single phase equivalent circuit in the model as well as in the analysis. However, it will not be adequate for the modeling and analysis of a distribution system. A distribution system is inherently imbalance and therefore, three-phase models of all the network components must be carried out in the investigation. Furthermore, the information requirements for the distribution system models are greater and more extensive (Kersting, 2002).

Instead, the three-phase modelling for major power components must be applied for the distribution network assessment. In the analysis, the distribution feeder will have to be mapped with the required information such as location, distance, rating and connection. Furthermore, the electrical characteristics of all the major components will also have to be acquired for the network evaluation.

4.1 Investigation setup

Modelling of HTS transformer can be different from that of conventional transformer and depends on the type of analysis to be carried out. Differences in material properties applied and design configurations employed will lead to variations in computational approaches. Initial electrical characteristics presented in Chapter 3 can be utilized to perform a power flow analysis (Ciric *et al.*, 2003; Ciric, Ochoa *et al.*, 2004; Kersting, 2002; Kersting & Dugan, 2006).

There is no existing modelling software found to be applied for the analysis on the application of HTS transformer in power distribution network. The computation in the study will be carried out according to the theoretical framework explained in chapter 3 and also under the analysis technique which will be presented in this chapter. Computational programs such as Matrix Laboratory (MATLAB) and Microsoft EXCEL will be employed for ease of calculation.

4.1.1 Analysis path

The modelling will be carried out on a three phase distribution feeder explained briefly in section 3.4 of chapter 3. The technical information on the HTS transformer will be

based on a preliminary baseline design (Kalsi, 2008). The analysis in this chapter will be on the feeder under normal steady-state operating condition for power flow and losses investigation. The study on the HTS transformer will be compared with that of a conventional transformer. An analysis from this research work on a different circuit configuration was presented previously (Abdul Rahman *et al.*, 2010). The calculation should provide better understanding of the operation of the HTS transformer.

Consequently, it is important to develop an understanding of the fundamental HTS transformer design issues that can provide guidance for developing practical devices of interest to the electric utility industry. The parameters of the HTS transformer need to be validated before any attempt to carry out to model the behaviour of a distribution network under a range of conditions. The predicted performance level of HTS transformers can then be verified through network modelling and analysis. The ultimate purpose is to furnish electric utilities precise information as to which HTS transformers work under various applications with greater technical efficiency and proven reliability.

4.1.2 Circuit analysis

The simulation was carried out on a distribution feeder. The source voltages were balanced three-phase 11 kV line-to-line. The system involved a short three-wire delta 11 kV tape screened underground cable and four four-wire wye 415 V line-to-line overhead lines with the transformer in-between. The network is shown in Figure 4.1 with the determined voltage nodes, current segments and load points.

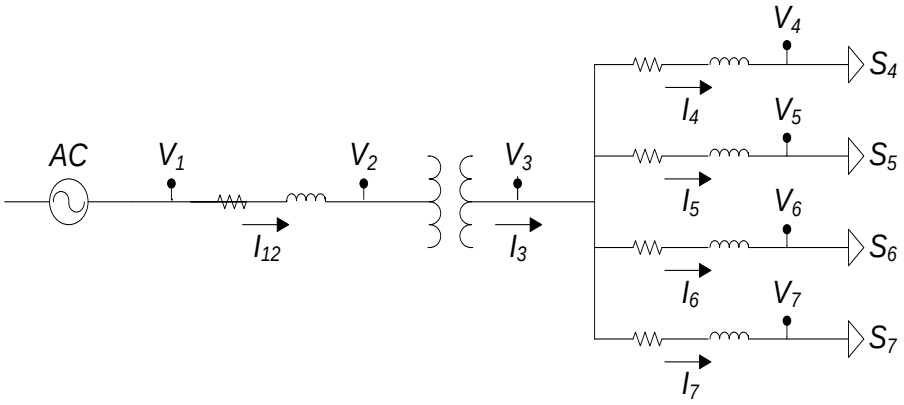

Figure 4.1: Network configurations for the analysis

The conventional and HTS distribution transformers were employed in the network study. The technical data on the HTS transformer were based on a preliminary baseline design the NZHTS transformer project group lead by Industrial Research Limited is working on (Kalsi, 2008). Several additional electrical characteristics for a typical conventional transformer compare with that of the HTS transformer are presented in Table 4.1.

Table 4.1: Electrical characteristics of the transformers

Electrical Characteristics	**Transformer Types**	
	Conventional	**HTS**
kVA Rating, S_{kVA}	1000	1000
Voltage Rating, kV	11/0.415	11/0.415
Load Loss at Rated Load, W_{CU}	7000	1250
Percent Impedance, Z	5	5
Connection	Δ-Y	Δ-Y

The transformer project group has decided to install the first prototype HTS transformer in one of Vector's power distribution network. The installation is expected to be on a

simple network and would not involve many customers. A combination of underground cable and overhead line was included in the analysis so that the model will have the flexibility of using either one or both types of line segment configurations when the actual location has been finalized. Both types of line segment configurations are common in Vector's network system. In addition to the modeling flexibility, the short length of underground cable was included for the evaluation on inrush current.

The underground cable was a 300 mm^2 three-core tape-screened XLPE cable as shown in Figure 3.6 and the overhead line structure was as per 3.5 using 500 kcmil 19-strands AAC for the phase and neutral conductors. Each line was short and assumed to be only 0.40km for the underground cable and 0.10km for the overhead lines. For the analysis, the loads for each phase a, b and c of each low voltage feeders were assumed to be between 10 kVA and 80 kVA at 0.85, 0.90 and 0.95 lagging power factor, respectively, which means the total loads for the circuit were between 120 kVA and 960 kVA. The parameters for the tape-screened underground cable are shown in Figure 4.2.

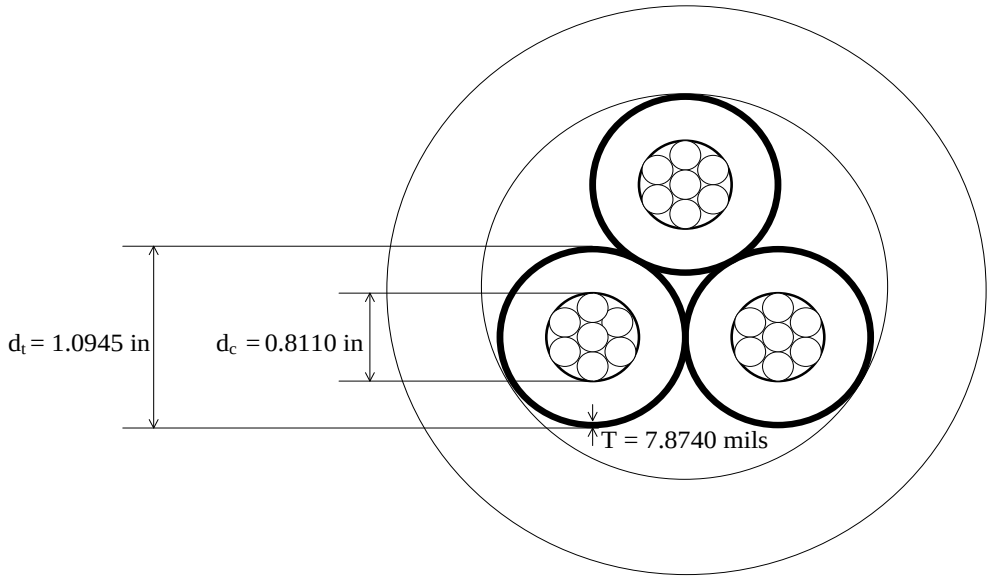

Figure 4.2: Parameters of the underground cable structure

From a cable standard table (Short, 2004), the values for the conductor resistance and Geometric Mean Radius were obtained as

$$r_c = 0.3231\ \Omega/\text{mile}$$

$$GMR_c = 0.0197\ \text{ft.}$$

Meanwhile, the resistivity of the tape was assumed to be 2.3715×10^{-8} Ω-m (Kulkarni & Khaparde, 2004). The copper tape resistance and Geometric Radius were calculated and the values were attained as

$$r_t = 2.1845\ \Omega/\text{mile}$$

$$GMR_t = 0.0453\ \text{ft.}$$

From the parameters, the values for self and mutual impedances were then calculated for the underground cable. Figure 4.3 shows the diagram for the cores and tapes.

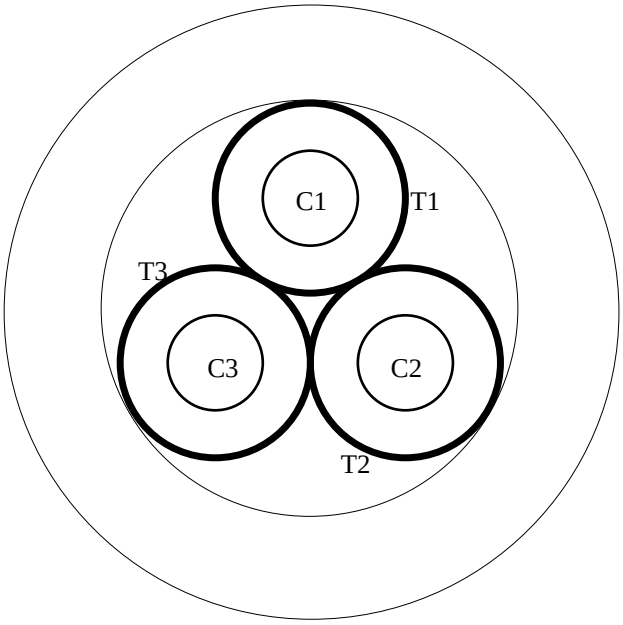

Figure 4.3: Design for the cores and tapes for the calculation

The impedance matrix for the underground cable was obtained from equation (3.47)

$$[\hat{z}_{UG}] = \begin{bmatrix} [\hat{z}_{ij}] & [\hat{z}_{in}] \\ [\hat{z}_{nj}] & [\hat{z}_{nn}] \end{bmatrix}$$

where equations (3.27) and (3.28) provide

$$\hat{z}_{ii} = r_i + \pi^2 fG + j4\pi fG\left(In\frac{1}{GMR_i} + 7.6786 + \frac{1}{2}In\frac{\rho}{f} \right)$$

$$\hat{z}_{ij} = \pi^2 fG + j4\pi fG\left(In\frac{1}{D_{ij}} + 7.6786 + \frac{1}{2}In\frac{\rho}{f} \right)$$

Figure 4.3 produces

$$[\hat{z}_{UG}] = \begin{bmatrix} z_{C1C1} & z_{C1C2} & z_{C1C3} & z_{C1T1} & z_{C1T2} & z_{C1T3} \\ z_{C2C1} & z_{C2C2} & z_{C2C3} & z_{C2T1} & z_{C2T2} & z_{C2T3} \\ z_{C3C1} & z_{C3C2} & z_{C3C3} & z_{C3T1} & z_{C3T2} & z_{C3T3} \\ z_{T1C1} & z_{T1C2} & z_{T1C3} & z_{T1T1} & z_{T1T2} & z_{T1T3} \\ z_{T2C1} & z_{T2C2} & z_{T2C3} & z_{T2T1} & z_{T2T2} & z_{T2T3} \\ z_{T3C1} & z_{T3C2} & z_{T3C3} & z_{T3T1} & z_{T3T2} & z_{T3T3} \end{bmatrix}$$

For the self impedances of the 400 m underground cable, the values were

$Z_{C1C1} = Z_{C2C2} = Z_{C3C3} = 0.1040 + j0.3577\ \Omega$

$Z_{T1T1} = Z_{T2T2} = Z_{T3T3} = 0.5666 + j0.3326\ \Omega.$

On the other hand, for the mutual impedances of the 400 m cable, the values were

$Z_{C1C2} = Z_{C1C3} = Z_{C2C1} = Z_{C2C3}$

$= Z_{C3C1} = Z_{C3C2}$

$= 0.0237 + j0.3117\ \Omega$

$$Z_{T1T2} = Z_{T1T3} = Z_{T2T1} = Z_{T2T3}$$

$$= Z_{T3T1} = Z_{T3T2}$$

$$= 0.5666 + j0.3326\ \Omega$$

$$Z_{C1T1} = \ldots = Z_{C1T3} = Z_{C2T1} = \ldots = Z_{C2T3}$$

$$= Z_{C3T1} = \ldots = Z_{C3T3}$$

$$= Z_{T1C1} = \ldots = Z_{T1C3}$$

$$= Z_{T2C1} = \ldots = Z_{T2C3}$$

$$= Z_{T3C1} = \ldots = Z_{T3C3}$$

$$= 0.0237 + j0.3326\ \Omega.$$

Thus, the primitive impedance matrix of the 400 m underground cable can be presented as

$$[\hat{Z}_{UG}] = \begin{bmatrix} 0.1040+j0.3577 & 0.0237+j0.3117 & 0.0237+j0.3117 & 0.0237+j0.3326 & 0.0237+j0.3326 & 0.0237+j0.3326 \\ 0.0237+j0.3117 & 0.1040+j0.3577 & 0.0237+j0.3117 & 0.0237+j0.3326 & 0.0237+j0.3326 & 0.0237+j0.3326 \\ 0.0237+j0.3117 & 0.0237+j0.3117 & 0.1040+j0.3577 & 0.0237+j0.3326 & 0.0237+j0.3326 & 0.0237+j0.3326 \\ 0.0237+j0.3326 & 0.0237+j0.3326 & 0.0237+j0.3326 & 0.5666+j0.3326 & 0.5666+j0.3326 & 0.5666+j0.3326 \\ 0.0237+j0.3326 & 0.0237+j0.3326 & 0.0237+j0.3326 & 0.5666+j0.3326 & 0.5666+j0.3326 & 0.5666+j0.3326 \\ 0.0237+j0.3326 & 0.0237+j0.3326 & 0.0237+j0.3326 & 0.5666+j0.3326 & 0.5666+j0.3326 & 0.5666+j0.3326 \end{bmatrix} \Omega$$

The parameters for the overhead line structure are shown in Figure 4.4.

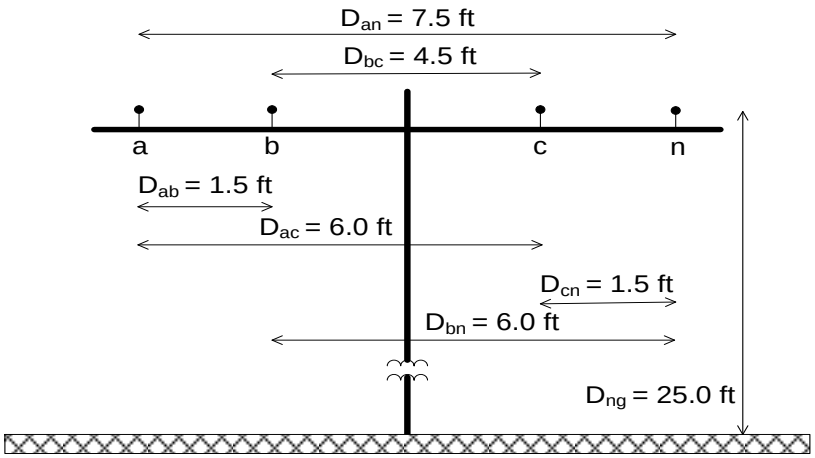

Figure 4.4: Parameters of the overhead line structure

The distances between the phases and the neutral are shown in the figure. Meanwhile, since the wires were the same for each phase and the neutral, the resistance and the Geometric Mean Radius for each wire were also the same (Short, 2004). The values were obtained as

$$r_a = r_b = r_c = r_n = 0.2249\ \Omega/\text{mile}$$

$$GMR_a = GMR_b = GMR_c = GMR_n = 0.0256\ \text{ft.}$$

The impedance matrix for the overhead line was obtained from equation (3.29)

$$\left[\hat{z}_{OH}\right] = \begin{bmatrix} \left[\hat{z}_{ij}\right] & \left[\hat{z}_{in}\right] \\ \left[\hat{z}_{nj}\right] & \left[\hat{z}_{nn}\right] \end{bmatrix}$$

where equations (3.27) and (3.28) provide

$$\hat{z}_{ii} = r_i + \pi^2 fG + j4\pi fG\left(In\frac{1}{GMR_i} + 7.6786 + \frac{1}{2}In\frac{\rho}{f}\right)$$

$$\hat{z}_{ij} = \pi^2 fG + j4\pi fG\left(In\frac{1}{D_{ij}} + 7.6786 + \frac{1}{2}In\frac{\rho}{f}\right)$$

Figure 4.4 produces

$$\left[\hat{z}_{OH}\right]=\begin{bmatrix} z_{aa} & z_{ab} & z_{ac} & z_{an} \\ z_{ba} & z_{bb} & z_{bc} & z_{bn} \\ z_{ca} & z_{cb} & z_{cc} & z_{cn} \\ z_{na} & z_{nb} & z_{nc} & z_{nn} \end{bmatrix}$$

For the self impedances of the 100 m overhead line, the values were

$Z_{aa} = Z_{bb} = Z_{cc} = Z_{nn} = 0.0199 + j0.0875\ \Omega.$

On the other hand, for the mutual impedances of the 100 m line, the values were

$Z_{ab} = Z_{ba} = 0.0059 + j0.0568\ \Omega$

$Z_{ac} = Z_{ca} = 0.0059 + j0.0463\ \Omega$

$Z_{bc} = Z_{cb} = 0.0059 + j0.0485\ \Omega$

$Z_{an} = Z_{na} = 0.0059 + j0.0446\ \Omega$

$Z_{bn} = Z_{nb} = 0.0059 + j0.0463\ \Omega$

$Z_{cn} = Z_{nc} = 0.0059 + j0.0568\ \Omega.$

Thus, the primitive impedance matrix of the 100 m overhead line can be presented as

$$\left[\hat{Z}_{OH}\right]=\begin{bmatrix} 0.0199+j0.0875 & 0.0059+j0.0568 & 0.0059+j0.0463 & 0.0059+j0.0446 \\ 0.0059+j0.0568 & 0.0199+j0.0875 & 0.0059+j0.0485 & 0.0059+j0.0463 \\ 0.0059+j0.0463 & 0.0059+j0.0485 & 0.0199+j0.0875 & 0.0059+j0.0568 \\ 0.0059+j0.0446 & 0.0059+j0.0463 & 0.0059+j0.0568 & 0.0199+j0.0875 \end{bmatrix}\Omega\,.$$

4.1.3 Network parameters

The three main equipment, *i.e.*, transformer, underground cable and overhead line were analysed as described in chapter 3. For the transformer, the first step was to obtain the three-phase impedance in matrix form. From the information provided, the impedance matrix for the conventional transformer was

$$[Z_{t1}] = \begin{bmatrix} 12.0540E-4 + j85.2390E-4 & 0 & 0 \\ 0 & 12.0540E-4 + j85.2390E-4 & 0 \\ 0 & 0 & 12.0540E-4 + j85.2390E-4 \end{bmatrix} \Omega.$$

Meanwhile, the impedance matrix for the HTS transformer was

$$[Z_{t2}] = \begin{bmatrix} 2.1525E-4 + j86.0724E-4 & 0 & 0 \\ 0 & 2.1525E-4 + j86.0724E-4 & 0 \\ 0 & 0 & 2.1525E-4 + j86.0724E-4 \end{bmatrix} \Omega.$$

From the transformer three-phase impedance values, the generalised matrices were obtained. The generalised matrices for the delta-grounded wye step-down conventional transformer were

$$[a_{t1}] = \begin{bmatrix} 0 & -30.5556 & -15.2778 \\ -15.2778 & 0 & -30.5556 \\ -30.5556 & -15.2778 & 0 \end{bmatrix}$$

$$[b_{t1}] = \begin{bmatrix} 0 & -0.0368 - j0.2605 & -0.0184 - j0.1302 \\ -0.0184 - j0.1302 & 0 & -0.0368 - j0.2605 \\ -0.0368 - j0.2605 & -0.0184 - j0.1302 & 0 \end{bmatrix}$$

$$[c_{t1}] = \begin{bmatrix} 0 & 0 & 0 \\ 0 & 0 & 0 \\ 0 & 0 & 0 \end{bmatrix}$$

$$[d_{t1}] = \begin{bmatrix} 0.0218 & -0.0218 & 0 \\ 0 & 0.0218 & -0.0218 \\ -0.0218 & 0 & 0.0218 \end{bmatrix}$$

$$[A_{t1}] = \begin{bmatrix} 0.0218 & 0 & -0.0218 \\ -0.0218 & 0.0218 & 0 \\ 0 & -0.0218 & 0.0218 \end{bmatrix}$$

$$[B_{t1}] = \begin{bmatrix} 0.0012 + j0.0085 & 0 & 0 \\ 0 & 0.0012 + j0.0085 & 0 \\ 0 & 0 & 0.0012 + j0.0085 \end{bmatrix}.$$

On the other hand, the generalised matrices for the HTS transformer were

$$[a_{t2}] = \begin{bmatrix} 0 & -30.5556 & -15.2778 \\ -15.2778 & 0 & -30.5556 \\ -30.5556 & -15.2778 & 0 \end{bmatrix}$$

$$[b_{t2}] = \begin{bmatrix} 0 & -0.0066 - j0.2630 & -0.0033 - j0.1315 \\ -0.0033 - j0.1315 & 0 & -0.0066 - j0.2630 \\ -0.0066 - j0.2630 & -0.0033 - j0.1315 & 0 \end{bmatrix}$$

$$[c_{t2}] = \begin{bmatrix} 0 & 0 & 0 \\ 0 & 0 & 0 \\ 0 & 0 & 0 \end{bmatrix}$$

$$[d_{t2}] = \begin{bmatrix} 0.0218 & -0.0218 & 0 \\ 0 & 0.0218 & -0.0218 \\ -0.0218 & 0 & 0.0218 \end{bmatrix}$$

$$[A_{t2}] = \begin{bmatrix} 0.0218 & 0 & -0.0218 \\ -0.0218 & 0.0218 & 0 \\ 0 & -0.0218 & 0.0218 \end{bmatrix}$$

$$[B_{t2}] = \begin{bmatrix} 0.0002 + j0.0086 & 0 & 0 \\ 0 & 0.0002 + j0.0086 & 0 \\ 0 & 0 & 0.0002 + j0.0086 \end{bmatrix}.$$

In the Chapter 3, it was mentioned that in many cases, the shunt admittance is very small and can be neglected in the computation with very little error (Kersting, 2002). The shunt components were not calculated and they were neglected in the computation. Distribution lines are typically so short that the shunt admittance can be ignored and this was used as a simplifying assumption. The phase impedance matrix for the 400 m underground cable was obtained after applying the Kron reduction method as

$$[Z_{UG}] = \begin{bmatrix} 0.2363 + j0.2522 & 0.1560 + j0.2062 & 0.1560 + j0.2062 \\ 0.1560 + j0.2062 & 0.2363 + j0.2522 & 0.1560 + j0.2062 \\ 0.1560 + j0.2062 & 0.1560 + j0.2062 & 0.2363 + j0.2522 \end{bmatrix} \Omega.$$

Meanwhile, the phase impedance matrix for the 100 m overhead line was acquired by applying the Kron reduction method as

$$[Z_{OH}] = \begin{bmatrix} 0.0190 + j0.0649 & 0.0051 + j0.0333 & 0.0056 + j0.0177 \\ 0.0051 + j0.0333 & 0.0192 + j0.0632 & 0.0057 + j0.0188 \\ 0..0056 + j0.0177 & 0.0057 + j0.0188 & 0.0205 + j0.0511 \end{bmatrix} \Omega.$$

From the phase impedance matrix for the underground cable, the general matrices for the high voltage cable were

$$[a_{UG}] = \begin{bmatrix} 1 & 0 & 0 \\ 0 & 1 & 0 \\ 0 & 0 & 1 \end{bmatrix}$$

$$[b_{UG}] = \begin{bmatrix} 0.2363 + j0.2522 & 0.1560 + j0.2062 & 0.1560 + j0.2062 \\ 0.1560 + j0.2062 & 0.2363 + j0.2522 & 0.1560 + j0.2062 \\ 0.1560 + j0.2062 & 0.1560 + j0.2062 & 0.2363 + j0.2522 \end{bmatrix}$$

$$[c_{UG}] = \begin{bmatrix} 0 & 0 & 0 \\ 0 & 0 & 0 \\ 0 & 0 & 0 \end{bmatrix}$$

$$[d_{UG}] = \begin{bmatrix} 1 & 0 & 0 \\ 0 & 1 & 0 \\ 0 & 0 & 1 \end{bmatrix}$$

$$[A_{UG}] = \begin{bmatrix} 1 & 0 & 0 \\ 0 & 1 & 0 \\ 0 & 0 & 1 \end{bmatrix}$$

$$[B_{UG}] = \begin{bmatrix} 0.2363 + j0.2522 & 0.1560 + j0.2062 & 0.1560 + j0.2062 \\ 0.1560 + j0.2062 & 0.2363 + j0.2522 & 0.1560 + j0.2062 \\ 0.1560 + j0.2062 & 0.1560 + j0.2062 & 0.2363 + j0.2522 \end{bmatrix}.$$

On the other hand, the general matrices for the low voltage line acquired from the phase impedance matrix of the overhead line were

$$[a_{OH}] = \begin{bmatrix} 1 & 0 & 0 \\ 0 & 1 & 0 \\ 0 & 0 & 1 \end{bmatrix}$$

$$[b_{OH}] = \begin{bmatrix} 0.0190 + j0.0649 & 0.0051 + j0.0333 & 0.0056 + j0.0177 \\ 0.0051 + j0.0333 & 0.0192 + j0.0632 & 0.0057 + j0.0188 \\ 0..0056 + j0.0177 & 0.0057 + j0.0188 & 0.0205 + j0.0511 \end{bmatrix}$$

$$[c_{OH}] = \begin{bmatrix} 0 & 0 & 0 \\ 0 & 0 & 0 \\ 0 & 0 & 0 \end{bmatrix}$$

$$[d_{OH}] = \begin{bmatrix} 1 & 0 & 0 \\ 0 & 1 & 0 \\ 0 & 0 & 1 \end{bmatrix}$$

$$[A_{OH}] = \begin{bmatrix} 1 & 0 & 0 \\ 0 & 1 & 0 \\ 0 & 0 & 1 \end{bmatrix}$$

$$[B_{OH}] = \begin{bmatrix} 0.0190 + j0.0649 & 0.0051 + j0.0333 & 0.0056 + j0.0177 \\ 0.0051 + j0.0333 & 0.0192 + j0.0632 & 0.0057 + j0.0188 \\ 0..0056 + j0.0177 & 0.0057 + j0.0188 & 0.0205 + j0.0511 \end{bmatrix}.$$

4.2 Power flow analysis

The power flow analysis was applied to determine the normal steady-state operating condition of the network under study. Various outputs such as voltage magnitudes and angles at all nodes in the network, power flow and power loss in each line segment and total network power input and power losses can be obtained from the analysis (Kersting, 2002, 2003). However, information such as three-phase voltages at the substation and complex power of all the loads and the load models should be made available prior to conducting the analysis.

4.2.1 Analysis technique

Ladder iterative technique was employed for the analysis (Ciric, Padilha-Feltrin, & Ochoa, 2004; Kersting, 2002, 2003). Kirchhoff's Voltage Law (KVL) and Kirchhoff's Current Law (KCL) were utilized to determine the node voltages and the line currents respectively. Nevertheless, the technique has to be adjusted to suit the radial system characteristic and nonlinear feature of the distribution network. The load currents were instead calculated by the conjugate of complex power loads over the node voltages. The forward and backward sweeps or the iterations were to be continued until the difference between the calculated and the specified voltage at the source meet the acceptable tolerance.

For a linear ladder circuit, all the line impedances and load impedances were made available prior to the analysis. The voltage at the source (V_s) was also known. Figure 4.5 presents a linear ladder circuit.

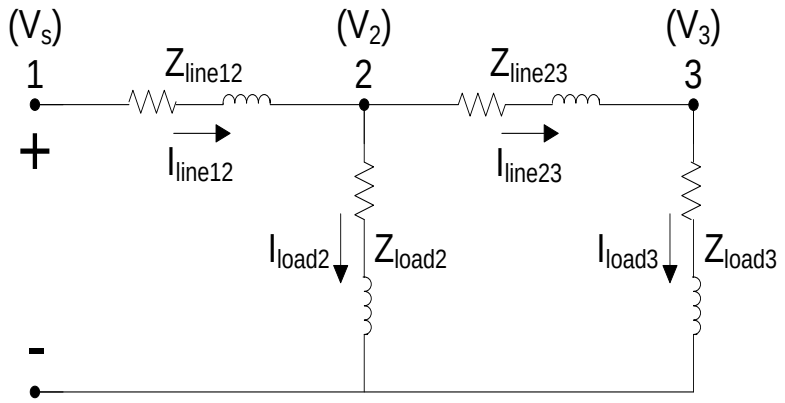

Figure 4.5: Linear ladder circuit

The solution to the circuit can be achieved by assuming the voltage at the most far end node (V_3). The load current can then be determined by

$$I_{load3} = \frac{V_3}{Z_{load3}}. \tag{4.1}$$

Applying KVL, the voltage at node 2 and current at load 2 can be determined by

$$V_2 = V_3 + Z_{line23} \cdot I_{line23} \tag{4.2}$$

$$I_{load2} = \frac{V_2}{Z_{load2}}. \tag{4.3}$$

Applying KCL, the line current 12 can be determined by

$$I_{line12} = I_{line23} + I_{load2}. \tag{4.4}$$

The calculation was continued until the voltage at node 1 (V_1) was computed at the source. The value can be compared to the specified voltage source as

$$Ratio = \frac{V_s}{V_1}. \tag{4.5}$$

For the linear ladder circuit, the line and load currents and the node voltages can be multiplied by the ratio to find the final solution of the circuit. Meanwhile, a nonlinear circuit is a modified linear circuit which replaces all constant load impedances by constant complex power loads. Figure 4.6 presents a nonlinear ladder circuit.

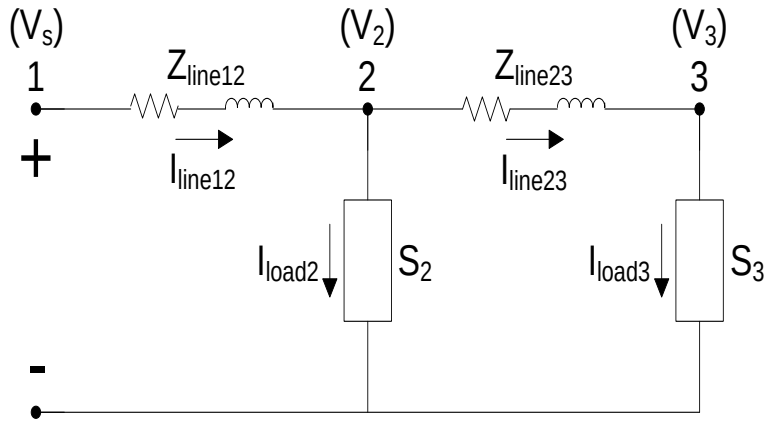

Figure 4.6: Nonlinear ladder circuit

The calculation procedure was still following the same outline except for the computation of load current at each node was given by

$$I_n = \left(\frac{S_n}{V_n} \right)^* . \tag{4.6}$$

The forward sweep calculation would produce a voltage not equal to the source voltage. For the nonlinear circuit, multiplication of current and voltage by the ratio would not provide the solution. The backward sweep calculation was the most direct modification for the ladder circuit computation. The method used the specified source voltage and the line currents from the forward sweep calculation. Applying KVL, the node voltage was given by

$$V_2 = V_s - Z_{line12} \cdot I_{line12} . \tag{4.7}$$

The calculation was repeated for the next line segments until a new voltage was computed for the last node. The second forward sweep can then be started to get a new computed voltage source. The forward and backward sweeps were to be continued until the difference between the calculated and the specified voltage source was within a suitable tolerance.

The analysis on the power network shown in Figure 4.1 was initiated with the load voltages V_4, V_5, V_6 and V_7 were set at the nominal voltage of 240 V. The load for each phase of low voltage feeders was assumed to be between 10 kVA and 80 kVA at 0.85, 0.90 and 0.95 lagging power factor, respectively. For the first iteration, the forward sweep began with the calculation for voltages and currents at node 3, followed by the voltage and current values at node 2 and node 1 using the matrix equations (3.5) and (3.6). The calculated value for V_1 was compared with the nominal source voltage V_S at 6.35 kV. The difference or the error was calculated to determine if the acceptable tolerance of 0.001 was met. If the tolerance was not achieved, the analysis went on with backward sweep. The backward sweep was carried out by calculating the voltage at node 2 by applying the matrix equation (3.7). The calculation continued for node 3 and the feeder nodes 4, 5, 6 and 7. The same calculation procedure was carried out for the second and subsequent iterations.

The unbalanced three-phase distribution network can be divided into series components and shunt components (Kersting, 2002). The series components are transformers, overhead lines, underground cables and voltage regulators. The components are connected in terms of generalized matrices through the input and output voltages and currents as defined in the previously mentioned general equations. Meanwhile, the shunt components are spot loads, distributed loads and capacitor banks. The spot loads and the capacitor banks are placed at nodes while the distributed loads are uniformly

distributed along overhead lines or underground cables. The spot loads are loads which are concentrated at one point or node. Meanwhile, for the distributed load, normally two thirds of the load is connected at a dummy node located at the one quarter point of the line and the remaining one third of the load is connected at the load end of the line segment. All the shunt components can be three-phase, two-phase or single-phase and they can be connected either in wye or delta connection. The spot and distributed loads can be modelled as constant impedance, constant current, constant complex power or a combination of them. Capacitor banks are modelled as constant admittance (Kersting, 2002).

The general matrices were employed in the calculation using the ladder iterative technique. The voltage drops computation for a series component of a node or segment will always produce the same results regardless of whether the component represents a transformer, overhead line, underground cable or voltage regulator. However, in the power flow study, the actual spacing and phasing of overhead lines or underground cables are very important in the calculation for the impedance and admittance. Unbalanced loading which will create unbalanced line currents could provide significant voltage drops due to the mutual coupling. Load imbalance is defined as imbalance in current detected by placement of load on feeder. The imbalance in current creates a neutral point "shift" which can cause voltage imbalance, either over-voltage or under-voltage. The heaviest loaded phase will have the largest voltage drop. However, the largest voltage rise doesn't necessarily happen on the lightest loaded phase.

The segment power loss calculation can be carried out by using two methods (Kersting, 2004; Ochoa *et al.*, 2005). The first method can particularly be applied on the line segments by performing the I^2R operation. The losses at each phases and the neutral can be calculated. The computed values are correct for each line phase, neutral and also the

total losses. The other method which will be applied later is by calculating the difference between the input power and the output power for the segment. The calculation for the power at the respective nodes is as per equation (4.6). This computation would not provide the actual real power loss in each phase. Using the difference between input and output power in each phase, the sum of the phase losses (a, b and c) gives the total losses, and it is not possible to compute the neutral losses. In this procedure, the value of total losses is correct, but the losses in each phase are incorrect.

The real power loss in a device can be computed by using the phase current squared times the phase resistance if the system is balance. Otherwise, the real power losses of a line segment must be computed as the difference (by phase) of the input power in a line segment minus the output power of the line segment. It is possible to have a negative power loss on a phase that is lightly loaded compared to the other two phases. Computing power loss as the phase current squared times the phase resistance does not give the actual real power loss in the phases, because the calculation must also take into account the power losses in the neutral conductor and the "ground" (Kersting, 2004; Ochoa *et al.*, 2005).

4.2.2 Results

Power flow analysis was carried out on the circuit. The first analysis was on the circuit with about 50 percent loading of the transformer capacity. This is a normal power utility practice especially for transformers installed in a parallel configuration. If one of the transformers is out of service, the other transformer should be able to take up the total load. For this analysis, the load on each phases a, b, and c for each feeder is assumed to

be 40 kVA with lagging power factors of 0.85, 0.90 and 0.95, respectively. All the feeders are identical.

After four iterations, the magnitudes of voltage errors were less than the acceptable tolerance of 0.001 per-units. The values of voltages and currents at the respective nodes for both transformers are shown in Table 4.2 and Table 4.3, respectively.

Table 4.2: Voltages at the respective nodes

Node Voltage	**Phase**	**Transformer**	
		Conventional	***HTS***
V_1 (V)	a	6351.00∠0°	6351.00∠0°
	b	6351.00∠-120°	6351.00∠-120°
	c	6351.10∠120°	6351.00∠120°
V_2 (V)	a	6348.60∠0°	6348.60∠0°
	b	6348.70∠-120°	6348.70∠-120°
	c	6348.50∠120°	6348.50∠120°
V_3 (V)	a	235.95∠-31°	236.54∠-31°
	b	236.46∠-151°	237.07∠-151°
	c	237.15∠89°	237.80∠89°
V_4 (V)	a	227.84∠-32°	228.45∠-32°
	b	233.08∠-153°	233.70∠-153°
	c	233.69∠88°	234.35∠88°

Table 4.3: Currents at the respective nodes

Line Current	Phase	Transformer	
		Conventional	***HTS***
I_{12} (A)	a	25.54∠-31°	25.47∠-32°
	b	24.81∠-145°	24.74∠-145°
	c	27.75∠93°	27.68∠93°
I_3 (A)	a	702.28∠-64°	700.40∠-64°
	b	686.48∠-179°	684.66∠-179°
	c	684.59∠69°	682.66∠69°
I_4= I_5= I_6= I_7 (A)	a	175.58∠-64°	175.11∠-64°
	b	171.62∠-179°	171.17∠-179°
	c	171.15∠69°	170.67∠69°

The line-to-neutral voltages at each node were within the acceptable range for the system voltages of 11 kV and 415 V line-to-line voltages. The currents were dependent on the loads and they were within the 450 A for the cable and 461 A for the overhead rating of the line segments (Short, 2004). The results showed that the voltage and current values were very close with less than 1% difference.

The study also looked into the network performance under low load and high load conditions. The low and high loads were considered at 10 kVA and 80 kVA respectively for each phase with the same lagging power factors of 0.85, 0.90 and 0.95. The total loads for the network were 120 kVA for the low load condition and 960 kVA for the high load situation. The resultant voltages for each load condition are presented in Table 4.4, Table 4.5, Table 4.6, and Table 4.7. Small differences for the voltage and current values of both transformers can be observed at low load condition. However, the variations grew larger as the load increased. The voltage drops particularly at V_3 and V_4 should be noted.

Table 4.4: Voltages at the respective nodes under low load condition

Node Voltage	**Phase**	**Transformer**	
		Conventional	***HTS***
V_1 (V)	a	6350.90∠0°	6350.90∠0°
	b	6350.90∠-120°	6350.90∠-120°
	c	6350.90∠120°	6350.90∠120°
V_2 (V)	a	6350.30∠0°	6350.30∠0°
	b	6350.30∠-120°	6350.30∠-120°
	c	6350.30∠120°	6350.30∠120°
V_3 (V)	a	239.05∠-30°	239.19∠-30°
	b	239.17∠-150°	239.32∠-150°
	c	239.33∠90°	239.49∠90°
V_4 (V)	a	237.09∠-30°	237.24∠-30°
	b	238.33∠-151°	238.48∠-151°
	c	238.50∠89°	238.66∠89°

Table 4.5: Currents at the respective nodes under low load condition

Line Current	**Phase**	**Transformer**	
		Conventional	***HTS***
I_{12} (A)	a	6.17∠-29°	6.16∠-29°
	b	6.08∠-143°	6.07∠-143°
	c	6.74∠95°	6.74∠95°
I_3 (A)	a	168.73∠-62°	168.63∠-62°
	b	167.84∠-177°	167.74∠-177°
	c	167.70∠71°	167.59∠71°
I_4= I_5= I_6= I_7 (A)	a	42.18∠-62°	42.16∠-62°
	b	41.96∠-177°	41.93∠-177°
	c	41.93∠71°	41.90∠71°

Table 4.6: Voltages at the respective nodes under high load condition

Node Voltage	**Phase**	**Transformer**	
		Conventional	***HTS***
V_1 (V)	a	6351.60∠0°	6351.60∠0°
	b	6351.90∠-120°	6351.80∠-120°
	c	6352.80∠120°	6352.60∠120°
V_2 (V)	a	6346.60∠0°	6346.60∠0°
	b	6347.20∠-120°	6347.10∠-120°
	c	6347.50∠120°	6347.30∠120°
V_3 (V)	a	231.18∠-32°	232.44∠-32°
	b	232.32∠-152°	233.57∠-152°
	c	233.81∠87°	235.14∠87°
V_4 (V)	a	213.93∠-34°	215.29∠-34°
	b	225.51∠-156°	226.79∠-156°
	c	226.48∠85°	227.87∠85°

Table 4.7: Currents at the respective nodes under high load condition

Line Current	**Phase**	**Transformer**	
		Conventional	***HTS***
I_{12} (A)	a	53.80∠-34°	53.47∠-35°
	b	51.14∠-147°	50.83∠-147°
	c	58.10∠91°	57.76∠91°
I_3 (A)	a	1494.90∠-66°	1485.50∠-66°
	b	1418.90∠-179°	1410.80∠-179°
	c	1412.60∠67°	1404.00∠67°
I_4= I_5= I_6= I_7 (A)	a	374.00∠-66°	371.64∠-66°
	b	354.77∠-179°	352.76∠-179°
	c	353.21∠67°	351.05∠67°

Power loss calculations were also carried out in the analysis. The losses were calculated at each network segment. Figure 4.7, Figure 4.8, and Figure 4.9 show the losses at different load conditions for line segments, transformer segment and total network respectively.

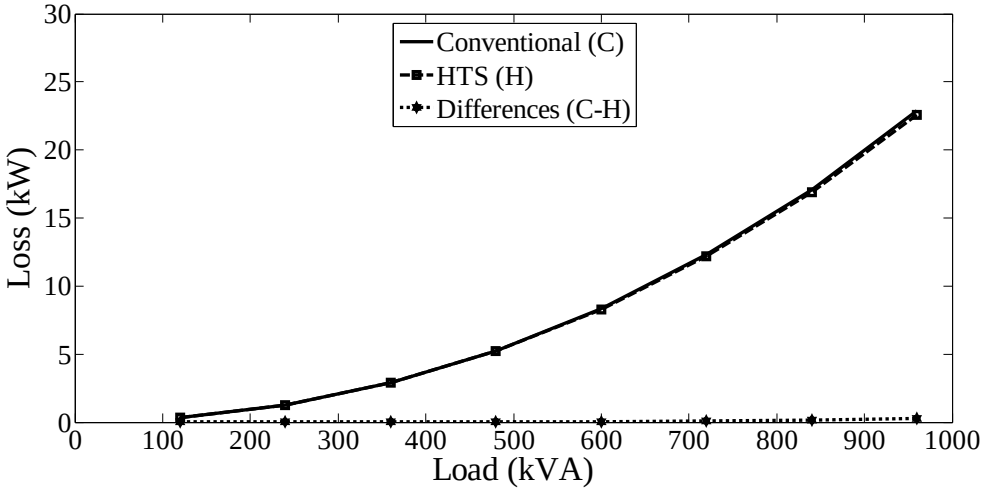

Figure 4.7: Line segments losses under various load conditions

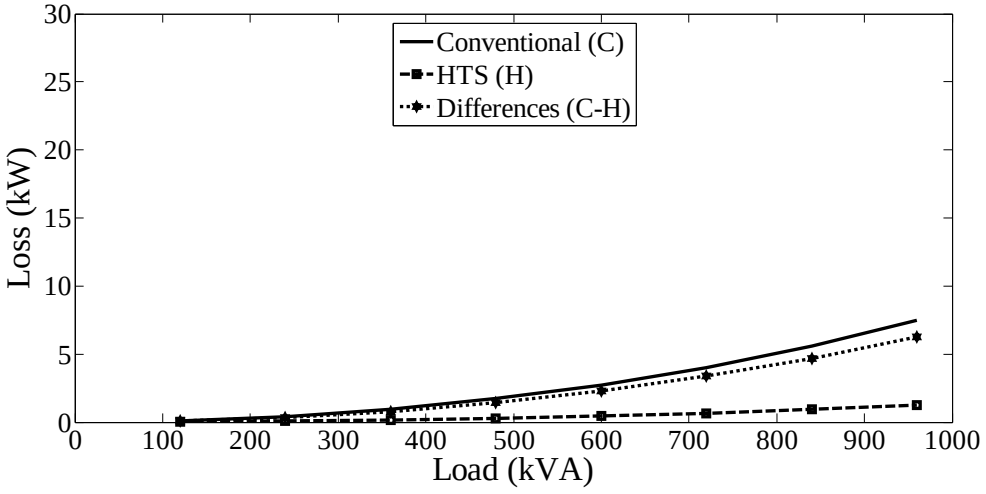

Figure 4.8: Transformer segment losses under various load conditions

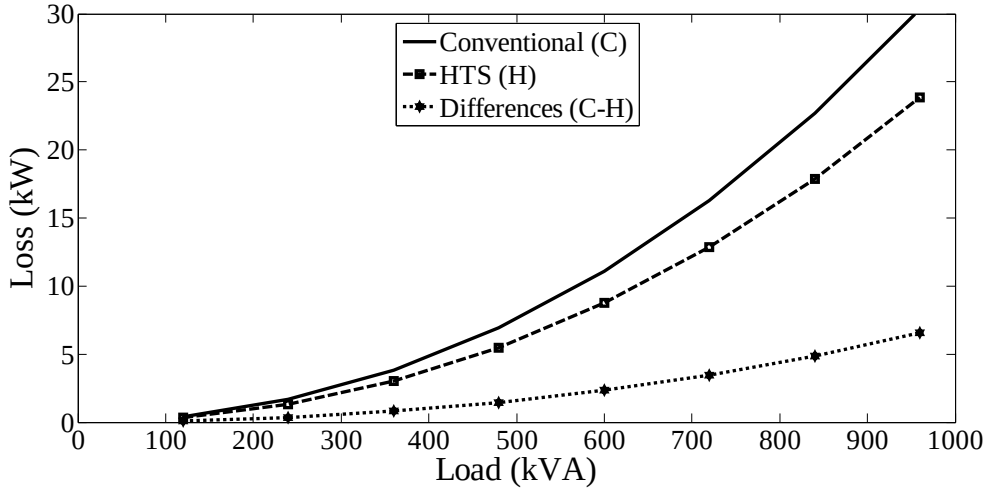

Figure 4.9: Total segment losses under various load conditions

Power losses were calculated for the line segments. The values are the difference between the input power and the output power for the segment. The power loss values for the line segments were the correct values for the segments. However, the losses for each phase of the line segments were not computed (Kersting, 2004; Ochoa *et al.*, 2005). Using both types of transformers would provide very slight differences in the loss values particularly at low and medium load condition. For the transformer segment, the computation was on the power losses of the transformer from the ohmic resistance of the windings. The calculation did not take into account the no-load or core loss of the transformer. The load loss from stray losses such as eddy loss and circulating current loss from the winding was also not taken into consideration. However, the variations between both transformers particularly at high load condition were very significant to indicate the improvement in energy efficiency.

4.3 Discussion

Applying the phase frame calculation method in the network modelling for the power flow computation gave eminently satisfactory results. The three-phase impedance and admittance matrices were very useful for the study. The method of solution appeared to be accurate and efficient. This validated the technique for more advanced and complicated circuit designs.

The load flow and system losses calculations were carried out in section 4.2 on the network with the application of both conventional and HTS transformers. The computation provided the actual losses on the line segments. The two transformers were evaluated on the same power network. Therefore, the minimal differences resulted on the line segments were expected. The reactive impedances for both transformers were nearly the same. However, the real impedance for conventional winding was almost six times that of the HTS winding. The results showed that the differences in power losses between the two transformers relied on the differences between the winding resistances of the transformers. Even though the actual transformer losses would not be available through network modelling, the load loss fraction of the losses can be employed as part of the comparison for the performance of the two transformers. The modeling focused on the losses from the ohmic resistance of the windings. The main idea was to observe the comparison on the usage of superconductor and copper for the transformer windings. The advantage of using HTS transformer can be observed through the reduction of real power requirement, especially on heavy loading networks.

CHAPTER 5

SHORT CIRCUIT AND INRUSH CURRENT ANALYSIS

Analyses on short circuit and inrush currents will require further information on the transformer winding such as number of turns, mean diameter and height (Blume, Camilli, Farnham, & Peterson, 1944; Ciric, Ochoa, Padilla-Feltrin, & Nouri, 2005; Holcomb, 1961; Kersting, 2002; Kersting & Phillips, 1990; Kulkarni & Khaparde, 2004; Specht, 1951). Moreover, differences between the resistance and critical current characteristics of the winding of conventional and HTS transformers will definitely influence the calculations. Additional information on the transformer core such as effective area, operating flux density and saturate flux density will also be necessary.

The next analysis will be on short circuit currents. The short circuit capacity design of a transformer is one of the most significant and challenging criteria. Additional generating capacity and interconnections due to the growth of electrical power demand have contributed to an increase in short circuit capacity of power networks. One of the consequences is that the short circuit current handled by transformers becomes more severe. The short circuit strength of a transformer should be designed to withstand any

fault currents due to external short circuit. Any weakness in the strength may result in a mechanical collapse of windings and deformation of clamping structures. The internal faults initiated by the external short circuits may lead to bushing blowouts, tank bursting, fire hazard, *etc*.

A couple of analyses from this research work on slightly different network configurations were presented (Abdul Rahman, Lie, & Prasad, 2011a, 2012) to determine the fault current values to be experienced by the conventional and HTS transformers when simulated with different types of short circuit conditions. The calculations provided the fault currents and voltages to be expected on the transformer for each fault classification. Since each utility has its own electrical network characteristics, the computed short circuit current and voltage values should fall within the specification set by the utility concerns.

The analysis will be continued with inrush current phenomena. The inrush current of a transformer can be as high as 7 to 10 times the rated current. Inrush current events are more frequent compared to short circuits. They also last for much longer duration compared to short circuits. The users are very anxious about the repeated switching of a transformer. Even though the inrush currents are usually not seriously looked into in the mechanical design considerations, the forces generated due to an extensive number of switching in a day may weaken the winding over a period of time. The continuous occurrences may lead to loosening of winding and subsequent failure.

The inrush current phenomena were also investigated as part of this research work on the conventional and HTS transformers for different circuit diagrams (Abdul Rahman *et al.*, 2011a, 2012). In this chapter, the peak values of inrush currents will be calculated for every cycle until they reach the primary winding rated current of the transformer to scrutinize the decay pattern. It is believed that the analysis will contribute further by

predicting the performance and reliability of HTS transformer before the installation in a distribution network system.

5.1 Short circuit analysis

The method of applying symmetrical components in the computation of short circuit currents for unbalanced faults is not suitable for distribution feeders that are inherently unbalanced. The unbalanced mutual coupling between the phases will lead to mutual coupling between the sequence components. Also, there will be limitation on the phases between which the faults may occur. Therefore, it is important to look into a suitable method for short circuit analysis of an unbalanced distribution system using the phase frame method (Kersting & Phillips, 1990).

5.1.1 Analysis technique

The model of an unbalanced feeder for short circuit calculation is presented in Figure 5.1. Short circuits can happen at any of the point 1, 2, 3, 4, and 5 shown in the model. The short circuit currents at point 1 are usually acquired from a transmission system short circuit analysis. The resultant short circuit MVAs will help to determine the zero and positive sequence impedances of the equivalent system (Kersting, 2002).

Figure 5.1 is a general description on the modelling for short circuit analysis. This study focuses only from point 2 to point 5 of the model which includes the primary line segment, the distribution transformer, and the secondary line segment. Therefore, there will only be one distribution transformer for this evaluation. Meanwhile, the primary line is an 11 kV medium voltage system and the secondary line is a 415 V low voltage

system. The short circuit analysis between point 4 and point 5 can then be carried out to observe the fault currents and voltages to be experienced by the distribution transformer (Ciric *et al.*, 2005; Kersting, 2002; Kersting & Phillips, 1990).

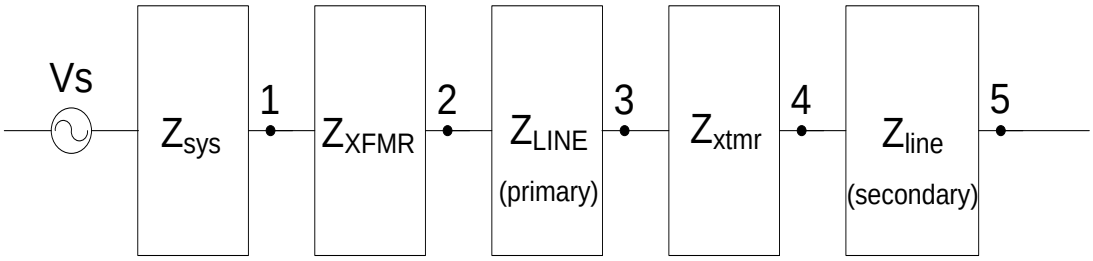

Figure 5.1: Model of an unbalanced distribution feeder for short circuit analysis

The calculation of short circuit currents and voltages for this study between point 4 and point 5 was carried out using the Thevenin equivalent three-phase circuit at the short circuit point. The Thevenin equivalent voltages (E_{th}) are the nominal line-to-ground voltages.

Figure 5.2 shows the Thevenin equivalent circuit at the faulted node. E_a, E_b and E_c are the Thevenin equivalent line-to-ground voltages. $[Z_{tot}]$ is the Thevenin equivalent phase impedance matrix at the faulted node. Z_f is the fault impedance. I_{fa}, I_{fb} and I_{fc} are the fault currents. V_{ax}, V_{bx} and V_{cx} are the phase voltages (a, b, c) to the point of fault (x). V_{xg} is the voltage from the point of fault (x) to the ground (g).

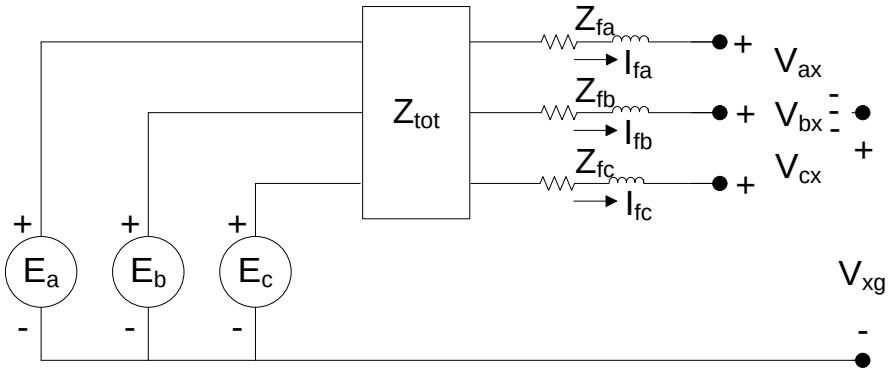

Figure 5.2: Thevenin equivalent circuit at the faulted node

Applying KVL to the Thevenin equivalent circuit, we have in matrix form as

$$\begin{bmatrix} E_a \\ E_b \\ E_c \end{bmatrix} = \begin{bmatrix} Z_{aa} & Z_{ab} & Z_{ac} \\ Z_{ba} & Z_{bb} & Z_{bc} \\ Z_{ca} & Z_{cb} & Z_{cc} \end{bmatrix} \cdot \begin{bmatrix} I_{fa} \\ I_{fb} \\ I_{fc} \end{bmatrix} + \begin{bmatrix} Z_f & 0 & 0 \\ 0 & Z_f & 0 \\ 0 & 0 & Z_f \end{bmatrix} \cdot \begin{bmatrix} I_{fa} \\ I_{fb} \\ I_{fc} \end{bmatrix} + \begin{bmatrix} V_{ax} \\ V_{bx} \\ V_{cx} \end{bmatrix} + \begin{bmatrix} V_{xg} \\ V_{xg} \\ V_{xg} \end{bmatrix}. \quad (5.1)$$

In equation (5.1), the Thevenin equivalent line to ground voltages are the summation of the Thevenin equivalent phase and fault impedance times the fault currents, the phase voltage to the point of fault, and the voltage from the point of fault to the ground (Kersting, 2002; Kersting & Phillips, 1990). We have known values of [y] (from [Z_{tot}] and [Z_f]) and [E_{abc}] (from [E_a], [E_b], [E_c]), then the equivalent injected currents are

$$\begin{bmatrix} I_{pa} \\ I_{pb} \\ I_{pc} \end{bmatrix} = \begin{bmatrix} I_{fa} \\ I_{fb} \\ I_{fc} \end{bmatrix} + \begin{bmatrix} y_{aa} & y_{ab} & y_{ac} \\ y_{ba} & y_{bb} & y_{bc} \\ y_{ca} & y_{cb} & y_{cc} \end{bmatrix} \cdot \begin{bmatrix} V_{ax} \\ V_{bx} \\ V_{cx} \end{bmatrix} + \begin{bmatrix} y_{sa} \\ y_{sb} \\ y_{sc} \end{bmatrix} \cdot \begin{bmatrix} V_{xg} \end{bmatrix} \quad (5.2)$$

where,

$$y_{sa} = y_{aa} + y_{ab} + y_{ac} \quad (5.3)$$

$$y_{sb} = y_{ba} + y_{bb} + y_{bc} \quad (5.4)$$

$$y_{sc} = y_{ca} + y_{cb} + y_{cc}. \quad (5.5)$$

The equations can be used to simulate all types of short circuits. The known values are the equivalent injected currents (I_{pa}, I_{pb}, I_{pc}), the equivalent admittances (y_{aa}, y_{ab}, y_{ac}, y_{ba}, y_{bb}, y_{bc}, y_{ca}, y_{cb}, y_{cc}) and the sum for each row of the admittances (y_{sa}, y_{sb}, y_{sc}). Meanwhile, the unknown values are the fault currents (I_{fa}, I_{fb}, I_{fc}), phase voltages to the point of fault (V_{ax}, V_{bx}, V_{cx}) and point of fault to ground voltage (V_{xg}). Therefore, the equations can be solved by specifying four additional independent equations which will depend on the type of fault being simulated. The validity of the results were verified by

using the line-to-ground voltages at node 4 [VLG_{4f} = (V_{ax}+V_{xg}, V_{bx}+V_{xg}, V_{cx}+V_{xg})] and the short circuit currents [I_{4f} = (I_{fa}, I_{fb}, I_{fc})], and then working backward through node 3 and node 2 to the source, using the relevant generalized matrices and applying equations (3.5) and (3.6) (Kersting, 2002). The seven equations can be presented in a matrix form by

$$\begin{bmatrix} I_{pa} \\ I_{pb} \\ I_{pc} \\ 0 \\ 0 \\ 0 \\ 0 \end{bmatrix} = \begin{bmatrix} 1 & 0 & 0 & y_{aa} & y_{ab} & y_{ac} & y_{sa} \\ 0 & 1 & 0 & y_{ba} & y_{bb} & y_{bc} & y_{sb} \\ 0 & 0 & 1 & y_{ca} & y_{cb} & y_{cc} & y_{sc} \\ \# & \# & \# & \# & \# & \# & \# \\ \# & \# & \# & \# & \# & \# & \# \\ \# & \# & \# & \# & \# & \# & \# \\ \# & \# & \# & \# & \# & \# & \# \end{bmatrix} \cdot \begin{bmatrix} I_{fa} \\ I_{fb} \\ I_{fc} \\ V_{ax} \\ V_{bx} \\ V_{cx} \\ V_{xg} \end{bmatrix} \tag{5.6}$$

where # is to be filled up depending on the type of fault.

Short circuits can be divided into five categories. The first category is the three-phase fault. The conditions will be $V_{ax} = V_{bx} = V_{cx} = 0$ and $I_{fa} + I_{fb} + I_{fc} = 0$. The equations can be presented in a matrix form as

$$\begin{bmatrix} I_{pa} \\ I_{pb} \\ I_{pc} \\ 0 \\ 0 \\ 0 \\ 0 \end{bmatrix} = \begin{bmatrix} 1 & 0 & 0 & y_{aa} & y_{ab} & y_{ac} & y_{sa} \\ 0 & 1 & 0 & y_{ba} & y_{bb} & y_{bc} & y_{sb} \\ 0 & 0 & 1 & y_{ca} & y_{cb} & y_{cc} & y_{sc} \\ 0 & 0 & 0 & 1 & 0 & 0 & 0 \\ 0 & 0 & 0 & 0 & 1 & 0 & 0 \\ 0 & 0 & 0 & 0 & 0 & 1 & 0 \\ 1 & 1 & 1 & 0 & 0 & 0 & 0 \end{bmatrix} \cdot \begin{bmatrix} I_{fa} \\ I_{fb} \\ I_{fc} \\ V_{ax} \\ V_{bx} \\ V_{cx} \\ V_{xg} \end{bmatrix}. \tag{5.7}$$

The second category is the three-phase to ground fault. The conditions will be $V_{ax} = 0$, $V_{bx} = 0$, $V_{cx} = 0$ and $V_{xg} = 0$. The equations can be shown in a matrix form as

$$\begin{bmatrix} I_{pa} \\ I_{pb} \\ I_{pc} \\ 0 \\ 0 \\ 0 \\ 0 \end{bmatrix} = \begin{bmatrix} 1 & 0 & 0 & y_{aa} & y_{ab} & y_{ac} & y_{sa} \\ 0 & 1 & 0 & y_{ba} & y_{bb} & y_{bc} & y_{sb} \\ 0 & 0 & 1 & y_{ca} & y_{cb} & y_{cc} & y_{sc} \\ 0 & 0 & 0 & 1 & 0 & 0 & 0 \\ 0 & 0 & 0 & 0 & 1 & 0 & 0 \\ 0 & 0 & 0 & 0 & 0 & 1 & 0 \\ 0 & 0 & 0 & 0 & 0 & 0 & 1 \end{bmatrix} \cdot \begin{bmatrix} I_{fa} \\ I_{fb} \\ I_{fc} \\ V_{ax} \\ V_{bx} \\ V_{cx} \\ V_{xg} \end{bmatrix}. \tag{5.8}$$

The third category is the phase to phase fault. There can be three conditions for this type of fault. Only one condition will be explained, *i.e.*, phase *a* and phase *b* are shorted while phase *c* is not faulty. The conditions will be $V_{ax} = 0$, $V_{bx} = 0$, $I_{fa} + I_{fb} = 0$ and $I_{fc} = 0$. In a matrix form, they are given by

$$\begin{bmatrix} I_{pa} \\ I_{pb} \\ I_{pc} \\ 0 \\ 0 \\ 0 \\ 0 \end{bmatrix} = \begin{bmatrix} 1 & 0 & 0 & y_{aa} & y_{ab} & y_{ac} & y_{sa} \\ 0 & 1 & 0 & y_{ba} & y_{bb} & y_{bc} & y_{sb} \\ 0 & 0 & 1 & y_{ca} & y_{cb} & y_{cc} & y_{sc} \\ 0 & 0 & 0 & 1 & 0 & 0 & 0 \\ 0 & 0 & 0 & 0 & 1 & 0 & 0 \\ 1 & 1 & 0 & 0 & 0 & 0 & 0 \\ 0 & 0 & 1 & 0 & 0 & 0 & 0 \end{bmatrix} \cdot \begin{bmatrix} I_{fa} \\ I_{fb} \\ I_{fc} \\ V_{ax} \\ V_{bx} \\ V_{cx} \\ V_{xg} \end{bmatrix}. \tag{5.9}$$

The fourth category is the two-phase to ground fault. As the previous category, there can also be three conditions and one of the conditions can be presented when phase *a* and phase *b* are shorted to the ground while the other phase, *i.e.*, phase *c*, is not faulty. The conditions will be $V_{ax} = 0$, $V_{bx} = 0$, $V_{xg} = 0$, and $I_{fc} = 0$. The equations in a matrix form are given by

$$\begin{bmatrix} I_{pa} \\ I_{pb} \\ I_{pc} \\ 0 \\ 0 \\ 0 \\ 0 \end{bmatrix} = \begin{bmatrix} 1 & 0 & 0 & y_{aa} & y_{ab} & y_{ac} & y_{sa} \\ 0 & 1 & 0 & y_{ba} & y_{bb} & y_{bc} & y_{sb} \\ 0 & 0 & 1 & y_{ca} & y_{cb} & y_{cc} & y_{sc} \\ 0 & 0 & 0 & 1 & 0 & 0 & 0 \\ 0 & 0 & 0 & 0 & 1 & 0 & 0 \\ 0 & 0 & 0 & 0 & 0 & 0 & 1 \\ 0 & 0 & 1 & 0 & 0 & 0 & 0 \end{bmatrix} \cdot \begin{bmatrix} I_{fa} \\ I_{fb} \\ I_{fc} \\ V_{ax} \\ V_{bx} \\ V_{cx} \\ V_{xg} \end{bmatrix}. \quad (5.10)$$

The final category is the one-phase to ground fault. There can also be three conditions for this type of fault. One of the conditions is when phase *a* is shorted to the ground while phase *b* and *c* are not faulty. The conditions will be $V_{ax} = 0$, $V_{xg} = 0$, $I_{fb} = 0$ and $I_{fc} = 0$. In the matrix form, the equations are

$$\begin{bmatrix} I_{pa} \\ I_{pb} \\ I_{pc} \\ 0 \\ 0 \\ 0 \\ 0 \end{bmatrix} = \begin{bmatrix} 1 & 0 & 0 & y_{aa} & y_{ab} & y_{ac} & y_{sa} \\ 0 & 1 & 0 & y_{ba} & y_{bb} & y_{bc} & y_{sb} \\ 0 & 0 & 1 & y_{ca} & y_{cb} & y_{cc} & y_{sc} \\ 0 & 0 & 0 & 1 & 0 & 0 & 0 \\ 0 & 0 & 0 & 0 & 0 & 0 & 1 \\ 0 & 1 & 0 & 0 & 0 & 0 & 0 \\ 0 & 0 & 1 & 0 & 0 & 0 & 0 \end{bmatrix} \cdot \begin{bmatrix} I_{fa} \\ I_{fb} \\ I_{fc} \\ V_{ax} \\ V_{bx} \\ V_{cx} \\ V_{xg} \end{bmatrix}. \quad (5.11)$$

5.1.2 Results

The three-phase fault and three-phase to ground fault analyses were carried out on the network with the conventional and HTS transformers. The circuit was shorted at various distances between the far end of the low voltage line segment, *i.e.*, 100 m and at the near end, *i.e.*, 0.1 m from the transformers. The fault current and voltage values at the far end and the near end are presented in Table 5.1 and Table 5.2, respectively. The fault currents and voltages will be experienced by the conventional and HTS transformers if the fault occurred.

Table 5.1: Currents and voltages for a three-phase fault

Short Circuit Values	Far End (100 m)		Near End (0.1 m)	
	Conventional	HTS	Conventional	HTS
I_{fa} (kA)	5.15∠-94°	5.19∠-95°	27.50∠-111°	27.54∠-118°
I_{fb} (kA)	5.64∠136°	5.67∠135°	27.51∠129°	27.55∠122°
I_{fc} (kA)	4.57∠16°	4.58∠15°	27.48∠9°	27.52∠2°
V_{ax} (V)	0	0	0	0
V_{bx} (V)	0	0	0	0
V_{cx} (V)	0	0	0	0
V_{xg} (V)	42.21∠111°	42.35∠110°	0.26∠104°	0.26∠97°

Table 5.2: Currents and voltages for a three-phase to ground fault

Short Circuit Values	Far End (100 m)		Near End (0.1 m)	
	Conventional	HTS	Conventional	HTS
I_{fa} (kA)	4.97∠-91°	5.02∠-92°	27.48∠-111°	27.52∠-118°
I_{fb} (kA)	5.58∠133°	5.61∠132°	27.50∠129°	27.54∠122°
I_{fc} (kA)	5.00∠18°	5.02∠17°	27.51∠9°	27.55∠2°
V_{ax} (V)	0	0	0	0
V_{bx} (V)	0	0	0	0
V_{cx} (V)	0	0	0	0
V_{xg} (V)	0	0	0	0

The phase to phase fault, two-phase to ground and one-phase to ground fault were also analysed on the circuit with both the conventional and HTS transformers. The shorted locations were also the same as for the three-phase and three-phase to ground faults. The fault currents and voltages which will have to be dealt with by the transformer are shown in Table 5.3, Table 5.4, and Table 5.5, respectively. The faults on other phases

than those presented for phase to phase, two-phase to ground, and one-phase to ground were not calculated in the analysis.

Table 5.3: Currents and voltages for a phase to phase fault

Short Circuit Values	Far End (100 m)		Near End (0.1 m)	
	Conventional	HTS	Conventional	HTS
I_{fa} (kA)	4.92∠-69°	4.96∠-70°	23.83∠-81°	23.86∠-88°
I_{fb} (kA)	4.92∠111°	4.96∠110°	23.83∠99°	23.86∠92°
I_{fc} (kA)	0	0	0	0
V_{ax} (V)	0	0	0	0
V_{bx} (V)	0	0	0	0
V_{cx} (V)	363.60∠89°	363.42∠89°	360.01∠90°	360.00∠90°
V_{xg} (V)	122.04∠-92°	121.96∠-92°	120.01∠-90°	120.00∠-90°

Table 5.4: Currents and voltages for a two-phase to ground fault

Short Circuit Values	Far End (100 m)		Near End (0.1 m)	
	Conventional	HTS	Conventional	HTS
I_{fa} (kA)	4.85∠-82°	4.90∠-83°	27.41∠-111°	27.44∠-118°
I_{fb} (kA)	5.22∠124°	5.24∠122°	27.60∠129°	27.63∠122°
I_{fc} (kA)	0	0	0	0
V_{ax} (V)	0	0	0	0
V_{bx} (V)	0	0	0	0
V_{cx} (V)	284.24∠88°	284.14∠88°	239.78∠90°	239.87∠90°
V_{xg} (V)	0	0	0	0

Table 5.5: Currents and voltages for a one-phase to ground fault

Short Circuit Values	Far End (100 m)		Near End (0.1 m)	
	Conventional	**HTS**	**Conventional**	**HTS**
I_{fa} (kA)	3.15∠-105°	3.16∠-105°	27.49∠-111°	27.52∠-118°
I_{fb} (kA)	0	0	0	0
I_{fc} (kA)	0	0	0	0
V_{ax} (V)	0	0	0	0
V_{bx} (V)	315.12∠-166°	314.48∠-166°	240.91∠-150°	240.94∠-150°
V_{cx} (V)	275.43∠100°	276.08∠100°	239.12∠90°	239.15∠90°
V_{xg} (V)	0	0	0	0

The three-phase fault and three-phase to ground fault analyses were carried out on the network with both conventional and HTS transformers. The circuit was shorted at various locations to observe the values of fault current experienced by the transformers. The fault current values for phases A, B, and C of the two types of faults are presented in Figure 5.3 to Figure 5.8, consecutively.

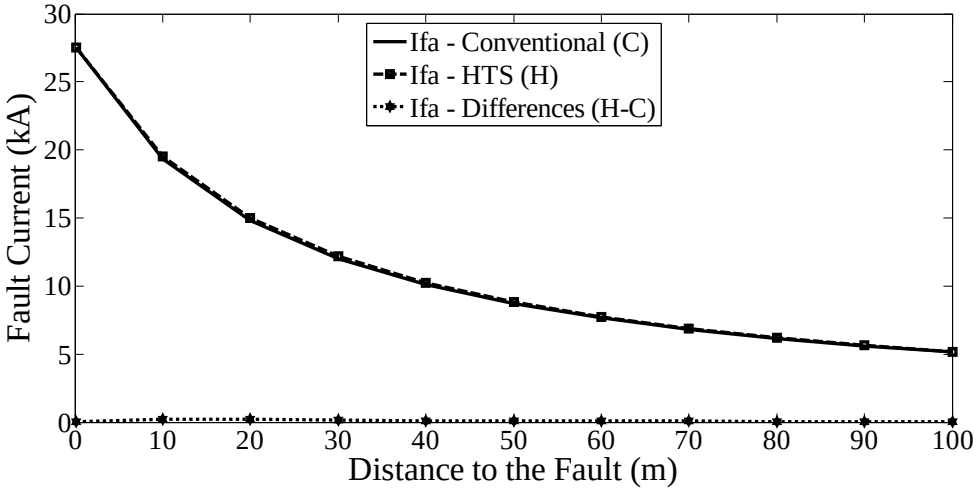

Figure 5.3: Three phase fault currents for phase A of the conventional and HTS transformers

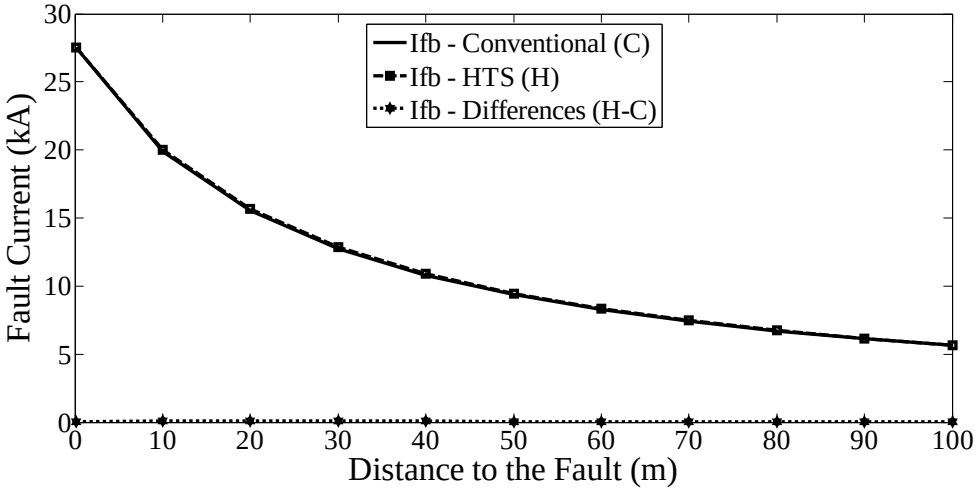

Figure 5.4: Three phase fault currents for phase B of the conventional and HTS transformers

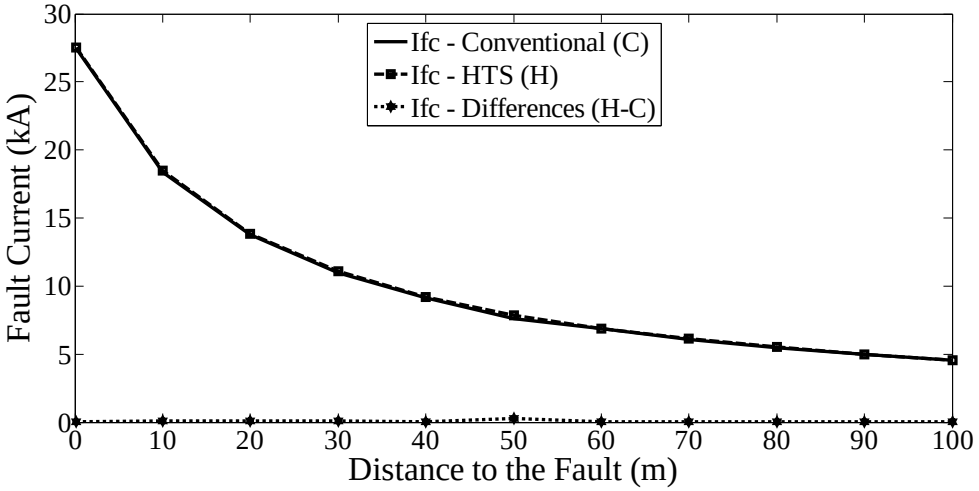

Figure 5.5: Three phase fault currents for phase C of the conventional and HTS transformers

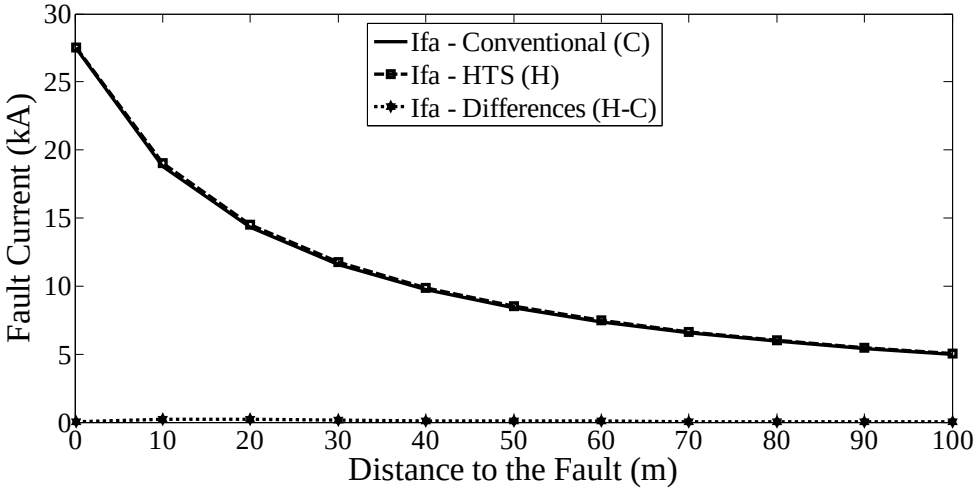

Figure 5.6: Three phase to ground fault currents for phase A of the conventional and HTS transformers

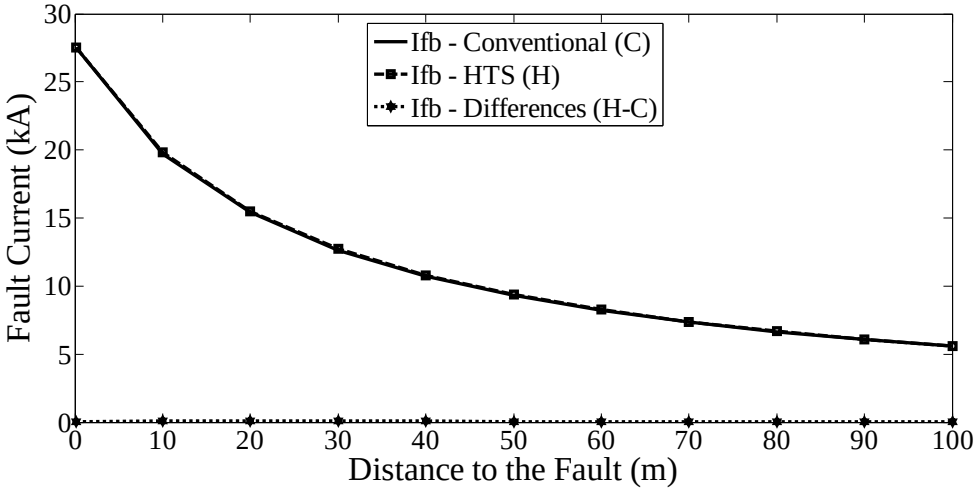

Figure 5.7: Three phase to ground fault currents for phase B of the conventional and HTS transformers

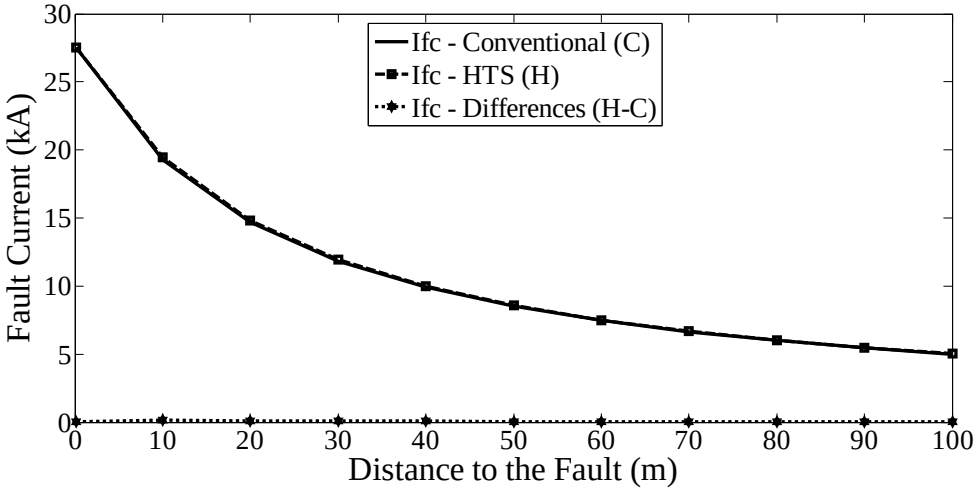

Figure 5.8: Three phase to ground fault currents for phase C of the conventional and HTS transformers

Meanwhile, the phase to phase fault, two-phase to ground and one-phase to ground faults were also analysed on the same circuit. The shorted locations were the same as those for the three-phase and three-phase to ground faults. The fault currents of the transformer experiencing the three faults are shown in Figure 5.9 to Figure 5.13.

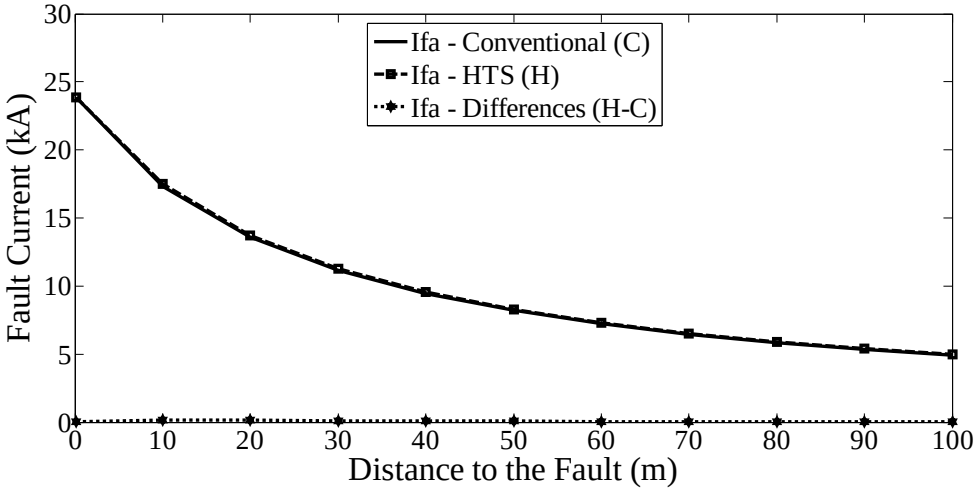

Figure 5.9: Phase to phase fault currents for phase A of the conventional and HTS transformers

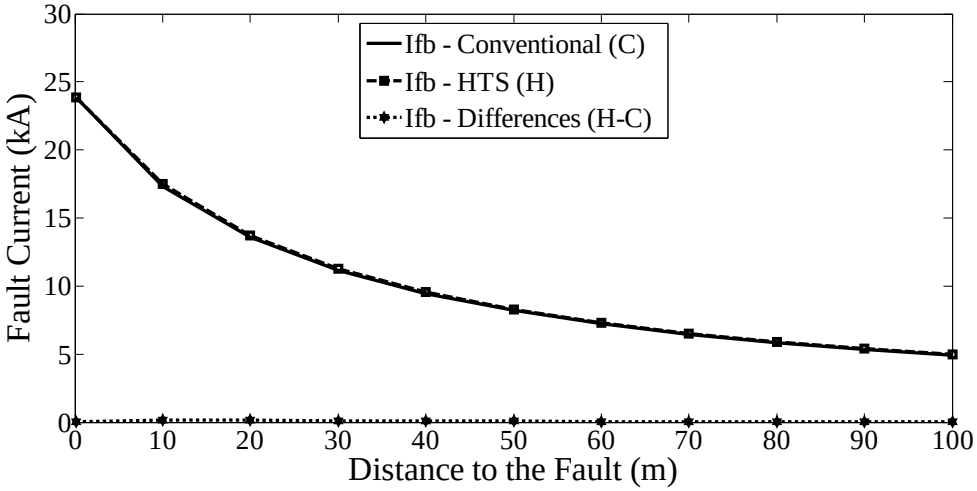

Figure 5.10: Phase to phase fault currents for phase B of the conventional and HTS transformers

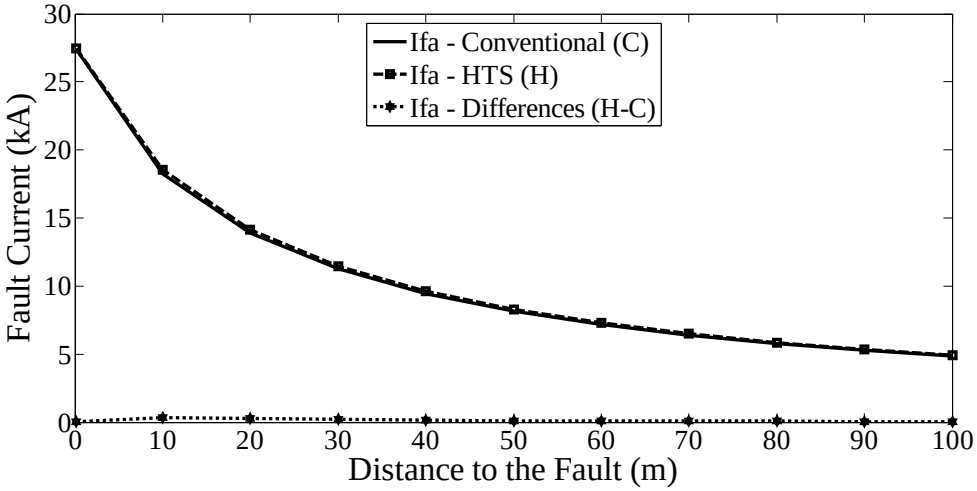

Figure 5.11: Two-phase to ground fault currents for phase A of the conventional and HTS transformers

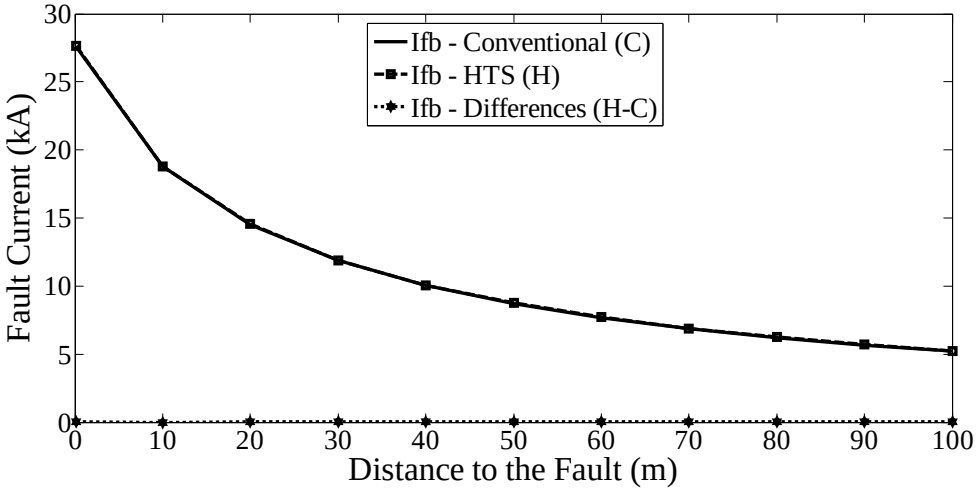

Figure 5.12: Two-phase to ground fault currents for phase B of the conventional and HTS transformers

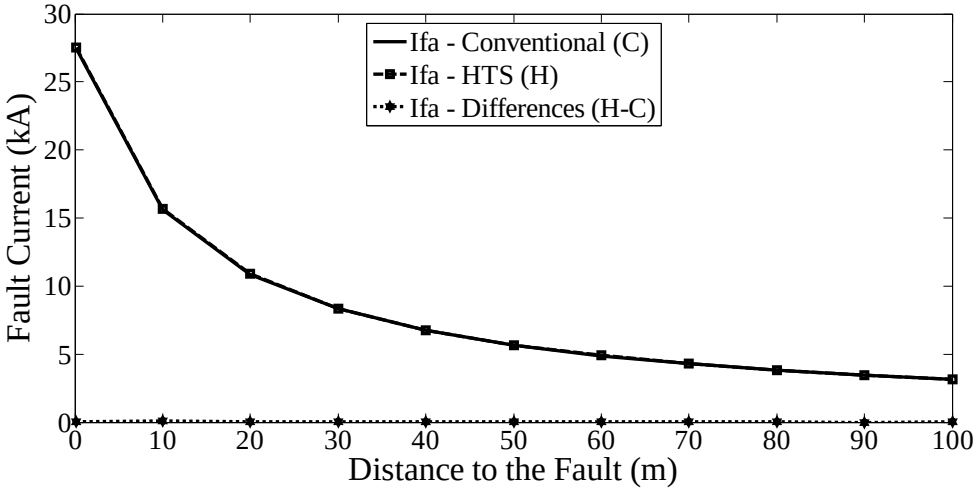

Figure 5.13: One-phase to ground fault currents for phase A of the conventional and HTS transformer

The figures show the trends of fault currents experienced by either conventional (CON) or HTS transformers installed in the circuit. The fault currents became higher as the fault locations moved nearer to the transformer or the source. Both types of transformers will therefore experience nearly the same kind of fault currents when a short circuit occurs.

Each utility has its own electrical network characteristics. For the low voltage distribution network applies in the analysis, a power utility, as an example, is specifying its transformers to meet the requirement characteristics of maximum service voltage at 1.1 kV_{rms} and low voltage short-circuit current at 31.5 kA. The short-circuit currents and voltages resulted from the analyses were found to be within the requirement.

5.2 Inrush current analysis

Magnetizing inrush current, which is also known as transient current, takes place the moment a transformer is energized. The inrush current will flow for a very short duration until the normal flux conditions are established. Under most of the power network conditions, the effects are of very little consequences. However, in rare cases, the current may disrupt momentarily the regular operation of the network system (Blume *et al.*, 1944). A part of this study is to investigate the consequences of inrush current on the superconducting transformer. The research will gather the effects of inrush current by the parameters and designs of the HTS transformer and compare with those of conventional transformers. The investigation will also look into the influence of transient current by the characteristics of network systems.

The inrush current will not take place if a transformer can be switched on at an instant of a voltage wave that corresponds to the actual flux density in the core at the same particular point of time. Nevertheless, the inrush phenomenon is difficult to prevent

because the instance of switching cannot be easily controlled and the instance of switching favourable to one phase is not favourable to the other two phases (Kulkarni & Khaparde, 2004). The instance of switching when the applied voltage is zero for maximum inrush current is shown in Figure 5.14. The inrush current can be as high as seven to ten times the rated current (Ishigohka, Uno, & Nishimiya, 2006). Inrush transients are more frequent than short circuits and they last for few seconds as compared to short circuits which are cleared in tens of milliseconds. In Figure 5.14, V is the applied voltage, i is the excitation current, B_r is the residual flux density, B_{mp} is the peak value of designed steady-state flux density in the core, and i_o is the instantaneous value of magnetizing current.

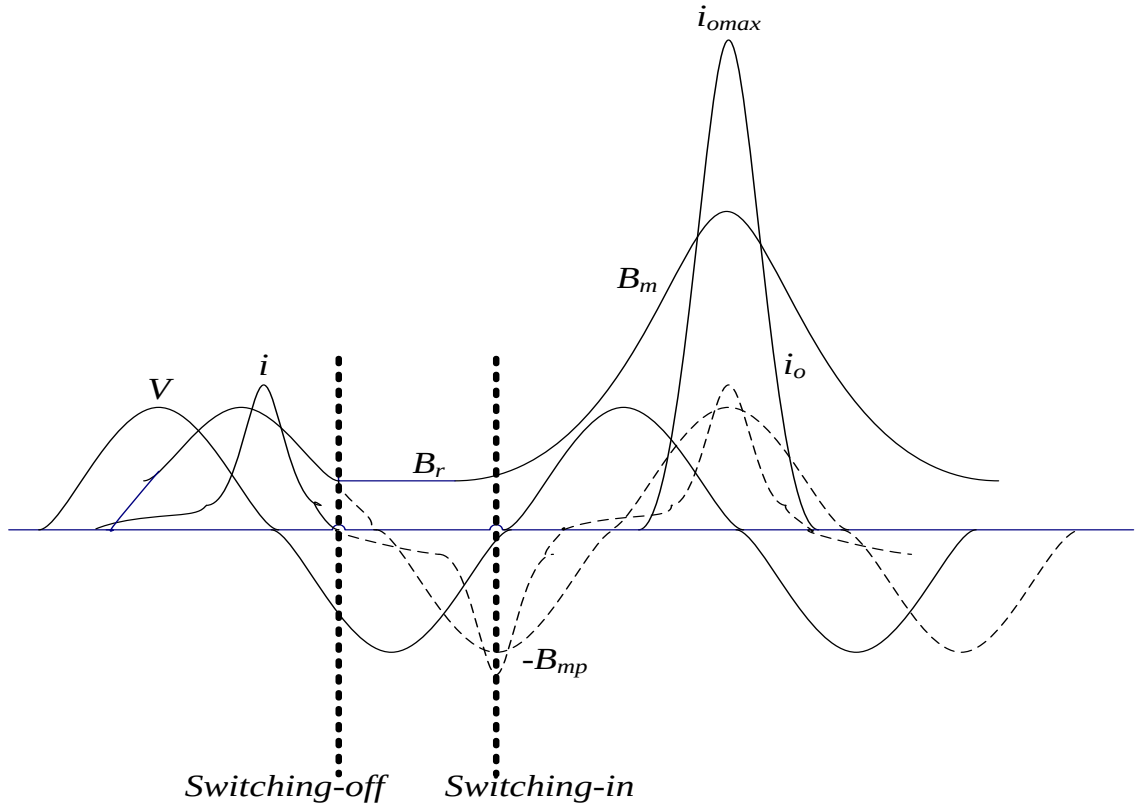

Figure 5.14: Maximum inrush current phenomenon

Figure 5.14 shows that when the transformer is switched-off, the excitation currents will follow the hysteresis curve to zero value and the flux density will change to a non-zero residual value (Kulkarni & Khaparde, 2004). The maximum inrush current is drawn from the residual flux density when the transformer is switched-on at the instance of the applied voltage equals zero. The dotted lines are to show the situation if the transformer is not switched-off.

The ratio of inductance over resistance of the circuit is not constant because the inductance value will change depends on the core saturation (Blume *et al.*, 1944; Kulkarni & Khaparde, 2004). The initial rate of decay will be quite high due to high saturation and low inductance. The losses will eventually damp the circuit which make the saturation to decline. The inductance will increase and the increment will slow down the inrush current decay. In short, the decay begins with high initial rate and decreases as the event progress. The phenomenon will subsequently keep on for few seconds. A smaller transformer will typically have higher rates of decay. Also, a lower efficient or higher losses transformer will experience higher inrush current decay rates.

5.2.1 Analysis technique

Utilities are very interested in the information on the maximum value and rate of decay of the inrush current. For a three phase delta connected primary transformer, each phase is independently connected to the network. The inrush phenomenon corresponding to flux of each phase of this transformer takes place as in the case of a single phase transformer (Kulkarni & Khaparde, 2004). The phase inrush current will therefore result in the same value as that of the single phase transformer. Meanwhile, the line inrush current will be less severe. The line current is square root three times the phase current

under normal condition. In inrush condition, only one phase which gets switched at the worst will be having large inrush current. Therefore, the line inrush current will be almost equal to the phase inrush current.

In the estimation of inrush current magnitude and decay pattern, operating engineers will be looking on the inrush current peak values for the first few cycles and the time after which the inrush current reduces to a value equal to the rated current. Two assumptions are made in the calculation. The first is that the transformer is energized at voltage equal to zero. The next is the residual flux is in the same direction as the initial flux change which gives maximum possible value of the inrush current (Holcomb, 1961; Kulkarni & Khaparde, 2004; Specht, 1951). In the event, after the core saturation, the inrush current is limited by air core reactance, X_s, which can be calculated as

$$X_s = \frac{\mu_\circ \cdot N^2 \cdot A_w}{h_w} \cdot 2 \cdot \pi \cdot f \tag{5.12}$$

where N is the number of turns of excited winding, A_w is the area inside the mean turn of excited winding and h_w is the height of energized winding. The angle, θ, at the instance which the core saturates is given by

$$\theta = K_1 \cos^{-1}\left(\frac{B_s \cdot B_{mp} \cdot B_r}{B_{mp}} \right) \tag{5.13}$$

where B_s is the saturation flux density, B_r is the residual flux density, B_{mp} is the peak value of designed steady-state flux density in the core and K_1 is the correction factor for saturation angle.

The inrush current peak, i_{omax}, for the first cycle is specified as

$$i_{o\max} = \frac{K_2 \cdot V \cdot \sqrt{2}}{X_s}(1-\cos\theta) \tag{5.14}$$

where V is the rms value of applied alternating voltage and K_2 is the correction factor for the peak value. The residual flux density will reduce at the end of the first cycle due to losses in the circuit. It is also a function of damping provided by the transformer losses. The new residual flux density, $B_{r(new)}$, is then presented as

$$B_{r(new)} = B_{r(old)} - \left[B_{mp} \cdot \frac{K_3 \cdot R}{X_s}\left(2 \cdot (\sin\theta - \theta\cos\theta)\right) \right] \tag{5.15}$$

where R is the sum of transformer winding resistance and system resistance and K_3 is the correction factor for the decay of inrush. The computations are repeated in order to calculate the peaks of the subsequent cycles. Each phase is independently connected to the network for a three phase delta connected primary transformer and this results in the same value of inrush phase current as that of a single phase transformer. Under normal conditions, the line current is equals √3 times the phase current. In inrush conditions, only one phase which gets switched. In the worst case the line current would be almost equal to the phase current (Kulkarni & Khaparde, 2004).

There are several factors affecting the magnetizing inrush current phenomenon. The first factor is the switching-on angle. The inrush current decreases when the switching angle on voltage wave increases. Hence, the maximum inrush current can be obtained when the angle equals 0° and the minimum value of the transient current is at the angle equal to 90^0 (Kulkarni & Khaparde, 2004). Another factor is the residual flux density. The residual flux density depends on the core material characteristics and the power factor of the connecting load. The core material characteristics are normally considered

as cold rolled or hot rolled. The maximum value is usually taken as at a certain percentage of the rated peak flux density of the core (60% for cold-rolled steel and 90% for hot rolled steel) (Kulkarni & Khaparde, 2004). Meanwhile, the type of load during switching off will affect the value of the residual flux density. The maximum value can be achieved before the moment at which the total current is switched off for no load, lagging load, and unity power factor load conditions. For the leading load condition, the maximum value can be obtained if the leading current component is less than the magnetizing component (Kulkarni & Khaparde, 2004). The next factor that can affect the inrush current phenomenon is the resistance of the line between the source and the transformer. The damping effect from the line resistance will reduce the maximum value of the initial inrush current and expedite the duration of the decay rate (Kulkarni & Khaparde, 2004).

The parameters for the HTS transformer and two conventional transformers of the same capacity are shown in Table 5.6. All the transformers have the same capacity of 1 MVA. The primary windings for the conventional transformers are rated at 52.5 A by the manufacturers. Meanwhile, the primary windings for the HTS transformer is rated lower at 30.3 A. However, the secondary windings for conventional transformers are rated almost the same at 1333 A as compared to 1391 A for the HTS transformer. The data were used in the calculation and the results were compared for the inrush current analysis between the transformers.

Table 5.6: Transformers parameters for inrush current calculation

Parameters	Transformer		
	HTS	Conventional 1	Conventional 2
Voltage - HV Winding (kV)	11	11	11
Number of Turn – HV Winding	1098	739	863
Mean Diameter – HV Winding (mm)	340.5	369.5	418.0
Height – HV Winding (mm)	311	458	500
Saturation Flux Density (T)	2.2	2.05	2.05
Peak Operating Flux Density (T)	1.600	1.584	1.728
Core Diameter (mm)	225	243	222
System & Winding Resistance (Ω)	0.150	1.263	1.110
Rated Current – HV Winding (A)	30.3	52.5	52.5
Critical Current – HV Winding (A)	112	n/a	n/a

A previous study had measured the magnetizing inrush for several transformer units and obtained the average values of the correction factors. The average values are the correction factor for saturation angle, K_1 = 0.90, the correction factor for the peak value, K_2 = 1.15, and the correction factor for the decay of inrush, K_3 = 2.26 (Kulkarni & Khaparde, 2004; Specht, 1951). The correction factors are the average constant values. The values were obtained from an analysis on seven units where their magnetizing inrush current measured from 10 kVA to 20,000 kVA (Specht, 1951). Meanwhile, the hot rolled steel was considered for the core application and therefore, the residual flux density was taken as 60% of the rated peak flux density (Kulkarni & Khaparde, 2004). Other alternatives for the core application were cold rolled steel and type C cores in which the residual flux densities were 90% and 50% of the rated peak flux density, respectively (Specht, 1951). The network resistance for the 400 m underground cable

was calculated to be around 0.05 Ohm (Short, 2004) and the resistance for the superconducting HV winding was assumed to be 0.1 Ohm (Kalsi, 2008).

5.2.2 Results

From the calculations on two conventional transformers 1 and 2 from two different manufacturers put into the distribution network presented, the inrush current peak values were found to increase up to 3 to 5 times the rated current. And, they took between 20 to 30 cycles or 0.4 to 0.6 second for the inrush current to reduce to the rated current as in Figure 5.15 and Figure 5.16, respectively.

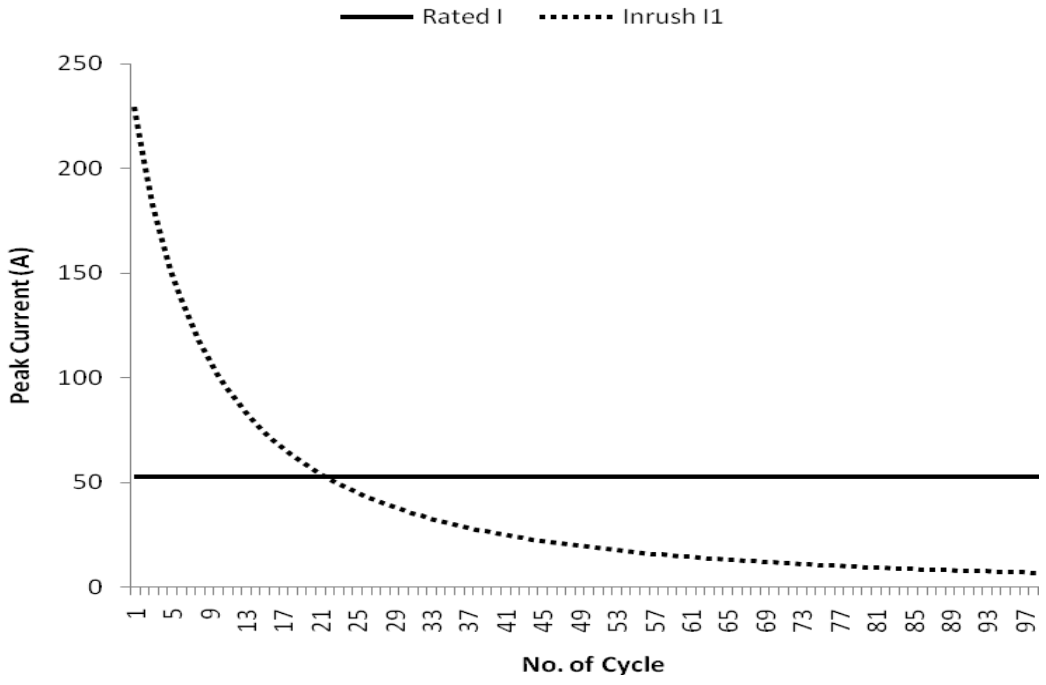

Figure 5.15: Peak inrush currents for conventional transformer 1

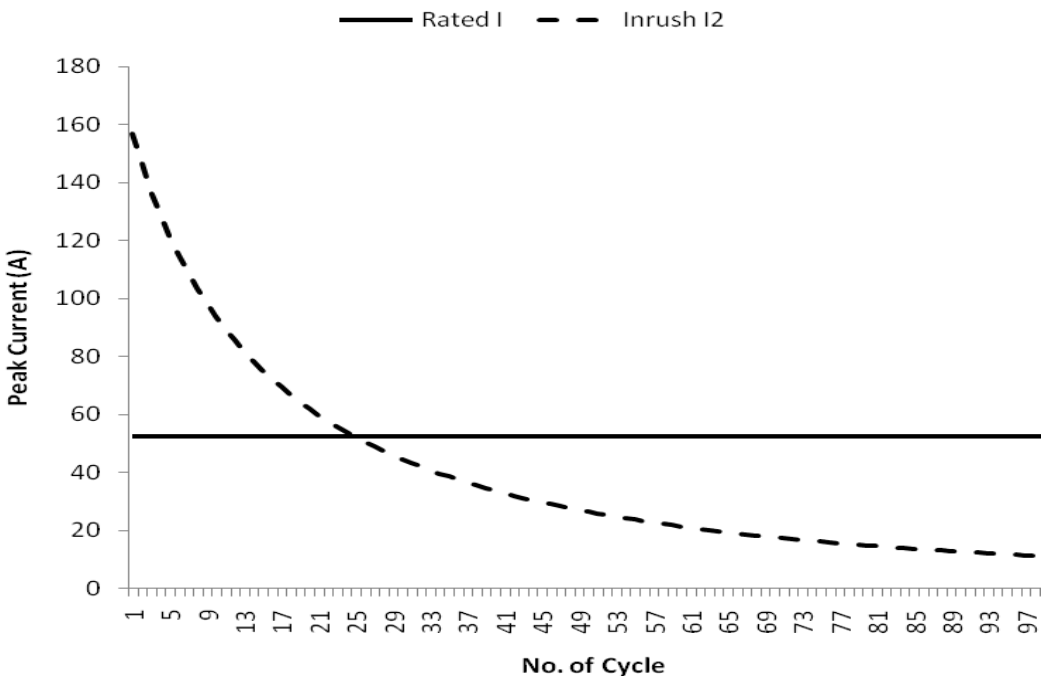

Figure 5.16: Peak inrush currents for conventional transformer 2

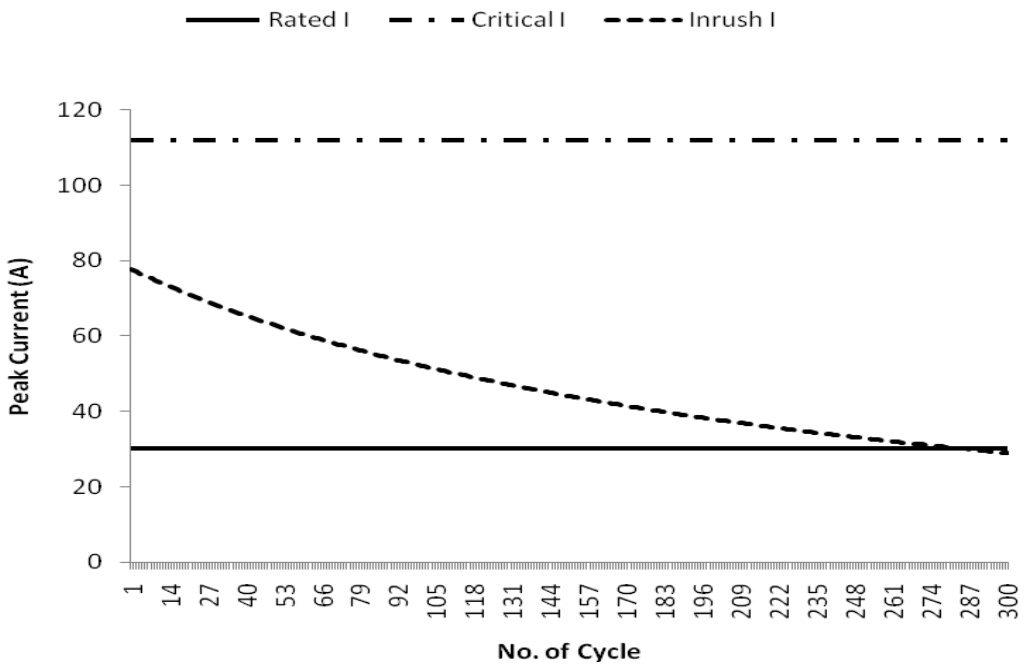

Figure 5.17: Peak inrush currents for the HTS transformer

Meanwhile, the inrush peak values went up to 2 to 3 times the rated current for the HTS transformer, as shown in Figure 5.17. Also, this value was found to be below the critical current value of the primary winding at operating temperature of 77 K. However, it was taking much longer time to reduce to its rated current, *i.e.*, almost 300 cycles or 6 seconds. It is very important to take into account the value of critical current for the primary winding of the HTS transformer. The transformer operates under normal condition at the temperature equals or less than 77 K. Beyond the critical current, the characteristics of the HTS transformer will change and this includes the superconducting properties of the primary winding.

The analysis continued with the investigation on the effects of various source impedances between the superconducting transformer and the source of sustained voltage. Figure 5.18 shows the outcome of applying different incoming cable sizes. The cable sizes employed were 150, 300, and 400 mm^2 for the 400 m length of cable. A lower cable size was not only reduced the magnitude of inrush current but also accelerated the rate of decay. Meanwhile, Figure 5.19 shows the results for different incoming cable lengths. The 300-mm^2 underground cable was evaluated for three different lengths of 0.1, 1.0, and 10.0 km. A shorter incoming cable increased the magnitude of the inrush current and delayed the rate of decay.

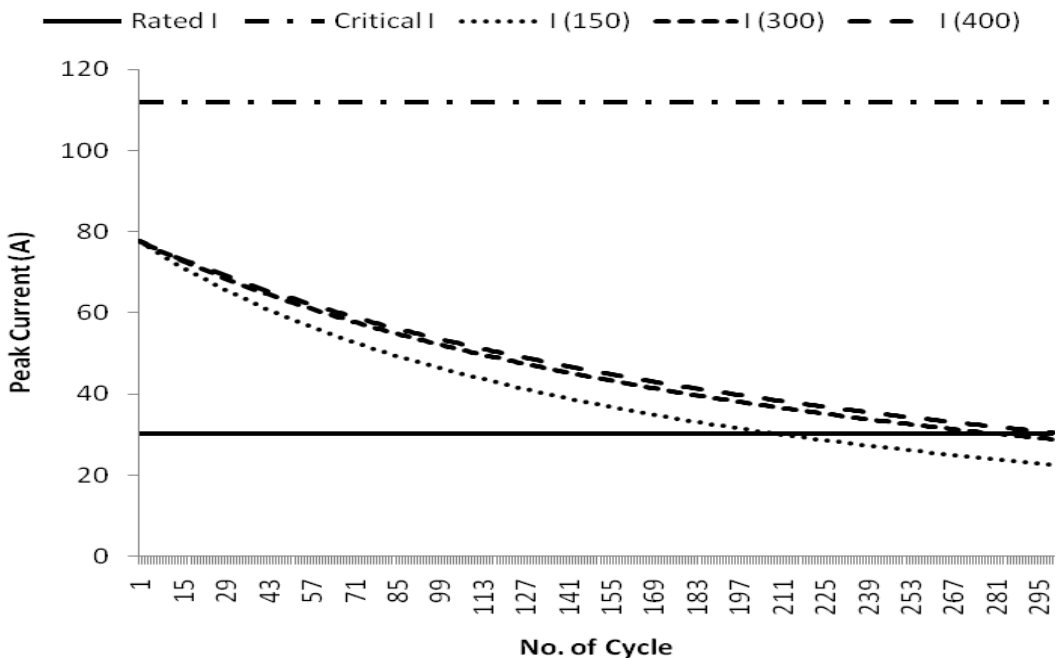

Figure 5.18: Peak inrush current of HTS transformer for different cable sizes (mm^2)

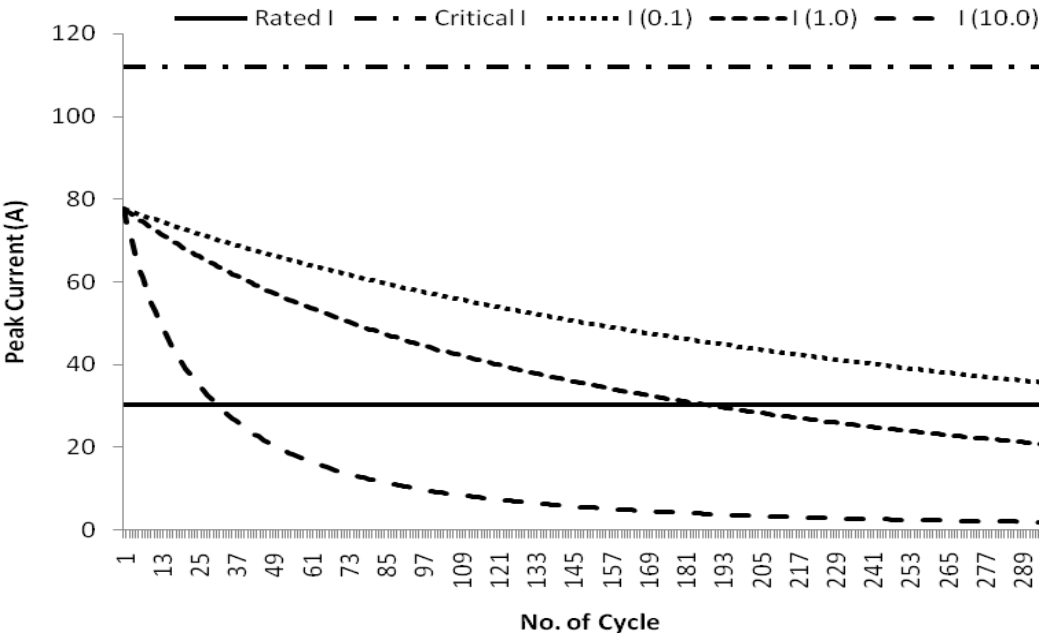

Figure 5.19: Peak inrush current of HTS transformer for different cable lengths (km)

The magnetizing inrush currents are more frequent than the short circuit currents. The inrush transients continue for few seconds as compared to short circuits currents which are limited to tens of milliseconds. Only the energized winding will be subjected to mechanical stresses due to the transient forces. The outer windings have a higher value of air-core reactance, X_s, compares to the inner winding. The transformer that is switched on from the outer winding will generate lower inrush current and subsequently lower corresponding forces. Meanwhile, the transformer that is switched on from the inner winding will experience higher inrush current. Switching on the transformer repeatedly could produce inrush current forces that may reduce the strength of the winding over a period of time that may then lead to winding looseness and subsequent transformer failure. Transformers are designed to withstand mechanical effects due to short circuit currents. Inrush currents may not be considered dangerous even though they may unnecessarily lead to the operation of protective equipment such as relays and fuses.

5.3 Discussion

The sample network with conventional and HTS transformers were simulated with different types of short-circuit conditions as shown in section 5.1. The calculation provided the fault currents and voltages for various fault locations to be expected on the transformers for each fault classification. The results were shown in Figure 5.3 through Figure 5.13. As expected, the three phase fault provided the highest fault current. The three-phase fault can normally be regarded as the most severe condition from the point of view of fault severity. Thus, the maximum possible value of the three-phase fault level normally determines the required short circuit rating of the power system circuit breaker. The current will be high because the fault current is only limited by the

inherent series impedance of the power system up to the point of faulty. The inherent series impedance is design to be as low as possible to get maximum power transfer to customer and to limit unnecessary losses in the network. However, the maximum value of a single-phase-to-earth fault current, in a solidly-earthed system, may exceed the maximum three phase fault current. Solid neutral earthing means high earth fault current but the value is limited by the inherent earth fault impedance of the system (Short, 2004). Since each utility have its own electrical network characteristics, the computed short-circuit current and voltage values should fall within the specification set by the utility concerns.

Section 5.2 describes several factors that were found to affect the magnitude of inrush currents, as shown in equations (5.12), (5.13) and (5.14). Equation (5.15) showed how the source impedance between the transformer and the source of sustained voltage functioned to reduce the magnitude of the peak inrush current. Generally, there will be some external impedance which will reduce the inrush current below the maximum.

For maximum inrush current, there is a linear relation between the maximum peak inrush current and the applied voltage. The linear relationship is explained by the fact that under conditions of residual flux and switching angle which produce the maximum inrush condition, the iron core is completely saturated. The maximum inrush current can be obtained when the transformer is energized at zero point on the voltage wave. The crest inrush current is reduced as the switching angle varies in either direction from a voltage zero.

The transient inrush currents decay at a rate determined by the resistance of the transformers themselves. Transformers having relatively high losses will in general have faster rates of decay than those which are more efficient, as shown in Figure 5.15, Figure 5.16, and Figure 5.17. Meanwhile, resistance in the circuit, *i.e.*, between the

transformer terminals and the source of sustained voltage not only reduces the maximum initial inrush current but also expedites its rate of decay and assists in restoring normal voltage wave shape more quickly.

CHAPTER 6

THERMAL EFFECTS OF SHORT CIRCUIT CURRENT

The expansion of generating capacity and the extension of interconnections due to the increase of electrical power requirement have contributed to the growth of short circuit capacity in power networks. Subsequently, the short circuit current the transformers have to cope with becomes more severe (Kulkarni & Khaparde, 2004). The short circuit capacity of a transformer should be tailored to withstand any fault current incidence due to external short circuit. Any shortcoming in the strength may contribute to mechanical collapse of the windings and deformation of the clamping structures. The short circuit fault that occurs in the power system outside the transformer will generate defects inside the transformer. The internal defects initiated by the external short circuit current may lead to bushing blowouts, tank bursting, fire hazard, *etc.*

6.1 Technology development

HTS winding applications for power transformers are captivating because they require a comparatively smaller amount of conductor for the same transformer capacity. In the United States, conventional transformers account for about 25% of the losses in the power transmission and distribution system and resistive heating is acknowledged to contribute a great portion of these losses (Schwenterly *et al.*, 1999). Therefore, the use of HTS transformers is able to bring about substantial energy savings and economized lifetime ownership costs. Other projected benefits include the capability to limit and withstand high currents and consequently minimize the loss of lifetime by thermal damage. They are also able to reduce potential fire and environmental hazards with the use of liquid nitrogen as a substitute to oil for cooling and insulation of the transformers. Last but not least, the weight and volume of HTS transformers are estimated to be about one-half to one-third that of conventional transformers (McConnell, 2000). This chapter focuses on modelling the effects of various distribution network conditions toward a distribution HTS transformer. This investigation looks comprehensively into the thermal effects of short circuit current on various architectural designs and fault current limiting properties of HTS transformer winding conductor.

Recent development on HTS transformer has focused on its capability to also operate as a Fault Current Limiter (FCL). A previous study (Jin *et al.*, 1997) has shown that the use of HTS-FCL devices can effectively reduce short circuit current in power transmission and distribution networks. The HTS-FCL transformer acts as a superconducting transformer under normal operating conditions and as a superconducting fault current limiter under short circuit conditions. The fault current that is limited by the HTS transformer will depend on the characteristics and

construction of the winding and the parameters of the HTS wire. Several investigations (Ahn *et al.*, 2007; Janowski, Kozak, Kondratowicz-Kucewicz, Wojtasiewicz, & Kozak, 2007; Kim *et al.*, 2010; Schmidt *et al.*, 2007) were carried out to study the behaviour of HTS-FCL conductors for the implementation in various power equipment.

The fault current limiting feature in HTS-FCL transformer could provide protection and reduce the wear and tear of other power equipment experiencing the short circuit current. It could also avoid power interruptions and damages to the power grid and equipment. The transformer is also able to improve the transient stability of power system in fault condition. Therefore, efficient and reliable power system can be established if the transformer could produce fault current limiting function only under fault conditions and could reduce the impedance under steady state conditions. However, the important concerns of HTS-FCL transformers are the current limiting factor, recovery characteristics and transformer function. This work scrutinizes the properties and characteristics of the materials adopted for the HTS-FCL transformer winding conductors. This information will eventually be used to carry out the analysis and determine the thermal effects of short circuit current on the HTS-FCL transformer windings.

6.2 Analyzing approach

The analysis looked into a couple of computational approaches to evaluate the thermal effects on the transformer secondary winding due to short circuit current. The investigation started with a standard calculation approach that was well established for evaluating conventional transformers. Another approach to determine the thermal effect was by the application of heat balance equation on a conventional transformer

experiencing a short circuit condition. The results for the calculation of the two approaches were compared and observed for any significant variation.

The short circuit near end and far end values calculated in Chapter 5 were employed in the calculation and scrutinized on how they will affect the analysis. Since the fault current values may vary depend on the conditions, the analysis also looked for another value which can be considered a high probable fault current to occur on the transformers. Finally, the analysis looked into the dynamics of alternative current electrical system by determining the asymmetrical short circuit current values from the symmetrical fault current magnitude and the X/R ratio of transformer winding coil. These fault current values were utilized to observe the thermal effect expected on the low voltage conductor.

6.2.1 Standard calculation

The ability to sustain without damage the thermal effect on the winding of a transformer from an external short circuit event is very important. The fault current which will run through the transformer winding is significantly higher than the normal operating current. This event will eventually contribute to the increase of the transformer winding temperature. However, the heat transfer through the cooling arrangement of the transformer winding should not be considered because the thermal time constant of the winding is usually several minutes and this is very much longer than the fault duration which is normally within 2 seconds before being interrupted by the protection system. International Electrotechnical Commission (IEC) has introduced a standard approach to exhibit the ability to withstand the thermal effect from the short circuit current in a conventional transformer (IEC60076-5, 2000). The standard shows the calculation procedures to determine and demonstrate the transformer capability to endure the

thermal and dynamic effects of the fault conditions. The formulation will provide the highest average temperature to be experienced by the winding conductor after a short circuit.

The equation applied in the standard for the average temperature (T) in the copper winding conductor of a conventional transformer after the short circuit is

$$T = T_o + \frac{2(T_o + 235)}{\frac{106000}{J^2 t} - 1} \tag{6.1}$$

where T_o is the initial winding temperature in Celsius (°C), J is the short circuit current density in Amperes per square millimetre (A/mm^2) and t is the duration of the short circuit in seconds (s).

Meanwhile, the next equation shows the relationship between the resistance growth and the resistivity at various temperatures on the low voltage winding during the short circuit period

$$R(T) = \rho(T) \cdot \frac{l}{A} \tag{6.2}$$

where l is the length of the conductor and A is the cross sectional area of the conductor. The resistivity values of copper at various temperatures are shown in Figure 6.1. The data was acquired from cryogenic and room temperature sources (Iwasa, 1994; Lide, 2003).

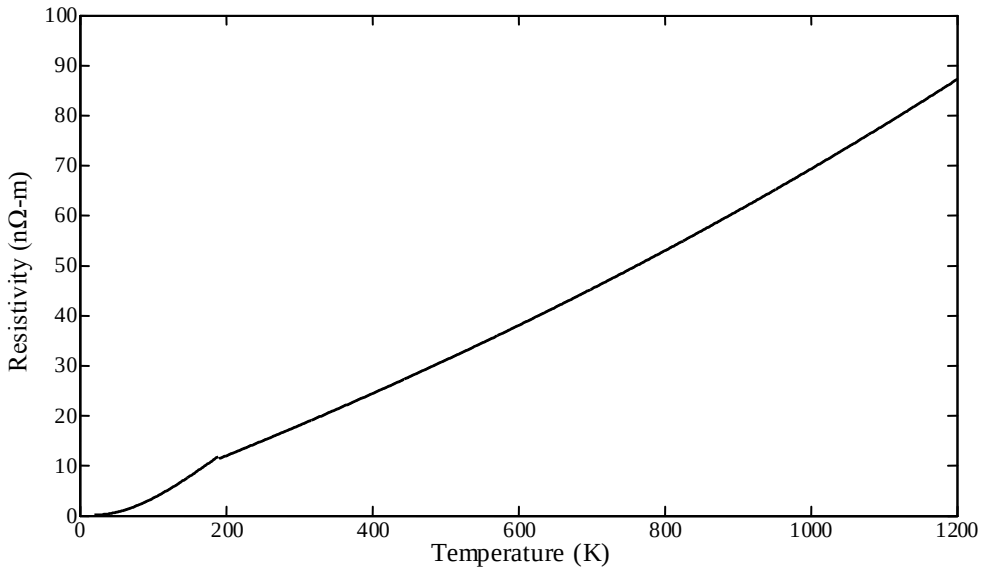

Figure 6.1: Resistivity of copper at various temperatures

Further information on the parameters of the conventional transformer would be required for the calculation. The data are presented in Table 6.1.

Table 6.1: Parameters for thermal effect calculation of the conventional transformer

Parameters for Low Voltage Winding	**Conventional Transformer**
Rated Current (I_r), A	1333
Cross Sectional Area (A), mm^2	430.00 × 1.30
Length (l), m	45
Copper Density (d), kg/m^3	8960
Resistance per phase at ambient (R), Ω	5.64×10^{-4}
Short Circuit Impedance (Z_{sc}), %	4.75
Overall Rated Current Density (J_r), A/mm^2	2.3846

For the calculation, the initial temperature was taken at 105 °C or 378 K, and the short circuit duration was 2 seconds. The temperature values after each 0.1 second are presented in Table 6.2.

Table 6.2: Winding temperatures by the standard calculation after short circuit

Total Short Circuit Duration (s)	**Winding Temperature (K)**
0	378.0000
0.1	379.6206
0.2	381.2490
0.3	382.8852
0.4	384.5292
0.5	386.1812
0.6	387.8411
0.7	389.5091
0.8	391.1851
0.9	392.8693
1.0	394.5616
1.1	396.2623
1.2	397.9712
1.3	399.6886
1.4	401.4144
1.5	403.1487
1.6	404.8916
1.7	406.6431
1.8	408.4033
1.9	410.1723
2.0	411.9501

6.2.2 Heat balance equation

Computations of the transformer short circuit parameters should be undertaken to determine the transformer capability to withstand the thermal effects. The thermal effects on the windings due to a short circuit event are very critical. The fault currents are significantly larger than the normal load currents. High winding temperatures are to

be expected from the incident. Another alternative to calculate the temperature rise in the transformer winding is by applying the presented heat balance equation.

$$C(T) \cdot m \cdot \frac{\Delta T}{\Delta t} = k(T) \cdot A \cdot \frac{\Delta T}{l} + \rho(T) \cdot J_{sc}^2 \cdot v \tag{6.3}$$

where $C(T)$ is the specific heat capacity, m is the mass of the winding, ΔT is the change in temperature, Δt is the time duration, $k(T)$ is the thermal conductivity, A is the cross-sectional area of the winding, l is the length of the winding, $\rho(T)$ is the resistivity, J_{sc} is the short circuit current density, and v is the volume of the winding. Equation (6.3) will be compared and validated later in this chapter for the calculation of the temperature rise in the transformer winding after short circuit with a computational approach from an international standard, IEC 60076-5 (2000): Power transformers – Ability to withstand short circuit. The temperature of the winding was calculated with an assumption that the heat developed during the event was retained in the winding itself, raising its temperature. For a conventional transformer, the heat transfer through the cooling medium was not taken into account because the thermal time constant of the winding is much larger than that of the short circuit current. Meanwhile, for an HTS transformer, the thermal time constant for the tape is small. However, the thermal power dissipated through the cooling medium when the applied current is much higher than the critical current is also small and hence neglected. The thermal power conducted through the conductors was very small compared to the thermal power due to the heat capacity and the resistivity. The heat balance equation applied during the short circuit duration was rewritten and the change in temperature was presented as

$$\Delta T = \frac{\rho(T) \cdot J_{sc}^2 \cdot v}{\dfrac{C(T) \cdot m}{\Delta t} - \dfrac{k(T) \cdot A}{l}} \tag{6.4}$$

The resistivity and specific heat capacity values are dependent on the temperature. The resistivity variation with temperature for copper was presented in Figure . Meanwhile, the specific heat capacities for copper, as a function of temperature, are shown in Figure . The specific heat data was taken from published sources (Brooks, Norem, Hendrix, Wright, & Northcutt, 1968; Jankowski, 2004; Mills, 1999; Thompson, Manganaro, & Fickett, 1990).

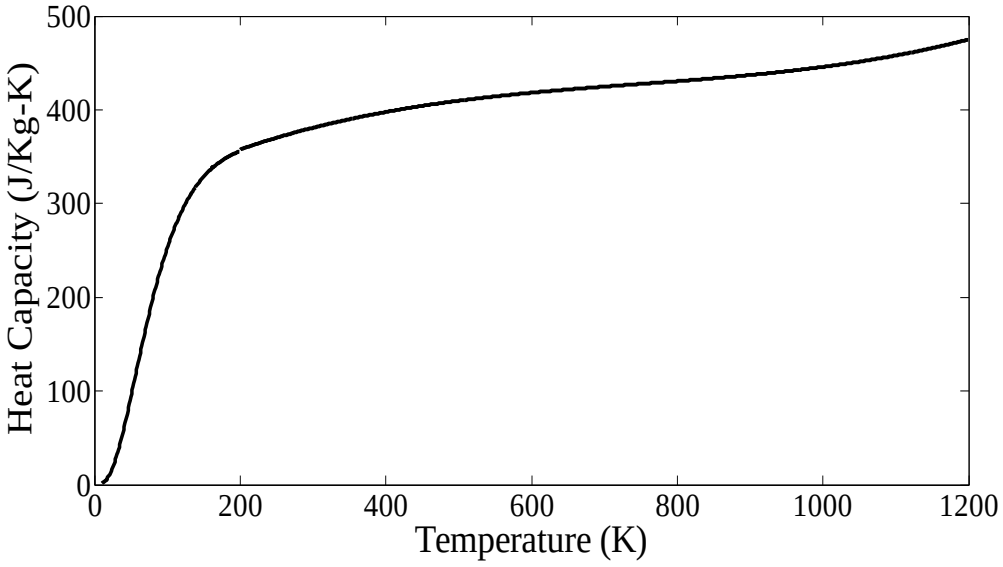

Figure 6.2: Specific heat capacity of copper at various temperatures

The information given in Table 6.1 was gathered and substituted into equation (6.4). The resistivity and heat capacity values at various temperatures were provided in Figure 6.1 and Figure 6.2, respectively. The short circuit current density for the secondary winding of the transformer (J_{sc}) is equal to the overall rated current density (J_r) or the rated current over the cross sectional area of the winding (I_r /A), divides by the short circuit percent impedance (%Z_{sc}) (Galloway & Mulkey, 2004).

$$J_{sc} = \frac{I_r / A}{\%Z_{sc}} = \frac{J_r}{\%Z_{sc}} \tag{6.5}$$

Meanwhile, the first initial winding temperature is 105 °C (378 K) which corresponded to the sum of the maximum permissible ambient temperature and the temperature rise allowed for the winding insulation system of the transformer (IEC60076-5, 2000). The calculation was done in steps with the fault duration (t) was taken at 0.1 second interval until it reached the maximum allowable period of 2 seconds. The results are presented in Table 6.3.

Table 6.3: Winding temperatures by heat balance equation after short circuit

Total Short Circuit Duration (s)	**Initial Winding Temperature (K)**	**Resistivity (nΩ-m)**	**Specific Heat Capacity (J/Kg-K)**	**New Winding Temperature (K)**
0.1	378.0000	23.0012	394.4659	379.6401
0.2	379.6401	23.1300	394.7703	381.2882
0.3	381.2882	23.1945	394.9217	382.9402
0.4	382.9402	23.3235	395.2231	384.6002
0.5	384.6002	23.4527	395.5224	386.2681
0.6	386.2681	23.5173	395.6713	387.9399
0.7	387.9399	23.6466	395.9677	389.6197
0.8	389.6197	23.7760	396.2620	391.3074
0.9	391.3074	23.8408	396.4084	392.9991
1.0	392.9991	23.9704	396.6997	394.6987
1.1	394.6987	24.1001	396.9890	396.4063
1.2	396.4063	24.1650	397.1330	398.1179
1.3	398.1179	24.2949	397.4194	399.8374
1.4	399.8374	24.4250	397.7039	401.5649
1.5	401.5649	24.5551	397.9864	403.3004
1.6	403.3004	24.6202	398.1269	405.0398
1.7	405.0398	24.7506	398.4066	406.7873
1.8	406.7873	24.8810	398.6843	408.5427
1.9	408.5427	25.0126	398.9602	410.3061
2.0	410.3061	25.0769	399.0974	412.0735

6.2.3 Calculation on a conventional transformer

The calculations for both methods were based on the parameters provided by the supplier of the conventional transformer. The results were almost identical, as shown in Table 6.2 and Table 6.3. The outcomes were utilized to justify the computational methods. The short circuit temperature values for the two approaches after the 2 seconds period were also well below the permissible 250°C (523 K) as described in the standard (IEC60076-5, 2000). The calculated values of 411.9501 K for the first approach and 412.0735 K for the other approach indicated that the cross sectional area of the winding was sufficient when it comes to the short circuit condition. The data from the two tables are graphically shown in Figure 6.3.

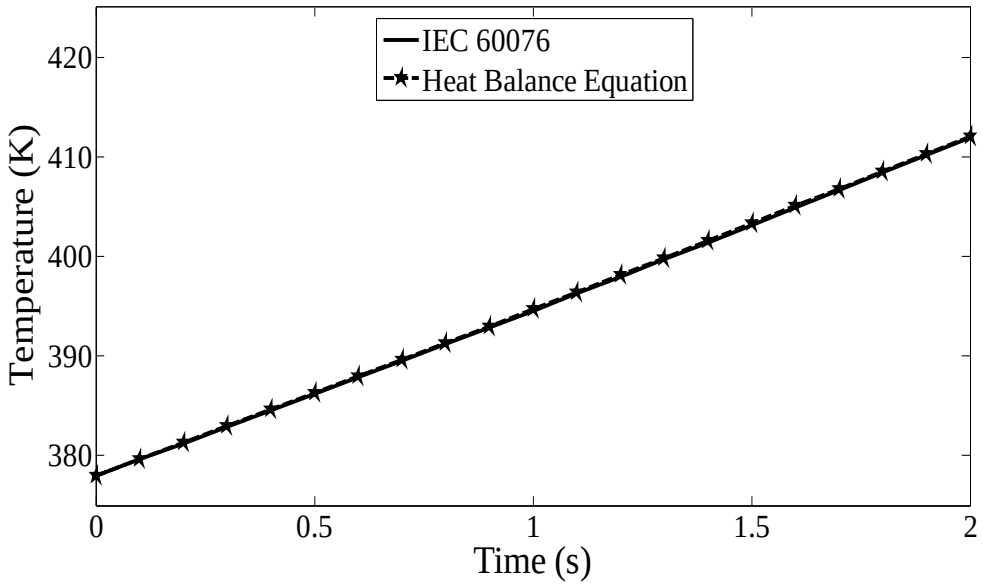

Figure 6.3: Comparison of the calculated temperature rise in the secondary winding

The resistance growth for the affected phase of the secondary copper winding can be developed through the calculation from equation (6.2). The temperature-resistance relationship for the second calculation method of the conventional transformer is shown

in Figure 6.4. The graph shows that the resistance of the copper winding will increase when the temperature rise. In this case, the temperature of the winding was increased because of the application of the short circuit current. The temperature can also rise due to other circumstances such as an increase in the network loading. However, the resistance growth of the winding will be much lower compared to the one from the short circuit current.

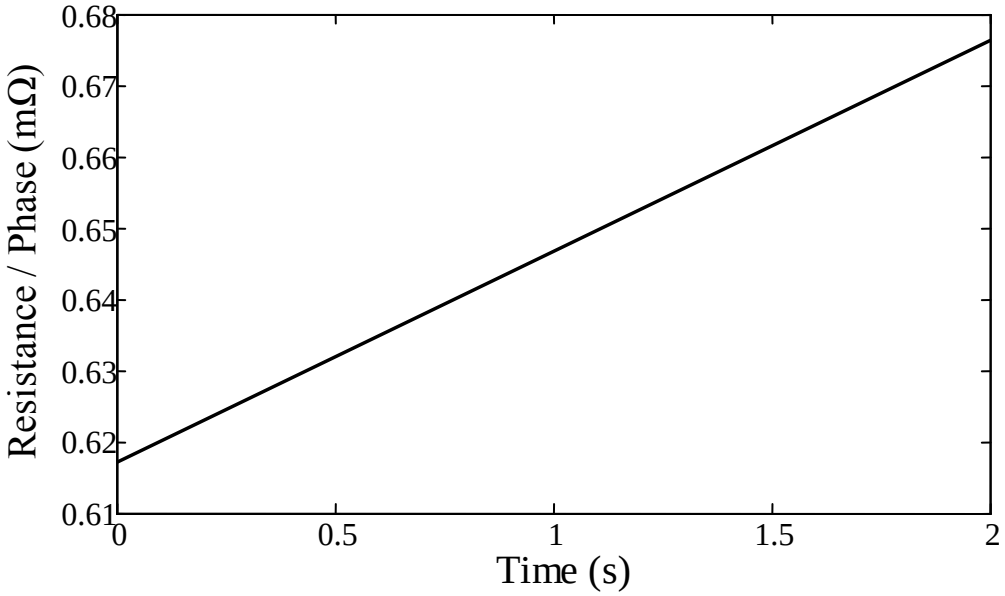

Figure 6.4: Resistance growth in the secondary winding during short circuit

6.2.4 Application of the calculated fault current values

The short circuit current density was calculated using equation (6.5) in the heat balance equation. The equation requires the values of the rated current of the winding (I_r), the short circuit impedance (Z_{sc}), and the cross-sectional area of the winding (A). The first two information can normally be acquired from the transformer name plate. However, the cross-sectional area of the low voltage winding would require further advice from the manufacturer.

Another alternative to compute the short circuit current density is by acquiring the short circuit current to be experienced by the transformer and then dividing the value with the cross sectional area of the transformer winding. Various type of faults have been discussed in chapter 5. The fault currents based on the type of faults at different fault locations were calculated and shown in the previous chapter. Since the three phase fault will normally produce the highest short circuit currents, the values were utilized for this analysis. The near end (0.1 m) and far end (100 m) fault currents for the conventional transformer, i.e 27.51 kA and 5.64 kA, respectively, were used and compared to observe the thermal effect in the winding conductor. The temperature rises for the two seconds period were calculated using equation (6.4). The results are presented in Table 6.4.

The data from the table shows that a greater short circuit current will contribute to a higher temperature rise in the winding conductor. The graphical comparison between the two fault currents applied to the transformer using the heat balance equation and the highest average temperature attained by the winding through the standard calculation in IEC60076 with the short circuit current of 28.06 kA is shown in Figure 6.5.

Table 6.4: Temperature rises from the calculated short circuit current values

Total Short Circuit Duration (s)	**Winding Temperature (K)**	
	I_{sc} = 27.51 kA (Near End)	**I_{sc} = 5.64 kA (Far End)**
0	378.0000	378.0000
0.1	379.5807	378.0670
0.2	381.1690	378.1339
0.3	382.7612	378.2009
0.4	384.3610	378.2678
0.5	385.9647	378.3348
0.6	387.5759	378.4017
0.7	389.1948	378.4687
0.8	390.8175	378.5356
0.9	392.4479	378.6027
1.0	394.0822	378.6699
1.1	395.7240	378.7370
1.2	397.3736	378.8041
1.3	399.0269	378.8712
1.4	400.6880	378.9383
1.5	402.3567	379.0054
1.6	404.0293	379.0726
1.7	405.7095	379.1397
1.8	407.3975	379.2068
1.9	409.0893	379.2739
2.0	410.7888	379.3410

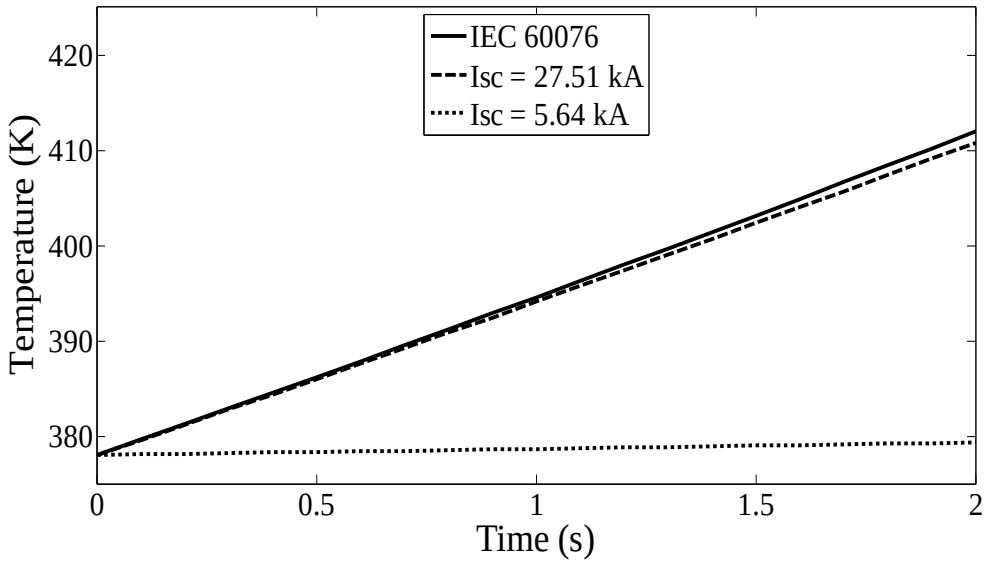

Figure 6.5: Comparison of the temperature rise at the two fault current conditions

The graph shows that the near end fault current provided a significant increase in the winding temperature. The temperature rise was almost to the highest average temperature calculated using the IEC standard. Meanwhile, for the far end fault current, the temperature rise was not as significant compares to the former.

6.2.5 Application of the dynamic asymmetrical fault current values

The Ohm's Law stated that if the voltage remains constant, when the impedance increases, the fault current decreases. The fault calculation at various location in the previous chapter has provided the evidence. However, this does not take into account the dynamics of alternative current (a.c.) electrical system. A fault is a sudden event which requires the electrical system some time to adapt. This transient response will only last for a very short time and may take less than one cycle or few milliseconds.

The impedance in AC electrical system has two components which are the resistance (r) and the reactance (x). The resistance is a measure on how hard it is for the current to flow through the material. Under normal operating condition, the current will flow through a material having resistance and the heat will be transferred from the material to the surrounding. Meanwhile, the reactance depends on two components, i.e. inductance and system frequency. The inductance is a reflection on how hard it is to change the current. All conducting materials have some inductance, but a good example is a coil of wire. The system frequency around the world is fixed at either 50 or 60 Hz, depending on the geographic location of the eletrical system. Therefore, the reactance is basically dependent upon the inductance.

The voltage and current in a linear a.c. electrical system are sinusoidal. A pure resistive system will have both the voltage and the current in phase. Meanwhile, a pure reactive system will have the voltage leading the current by 90^0. When a fault occurs, the current waveform is no longer a sinusoidal waveform. Instead, the waveform is now the sum of a symmetrical sinusoidal waveform and a decaying exponential. The summation value will cause the current to have a much larger value than the sinusoidal waveforme alone. The waveform is called the asymmetrical current because it does not have symmetry above and below the time axis. The asymmetrical short circuit current waveform can be broken down into two components, i.e., a unidirectional (d.c.) component and a symmetrical alternating (a.c.) component. The d.c. component exponentially decays to zero, while the envelope of the symmetrical a.c. component eventually decays to a constant amplitude sine wave in the steady-state. The rate of exponential decay (or time constant) of the d.c. component is related to the short circuit *x/r* ratio, where *x* and *r* are the equivalent reactance and resistance at the fault location, respectively.

The actual waveform of the asymmetrical short circuit current is not easy to predict because it depends on the actual time in the voltage cycle waveform when the fault occurs. However, the largest fault current value can be acquired when the fault occurs at the point when the voltage is zero. Therefore, the asymmetrical fault current will depend solely on the x/r ratio and the magnitude of the symmetrical fault current. The peak asymmetrical short circuit current can be calculated using the following equation.

$$I_{sc(peak-asymmetrial)} = k \cdot I_{sc(symmetrical)} \tag{6.6}$$

The peak asymmetrical short circuit current can be converted to the rms value by dividing it with square root of two. The *k* factor is also called the asymmetry factor and is given by

$$k = \sqrt{2} \cdot \left\{ 1 + \exp\left[-\left(\theta + \frac{\pi}{2} \right) \cdot \frac{r}{x} \right] \cdot \sin\theta \right\} \tag{6.7}$$

$$\theta = \tan^{-1}\left(\frac{x}{r} \right) \tag{6.8}$$

where *r* is the resistance, *x* is the reactance, and θ is in radians (Vecchio, Poulin, Feghali, Shah, & Ahuja, 2002). The resistance and the reactance values of the winding conductors are used in the calculation to determine the asymmetrical fault current through the conductors. The initial resistance and the reactance values of the low voltage winding are provided in Chapter 4. The *k* value is calculated at every cycle and the resistance value increases as the winding temperature increases. The symmetrical short circuit currents of the near end fault (27.51 kA) and the far end fault (5.64 kA) are used to calculate the asymmetrical fault currents for the two conditions. The asymmetrical short circuit currents for every cycle until reaching the two second duration are shown in Figure 6.6.

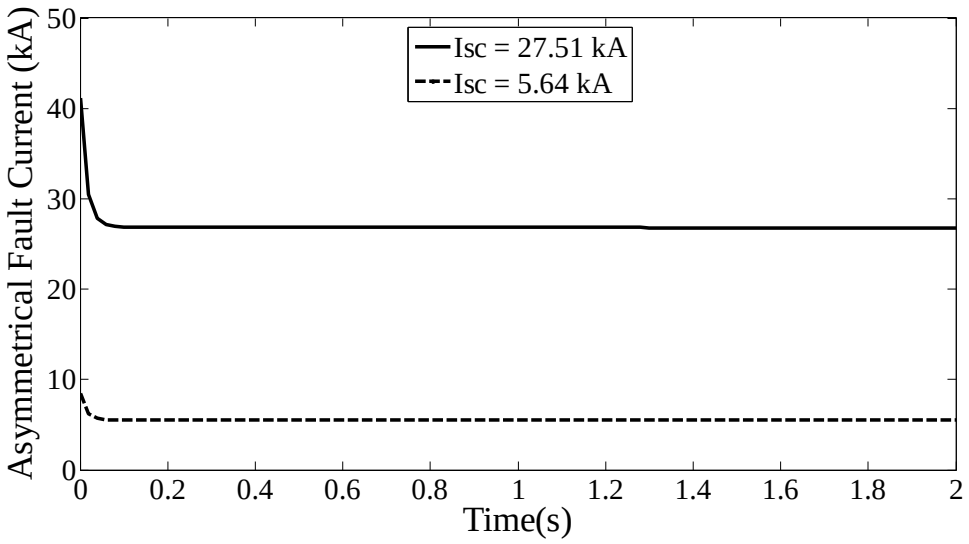

Figure 6.6: Asymmetrical fault current for the conventional transformer

The thermal effect on the secondary winding can be observed by applying the dynamic short circuit current, resistivity, and heat capacity values into the heat balance equation. The temperature rises of the secondary winding due to the two short circuit conditions compare to the standard IEC calculation are depicted in Figure 6.7. The values are expected to increase at the first few cycles and decrease at the later stage when compare to the result shown in Figure 6.5. Short circuit current normally takes on the asymmetrical characteristic during the first few cycles of duration before decaying to the steady state of the symmetrical fault.

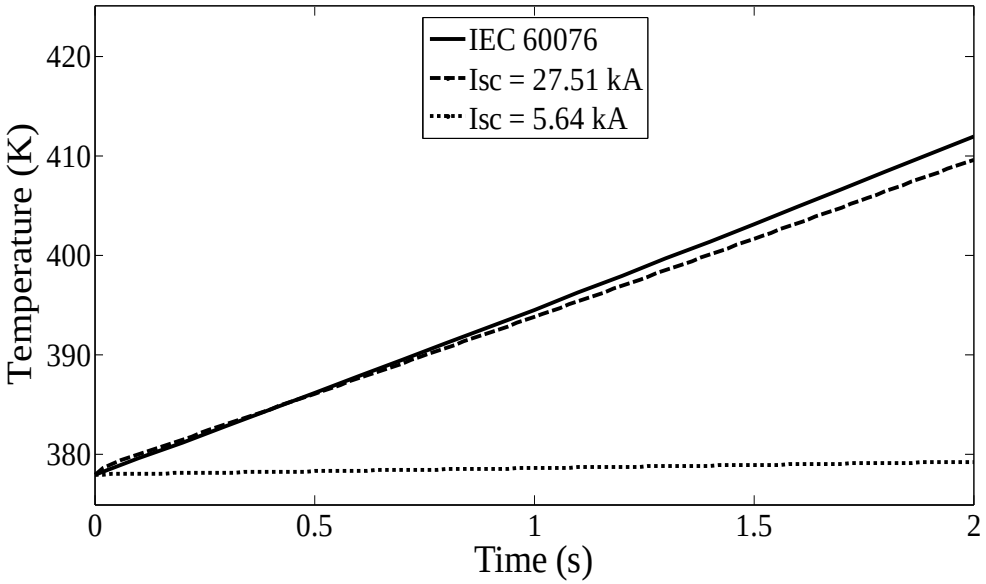

Figure 6.7: Dynamic temperature rise for the two fault conditions

The consideration of the x/r ratio is very important in performing the short circuit current calculation. The higher the ratio, the higher the asymmetrical fault current. The application in this part of the analysis would be utilized in the next investigation on the thermal effect of the winding conductor due to the short circuit current on the HTS transformer winding.

6.3 Analysis of HTS transformer winding

The following step of the analysis is to investigate the thermal effects in the secondary winding of the HTS transformer during a short circuit event. However, the structure of the HTS secondary winding conductor needs to be understood prior to going further into the analysis. This is significant in order to anticipate what the winding conductor will be actually undergoing during the period. The structure for the HTS winding conductor to be explained is based on a baseline design this study is working on (Kalsi, 2008).

6.3.1 Architectural design

The HTS conductors are built up into a continuously transposed cable. These conductors are very thin and fragile tapes. The superconducting layer is a very thin layer of a special ceramic material implanted on a Hastelloy substrate and enclosed by copper plating. The architectural structure is shown in Figure 6.8 where the overall thickness is only about 0.1 mm. Any substantial lateral bending cannot be tolerated because it will damage the superconducting layer. Special methods are employed to assemble the conductor and produce the cable.

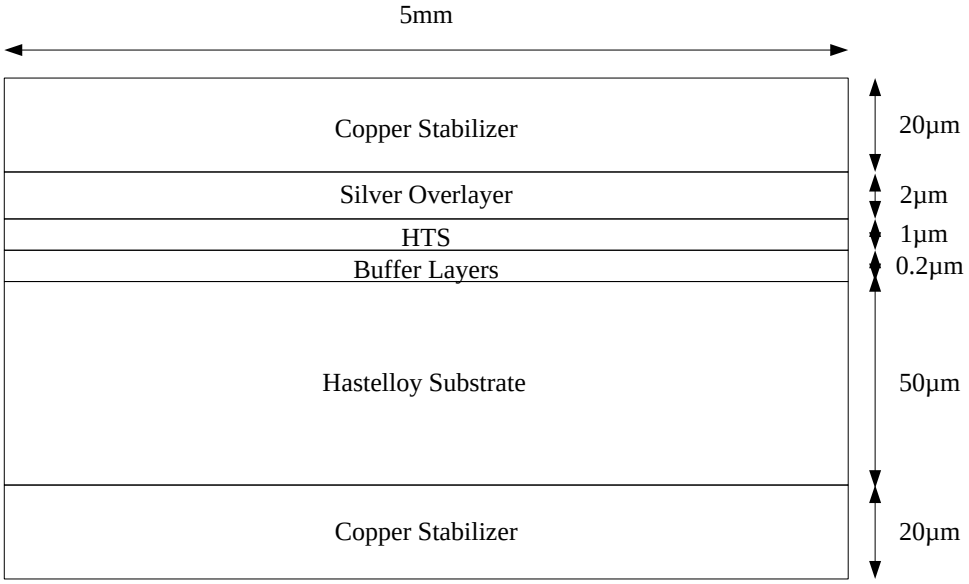

Figure 6.8: Structure of the HTS Winding Conductor

In this part of the study, it was assumed that the short circuit current would be shifted to the copper stabilizer layer after the occurrence of the fault. Another research study also applied the same assumption in its analysis that the fault current will be shifted to the stabilizing layer (Staines *et al.*, 2012). The superconductor should not be damaged if the fault duration can be reduced to an acceptable period. Since the copper layer would take

over the duty of transmitting the short circuit current, the next step was to observe its characteristics in withstanding the situation.

6.3.2 Thermal effects on the existing design

After the short circuit, the temperature of the conductor is expected to rise due to heat from excessive current. Particular attention was focused on the specific heat capacity of copper. The specific heat capacity of copper as a function of temperature was presented in Figure 6.2. Meanwhile, the resistivity of copper with respect to temperature was provided previously in Figure 6.1.

Applying the same computation steps in the heat balance equation in (6.3) and (6.4) as for the conventional transformer, the analysis on the HTS transformer was carried out. The reactance value for the HTS transformer was provided in Chapter 4. The value can also be acquired through per unit (p.u.) calculation method as shown in Table 6.5 in which the winding was limited by the 0.05 p.u. leakage reactance. Meanwhile, the resistance was based on that of copper stabilizer layer.

Table 6.5: Reactance value as per unit calculation

Parameters	**Calculation & Values**
Power, S_{base}	1000000 VA
Voltage, V_{base}	415 V
Current, I_{base}	$\frac{S_{base}}{V_{base}} = 2410\,A$
Impedance, Z_{base}	$\frac{V_{base}^2}{S_{base}} = 0.1722\,\Omega$
Per Unit Leakage Reactance, $X_{p.u.}$	0.05
Low Voltage Reactance, X_{LV}	$Z_{base} \cdot X_{p.u.} = 0.0086\,\Omega$

The heat balance equation (6.4) was applied with all the parameters acquired to calculate the temperature rise during the fault condition. These additional parameters are presented in Table 6.6. The transformer was not expected to be able to withstand the required 2 second period as per IEC standard. Therefore, instead of 2 second duration as for the conventional transformer, the observation for the HTS transformer was only focused on the first 1 second period. The temperature was expected to grow faster compared to that of conventional transformer due to the very much smaller cross sectional area of the copper stabilizer compares to that of conventional winding which should contribute to higher resistance value for the fault current to flow through.

Table 6.6: Parameters for thermal effect calculation of the HTS transformer

Parameters for Low Voltage Winding	**HTS Transformer**
Cross Sectional Area per strand (A), mm^2	5.00 × 0.04
Number of Strands	17
Length (l), m	23
Copper Density (d), kg/m^3	8960
Short Circuit Impedance (Z_{sc}), %	5.00

A huge current will run through the HTS winding conductor when a short circuit occurs. After a short moment, the superconductor will be expected to quench. The quench response time is normally of the order of few milliseconds. The second generation (2G) superconductor wires will normally quench at currents around 2-3 times the critical current (Xie, Tekletsadik, Hazelton, & Selvamanickam, 2007). For the calculation, the short circuit was simulated to occur at t = 0 and the superconductor winding was assumed to quench at the response time of t_o. These situations are depicted in the following figures on the temperature rise of various stabilizer types and thicknesses.

The temperature rises for the copper stabilizer of the HTS winding over short circuit duration are shown in Figure 6.9. Three values of short circuit current were employed in the calculations. Two of them were the near end fault current (27.55 kA) and the far end fault current (5.67 kA) which were based on the calculations on the circuit presented in Chapter 5. The other value was a predicted peak current in the LV winding (14.30 kA) based on 0.14 p.u. fault impedance (Staines *et al.*, 2012).

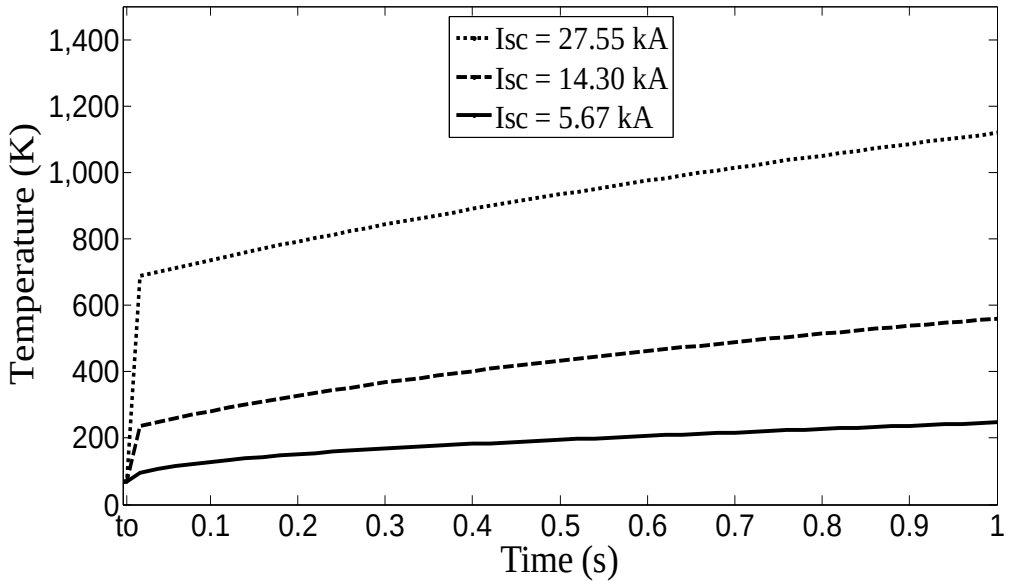

Figure 6.9: Temperature rise in the copper stabilizer of the HTS secondary winding

From the graph, it can be observed that the HTS transformer would not be able to withstand the required 2 second short circuit condition, as prescribed in IEC 60076 standards (IEC60076-5, 2000). The temperature of the copper layer in the winding would rise beyond its withstand value. The fault current would damage the winding if it was permitted to run during the period. Therefore, the HTS transformer, with the present design parameters as shown in Table 6.6, needs to be isolated sooner.

From the calculation and observation, there are two key elements that influence the curve of the graph. One is the value of short circuit currents and the other one is the size of conductor's cross-sectional areas. The higher the fault current or the smaller the cross-sectional area, the steeper the curve of the graph that causes the knee point, before the temperature rise becomes more stable. The low fault current of 5.67 kA would let the transformer to experience a temperature lower than the room temperature of 298 K even after 1 second compared to the medium fault current of 14.30 kA, which would experience the rise to the room temperature only after 0.1 second. Any higher fault

current value would bring about a potentially damaging temperature to the transformer winding.

Several alternatives can be considered to address the problem. The first is to limit the fault duration for the HTS transformer to less than 2 seconds withstand time. The set up would require re-coordination of protection system in the power network. Consensus between the relevant parties, especially the users or utilities, must be obtained since the duration is quite short for the distribution system. This option is currently being considered. The other option is to look into the design parameters of the HTS winding conductors. The temperature rise can be reduced by using thicker copper stabilizer or replacing it with stainless steel or high resistance alloy strip. Further analysis needs to be carried out in order to ensure that the size and weight advantage of HTS transformer will not be sacrificed and the load loss of the transformer windings should be within the acceptable value or the transformer's load loss rated value.

6.3.3 Thermal effects on various stabilizer thicknesses

Further investigation was carried out for the HTS winding conductor with various copper stabilizer thicknesses. A previous study (Bae, Park, Eom, Seong, & Baik, 2010) has looked at thermal stability of the same winding conductor architecture as the operating current approaches the critical current. The present work, meanwhile, explored the effects on the conductor due to short circuit current which would first rise beyond the critical current but will then subside throughout the fault duration.

Three different copper stabilizer thicknesses, *i.e.*, the original 40 µm, and the alternative 60 and 80 µm, were employed in the analysis. The stabilizer thicknesses were the total thickness of copper in the structure. This means that the 80 µm thickness was made up

of a 40 µm copper layer on each side. The analysis was looking into the temperature rise of the secondary winding for the various copper layer thicknesses during the fault duration. The predicted fault current of 14.30 kA was applied in the computation. The results are shown in Figure 6.10.

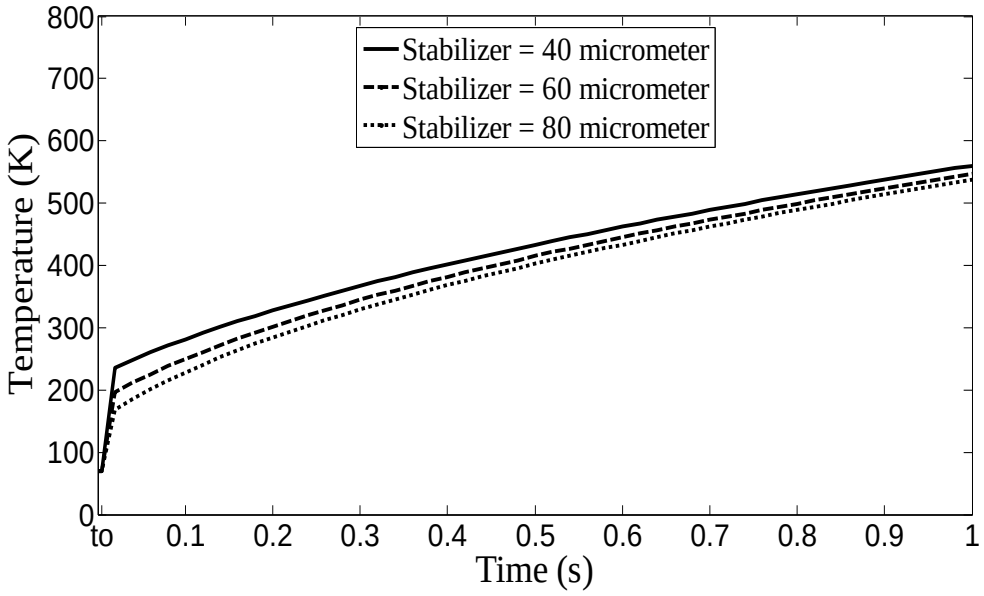

Figure 6.10: Temperature rise for various copper stabilizer thicknesses

The graph shows the temperature rise in the secondary winding due to the short circuit current. The increase was greater with thinner copper stabilizer. However, each conductor would still experience the temperature rise beyond the room temperature limit if allowed to operate until the end of the one second period.

6.3.4 Effects on stabilizer free with thicker silver overlayer

A study was conducted previously (Yazawa *et al.*, 2008) on superconducting yttrium barium copper oxide (YBCO) tapes with ion beam assisted deposition (IBAD) substrate. Parts of the analysis were to investigate short circuit effects on stabilizer free conductors. The construction of the tapes was the same as in Figure 6.8 but without the

copper stabilizer. However, various thicknesses of silver over layer, which dominates the resistance, were applied. In this study, another analysis was carried out on the stabilizer free superconducting wires with silver protective layer of 10, 20 and 30 μm thicknesses instead of the normal 2 μm.

The resistivity and heat capacity of silver at various temperatures are presented in Figure 6.11 and Figure 6.12, respectively. The resistivity data were acquired from cryogenic and room temperature sources (Iwasa, 1994; Jankowski, 2004; Lide, 2003). Meanwhile, the heat capacity tabulated data were gathered also from cryogenic and room temperature sources (Jankowski, 2004; Johnson, 1960; Mills, 1999)

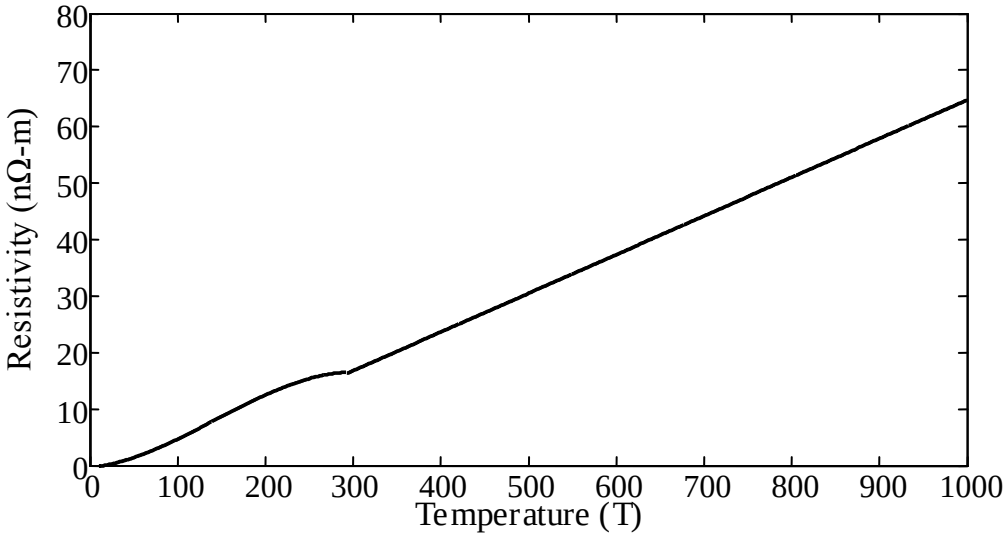

Figure 6.11: Resistivity of silver at various temperatures

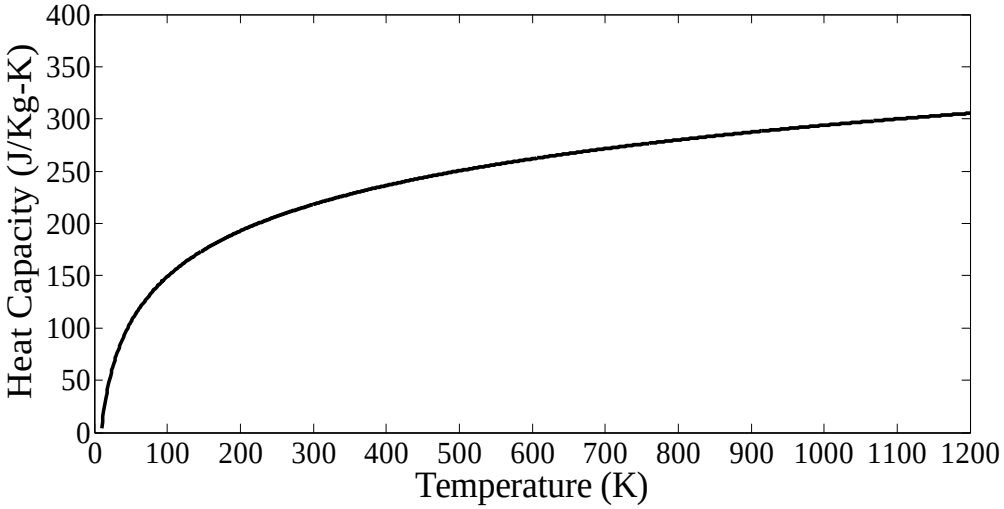

Figure 6.12: Specific heat capacity of silver at various temperatures

The values of the temperature rise for the first 1 second duration are shown in Figure 6.13. The high temperature rises demonstrated that the conductor would not withstand the required 2 seconds period. The values seemed not to improve much even with thicker silver protective layer.

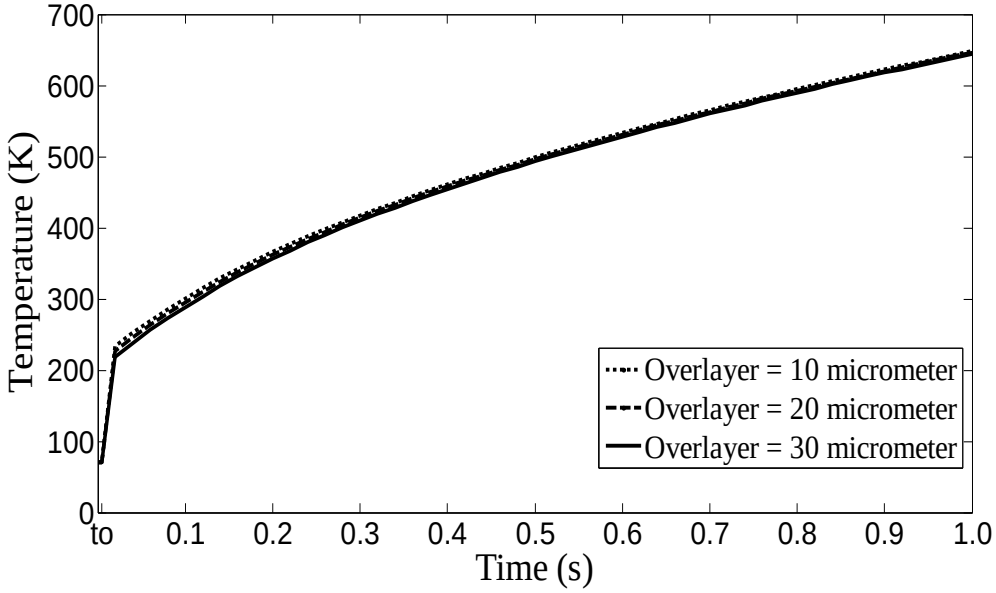

Figure 6.13: Temperature rise for various stabilizer free silver overlayer thicknesses

6.4 Analysis of HTS-FCL transformer winding

Present studies on HTS-FCL transformer are currently investigating varieties of winding conductor architecture to suppress the fault current and protect the transformer. The transformer will operate as a superconducting transformer in steady state condition and as a superconducting fault current limiter in fault condition. This research work has evaluated various HTS conductor designs such as superconductors with high resistance alloy strip, stabilizer free superconductors and hybrid HTS coils (Abdul Rahman, Lie, & Prasad, 2011b). The superconductor wire designs can be simulated with the HTS transformer to observe the thermal effects from short circuit currents.

6.4.1 Options for HTS-FCL winding construction

For the first option, the HTS tape was put in parallel with a resistive conductor for stability and fault handling (Rey *et al.*, 2011). The original design used copper as the parallel conductor to meet the required fault withstands duration. However, the transformer would require the amount of copper nearly as much as a conventional unit in order to meet the standard requirement of 2 seconds duration. A high resistant alloy, stainless steel, is proposed for the co-wound winding conductor to meet the requirement of 2 second fault duration. The original design used co-wound copper which had the disadvantages as the required amount of copper is nearly as much as in a conventional transformer. Therefore, high resistance alloys are being considered as the replacement to reduce the fault current The HTS-FCL wire with high resistance alloy strip is developed as in Figure 6.14. The design presents robust HTS-FCL wire construction that can be insulated on uncomplicated insulating equipment.

The next alternative employs the second generation superconducting tape which operates with low resistivity in superconducting state and high resistivity in normal state (Janowski *et al.*, 2011). The stabilizer free wire must provide high resistance-per-length in normal state at 77 K and also high mechanical strength to withstand the short circuit force. This is very important since the superconductor layer is only about 1 percent of the total thickness of the wire. The wire design construction is as in Figure 6.8 but without the copper stabilizer.

In the other option, a hybrid coil is utilized. The hybrid HTS coil is a combination of limiting and non-limiting coils. The limiting coil is a stabilizer free HTS wire as described in the second alternative. Meanwhile, the non-limiting coil is a surround copper stabilizer HTS wire as applied in the author's preliminary baseline design HTS transformer and shown in Figure 6.8. Both of the HTS coils are connected in series. The hybrid HTS coil using different types of HTS tapes in the low voltage coils is claimed to bring about a higher flexibility for both transformer and current limiter designs by the variation of the length and its ratio between the limiting and non-limiting coils (Kojima *et al.*, 2011).

This investigation focused on the first FCL-HTS wire architectural design mentioned earlier. Several previous studies have worked on this design (Ahn *et al.*, 2007; Du *et al.*, 2010; Tomioka *et al.*, 2011). They were carried out on certain high resistance alloy strips at various thicknesses. The effectiveness of current limiting characteristics in a combination of YBCO tape and cupronickel (C71500) tape was verified *(Tomioka et al.*, 2011). The AC over-current tests beyond the critical current in which the test current was damped with time were conducted. The study was looking into the possibility of stabilizing the power system by improving the function of fault current limiting.

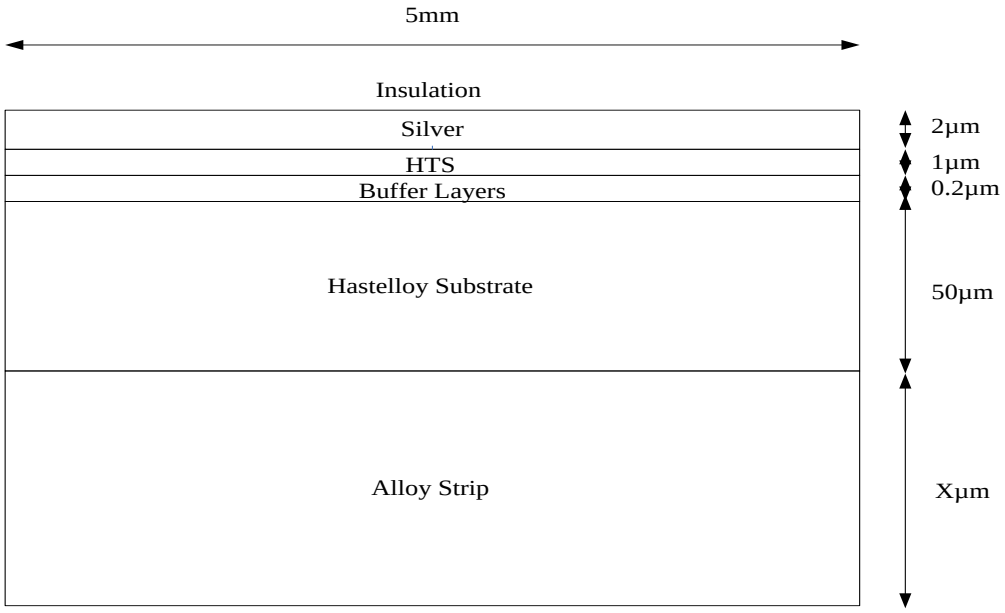

Figure 6.14: HTS wire with high resistance alloy strip

In addition to the first high resistance alloy, stainless steel (SS316L) was also considered for the coated conductor. Over-current characteristics of HTS wire with stainless steel as the stabilizer material were investigated (Ahn *et al.*, 2007). Among the commercialized HTS conductor, the wire was considered at that time by the investigation to be more proper than others for HTS-FCL function. Another study on HTS wire with stainless steel stabilizer (Du *et al.*, 2010) was also conducted by applying a fault current and observing the resistance increase trends. This study indicated that the HTS wire with stainless steel stabilizing layers can have positive effects on the performance of the current-limiting elements.

6.4.2 Analytical approach for conductor with stainless steel stabilizer

In section 6.3, the heat balance equation was applied to calculate the temperature rise in the copper stabilizer of the secondary winding conductor of an HTS transformer. The simulation took into account the structural design of HTS conductor and assumed the

conductor to quench after a short time by the fault current. The calculation also assumed the short circuit current was forced to be diverted from the HTS filaments to the copper stabilizer layers. The fault current generates heat and increases the resistance in the winding. The result shows that the transformer secondary winding conductor can be damaged due to the thermal effect if the fault current is to be allowed for a period of 2 seconds as specified in IEC 60076 standards.

This study investigated a high resistance alloy, stainless steel (SS316L), which has very high resistivity and can be used as a stabilizing metal. Fundamental data for the material such as resistivity and specific heat capacity were gathered for computation in the analysis. The resistivity and heat capacity values for the alloy with respect to temperature are presented in Figure 6.15 and Figure 6.16, respectively. The architectural design of the HTS wire was based on that of in Figure 6.14. Three different short circuit current values were considered in the investigation to observe the performance of the high resistance alloy. The same simulation as for the HTS transformer with copper stabilizer was carried out taking into account the fault current resulted on the short circuit from the network presented in Chapter 5.

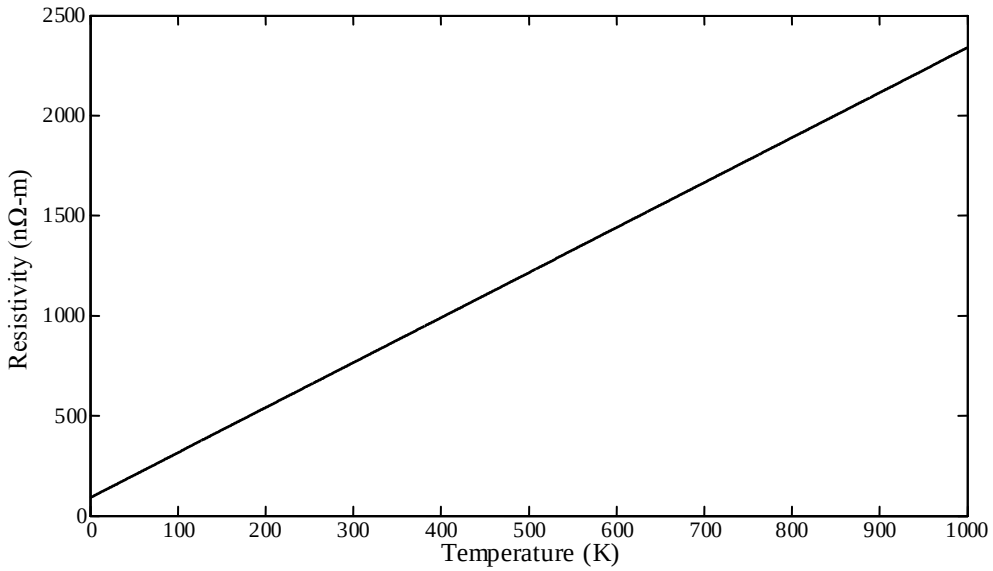

Figure 6.15: Resistivity of stainless steel at various temperatures

The resistivity value of stainless steel at 293 K was used as the reference. At this temperature, the resistivity is 7.496×10^{-7} Ω-m (Ugur, 2006) and the temperature coefficient for resistivity is assumed to be 0.003 (Kuphaldt, n.d.). The resistivity values of the material at other temperatures are calculated based on this reference value. Meanwhile, the values for heat capacity are from several sources (Mann, 1977; Tavassoli, 1995; Touloukian & Ho, 1976).

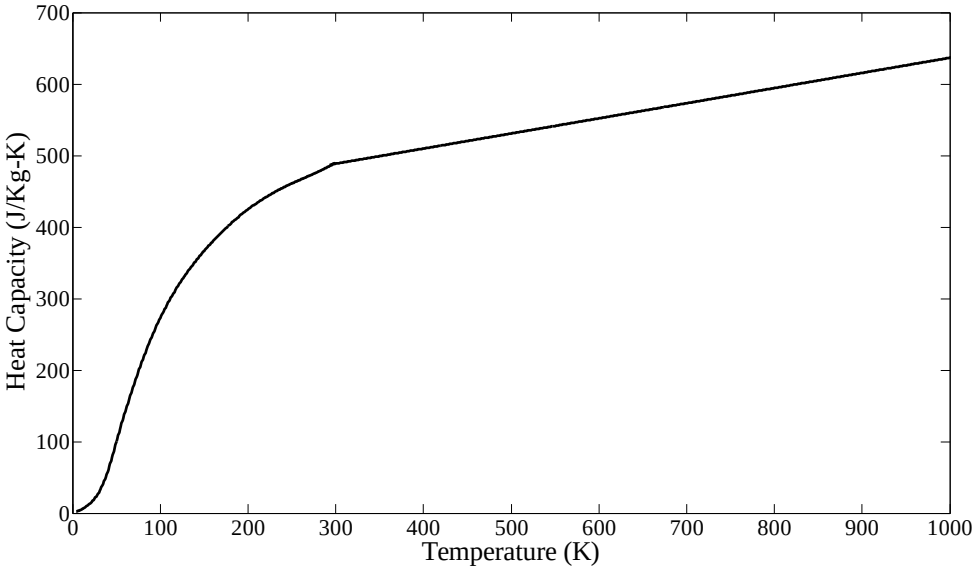

Figure 6.16: Heat capacity of stainless steel at various temperatures

6.4.3 Thermal effects on the stainless steel stabilizer

The results for the calculation of the temperature rise on the winding conductor with stainless steel stabilizer are shown in Figure 6.17. The thickness of the stainless steel stabilizer was the same as the copper stabilizer, *i.e.*, 40 µm. The temperature rises for all the applied short circuit currents were very much lower compare to the conductor with copper stabilizer. The temperature values have not reached the room temperature even after the 1 second period. The results showed on how the HTS-FCL winding conductor was able to withstand the thermal effects of the short circuit currents.

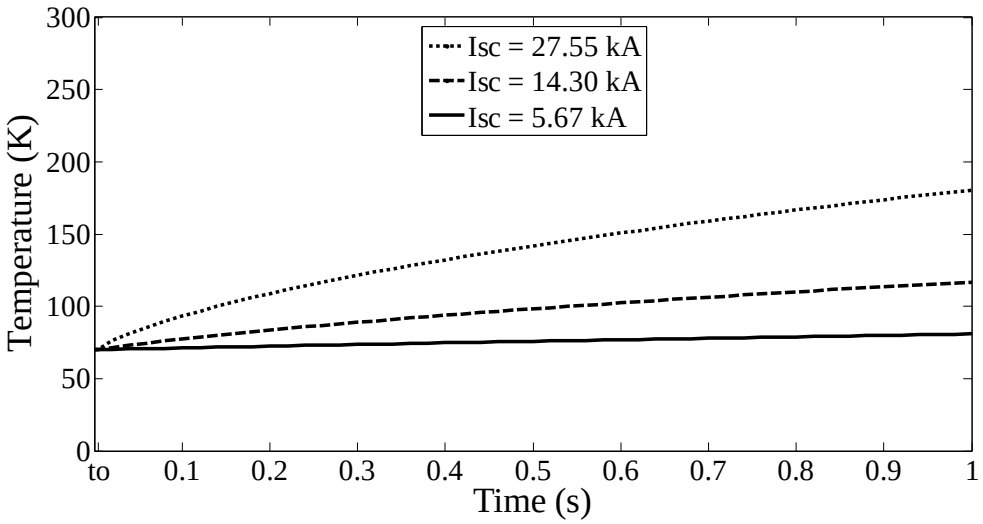

Figure 6.17: Temperature rise in stainless steel stabilizer from the fault currents

The conductor was also simulated with different stabilizer thicknesses. The range of thicknesses investigated was the same as for the copper stabilizer, *i.e.*, 40, 60 and 80 µm. The applied fault current was 14.30 kA, also the same as the previous simulation. The results are presented in Figure 6.18. The temperature rises were found to be identical for all the three stabilizer thicknesses. The finding indicated that there would not be significant differences in term of thermal effect by applying the stainless steel stabilizer within the evaluated thickness range of between 40 and 80 µm.

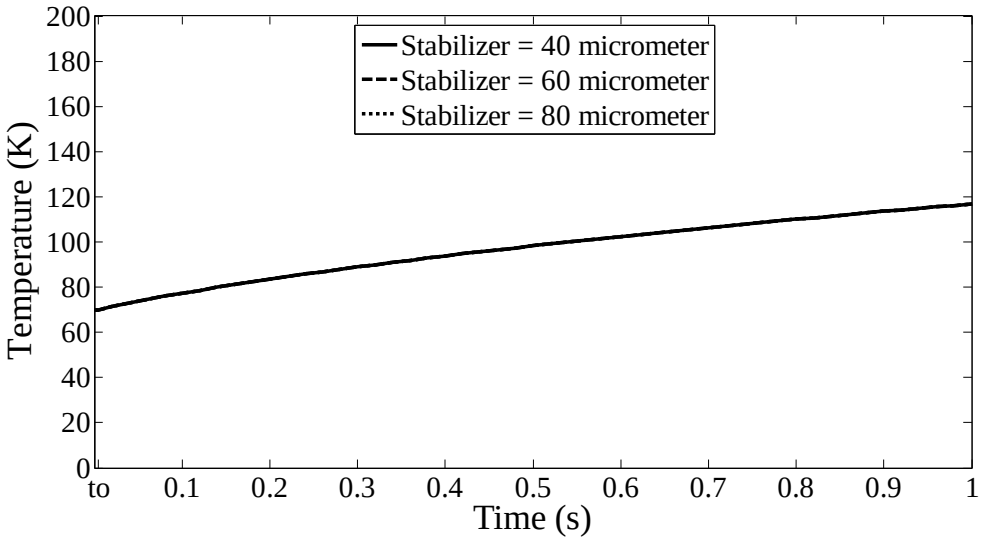

Figure 6.18: Temperature rise for various stainless steel stabilizer thicknesses

6.4.4 Comparison on the performance of the HTS and HTS-FCL conductors

The analysis on copper stabilizer has shown its inability to withstand high fault currents for the duration required by the normal standard. The transformer has to be protected by the protection system sooner in order to avoid any damage to the equipment. Meanwhile, the investigation on stainless steel stabilizer has demonstrated that it was able to endure the thermal effect better than copper.

Figure 6.19 presents the temperature rise in both stabilizers when the 14.30 kA fault current was applied on to the network system. While the temperature for copper went up higher than the room temperature just after 0.1 second, the temperature for stainless steel was still very much lower than the room temperature even after reaching the one second period. The high resistance alloy would be able to provide the HTS-FCL winding conductor the capability to perform as superconducting transformer under normal operating condition and superconducting fault current limiter under short circuit condition.

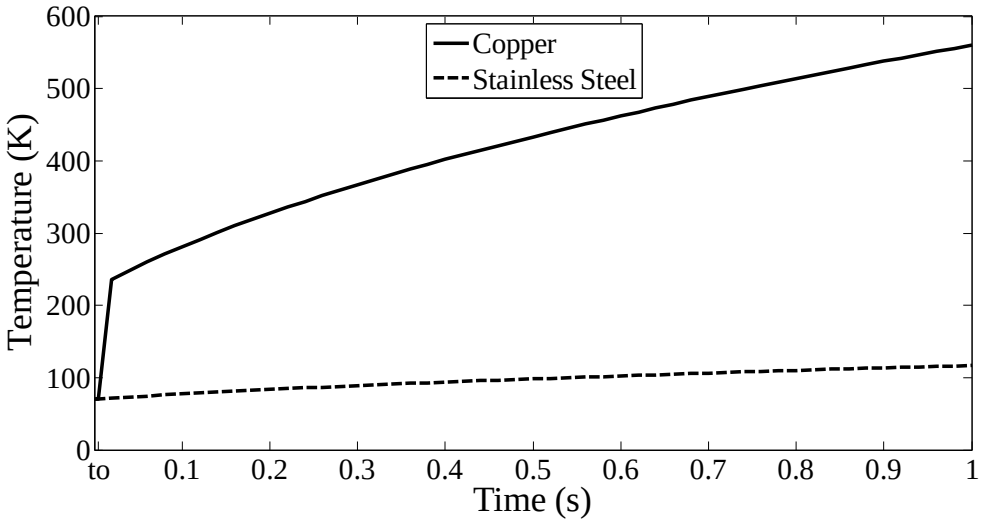

Figure 6.19: Temperature rise in copper and stainless steel stabilizers due to the fault current

6.5 Discussion

An analysis was carried out to determine the thermal effects of short circuit phenomena on an HTS transformer winding. The mathematical model presented enables the estimation of temperature rise developed in the transformer winding during short circuit. The investigation was conducted to observe the findings on HTS wires with various specified copper stabilizer thicknesses and stabilizer free HTS conductors with various specified silver protective layer thicknesses. Further analysis was executed to investigate the outcomes of an HTS-FCL superconductor winding design.

The fault current values applied in the calculation was based on the short circuit at the near end and far end of the line of the power network presented in the previous chapter. The fault current computation included the reactance of the relevant HTS conductor coil of the secondary winding and the resistance of the materials expected to carry the fault current. The heat balance equation was then utilized to calculate the temperature rise in secondary winding. The calculation took into account the structural design of HTS

conductor and assumed the conductor to quench after a short time by the fault current, forced the current to be diverted from the HTS filaments to the stabilizer layers. The fault current generated heat and increases the resistance in the winding. The resistance growth was determined by the temperature-resistance relationship. The specified thicknesses for the relevant conductor layers selected for each analysis in this study were referred to several previously mentioned studies.

The investigation on HTS wire with various copper stabilizer thicknesses showed that the fault current would not be sufficiently suppressed. Thicker stabilizer would allow higher fault current to pass through the winding and this would reduce the temperature rise. The conductor configuration would not permit the HTS transformer to operate as a good fault current limiter. Meanwhile, the results from the heat balance equation calculation showed that the transformer secondary winding with any of the three copper stabilizer thicknesses could still be damaged due to the thermal effect if the fault current was to be allowed for a period of 2 seconds as specified in IEC 60076 standards. Therefore, the protection system would have to be coordinated so that the system would trip in less than 2 seconds. The set up would depend on the transformer withstand temperature and the consensus between the relevant parties.

A short circuit analysis on stabilizer free conductors with various specified silver protective layer thicknesses also suggested the same outcomes. As per analysis on copper stabilizer conductor, the short circuit current was assumed to be diverted to the silver layer which dominates the resistance. Any thickness beneath the specified values would result in better fault current suppression, but the silver layer would not be able to withstand the thermal effect. Moreover, the superconducting wire design configuration without any metal stabilizer would not be easy to handle. The fabrication of a conductor

coil from this conductor would be very complicated to prevent any chemical or mechanical damage.

Further advancement in the technology enables the research and development of HTS-FCL transformer. Several alternatives for HTS-FCL wire have been introduced. Since the architectural design of the wire has been altered, the previous assumption considered in the calculation must be re-established. During the short circuit duration, the HTS-FCL wire will be transformed from superconducting state into normal or high resistance state. In the superconducting state, the short circuit impedance depends only on the reactance. Meanwhile, in the normal state, the resistance of the materials will be the dominant factor. The resistance of the wire will be equal to the equivalent resistance of all the parallel layers in the wire. The resistance value will depend on the resistivity, thickness and cross-sectional percentage of each layer material. However, the analysis of this study focused only on the dominant layer of the conductor.

The winding resistance will eventually increase the impedance of the transformer. Due to the high resistance of the winding in the normal state, the fault current can be suppressed below the permissible value, *i.e.*, the critical current of the superconductor. The restricted short circuit current should generate less heat on the winding. Therefore, the temperature rise and the resistance growth on the HTS-FCL wire should also be reduced. The temperature rises for the stainless steel stabilizer at three different thicknesses throughout the one second short circuit period were presented in the previous section.

The overall performance based on the analysis carried out showed that stainless steel was a good stabilizer or high resistance alloy strip for the HTS-FCL conductor. However, other factors should also be considered when deciding the optimum selection. One of them should be the suitability for the application. This study focused on the

utilization of HTS-FCL conductor on the secondary winding of a distribution power transformer. Therefore, the design of the winding coil and the transformer itself must be taken into consideration in the selection of the type and thickness of the stabilizer. Different applications such as switchgear and fault current limiter should have different considerations for the selection. Another major factor should be the cost of the alloys and the manufacturing process. The economy factor is very critical since the HTS-FCL transformer will not only be compared with the conventional transformer but also with the normal HTS transformer.

CHAPTER 7

CONCLUSIONS

7.1 Summary and conclusions

An analysis was carried out to validate the parameters of a typical HTS transformer design in a distribution feeder and was compared with that of a conventional transformer to demonstrate that the HTS transformer with the set up parameters should be performing as well as a conventional transformer in a normal distribution network. Applying the phase frame calculation method gave eminently satisfactory results. The three-phase impedance and admittance matrices were very useful for the study. The method of solution appeared to be accurate and efficient. This validated the technique for more advanced and complicated circuit designs.

Several evaluations were conducted in the study, *i.e.*, load flow, short circuit, inrush, and thermal effects. These investigation required different analytical methods. The thesis presents step by step approach for each analysis. However, the parameters required for each investigation were not all the same. Conventional transformers have basically established designs. People are still working on optimum designs for HTS transformers.

Development of software for the application of HTS transformer will be possible, but it must be incorporated with several alternative designs of HTS transformer.

Load flow and system losses calculations were carried out on the case study network with the application of both conventional and HTS transformers. The computation provided the actual losses on the line segments. Even though the actual transformer losses would not be available through network modelling, the load loss fraction of the losses could be employed as part of the comparison for the performance of the two transformers. The advantage of using HTS transformer could be observed through the reduction of real power requirement, especially on heavy loading networks.

The sample network with HTS transformer was simulated with different types of short circuit conditions. The calculation provided the fault currents and voltages to be expected on the transformer for each fault classification. Since each utility would have its own electrical network characteristics, the computed short-circuit current and voltage values should fall within the specification set by the utility concerns. The findings from the phase frame method of analysis have led to further investigation on the HTS transformer into various distribution network conditions such as inrush current phenomena toward the transformer primary windings and thermal effects of the short circuit currents toward the secondary windings.

Investigations were carried out to determine the effects of short circuit and inrush current phenomena on the HTS transformer windings. The outcomes on the application of different type of short circuits toward HTS transformer were analysed. Also, the results on the application of inrush current toward the transformer were compared with that of conventional transformers. The short circuit and inrush current patterns were shown to be quite different from each other. The secondary winding was first to experience the larger short circuit current which was cleared in tens of milliseconds.

Meanwhile, the smaller inrush force acted on the energized winding and could last for few seconds. The study demonstrated the expected performance level of the HTS transformers in dealing with short circuit and inrush currents.

The analysis presented in this thesis showed that inrush currents may not be considered dangerous to HTS transformer. The inrush peak values could increase several times the rated current value, but as long as they were below the critical current value, the characteristics of HTS winding would not change. However, precautions have to be taken into the network design because their lengthy existence may unnecessarily overwork the protective equipment such as relays and fuses.

The basic operational principles of conventional and HTS transformers are still the same. The major differences are on the technological advancement of the winding and the insulation. The analysis methods for conventional transformer applied in the investigation are already established and accepted. The evaluation on thermal effects was based on a heat balance equation which was compared and validated with a computational approach from an international standard. The results were found to fall within the expected values or operational ranges.

The mathematical model presented in chapter 6 enables the estimation of temperature rise developed in the transformer secondary winding during the short circuit. Simplifying assumptions made in the computation appear not to significantly affect the model's accuracy. Comparison of the presented model with the ones provided in the IEC 60076 standards was shown and found to be comparable. The calculation on short circuit current even with various copper stabilizer thicknesses showed the normal HTS transformer was unable to withstand the duration of 2 seconds as prescribed in the IEC standards.

The temperature of the secondary winding increased tremendously and increased beyond the allowable limit during the period. Therefore, certain arrangement must be made to isolate the transformer sooner in order to prevent any damage to the transformer and loss of power supply to the customers. The transformer should be limited to fault duration below 2 seconds. Another analysis on winding conductor without metal stabilizer with specified silver protective layer thicknesses also provided the same findings. However, stabilizer free conductor would not be easy to fabricate into a coil.

Development of HTS-FCL transformer should be able to minimize the obstacles due to short circuit current. The fault current would be limited because of high winding resistance in the normal state. The limited fault current would then reduce the increase in heat generated. This circumstance would eventually reduce the growth of the winding resistance. An analysis on a high resistance alloy of stainless steel as the stabilizer metal for HTS-FCL conductor was also carried out. The results showed that the alloy should be able to suppress the fault current to a certain designated level with the right thickness. The alloy was also capable to restrain the temperature rise of the superconductor winding.

7.2 Suggestions for future work

The findings from the inrush current phenomena could establish further investigation on the HTS transformer into various distribution network conditions such as the effects of different switching scenarios. It will also be interesting to investigate further on either both the design and connections of the HTS transformer or the characteristics of the

power network system that will have more influence on the effect towards the resultant inrush current.

The short circuit and inrush current patterns were shown to be quite different from each other. The secondary winding would experience the larger short circuit force earlier and is cleared in tens of milliseconds. Meanwhile, the smaller inrush force would be subjected to the energized winding which can last for longer time (few seconds). It will be beneficial to explore further on how these two forces could weaken the HTS windings electrically and mechanically over a period of time.

The current design of the HTS transformer has been proved not to be able to withstand the specified fault duration established in the current operational standard. This could be a setback with the forthcoming development of HTS-FCL transformer. This study has demonstrated that superconductor winding with stainless steel stabilizer should be able to limit the fault current and suppress the temperature rise from short circuit conditions. Other materials such as cupronickel (C71500) have also been investigated for the same objective. Therefore, further research can be developed to determine the optimum selection of stabilizer metal where other factors such as the application of the HTS-FCL conductor and the economy of the implementation have to be considered.

REFERENCES

Abdul Rahman, M. A., Lie, T. T., & Prasad, K. (2010, October). *Three-phase modeling of HTS transformer in distribution networks.* Paper presented at the meeting of the International Power and Energy Conference, Singapore. doi:10.1109/IPECON.2010.5697133

Abdul Rahman, M. A., Lie, T. T., & Prasad, K. (2011a, August). *Modelling of short-circuit and inrush currents of HTS transformer in distribution networks*. Paper presented at the meeting of the Power Systems Computation Conference, Stockholm, Sweden. Retrieved from http://www.pscc-central.org/en/background/papers-from-previous-psccs.html

Abdul Rahman, M. A., Lie, T. T., & Prasad, K. (2011b, December). *Performance analysis of HTS transformer with fault current limiting properties on short circuit current*. Paper presented at the meeting of the International Conference on Applied Superconductivity and Electromagnetic Devices, Sydney, Australia. doi:10.1109/ASEMD.2011.6145066

Abdul Rahman, M. A., Lie, T. T., & Prasad, K. (2012). The Effects of Short-Circuit and Inrush Currents on HTS Transformer Windings. *IEEE Transactions on Applied Superconductivity, 22*(2), 5500108. doi:10.1109/TASC.2011.2173571

Ahn, M. C., Park, D. K., Yang, S. E., Kim, M. J., Kim, H. M., Kang, H., et al. (2007). A Study on the design of the stabilizer of coated conductor for applying to SFCL. *IEEE Transactions on Applied Superconductivity, 17*(2), 1855-1858. doi:10.1109/TASC.2007.898130

Amoiralis, E. I., Tsili, M. A., & Kladas, A. G. (2009). Transformer design and optimization: A literature survey. *IEEE Transactions on Power Delivery, 24*(4), 1999-2024. doi:10.1109/TPWRD.2009.2028763

Appleton, A. D. (1994). Near term engineering applications of high T_c superconductors. *Cryogenics, 34*(Supplement 1), 31-38. doi:10.1016/S0011-2275(05)80007-4

Appleton, A. D., & Prothero, D. H. (1998). An introduction to the power applications of superconductivity. In B. Seeber (Ed.), *Handbook of applied superconductivity* (Vol. 2, pp. 1487-1495). Bristol, United Kingdom: Institute of Physics Publishing.

Bae, J. H., Park, H. Y., Eom, B. Y., Seong, K. C., & Baik, S. K. (2010). Thermal stability of YBCO coated conductor with different Cu stabilizer thickness. *Physica C: Superconductivity, 470*(20), 1880-1882. doi:10.1016/j.physc.2010.05.227

Bardeen, J., Cooper, L. N., & Schrieffer, J. R. (1957). Theory of superconductivity. *Physical Review, 108*(5), 1175-1204. doi:10.1103/PhysRev.108.1175

Bednorz, J. G., & Muller, K. A. (1986). Possible high-T_c superconductivity in the Ba-La-Cu-O system [Chemistry and Materials Science]. *Zeitschrift für Physik B Condensed Matter, 64*(2), 189-193. doi:10.1007/BF01303701

Blaugher, R. D., Bhattacharya, R. N., Chen, J., & Padmanabhan, R. (2002). Alternative HTS coated conductors. *Physica C: Superconductivity, 382*(1), 72-79. doi:10.1016/S0921-4534(02)01201-7

Blume, L. F., Camilli, G., Farnham, S. B., & Peterson, H. A. (1944). Transformer magnetizing inrush currents and influence on system operation. *Transactions of the American Institute of Electrical Engineers, 63*(6), 366-375. doi:10.1109/T-AIEE.1944.5058946

Brooks, C. R., Norem, W. E., Hendrix, D. E., Wright, J. W., & Northcutt, W. G. (1968). The specific heat of copper from 40 to 920°C. *Journal of Physics and Chemistry of Solids, 29*(4), 565-574. doi:10.1016/0022-3697(68)90023-1

Carson, J. R. (1926). Wave propagation in overhead wires with ground return. *Bell System Technical Journal, 5*, 539-554. Retrieved from http://www.alcatel-lucent.com/bstj/vol505-1926/articles/bstj1925-1924-1539.pdf.

Chen, M., Donzel, L., Lakner, M., & Paul, W. (2004). High temperature superconductors for power applications. *Journal of the European Ceramic Society, 24*(6), 1815-1822. doi:10.1016/S0955-2219(03)00443-6

Chen, T. H., Chen, M. S., Hwang, K. J., Kotas, P., & Chebli, E. A. (1991). Distribution system power flow analysis - a rigid approach. *IEEE Transactions on Power Delivery, 6*(3), 1146-1152. doi:10.1109/61.85860

Chen, T. H., Chen, M. S., Inoue, T., Kotas, P., & Chebli, E. A. (1991). Three-phase cogenerator and transformer models for distribution system analysis. *IEEE Transactions on Power Delivery, 6*(4), 1671-1681. doi:10.1109/61.97706

Chen, T. H., Chen, M. S., Lee, W. J., Kotas, P., & Van Olinda, P. (1992). Distribution system short circuit analysis - a rigid approach. *IEEE Transactions on Power Systems, 7*(1), 444-450. doi:10.1109/59.141741

Cheon, H. G., Kwag, D. S., Choi, J. H., Min, C. H., Park, T. S., Kim, H. H. (2008). Insulation design and experimental results for transmission class HTS transformer with composite winding. *IEEE Transactions on Applied Superconductivity, 18*(2), 648-651. doi:10.1109/TASC.2008.920837

Ciric, R. M., Fadilha-Feltrin, A., & Ochoa, L. F. (2003). Power flow in four-wire distribution networks - general approach. *IEEE Transactions on Power Systems, 18*(4), 1283-1290. doi:10.1109/TPWRS.2003.818597

Ciric, R. M., Ochoa, L. F., & Padilha-Feltrin, A. (2004). Power flow in distribution networks with earth return. *International Journal of Electrical Power & Energy Systems, 26*(5), 373-380. doi:10.1016/j.ijepes.2003.11.006

Ciric, R. M., Ochoa, R. F., Padilla-Feltrin, A., & Nouri, H. (2005). Fault analysis in four-wire distribution networks. *IEE Proceedings - Generation, Transmission and Distribution, 152*(6), 977-982. doi:10.1049/ip-gtd:20045226

Ciric, R. M., Padilha-Feltrin, A., & Ochoa, L. F. (2004, June). *Power flow in four-wire distribution networks - general approach*. Paper presented at the meeting of the IEEE Power Engineering Society General Meeting, Denver, CO. doi:10.1109/PES.2004.1372952

David, L., Alex, G., Feldmann, D. M., & Anatoly, P. (2001). High-Tc superconducting materials for electric power applications. *Nature, 414*(6861), 368.

Djurek, D., Medunić, Z., Tonejc, A., & Paljević, M. (2001). $PbCO_3 \cdot 2PbO + Ag_2O$ and $PbCO_3 \cdot PbO + Ag_2O$ (PACO) systems: route for novel superconductors. *Physica C: Superconductivity, 351*(1), 78-81. doi:10.1016/S0921-4534(00)01696-8

Donnier-Valentin, G., Tixador, P., & Vinot, E. (2001). Considerations about HTS superconducting transformers. *IEEE Transactions on Applied Superconductivity, 11*(1), 1498-1501. doi:10.1109/77.920059

Du, H. I., Kim, M. J., Kim, Y. J., Lee, D. H., Han, B. S., & Song, S. S. (2010). Study on resistance characteristics and operating conditions of YBCO thin-film wire for current limitation considering insulation layer. *Physica C: Superconductivity, 470*(20), 1666-1670. doi:10.1016/j.physc.2010.05.184

Formisano, A., Marignetti, F., Martone, R., Masullo, G., Matrone, A., Quarantiello, R., et al. (2006). Performance evaluation for a HTS transformer. *IEEE Transactions on Applied Superconductivity, 16*(2), 1501-1504. doi:10.1109/TASC.2006.869552

Funaki, K., Iwakuma, M., Kajikawa, K., Hara, M., Suchiro, J., Ito, T., et al. (2001). Development of a 22 kV/6.9 kV single-phase model for a 3 MVA HTS power transformer. *IEEE Transactions on Applied Superconductivity, 11*(1), 1578-1581. doi:10.1109/77.920079

Galloway, D. L., & Mulkey, D. (2004). Distribution transformers. In J. H. Harlow (Ed.), *Electric power transformer engineering*. Boca Raton, FL: CRC Press LLC.

Garlick, W. G. (1997). Power system applications of high temperature superconductors. *Cryogenics, 37*(10), 649-652. doi:10.1016/S0011-2275(97)00052-0

Giese, R. F., Sheahen, T. P., Wolsky, A. M., & Sharma, D. K. (1992). High-temperature superconductors: their potential for utility applications. *IEEE Transactions on Energy Conversion, 7*(3), 589-597. doi:10.1109/60.148582

Glasson, N., Staines, M., Buckley, R., Pannu, M., & Kalsi, S. (2010). Development of a 1 MVA 3-phase superconducting transformer using YBCO roebel cable. *IEEE Transactions on Applied Superconductivity, 21*(3), 1393-1396. doi:10.1109/TASC.2010.2087738

Golubov, A. A. (1998a). The evolution of superconducting theories. In B. Seeber (Ed.), *Handbook of applied superconductivity* (Vol. 1, pp. 3-36). Bristol, United Kingdom: Institute of Physics Publishing.

Golubov, A. A. (1998b). High-temperature superconductivity. In B. Seeber (Ed.), *Handbook of applied superconductivity* (Vol. 1, pp. 53-62). Bristol, United Kingdom: Institute of Physics Publishing.

Hawsey, R. A., & Christen, D. K. (2006). Progress in research, development, and pre-commercial deployment of second generation HTS wires in the USA. *Physica C: Superconductivity, 445-448*, 488-495. doi:10.1016/j.physc.2006.04.062

Holcomb, J. E. (1961). Distribution transformer magnetizing inrush current. *Transactions of the American Institute of Electrical Engineers: Power Apparatus and Systems - Part III., 80*(3), 697-702. doi:10.1109/AIEEPAS.1961.4501117

Hornfeldt, S. P. (2000). HTS in electric power applications, transformers. *Physica C: Superconductivity, 341-348*(Part 4), 2531-2533. doi:10.1016/S0921-4534(00)01307-1

IEC60076-3. (2000). Power transformers - part 3: Insulation levels, dielectric tests and external clearances in air (2nd ed.): International Electrotechnical Commission.

IEC60076-5. (2000). Power transformers - part 5: Ability to withstand short circuit (2nd ed.): International Electrotechnical Commission.

Ishigohka, T., Uno, K., & Nishimiya, S. (2006). Experimental study on effect of in-rush current of superconducting transformer. *IEEE Transactions on Applied Superconductivity, 16*(2), 1473-1476. doi:10.1109/TASC.2005.864355

Iwakuma, M., Hayashi, H., Okamoto, H., Tomioka, A., Konno, M., Saito, T., et al. (2009). Development of REBCO superconducting power transformers in Japan. *Physica C: Superconductivity, 469*(15-20), 1726-1732. doi:10.1016/j.physc.2009.05.246

Iwasa, Y. (1994). *Case studies in superconducting magnets*. New York, NY: Plenum Press.

Jankowski, J. E. (2004). *Convective heat transfer model for determining quench recovery of high temperature superconducting YBCO in liquid nitrogen* (Master Thesis). Massachusetts Institute of Technology, Cambridge, MA. Retrieved from http://dspace.mit.edu/bitstream/handle/1721.1/30297/61048634.pdf

Janowski, T., Glowacki, B. A., Wojtasiewicz, G., Kozak, S., Kozak, J., Kondratowicz-Kucewicz, B., et al. (2011). Fault current limitation in power network by the superconducting transformers made of 2G HTS. *IEEE Transactions on Applied Superconductivity, 21*(3), 1413 - 1416. doi:10.1109/TASC.2011.2112325

Janowski, T., Kozak, S., Kondratowicz-Kucewicz, B., Wojtasiewicz, G., & Kozak, J. (2007). Analysis of transformer type superconducting fault current limiters.

IEEE Transactions on Applied Superconductivity, 17(2), 1788-1790. doi:10.1109/TASC.2007.898134

Jeehoon, C., Seungwook, L., Sukjin, C., Myungjin, P., Wooseok, K., Jikwang, L., et al. (2008). Conceptual design of a 5 MVA single phase high temperature superconducting transformer. *IEEE Transactions on Applied Superconductivity, 18*(2), 636-639. doi:10.1109/TASC.2008.921309

Jianxun, J., & Xiaoyuan, C. (2008, April). *Development of HTS transformers.* Paper presented at the meeting of the IEEE International Conference on Industrial Technology, Chengdu, China. doi:10.1109/ICIT.2008.4608455

Jin, J. X., Dou, S. X., Liu, H. K., Grantham, C., Zeng, Z. J., Liu, Z. Y., et al. (1997). Electrical application of high T_c superconducting saturable magnetic core fault current limiter. *IEEE Transactions on Applied Superconductivity, 7*(2), 1009-1012. doi:10.1109/77.614678

Johnson, V. (1960). *A compendium of the properties of materials at low temperature (phase II)*. Wright-Patterson Air Force Base, OH: Wright Air Development Division, Air Research and Development Command, United States Air Force.

Jones, H. (2008). Superconductors in the transmission of electricity and networks. *Energy Policy, 36*(12), 4342-4345. doi:10.1016/j.enpol.2008.09.063

Kalsi, S. (2008). *HTS transformer development utilizing IRL's continuously transposed cable (CTC)*: Kalsi Green Power System, LLC.

Kersting, W. H. (2002). *Distribution system modeling and analysis*. Boca Raton, FL: CRC Press LLC.

Kersting, W. H. (2003, September). *The computation of neutral and dirt currents and power losses*. Paper presented at the meeting of the IEEE PES Transmission and Distribution Conference and Exposition, Dallas, TX. doi:10.1109/TDC.2003.1335074

Kersting, W. H. (2004, October). *The computation of neutral and dirt currents and power losses*. Paper presented at the meeting of the IEEE PES Power Systems Conference and Exposition, New York, NY. doi:10.1109/PSCE.2004.1397573

Kersting, W. H. (2006). The modeling and analysis of parallel distribution lines. *IEEE Transactions on Industry Applications, 42*(5), 1126-1132. doi:10.1109/TIA.2006.880897

Kersting, W. H., & Dugan, R. C. (2006, October). *Recommended practices for distribution system analysis*. Paper presented at the meeting of the IEEE PES Power Systems Conference and Exposition, Atlanta, GA. doi:10.1109/PSCE.2006.296364

Kersting, W. H., & Phillips, W. H. (1990, August). *Distribution system short circuit analysis*. Paper presented at the meeting of the Intersociety Energy Conversion Engineering Conference, Reno, NV. doi:10.1109/IECEC.1990.716901

Kersting, W. H., & Phillips, W. H. (1992). Modeling and analysis of rural electric distribution feeders. *IEEE Transactions on Industry Applications, 28*(4), 767-773. doi:10.1109/28.148441

Kersting, W. H., & Phillips, W. H. (1995). Distribution feeder line models. *IEEE Transactions on Industry Applications, 31*(4), 715-720. doi:10.1109/28.395276

Kersting, W. H., & Phillips, W. H. (1996). Modeling and analysis of unsymmetrical transformer banks serving unbalanced loads. *IEEE Transactions on Industry Applications, 32*(3), 720-725. doi:10.1109/28.502187

Kersting, W. H., Phillips, W. H., & Carr, W. (1999). A new approach to modeling three-phase transformer connections. *IEEE Transactions on Industry Applications, 35*(1), 169-175. doi:10.1109/28.740861

Khare, N. (2003). Introduction to high-temperature superconductors. In N. Khare (Ed.), *Handbook of high-temperature superconductor electronics*. New York, NY: Marcel Dekker.

Kim, Y. J., Park, D. K., Yang, S. E., Kim, W. C., Ahn, M. C., Yoon, Y. S., et al. (2010). Analytical design method of high-T_c coated conductor for a resistive superconducting fault current limiter using finite element method. *IEEE Transactions on Applied Superconductivity, 20*(3), 1172-1176. doi:10.1109/TASC.2010.2040385

Kimura, H., Honda, K., Hayashi, H., Tsutsumi, K., Iwakuma, M., Funaki, K., et al. (2002). Test results of a HTS power transformer connected to a power grid. *Physica C: Superconductivity, 372-376*(Part 3), 1694-1697. doi:10.1016/S0921-4534(02)01103-6

Koblischka-Veneva, A., Sakai, N., Tajima, S., & Murakami, M. (2003). YBCO. In D. A. Cardwell & D. S. Ginley (Eds.), *Handbook of superconducting materials* (Vol. 1, pp. 893-945). Bristol, United Kingdom: Institute of Physics Publishing.

Kojima, H., Kotari, M., Kito, T., Hayakawa, N., Hanai, M., & Okubo, H. (2011). Current limiting and recovery characteristics of 2 MVA class superconducting fault current limiting transformer (SFCLT). *IEEE Transactions on Applied Superconductivity, 21*(3), 1401 - 1404 doi:10.1109/TASC.2010.2089413

Kotari, M., & et al. (2010). Development of 2 MVA class superconducting fault current limiting transformer (SFCLT) with YBCO coated conductors. *Journal of Physics: Conference Series, 234*(3), 032070. doi:10.1088/1742-6596/234/3/032070

Kulkarni, S. V., & Khaparde, S. A. (2004). *Transformer engineering - design and practice*. New York, NY: Marcel Dekker, Inc.

Kunzler, J. E. (1961). Superconductivity in high magnetic fields at high current densities. *Reviews of Modern Physics, 33*(4), 501-509. doi:10.1103/RevModPhys.33.501

Kuphaldt, T. R. (n.d.). Temperature coefficient of resistance. Retrieved from http://www.allaboutcircuits.com/vol_1/chpt_12/6.html

Larbalestier, D., Gurevich, A., Feldmann, D. M., & Polyanski, A. (2001). High-T_c superconducting materials for electric power applications. *Nature, 414*(6861), 368-377. doi:10.1038/35104654

Leghissa, M., Gromoll, B., Rieger, J., Oomen, M., Neumüller, H. W., Schlosser, R., et al. (2002). Development and application of superconducting transformers. *Physica C: Superconductivity, 372-376*(Part 3), 1688-1693. doi:10.1016/S0921-4534(02)01102-4

Lide, D. R. (Ed.). (2003). *CRC handbook of chemistry and physics* (84th ed.). Boca Raton, FL: CRC Press.

Liye, X., & Liangzhen, L. (2007). Recent progress of power application of superconductor in China. *IEEE Transactions on Applied Superconductivity, 17*(2), 2355-2360. doi:10.1109/TASC.2007.898160

Maeda, H., Tanaka, Y., Fukutomi, M., Asano, T., Togano, K., Kumakura, H., et al. (1988). New high-T_c superconductors without rare earth element. *Physica C: Superconductivity, 153-155*(Part 1), 602-607. doi:10.1016/0921-4534(88)90727-7

Makram, E. B., Bou-Rabee, M. A., & Girgis, A. A. (1987). Three-phase modeling of unbalanced distribution systems during open conductors and/or shunt fault conditions using the bus impedance matrix. *Electric Power Systems Research, 13*(3), 173-183. doi:10.1016/0378-7796(87)90002-2

Makram, E. B., & Girgis, A. A. (1988). A generalized computer technique for the development of the three-phase impedance matrix for unbalanced power systems. *Electric Power Systems Research, 15*(1), 41-50. doi:10.1016/0378-7796(88)90038-7

Makram, E. B., & Girgis, A. A. (1989). A fault-induced transient analysis of unbalanced distribution systems with harmonic distortion. *Electric Power Systems Research, 17*(2), 89-99. doi:10.1016/0378-7796(89)90041-2

Mann, D. (Ed.). (1977). *LNG materials and fluids* (1st ed.). Boulder, CO: National Bureau of Standards.

Manuel, P., Camescasse, F. X., Coevoet, M., Leitloff, V., Lesur, F., Serres, E., et al. (2002). Prospects for application of high temperature superconductors to electric power networks. *Physica C: Superconductivity, 372-376*(Part 3), 1591-1597. doi:10.1016/S0921-4534(02)01068-7

Masur, L. J., Kellers, J., Pegrum, C. M., & Cardwell, D. A. (2003). Applied properties of superconducting materials. In D. A. Cardwell & D. S. Ginley (Eds.), *Handbook of superconducting materials* (Vol. 1, pp. 27-52). Bristol, United Kingdom: Institute of Physics Publishing.

McConnell, B. W. (2000). Transformers - a successful application of high temperature superconductors. *IEEE Transactions on Applied Superconductivity, 10*(1), 716-720. doi:10.1109/77.828332

McConnell, B. W., Mehta, S. P., & Walker, M. S. (2000). HTS transformers. *IEEE Power Engineering Review, 20*(6), 7-11. doi:10.1109/39.846102

McGowan, F. (1988). New developments in superconducting materials : Implications for the electricity supply industry. *Energy Policy, 16*(5), 506-513. doi:10.1016/0301-4215(88)90050-X

Mehta, S. P., Aversa, N., & Walker, M. S. (1997). Transforming transformers [superconducting windings]. *IEEE Spectrum, 34*(7), 43-49. doi:10.1109/6.609815

Meissner, W., & Ochsenfeld, R. (1933). Ein neuer effekt bei eintritt der supraleitfähigkeit. *Naturwissenschaften 21*(44), 787-788. doi:10.1007/BF01504252

Mills, A. F. (1999). *Heat transfer* (2nd ed.). Upper Saddle River, NJ: Prentice Hall.

Minwon, P., Young-Sik, J., & Kang-Sik, R. (2007). Recent activities of HTS power application in Korea. *International Journal of Applied Ceramic Technology, 4*(3), 217-224. doi:10.1111/j.1744-7402.2007.02135.x

Morandi, A., Trevisani, L., Ribani, P. L., Fabbri, M., Martini, L., & Bocchi, M. (2008). Superconducting transformers: key design aspects for power applications. *Journal of Physics: Conference Series, 97*(1), 012318. doi:10.1088/1742-6596/97/1/012318

Nagasawa, T., Yamaguchi, M., & Fukui, S. (2003). Design study of a high-temperature superconducting transformer. *Electrical Engineering in Japan, 142*(1), 25-31. doi:10.1002/eej.10087

Ochoa, L. F., Ciric, R. M., Feltrin, A. P., & Harrison, G. P. (2005, August). *Evaluation of distribution system losses due to load unbalance*. Paper presented at the meeting of the Power System Computation Conference, Liege, Belgium. Retrieved from http://www.montefiore.ulg.ac.be/services/stochastic/pscc05/papers/fp498.pdf

Oomen, M. P. (2000). *AC loss in superconducting tapes and cables* (Doctoral Thesis). University of Twente, Enschede, The Netherland. Retrieved from http://purl.org/utwente/23468

Pan, S. H., Hudson, E. W., Lang, K. M., Eisaki, H., Uchida, S., & Davis, J. C. (2000). Imaging the effects of individual zinc impurity atoms on superconductivity in $Bi_2Sr_2CaCu_2O_{8+\delta}$. *Nature, 403*(6771), 746-750. doi:10.1038/35001534

Pippard, B. (2003). Historical development of superconductivity. In D. A. Cardwell & D. S. Ginley (Eds.), *Handbook of superconducting materials* (Vol. 1, pp. 5-12). Bristol, United Kingdom: Institute of Physics Publishing.

Reis, C. T., Mehta, S. P., McConnell, B. W., & Jones, R. H. (2001, January). *Development of high temperature superconducting power transformers*. Paper presented at the meeting of the IEEE Power Engineering Society Winter Meeting, Columbus, OH. doi:10.1109/PESW.2001.916880

Reis, C. T., Mehta, S. P., McConnell, B. W., & Jones, R. H. (2002, January). *Development of high temperature superconducting power transformers*. Paper presented at the meeting of the IEEE Power Engineering Society Winter Meeting, New York, NY. doi:10.1109/PESW.2002.984977

Rey, C. M., Duckworth, R. C., Schwenterly, S. W., & Pleva, E. (2011). Electrical AC loss measurements on a 2G YBCO coil. *IEEE Transactions on Applied Superconductivity, 21*(3), 2424-2427. doi:10.1109/TASC.2011.2112324

Schilling, A., Cantoni, M., Guo, J. D., & Ott, H. R. (1993). Superconductivity above 130 K in the Hg-Ba-Ca-Cu-O system. *Nature, 363*(6424), 56-58. doi:10.1038/363056a0

Schmidt, W., Kraemer, H. P., Neumueller, H. W., Schoop, U., Verebelyi, D., & Malozemoff, A. P. (2007). Investigation of YBCO coated conductors for fault current limiter applications. *IEEE Transactions on Applied Superconductivity, 17*(2), 3471-3474. doi:10.1109/TASC.2007.899709

Schwenterly, S. W., McConnell, B. W., Demko, J. A., Fadnek, A., Hsu, J., List, F. A., et al. (1999). Performance of a 1-MVA HTS demonstration transformer. *IEEE Transactions on Applied Superconductivity, 9*(2), 680-684. doi:10.1109/77.783387

Schwenterly, S. W., Mehta, S. P., Walker, M. S., & Jones, R. H. (2002). Development of HTS power transformers for the 21st century: Waukesha Electric Systems/IGC-SuperPower/RG&E/ORNL SPI collaboration. *Physica C: Superconductivity, 382*(1), 1-6. doi:10.1016/S0921-4534(02)01168-1

Shaw, D. (2003). Introduction to section C: High temperature superconductors. In D. A. Cardwell & D. S. Ginley (Eds.), *Handbook of superconducting materials* (Vol. 1, pp. 891-892). Bristol, United Kingdom: Institute of Physics Publishing.

Sheahen, T. P. (1994). *Introduction to high-temperature superconductivity*. New York, NY: Plenum Press.

Sheahen, T. P., McConnell, B. W., & Mulholland, J. W. (2002). Method for estimating future markets for high-temperature superconducting power devices. *IEEE Transactions on Applied Superconductivity, 12*(2), 1784-1789. doi:10.1109/TASC.2002.1020337

Sheng, Z. Z., & Hermann, A. M. (1988). Superconductivity in the rare-earth-free Tl–Ba–Cu–O system above liquid-nitrogen temperature. *Nature, 332*(6159), 55-58. doi:10.1038/332055a0

Short, T. A. (2004). *Electric power distribution handbook*. Boca Raton, FL: CRC Press LLC.

Sissimatos, E., Harms, G., & Oswald, B. R. (2001a). Design rules for high-temperature superconducting power transformers. *Physica C: Superconductivity, 354*(1-4), 23-26. doi:10.1016/S0921-4534(01)00017-X

Sissimatos, E., Harms, G., & Oswald, B. R. (2001b). Optimization of high-temperature superconducting power transformers. *IEEE Transactions on Applied Superconductivity, 11*(1), 1574-1577. doi:10.1109/77.920078

Smith, G. J., Alexander, J. A., Buyrn, A. B., & Alic, J. A. (1989). High temperature superconductivity: Prospects and policies. *Futures, 21*(3), 235-248. doi:10.1016/0016-3287(89)90021-9

Specht, T. R. (1951). Transformer magnetizing inrush current. *Transactions of the American Institute of Electrical Engineers, 70*(1), 323-328. doi:10.1109/T-AIEE.1951.5060409

Staines, M., Glasson, N., Pannu, M., Thakur, K. P., Badcock, R., Allpress, N., et al. (2012). The development of a roebel cable based 1 MVA HTS transformer. *Superconductor Science and Technology, 25*(1), 014002. doi:10.1088/0953-2048/25/1/014002

Sykulski, J. K. (1997, January). *Modelling electromagnetic fields and power losses in high temperature superconductors*. Paper presented at the meeting of the IEE Colloquium on Computer Methods for Material Modelling in Electromagnetics, London, United Kingdom. doi:10.1049/ic:19970360

Tavassoli, A. A. (1995). Assessment of austenitic stainless steels. *Fusion Engineering and Design, 29*, 371-390. doi:10.1016/0920-3796(95)80044-X

Thompson, C. A., Manganaro, W. M., & Fickett, F. R. (1990). *Cryogenic properties of copper*. Boulder, CO: National Institute of Standards and Technology.

Tomioka, A., Otonari, T., Ogata, T., Iwakuma, M., Okamoto, H., Hayashi, H., et al. (2011). AC over-current test results of YBCO conductor for YBCO power transformer with fault current limiting function. *Physica C: Superconductivity, 471*(21-22), 1367-1373. doi:10.1016/j.physc.2011.05.196

Touloukian, Y. S., & Ho, C. Y. (Eds.). (1976). *Thermophysical properties of selected aerospace materials. Part II: Thermophysical properties of seven materials*. West Lafayette, IN: Thermophysical and Electronic Properties Information Center, CINDAS, Purdue University.

Tsai-Hsiang, C., & Wen-Chih, Y. (2001). Analysis of multi-grounded four-wire distribution systems considering the neutral grounding. *IEEE Transactions on Power Delivery, 16*(4), 710-717. doi:10.1109/61.956760

Tsukamoto, O. (2005). Roads for HTS power applications to go into the real world: Cost issues and technical issues. *Cryogenics, 45*(1), 3-10. doi:10.1016/j.cryogenics.2004.06.008

Tsukamoto, O., & Akita, S. (2002). Overview of R&D activities on applications of superconductivity to power apparatuses in Japan. *Cryogenics, 42*(6-7), 337-344. doi:10.1016/S0011-2275(02)00054-1

Ugur, U. (2006). Resistivity of steel. Retrieved from http://hypertextbook.com/facts/2006/UmranUgur.shtml

Vajda, I., Hyde, A., Gyore, A., Nador, G., Trollier, T., Sailer, B., et al. (2011). Slimformer - self-limiting transformer pre-prototype and pilot plant design, construction, and tests. *IEEE Transactions on Applied Superconductivity, 21*(3), 1298-1302. doi:10.1109/TASC.2011.2108251

Vecchio, R. M. D., Poulin, B., Feghali, P. T., Shah, D. M., & Ahuja, R. (2002). *Transformer design principles*. Boca Raton, FL: CRC Press

Weber, C. S., Reis, C. T., Hazelton, D. W., Schwenterly, S. W., Cole, M. J., Demko, J. A., et al. (2005). Design and operational testing of a 5/10-MVA HTS utility power transformer. *IEEE Transactions on Applied Superconductivity, 15*(2), 2210-2213. doi:10.1109/TASC.2005.849614

Wesche, R. (1998). *High-temperature superconductors: materials, properties, and applications*. Boston, MA: Kluwer Academic Publishers.

Wu, M. K., Ashburn, J. R., Torng, C. J., Hor, P. H., Meng, R. L., Gao, L., et al. (1987). Superconductivity at 93 K in a new mixed-phase Y-Ba-Cu-O compound system at ambient pressure. *Physical Review Letters, 58*(9), 908-910. doi:10.1103/PhysRevLett.58.908

Xie, Y. Y., Tekletsadik, K., Hazelton, D., & Selvamanickam, V. (2007). Second generation high-temperature superconducting wires for fault current limiter applications. *IEEE Transactions on Applied Superconductivity, 17*(2), 1981-1985. doi:10.1109/TASC.2007.898186

Yazawa, T., Koyanagi, K., Takahashi, M., Ono, M., Toba, K., Takigami, H., et al. (2008). Superconducting fault current limiter using high-resistive YBCO tapes. *Physica C: Superconductivity, 468*(15-20), 2046-2049. doi:10.1016/j.physc.2008.05.123

Yinshun, W., Xiang, Z., Junjie, H., Huidong, L., Ying, G., Qing, B., et al. (2007). Development of a 630 kVA three-phase HTS transformer with amorphous alloy cores. *IEEE Transactions on Applied Superconductivity, 17*(2), 2051-2054. doi:10.1109/TASC.2007.898162

Zueger, H. (1998). 630 kVA high temperature superconducting transformer. *Cryogenics, 38*(11), 1169-1172. doi:10.1016/S0011-2275(98)00104-0

APPENDICES

Appendix A: List and relevant research outputs

Abdul Rahman, M. A., Lie, T. T., & Prasad, K. (2010, February). *Distribution Network Modeling and Analysis of the Application of HTS Transformer*. Poster presentation of 18th International Superconductivity Industry Summit, Wellington, New Zealand.

Abdul Rahman, M. A., Lie, T. T., & Prasad, K. (2010, October). *Three-phase modeling of HTS transformer in distribution networks.* Paper presented at the meeting of the International Power and Energy Conference, Singapore. doi:10.1109/IPECON.2010.5697133

Abdul Rahman, M. A. (2011, February). *Three-Phase Modelling of HTS Transformer in Distribution Networks*. Oral Presentation at the Engineering Lunchtime Seminar Series (25/02/2011), School of Engineering, Auckland University of Technology, Auckland, New Zealand.

Abdul Rahman, M. A., Lie, T. T., & Prasad, K. (2011, August). *Modelling of short-circuit and inrush currents of HTS transformer in distribution networks*. Paper presented at the meeting of the Power Systems Computation Conference, Stockholm, Sweden. Retrieved from http://www.pscc-central.org/en/background/papers-from-previous-psccs.html

Abdul Rahman, M. A. (2011, November). *Performance Analysis of HTS Transformer with Fault Current Limiting Properties on Short Circuit Current*. Oral Presentation at the Engineering Lunchtime Seminar Series (23/11/2011), School of Engineering, Auckland University of Technology, Auckland, New Zealand.

Abdul Rahman, M. A., Lie, T. T., & Prasad, K. (2011, December). *Performance analysis of HTS transformer with fault current limiting properties on short circuit current*. Paper presented at the meeting of the International Conference on Applied Superconductivity and Electromagnetic Devices, Sydney, Australia. doi:10.1109/ASEMD.2011.6145066

Abdul Rahman, M. A., Lie, T. T., & Prasad, K. (2012). The Effects of Short-Circuit and Inrush Currents on HTS Transformer Windings. *IEEE Transactions on Applied Superconductivity, 22*(2), 5500108. doi:10.1109/TASC.2011.2173571

Abdul Rahman, M. A., Lie, T. T., & Prasad, K. (2012). Modelling and Analysis of Distribution Network with HTS Transformer. Accepted for publication in the *DPC Transactions on Energy and Power Engineering*

Abdul Rahman, M. A., Lie, T. T., & Prasad, K. (2012). Computation of the Thermal Effects of Short Circuit Currents on HTS Transformer Windings. Accepted for publication in the *IEEE Transactions on Applied Superconductivity*

Appendix A1: Conference paper (IPEC 2010)

International Power and Energy Conference,

Singapore.

Three-Phase Modeling of HTS Transformer in Distribution Networks

M. A. Abdul Rahman, T. T. Lie, K. Prasad
Faculty of Designs & Creative Technologies
Auckland University of Technology
Auckland, New Zealand
muhammad.rahman@aut.ac.nz, tek.lie@aut.ac.nz, krishnamachar.prasad@aut.ac.nz

***Abstract* — Transformers utilizing high temperature superconductors (HTS) are considered as a timely invention. The number of power transformers age more than 30 years old and nearing retirement is increasing. If this window of opportunity is not grabbed, there would be great reluctance to replace recently installed highly priced capital asset. Major projects of developing HTS transformers are well making progress in the United States, Europe, Japan, Korea and China which indicate the interest. The efforts must have been appropriately verified through the economic interest of the discounted losses. Consequently, it is very important to develop an understanding of the fundamental HTS transformer design issues that can provide guidance for developing practical devices of interest to the electric utility industry. The parameters of HTS transformer need to be validated before any effort is to carry out to model the behaviour of a distribution network under a range of conditions. The predicted performance and reliability of HTS transformers can then be verified through the network modelling and analysis calculation. The ultimate purpose is to furnish electric utilities precise information as to which HTS transformers work under various applications with greater technical efficiency and proven reliability.**

Keywords – high temperature superconductor; transformer; distribution system; network modelling.

I. INTRODUCTION

The introduction of high temperature superconductors (HTS) in 1986 by Georg Bednorz and Alex Muller [1] has created many new prospects for the practical application of superconductivity in utility power equipment such as transformers, cables, current limiters and so on. The feasibility of HTS transformers has been weighted from perspectives of high performance of the windings and lower cost of refrigeration on basis of advanced HTS wires with high critical current and low AC loss. The load loss generated mostly in the windings is expected to reduce drastically in comparison with copper windings. Meanwhile, the coolant as liquid nitrogen has a function of electrical insulation nearly comparable to insulation oil for conventional transformers. The HTS properties of higher refrigeration reliability and lower refrigeration cost make it achievable to overcome the limitations experienced in the low temperature semiconductor (LTS) transformer designs of the 1970s and 1980s.

The research is developed into several measures starting with the review and assessment of the state-of-the-art of HTS transformer designs and technologies. Then, a set of parameters is built up to represent the HTS transformer that can be correlated with existing distribution network designs and model accordingly under various network conditions. A real distribution network, which is inherently unbalanced, will be modelled while taking into account the three phase models of all the other relevant network components. The ultimate tasks of the study are to establish the distribution network model with the application of HTS transformer in relation to power flow and short circuit analysis and to scrutinize the effects of different switching scenarios towards the network modelling.

II. HTS TRANSFORMER

The discovery by Georg Bednorz and Alex Muller has opened up interest in research and development for the technology and many superconductors have been found since then. The most common high temperature superconductors are $Bi_2Sr_2Ca_2Cu_3O_x$ (Bi-2223), $YBa_2Cu_3O_x$ (Y-123 or YBCO) and $Bi_2Sr_2Ca_1Cu_2O_x$ (Bi-2212). These materials have exhibited a superconducting behaviour at the temperature below 110, 92 and 85K respectively which allow them to be operated in liquid nitrogen. However, the search for superconductivity at higher temperature is still continued [2]. The technical properties of high temperature superconductors are subjects to ongoing research [3]. The basic advantages of high temperature superconductors are relatively high operating temperature and heat capacity. These characteristics allow simple cooling and high stability against disturbances.

Power transformers have evolved little in the last fifty years with the exception of core steel and improvements in insulation. While the fundamental design principles and overall construction techniques have changed little, today's utility power transformer has losses that are less than 0.4% of total rating. Modern power transformers are very reliable, robust equipment which operate under less than perfect environmental conditions from near zero loads to greater than 125% of nameplate for over thirty years under limited human surveillance. Even though protected externally by voltage surge arresters the devices are designed and tested to withstand simulated lightning impulse. While current limiting relaying systems and fuses protect transformers against the high currents induced by short circuit faults, transformer windings must be

The research project is supported by Industrial Research Limited, New Zealand through the Foundation for Research, Science and Technology (FRST) High Temperature Superconductors (HTS) Accelerated Development Transformational Research, Science and Technology (TRST) funding.

designed to survive significant current overloads of 10-20 times normal full load for 1-2 seconds. This requirement insures the mechanical integrity of both the windings and insulation system. The superconducting transformers must be designed and developed to meet these or similar strenuous specifications.

Strong international interest in the development and commercialization of the high temperature superconducting transformer can be observed. Some have estimated that in the year 2020 up to 80% of new power transformers will be using high temperature superconductors instead of copper [4]. The expectations are seem rather high in the power engineering sector. Several studies have been carried out to compare conventional and high temperature superconducting power transformers [5]. The viability of a superconducting transformer is dealt not only with technical points of view but also economical aspects. The conventional copper transformers have been produced for almost a century and have reached physical and technological limits in many aspects. The crucial expectation will be of what cost-effective conditions the overall benefits of a high temperature superconducting transformer can be made higher than that of a conventional copper transformer.

III. DISTRIBUTION NETWORK MODELLING

More and more people have dedicated for the development of modelling and analysis on distribution network. Previously, most advancement has been devoted to large transmission networks and synchronous generators. Various tools are now available for distribution engineers to run power flow studies and simulate loading conditions on the network. Such progression on the analysing tools allows for in-depth studies in short circuit, switching scenarios, losses, etc. The major network components are overhead lines, underground cables, transformers and loads. This paper is looking especially into the transformer and overhead lines in the modelling and analysis.

A. Transformer

Distribution transformers transform transmission or sub-transmission voltage to low voltage from the capacity rating of a few kVA to a few MVA which will be connected to the customer's load. The transformers can either be of a combination of single-phase components or a three-phase unit with normally a no-load tap changer on the high voltage winding. Several types of phase connection are available from the combinations of delta, grounded wye, ungrounded wye, open wye and open delta. The most common connection for a four-wire feeder is the delta-grounded wye. The transformers come in different styles such as pole mounted, ground mounted and cubicle depend on the required rating and field application.

Distribution transformer impedances are normally between the range of 3% and 6%. These low impedances serve better voltage regulation and less voltage flicker for motor starting or the fluctuating loads. However, they raise fault currents on the secondary which result in deeper voltage sags and higher fault current on the primary. The percent impedance can be derived from the triangle with the percentage values of the resistance and inductance.

$$\%Z_t^2 = \%R_t^2 + \%X_t^2 \tag{1}$$

where,

$$\%R_t = \frac{load\ loss}{10 \cdot kVA} = \frac{\Omega_R \cdot kVA}{kV^2} \tag{2}$$

$$\%X_t = \frac{apparent\ watts}{10 \cdot kVA} = \frac{\Omega_L \cdot kVA}{kV^2} \tag{3}$$

Hence, the phase impedance for a three-phase transformer in matrix form,

$$[Zt_{abc}] = \begin{bmatrix} \Omega_R + j\Omega_L & 0 & 0 \\ 0 & \Omega_R + j\Omega_L & 0 \\ 0 & 0 & \Omega_R + j\Omega_L \end{bmatrix} \tag{4}$$

The research study is focusing on three-phase step down distribution transformer models with delta-grounded wye connection. This is a popular connection to serve a four-wire feeder system and to provide service to loads which are primarily single phase [6]. The transformer models are generalized for the connection with other series components of the network such as line segments and voltage regulators. The matrix equations to calculate the voltages and currents at the input point as a function of the voltages and currents at the output point are,

$$[VLN_{abc}]_{in} = [a] \cdot [VLN_{abc}]_{out} + [b] \cdot [I_{abc}]_{out} \tag{5}$$

$$[I_{abc}]_{in} = [c] \cdot [VLN_{abc}]_{out} + [d] \cdot [I_{abc}]_{out} \tag{6}$$

The equation for the voltages at the output point as a function of voltages at the input point and the currents at the output point is also required,

$$[VLN_{abc}]_{out} = [A] \cdot [VLN_{abc}]_{in} + [B] \cdot [I_{abc}]_{out} \tag{7}$$

The voltages are equivalent to line-to-neutral voltages for a delta connection. Meanwhile, for a grounded wye connection, the voltages are the line-to-ground voltages. The currents are the line currents regardless of the types of connection. The connection with relation to voltages is shown in Fig. 1.

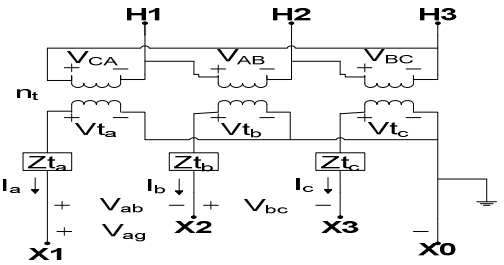

Figure 1. Delta-Grounded Wye Connection With Reference To Voltages

From the above figure, the actual winding turn ratio (n_t) is,

$$n_t = \frac{V(line-to-line)_{rated\ HV}}{V(line-to-neutral)_{rated\ LV}} \tag{8}$$

Meanwhile, the transformer ratio (a_t) is,

$$a_t = \frac{n_t}{\sqrt{3}} = \frac{V(line-to-line)_{rated\ HV}}{V(line-to-line)_{rated\ LV}} \tag{9}$$

From the figure also, the primary line-to-line voltages as a function of the ideal secondary voltages can be defined in matrix form.

$$\begin{bmatrix} V_{AB} \\ V_{BC} \\ V_{CA} \end{bmatrix} = \begin{bmatrix} 0 & -n_t & 0 \\ 0 & 0 & -n_t \\ -n_t & 0 & 0 \end{bmatrix} \cdot \begin{bmatrix} V_{ta} \\ V_{tb} \\ V_{tc} \end{bmatrix} \tag{10}$$

Fig. 2 shows the delta-grounded wye connection with the currents. The polarity marks on the transformer windings are indicated in the figure.

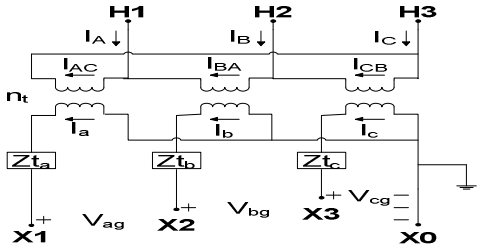

Figure 2. Delta-Grounded Wye Connection With Reference To Currents

By applying Kirchhoff's Current Law, the line currents as functions of the delta currents in matrix form.

$$\begin{bmatrix} I_A \\ I_B \\ I_C \end{bmatrix} = \begin{bmatrix} 1 & -1 & 0 \\ 0 & 1 & -1 \\ -1 & 0 & 1 \end{bmatrix} \cdot \begin{bmatrix} I_{AC} \\ I_{BA} \\ I_{CB} \end{bmatrix} \tag{11}$$

In summary, the generalized matrices for a delta-grounded wye step down transformer to be applied for connection with other network components are,

$$[a_t] = \frac{-n_t}{3} \begin{bmatrix} 0 & 2 & 1 \\ 1 & 0 & 2 \\ 2 & 1 & 0 \end{bmatrix} \tag{12}$$

$$[b_t] = \frac{-n_t}{3} \begin{bmatrix} 0 & 2Z_{tb} & Z_{tc} \\ Z_{ta} & 0 & 2Z_{tc} \\ 2Z_{ta} & Z_{tb} & 0 \end{bmatrix} \tag{13}$$

$$[c_t] = \begin{bmatrix} 0 & 0 & 0 \\ 0 & 0 & 0 \\ 0 & 0 & 0 \end{bmatrix} \tag{14}$$

$$[d_t] = \frac{1}{n_t} \begin{bmatrix} 1 & -1 & 0 \\ 0 & 1 & -1 \\ -1 & 0 & 1 \end{bmatrix} \tag{15}$$

$$[A_t] = \frac{1}{n_t} \begin{bmatrix} 1 & 0 & -1 \\ -1 & 1 & 0 \\ 0 & -1 & 1 \end{bmatrix} \tag{16}$$

$$[B_t] = \begin{bmatrix} Z_{ta} & 0 & 0 \\ 0 & Z_{tb} & 0 \\ 0 & 0 & Z_{tc} \end{bmatrix} \tag{17}$$

Several electrical characteristics of the distribution transformers are required to develop the model. These parameters are significant especially to observe the operational differences between the conventional transformers and the HTS transformers. Those parameters are voltage ratings at the high voltage and low voltage sides, capacity rating of the transformers in kVA, impedance (Z), resistance (R) and reactance (X) in ohms, no load power loss in Watt, and load loss at rated load in Watt. The parameters will be used to calculate the generalized matrices for the modelling of the transformers.

B. Overhead Line

Distribution line models are also generalized for the connection with other series components of the distribution network. The matrix equations are basically the same as (5), (6), and (7). The voltages and currents in term of the types of connection are also similar as explained in the earlier section. The major parameters for modelling of lines segments will be the series impedance and shunt admittance. The accurate measurements are significant prior to carrying out the analysis of a distribution feeder [7], [8].

Several factors must be taken into the measurements for the series impedance. These factors are the resistance of each conductor and the magnetic fields i.e. self inductive reactance and mutual inductive reactance which surround each conductor. In 1926, John Carson developed a set of equations to calculate the self and mutual impedances of power lines which took the ground as the return path of the currents. At this stage, several unknown values have been identified. The Carson's equations were modified to solve the problem regarding the identified unknown values. Approximations are made in deriving the modified equations and therefore, we have the self and mutual impedances of

$$\hat{z}_{ii} = r_i + \pi^2 fG + j4\pi fG\left(In\frac{1}{GMR_i} + 7.6786 + \frac{1}{2} In\frac{\rho}{f} \right) \tag{18}$$

$$\hat{z}_{ij} = \pi^2 fG + j4\pi fG\left(In\frac{1}{D_{ij}} + 7.6786 + \frac{1}{2} In\frac{\rho}{f} \right) \tag{19}$$

where f is the system frequency, ρ is the resistivity of earth, G equals 0.1609344e-3 ohm/mile, r_i is the resistance of conductor i, GMR_i is the Geometric Mean Radius of conductor i and D_{ij} is the distance between conductor i and j.

The modified Carson's equations are used to compute the primitive self and mutual impedances of overhead lines. For the phase frame analytical method, the primitive impedance matrix needs to be converted to a 3x3 phase impedance matrix for connection with other components. Kron reduction method can be applied to achieve the required matrix size [9]. Applying Kirchhoff's Voltage Law, we get in partition form

$$\begin{bmatrix} [V_{abc}] \\ [V_{ng}] \end{bmatrix}_{in} = \begin{bmatrix} [V_{abc}] \\ [V_{ng}] \end{bmatrix}_{out} + \begin{bmatrix} [\hat{z}_{ij}] & [\hat{z}_{in}] \\ [\hat{z}_{nj}] & [\hat{z}_{nn}] \end{bmatrix} \cdot \begin{bmatrix} [I_{abc}] \\ [I_n] \end{bmatrix} \tag{20}$$

Since the neutrals are grounded, V_{ng} values will be zero. Solving the equation will provide the phase impedance matrix as,

$$[z_{abc}] = [\hat{z}_{ij}] - [\hat{z}_{in}] \cdot [\hat{z}_{nn}]^{-1} \cdot [\hat{z}_{nj}] \quad (21)$$

Hence, the final phase impedance matrix,

$$[z_{abc}] = \begin{bmatrix} z_{aa} & z_{ab} & z_{ac} \\ z_{ba} & z_{bb} & z_{bc} \\ z_{ca} & z_{cb} & z_{cc} \end{bmatrix} \quad (22)$$

On the other hand, the shunt admittance calculation will include the conductance and capacitive susceptance of the line. However, the conductance is normally very small and ignored. The general application applied in Carson's equations is also employed in the calculation of the shunt capacitance. The self and mutual potential coefficients are acquired.

$$\hat{P}_{ii} = \frac{1}{2\pi\varepsilon} q_i In \frac{S_{ii}}{RD_i} \quad (23)$$

$$\hat{P}_{ij} = \frac{1}{2\pi\varepsilon} q_j In \frac{S_{ij}}{D_{ij}} \quad (24)$$

where ε is the permittivity of the medium, q_i and q_j are the charge densities on conductor i and j respectively, S_{ii} and S_{ij} are distance from conductor i to its own image and the image of conductor j respectively, RD_i is the radius of conductor i and D_{ij} is the distance between conductor i and j. The primitive potential coefficient matrix in partition form,

$$[\hat{p}_{primitive}] = \begin{bmatrix} \begin{bmatrix} \hat{P}_{ij} \\ \hat{P}_{nj} \end{bmatrix} & \begin{bmatrix} \hat{P}_{in} \\ \hat{P}_{nn} \end{bmatrix} \end{bmatrix} \quad (25)$$

Again, since the neutral is grounded, the matrix can be reduced by using the Kron reduction method to acquire the 3x3 phase potential coefficient matrix,

$$[P_{abc}] = [\hat{P}_{ij}] - [\hat{P}_{in}] \cdot [\hat{P}_{nn}]^{-1} \cdot [\hat{P}_{nj}] \quad (26)$$

The capacitance matrix is the inverse of the potential coefficient matrix.

$$[C_{abc}] = [P_{abc}]^{-1} \quad (27)$$

And, the phase shunt admittance matrix,

$$[y_{abc}] = 0 + j\omega[C_{abc}] \quad (28)$$

Fig. 3 shows the three phase distribution overhead line model. The generalized matrices for the line are developed from the model of the phase impedance matrices and the phase admittance matrices deliberated earlier.

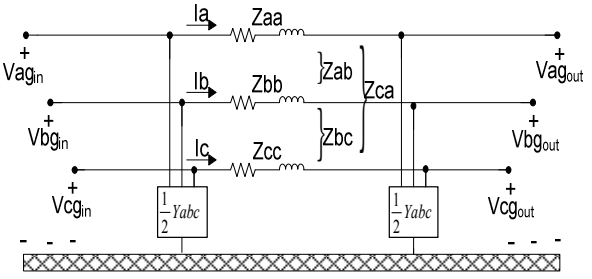

Figure 3. Three-Phase Distribution Line Segment

Applying KVL and KCL to the line segment, we get the condensed equations for the generalized matrices of overhead line segments,

$$[a_l] = [U] + \frac{1}{2}[z_{abc}] \cdot [y_{abc}] \quad (29)$$

$$[b_l] = [z_{abc}] \quad (30)$$

$$[c_l] = [y_{abc}] + \frac{1}{4}[y_{abc}] \cdot [z_{abc}] \cdot [y_{abc}] \quad (31)$$

$$[d_l] = [U] + \frac{1}{2}[y_{abc}] \cdot [z_{abc}] \quad (32)$$

$$[A_l] = [a]^{-1} \quad (33)$$

$$[B_l] = [a]^{-1} \cdot [b] \quad (34)$$

The critical steps in the analysis are to determine the actual phasing of the lines and the correct spacing between conductors. Several parameters are significant in the calculation for the modelling of overhead lines. They are voltage rating, type of insulation, conductor size, phase connection, spacing between conductors (including neutral conductor), distances between conductors and ground level, Geometric Mean Radius of the conductors, diameter of the conductors and resistance of the conductors. These parameters are used to calculate the generalized matrices for the modelling of the overhead lines.

IV. ANALYZING TECHNIQUE

The evaluation of distribution power network can be well distinguished from that of transmission for its unbalanced loading characteristic [10], [11]. The main contributing features for the analysis are the unequal single-phase loads and the inequilateral conductor spacing either for overhead lines or underground cables. The conventional power flow and short circuit programs which are implemented in the transmission network studies would not be adequate. Those programs are based on balanced network where the single-phase equivalent system is employed. For the distribution network assessment, three-phase modelling for the major power components must be applied. In the analysis, the distribution feeder will have to be mapped with the required information such as location, distance, rating and connection. Furthermore, the electrical characteristics of all the major components will also have to be acquired for the network evaluation.

A. Power Flow Analysis

The power flow analysis is applied to determine the normal steady-state operating condition of the network under study. Various output can be obtained from the analysis such as voltage magnitudes and angles at all nodes in the network, power flow and power loss in each line segment and total network power input and power losses. However, information such as three-phase voltages at the substation and complex power of all the loads and the load models should be made available prior to conducting the analysis. Ladder iterative technique is employed for the analysis. KVL and KCL are utilized to determine the node voltages and the line currents respectively. Nevertheless, the technique has to be adjusted to

suit the radial system characteristic and nonlinear feature of the distribution network. The load currents are instead calculated by the conjugate of complex power loads over the node voltages. The forward and backward sweep or the iteration will be continued until the difference between the calculated and the specified voltage at the source meet the acceptable tolerance.

The unbalanced three-phase distribution network can be divided into series components and shunt components. The series components are transformers, overhead lines, underground cables and voltage regulators. The components are connected in terms of generalized matrices through the input and output voltages and currents as defined in general equations (1), (2) and (3). Meanwhile, the shunt components are spot loads, distributed loads and capacitor banks. The spot loads and the capacitor banks are placed at nodes while the distributed loads are uniformly distributed along overhead lines or underground cables. The real power losses of unbalanced distribution network for overhead lines or underground cables should not be calculated by applying the phase current squared times the phase resistance. The calculation works for balanced transmission network but it would not provide the actual real power loss in the phases. Instead, the computation should be on the difference of the input power minus the output power for each phase of the line segment.

V. CASE STUDY

A. Network Characteristics

A case study was carried out on a simple distribution feeder. The source voltages are balanced three-phase of 11kV line-to-line. The system involves one three-wire delta 11kV and four four-wire wye 415V line-to-line overhead lines with the transformer in-between. The network is shown in Fig. 4.

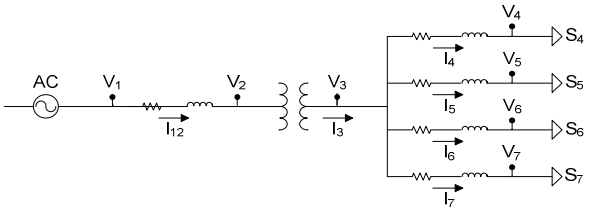

Figure 4. Network of a Simple Distribution Feeder

Conventional and HTS distribution transformers are employed in the network study. The technical information on the HTS transformer is based on a preliminary baseline design the authors are working on. The electrical characteristics for a typical conventional transformer and the under study HTS transformer are shown in Table 1.

TABLE I. TYPICAL ELECTRICAL CHARACTERISTICS OF TRANSFORMERS

Transformer Types	Electrical Characteristics	
	Conventional	*HTS*
kVA Rating, S_{kVA}	1000	1000
Voltage Rating, kV	11/0.415	11/0.415
Load Loss at Rated Load, W_{CU}	7000	1250
No Load Loss, W_{NL}	1400	800
Percent Impedance, Z	5	5
Connection	Δ-Y	Δ-Y

Meanwhile, both overhead line segments use the same 500kcmil 19 strands AAC for phase conductors and the line on the low voltage side use 266.8kcmil 7 strands AAC for neutral conductor. Each line is short and assumed to be only 0.40km for the 11kV side and 0.10km for the low voltage side. The loads for phase a, b and c are assume to be 40kVA each at 0.85, 0.90 and 0.95 lagging power factor respectively.

B. Results

Power flow analysis was carried out on the circuit. After four iterations, the magnitudes of voltage errors are less than the acceptable tolerance of 0.001 per-units. The values of voltages and currents at the respective nodes for both transformers are shown in Table II and Table III.

TABLE II. VOLTAGES AT THE RESPECTIVE NODES

Node Voltage	Phase	Transformer	
		Conventional	*HTS*
V1	a	$6350.85\angle 30^0$	$6350.85\angle 30^0$
	b	$6350.85\angle -90^0$	$6350.85\angle -90^0$
	c	$6350.85\angle 150^0$	$6350.85\angle 150^0$
V2	a	$6347.10\angle 0^0$	$6347.10\angle 0^0$
	b	$6348.60\angle -120^0$	$6348.60\angle -120^0$
	c	$6347.80\angle 120^0$	$6347.80\angle 120^0$
V3	a	$235.91\angle -31^0$	$236.50\angle -31^0$
	b	$236.42\angle -151^0$	$237.04\angle -151^0$
	c	$237.12\angle 89^0$	$237.76\angle 89^0$
V4	a	$229.20\angle -32^0$	$229.80\angle -32^0$
	b	$231.74\angle -153^0$	$232.37\angle -153^0$
	c	$233.85\angle 87^0$	$234.51\angle 87^0$

TABLE III. CURRENTS AT THE RESPECTIVE NODES

Line Current	Phase	Transformer	
		Conventional	*HTS*
I_{12}	a	$25.50\angle -31^0$	$25.43\angle -31^0$
	b	$24.95\angle -145^0$	$24.88\angle -145^0$
	c	$27.63\angle 93^0$	$27.56\angle 93^0$
I_3	a	$698.11\angle -64^0$	$696.27\angle -64^0$
	b	$690.42\angle -178^0$	$688.56\angle -178^0$
	c	$684.12\angle 69^0$	$682.21\angle 69^0$
$I_4 = I_5 = I_6 = I_7$	a	$174.54\angle -64^0$	$174.08\angle 64^0$
	b	$172.61\angle -178^0$	$172.15\angle -178^0$
	c	$171.03\angle 69^0$	$170.55\angle 69^0$

The line-to-neutral voltages at each node are within the acceptable range for the system voltages of 11kV and 415V line-to-line voltages. The currents are dependent on the loads and they are within the 350A rating of the line segments. The results show that the voltage and current values are very close with less than 1% differences.

Power loss calculation can also be carried out in the analysis. The losses are calculated at each network segment. Figures 5, 6 and 7 show the losses at different load conditions for line segments, transformer segment and total network respectively.

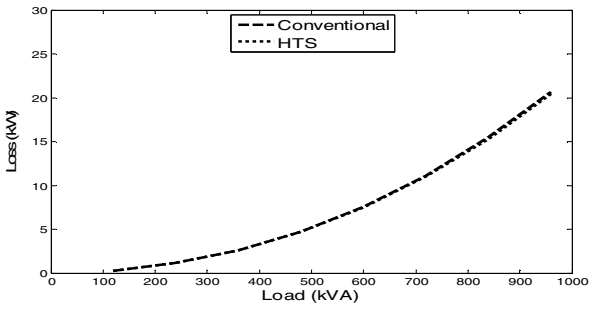

Figure 5. Line Segments Losses at Various Load Conditions

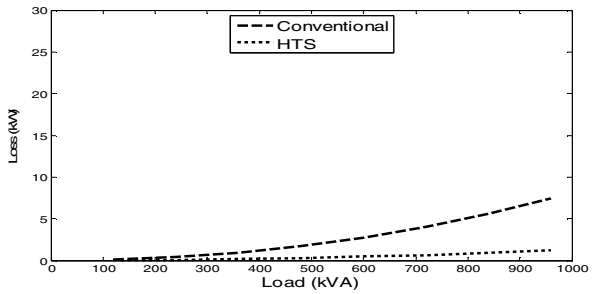

Figure 6. Transformer Segment Losses at Various Load Conditions

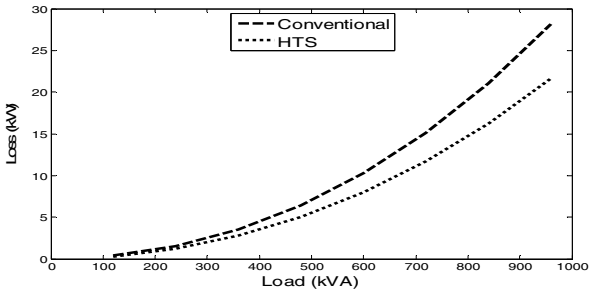

Figure 7. Total Segment Losses at Various Load Conditions

Power losses for the line segments are the correct values for all the three phases. The losses for each phase of the line segments are not computed. Applying both types of transformers would provide very slight differences in the loss values particularly at low and medium load condition. For the transformer segment, the values are not the actual transformer losses. They are more of load losses, and these values are without the winding losses on unloaded condition. No-load losses from hysteresis losses, eddy currents, etc are also not included in the loss values. However, the variations between both transformers particularly at high load condition are very significant to indicate the improvement in energy efficiency.

VI. CONCLUSION

The case study was carried out to validate the parameters of a typical HTS transformer design in a simple distribution feeder. The results were compared with the application of a conventional transformer. The main purpose is to demonstrate that HTS transformer with the set up parameters should be performing as well as conventional transformer in a normal distribution network. Applying the phase frame calculation method gave eminently satisfactory results. The three-phase impedance and admittance matrices are very useful for the study. The method of solution appears to be accurate and efficient. This validates the technique for more advanced and complicated circuit designs.

Load flow and system losses calculation were carried out on the network with the application of both conventional and HTS transformers. The computation provides the actual losses on the line segments. Even tough the actual transformer losses would not be available through network modelling; the load loss fraction of the losses can be employed as part of the comparison for the performance of the two transformers. The advantage of using HTS transformer can be observed through the reduction of real power requirement especially on heavy loading networks.

The findings will establish further investigation on HTS transformer into various distribution network conditions such as short circuits and the effects of different switching scenarios. These analyses will contribute further in predicting the performance and reliability of HTS transformer before the installation in a distribution network system.

REFERENCES

[1] J. G. Bednorz and K. A. Müller, "Possible high-Tc superconductivity in the Ba-La-Cu-O system," *Zeitschrift für Physik B Condensed Matter,* vol. 64, p. 5, June 1986.

[2] D. Djurek, Z. Medunić, A. Tonejc, and M. Paljević, "PbCO3·2PbO+Ag2O and PbCO3·PbO+Ag2O (PACO) systems: route for novel superconductors," *Physica C: Superconductivity,* vol. 351, p. 4, March 2001.

[3] R. Wesche, High-Temperature Superconductors: Materials, Properties, and Applications. Boston/Dordrecht/London: Kluwer Academic Publishers, 1998.

[4] T. P. Sheahen, B. W. McConnell, and J. W. Mulholland, "Method for estimating future markets for high-temperature superconducting power devices," *Applied Superconductivity, IEEE Transactions on,* vol. 12, pp. 1784-1789, 2002.

[5] B. W. McConnell, S. P. Mehta, and M. S. Walker, "HTS transformers," *Power Engineering Review, IEEE,* vol. 20, pp. 7-11, 2000.

[6] W. H. Kersting, "Transformer model test system," in *Transmission and Distribution Conference and Exposition*, 2003, pp. 1022-1026.

[7] W. H. Kersting and W. H. Phillips, "Distribution feeder line models," *Industry Applications, IEEE Transactions on,* vol. 31, pp. 715-720, 1995.

[8] R. M. Ciric, A. P. Feltrin, and L. F. Ochoa, "Power flow in four-wire distribution networks-general approach," *Power Systems, IEEE Transactions on,* vol. 18, pp. 1283-1290, 2003.

[9] E. B. Makram, M. A. Bou-Rabee, and A. A. Girgis, "Three-phase modeling of unbalanced distribution systems during open conductors and/or shunt fault conditions using the bus impedance matrix," *Electric Power Systems Research,* vol. 13, pp. 173-183, 1987.

[10] W. H. Kersting and R. C. Dugan, "Recommended Practices for Distribution System Analysis," in *Power Systems Conference and Exposition,* 2006, pp. 499-504.

[11] E. B. Makram and A. A. Girgis, "A generalized computer technique for the development of the three-phase impedance matrix for unbalanced power systems," *Electric Power Systems Research,* vol. 15, pp. 41-50, 1988.

Appendix A2: Conference paper (PSCC 2011)

Power Systems Computation Conference,

Stockholm, Sweden.

MODELLING OF SHORT-CIRCUIT AND INRUSH CURRENTS OF HTS TRANSFORMER IN DISTRIBUTION NETWORKS

Muhammad Azizi Abdul Rahman, Tek Tjing Lie, Krishnamachar Prasad
Auckland University of Technology
Auckland, New Zealand
muhammad.rahman@aut.ac.nz, tek.lie@aut.ac.nz, krishnamachar.prasad@aut.ac.nz

Abstract – Rapid changes and developments are being witnessed in the transformer design technologies. The phenomenal growth of power systems has put tremendous responsibilities on the industry to supply reliable and cost effective transformers. Advent of High Temperature Superconductor (HTS) materials has increased interest in research and development of superconducting transformers with major projects being carried out worldwide. Among major challenges in the design and development of HTS transformers is the modelling of short circuit and inrush currents the transformer can withstand. The performance and reliability need to be proven to the users and customers. Even though HTS technology is claimed to be more efficient, reliable and eco-friendly, its use must be appropriately verified through proper modelling of the power system network.

Keywords: Modelling, Transformer, Superconductor, Distribution, Short Circuit, Inrush

1 INTRODUCTION

The short circuit design of a transformer is one of the most significant and challenging criteria. Additional generating capacity and interconnections due to the growth of electrical power demand have contributed to an increase in short circuit capacity of power networks. One of the consequences is that the short circuit duty to be undertaken by transformers becomes more severe. The short circuit strength of a transformer is designed to withstand through fault currents due to external short circuit. Any weakness in the strength may result in a mechanical collapse of windings and deformation of clamping structures. The internal faults initiated by the external short circuits may lead to bushing blowouts, tank bursting, fire hazard, *etc*.

Meanwhile, the inrush current of a transformer can be as high as seven to ten times the rated current. Inrush current events are more frequent compared to short circuits. They also last for much longer time compared to short circuits. The users are very anxious about the repeated switching of a transformer. Even though the inrush currents are usually not seriously looked into in the mechanical design considerations, the forces generated due to an extensive number of switching in a day may weaken the winding over a period of time. Their continuous occurrences may lead to winding looseness and subsequent failure.

Consequently, it is important to develop an understanding of the fundamental High Temperature Superconducting (HTS) transformer design issues that can provide guidance for developing practical devices of interest to the electric utility industry. The parameters of HTS transformer need to be validated before any attempt to carry out to model the behaviour of a distribution network under a range of conditions [1]. The predicted performance and reliability of HTS transformers can then be verified through network modelling and analysis. The ultimate purpose is to furnish electric utilities precise information as to which HTS transformers work under various applications with greater technical efficiency and proven reliability.

The modelling is carried out on a three phase distribution feeder which is inherently unbalanced [2]. The technical information on the HTS transformer is based on a preliminary baseline design. The results are subsequently compared with the application of typical conventional transformers.

The sample network with HTS transformer is simulated with different types of short circuit conditions [3]. The calculations provide the fault currents and voltages to be expected on the transformer for each fault classification. Since each utility has its own electrical network characteristics, the computed short circuit current and voltage values should fall within the specification set by the utility concerns.

The findings establish further investigation on HTS transformer into other distribution network conditions. Several factors affecting the inrush phenomena are investigated [4]. The peak values of inrush currents are calculated for every cycle until they reach the primary winding rated current of the

transformer to scrutinize the decay pattern. The analysis will contribute further in predicting the performance and reliability of HTS transformer before the installation in a distribution network system.

2 NETWORK MODEL

A simulation was carried out on a simple distribution feeder. The source voltages are balanced three-phase 11 kV line-to-line. The system involves a short three-wire Delta 11 kV tape screened underground cable and four four-wire Wye 415 V line-to-line overhead lines with the transformer in-between. The network is shown in Figure 1.

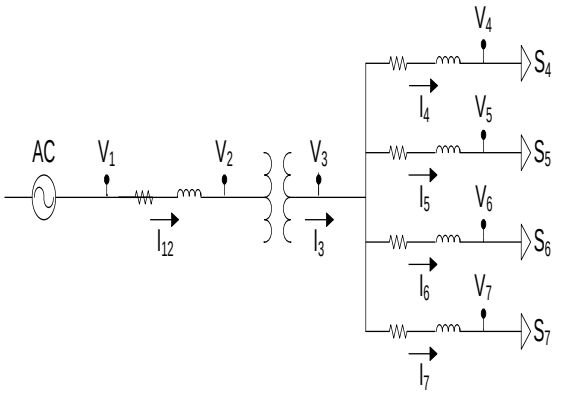

Figure 1: Network of a Simple Distribution Feeder

Conventional and HTS distribution transformers are employed in the network study. The electrical characteristics for a typical conventional transformer are based on those used in distribution system by a utility company. Meanwhile, the technical information on the HTS transformer is based on a preliminary baseline design the authors are working on [5].

The underground cable is a 300 mm^2 three-core tape screened XLPE cable and the overhead line structure is using 500 kcmil 19 strands AAC for both the phase and neutral conductors. Each line is short and assumed to be only 0.40 km for the underground cable and 0.10 km for the overhead lines.

3 SHORT CIRCUIT CURRENT ANALYSIS

The method of applying symmetrical components in the computation of short circuit currents for unbalanced faults is not suitable for distribution feeders that are inherently unbalanced. The unbalanced mutual coupling between the phases will lead to mutual coupling between the sequence components. Also, there will be limitation on the phases between which the faults may occur. Therefore, it is important to look into a suitable method for short circuit analysis of an unbalanced distribution system such as the phase frame method [6].

The model of an unbalanced feeder for short circuit calculation is presented in Figure 2. Short circuits can occur at any of the points shown in the model. The short circuit currents at point 1 are usually acquired from a transmission system short circuit analysis. The resultant short circuit MVAs will help to determine the zero and positive sequence impedances of the equivalent system. The short circuit analysis for points 2, 3, 4 and 5 can then be carried out with the supporting information.

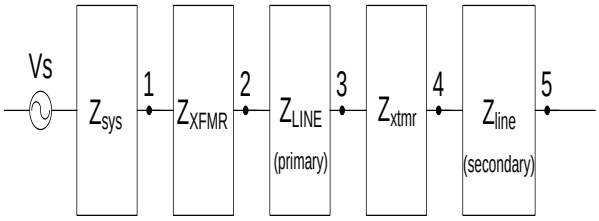

Figure 2: Model of An Unbalanced Feeder for Short Circuit Analysis

The calculation for short circuits at points 2, 3, 4 and 5 can be carried out using the Thevenin equivalent three-phase circuit at the short circuit point. The Thevenin equivalent voltages (E_{th}) are the nominal line-to-ground voltages.

Figure 3 shows the Thevenin equivalent circuit at the faulted node. E_a, E_b and E_c are the Thevenin equivalent line-to-ground voltages. $[Z_{tot}]$ is the Thevenin equivalent phase impedance matrix at the faulted node. Z_f is the fault impedance. I_{fa}, I_{fb} and I_{fc} are the fault currents. V_{ax}, V_{bx} and V_{cx} are the phase voltages (a, b, c) to the point of fault (x). V_{xg} is the voltage from the point of fault (x) to the ground (g).

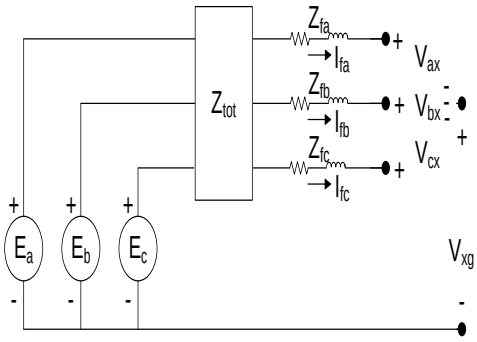

Figure 3: Thevenin Equivalent Circuit at the faulted node

Applying KVL to the Thevenin equivalent circuit, we obtain an equation as follows:

$$\begin{bmatrix} E_a \\ E_b \\ E_c \end{bmatrix} = \begin{bmatrix} Z_{aa} & Z_{ab} & Z_{ac} \\ Z_{ba} & Z_{bb} & Z_{bc} \\ Z_{ca} & Z_{cb} & Z_{cc} \end{bmatrix} \cdot \begin{bmatrix} I_{fa} \\ I_{fb} \\ I_{fc} \end{bmatrix} + \begin{bmatrix} Z_f & 0 & 0 \\ 0 & Z_f & 0 \\ 0 & 0 & Z_f \end{bmatrix} \cdot \begin{bmatrix} I_{fa} \\ I_{fb} \\ I_{fc} \end{bmatrix} + \begin{bmatrix} V_{ax} \\ V_{bx} \\ V_{cx} \end{bmatrix} + \begin{bmatrix} V_{xg} \\ V_{xg} \\ V_{xg} \end{bmatrix} \quad (1)$$

We know the values of $[y]$ (from $[Z_{tot}]$ and $[Z_f]$) and $[E_{abc}]$ (from $[E_a]$, $[E_b]$, $[E_c]$), then the equivalent injected currents is obtained as follows:

$$\begin{bmatrix} I_{pa} \\ I_{pb} \\ I_{pc} \end{bmatrix} = \begin{bmatrix} I_{fa} \\ I_{fb} \\ I_{fc} \end{bmatrix} + \begin{bmatrix} y_{aa} & y_{ab} & y_{ac} \\ y_{ba} & y_{bb} & y_{bc} \\ y_{ca} & y_{cb} & y_{cc} \end{bmatrix} \cdot \begin{bmatrix} V_{ax} \\ V_{bx} \\ V_{cx} \end{bmatrix} + \begin{bmatrix} y_{sa} \\ y_{sb} \\ y_{sc} \end{bmatrix} \cdot [V_{xg}] \quad (2)$$

where,

$$y_{sa} = y_{aa} + y_{ab} + y_{ac} \quad (3)$$

$$y_{sb} = y_{ba} + y_{bb} + y_{bc} \quad (4)$$

$$y_{sc} = y_{ca} + y_{cb} + y_{cc} \quad (5)$$

These equations can be used to simulate all types of short circuits. The known values are the equivalent injected currents (I_{pa}, I_{pb}, I_{pc}), the equivalent admittances (y_{aa}, y_{ab}, y_{ac}, y_{ba}, y_{bb}, y_{bc}, y_{ca}, y_{cb}, y_{cc}) and the sum for each row of the admittances (y_{sa}, y_{sb}, y_{sc}). Meanwhile, the unknown values are the fault currents (I_{fa}, I_{fb}, I_{fc}), phase voltages to the point of fault (V_{ax}, V_{bx}, V_{cx}) and point of fault to ground voltage (V_{xg}). Therefore, the equations can be solved by specifying four additional independent equations which will depend on the type of fault being simulated. The seven equations can be presented in the matrix form,

$$\begin{bmatrix} I_{pa} \\ I_{pb} \\ I_{pc} \\ 0 \\ 0 \\ 0 \\ 0 \end{bmatrix} = \begin{bmatrix} 1 & 0 & 0 & y_{aa} & y_{ab} & y_{ac} & y_{sa} \\ 0 & 1 & 0 & y_{ba} & y_{bb} & y_{bc} & y_{sb} \\ 0 & 0 & 1 & y_{ca} & y_{cb} & y_{cc} & y_{sc} \\ \# & \# & \# & \# & \# & \# & \# \\ \# & \# & \# & \# & \# & \# & \# \\ \# & \# & \# & \# & \# & \# & \# \\ \# & \# & \# & \# & \# & \# & \# \end{bmatrix} \cdot \begin{bmatrix} I_{fa} \\ I_{fb} \\ I_{fc} \\ V_{ax} \\ V_{bx} \\ V_{cx} \\ V_{xg} \end{bmatrix} \quad (6)$$

where # to be filled up depends on the type of fault.

The three-phase fault and three-phase-to-ground fault analysis are carried out on the network with HTS transformer. The circuit is shorted at the far end of the low voltage line segment i.e. 100 m and at the near end i.e. 0.1 m from the transformer. The fault current and voltage values for the two types of faults are presented in Tables 1 and 2 respectively. The fault currents and voltages will be experienced by the HTS transformer if the fault occurred.

Short-Circuit Values	3 Phase Fault	
	Far End	Near End
I_{fa} (kA)	4.88∟-99°	27.93∟-118°
I_{fb} (kA)	5.37∟134°	27.94∟122°
I_{fc} (kA)	4.61∟12°	27.92∟2°
V_{ax} (V)	0	0
V_{bx} (V)	0	0
V_{cx} (V)	0	0
V_{xg} (V)	8.58∟102°	0.05∟92°

Table 1: Currents and Voltages for 3-Ph Faults

Short-Circuit Values	3 Phase to Ground Fault	
	Far End	Near End
I_{fa} (kA)	4.84∟-98°	27.93∟-118°
I_{fb} (kA)	5.35∟133°	27.94∟122°
I_{fc} (kA)	4.68∟12°	27.92∟2°
V_{ax} (V)	0	0
V_{bx} (V)	0	0
V_{cx} (V)	0	0
V_{xg} (V)	0	0

Table 2: Currents and Voltages for 3-Ph to G Faults

The phase-to-phase, two-phase-to-ground and one-phase-to-ground faults are also analysed on the circuit with the HTS transformer. The shorted locations are also the same as for the three-phase and three-phase-to-ground faults. The fault currents and voltages which will be dealt with by the transformer by the two faults are shown in Tables 3, 4 and 5.

Short-Circuit Values	Phase to Phase Fault	
	Far End	Near End
I_{fa} (kA)	4.62∟-73°	24.2∟-88°
I_{fb} (kA)	4.62∟107°	24.2∟92°
I_{fc} (kA)	0	0
V_{ax} (V)	0	0
V_{bx} (V)	0	0
V_{cx} (V)	365∟88°	360∟90°
V_{xg} (V)	122∟-92°	120∟-90°

Table 3: Currents and Voltages for 2-Ph Faults

Short-Circuit Values	2 Phase to Ground Fault	
	Far End	Near End
I_{fa} (kA)	4.64∟-88°	27.88∟-118°
I_{fb} (kA)	4.90∟122°	27.98∟122°
I_{fc} (kA)	0	0
V_{ax} (V)	0	0
V_{bx} (V)	0	0
V_{cx} (V)	295∟88°	240∟90°
V_{xg} (V)	0	0

Table 4: Currents and Voltages for 2-Ph to G Faults

Short-Circuit Values	Phase to Ground Fault	
	Far End	Near End
I_{fa} (kA)	3.27∟-106°	27.91∟-118°
I_{fb} (kA)	0	0
I_{fc} (kA)	0	0
V_{ax} (V)	0	0
V_{bx} (V)	299∟-164°	241∟-150°
V_{cx} (V)	279∟102°	240∟90°
V_{xg} (V)	0	0

Table 5: Currents and Voltages for 1-Ph to G Faults

Each utility has its own electrical network characteristics. For the low voltage distribution network used in the analysis, certain utilities are specifying their transformers to meet the requirement characteristics of maximum service voltage at 1.1 kV (RMS) and low voltage short-circuit current at 31.5 kA. The short-circuit currents and voltages resulting from the analysis fall within the requirement if the transformer is specified according to the characteristics.

4 INRUSH CURRENT ANALYSIS

Inrush current will not take place if a transformer can be switched on at an instance of a voltage wave that corresponds to the actual flux density in the core at the same particular point of time. Nevertheless, the inrush phenomenon is difficult to prevent because the instance of switching cannot be easily controlled and the instance of switching favorable to one phase is not favorable to the other two phases.

When a transformer is energized, the magnetizing inrush current will flow for a short period of time. The phenomenon will continue until the normal flux conditions are established. Under most conditions, the phenomenon will produce little consequences. However, in rare cases, it can impair momentarily the proper operation of the system.

The inrush current can be as high as seven to ten times the rated current [7]. Inrush transients are more frequent than short circuits and they last for few seconds as compared to short circuits which are cleared in tens of milliseconds.

Utilities are very interested in the information on the maximum value and rate of decay of the inrush current. For a three-phase Delta connected primary transformer, each phase is independently connected to the network. The inrush phenomenon corresponding to flux of each phase of this transformer takes place as in the case of a single phase transformer. The phase inrush current will therefore result in the same value as that of the single phase transformer. Meanwhile, the line inrush current will be less severe. The line current is √3 times the phase current under normal condition. In the inrush condition, only one phase which gets switched at the worst instance will be having large inrush current. Therefore, the line inrush current will be almost equal to the phase inrush current.

In the estimation of inrush current magnitude and decay pattern, operating engineers will be looking at the inrush current peak values for the first few cycles and the time after which the inrush current reduces to a value equal to the rated current. Two assumptions are made in the calculations, *viz.,* the transformer is energized at voltage equal to zero and the residual flux is in the same direction as the initial flux change which gives maximum possible value of the inrush current.

In the event, after the core saturation, the inrush current was limited by air core reactance, X_s, which can be calculated by the following equation,

$$X_s = \frac{\mu_o \cdot N^2 \cdot A_w}{h_w} \cdot 2 \cdot \pi \cdot f \tag{7}$$

where,
N = number of turns of excited winding
A_w = area inside the mean turnoff excited winding
h_w = height of energized winding

The angle, θ, at the instance which the core saturates is given by,

$$\theta = K_1 \cos^{-1}\left(\frac{B_s \cdot B_{mp} \cdot B_r}{B_{mp}}\right) \tag{8}$$

where,
B_s = saturation flux density
B_r = residual flux density
B_{mp} = peak value of the designed steady-state flux density in the core
K_1 = correction factor for the saturation angle

The inrush current peak, i_{omax}, for the first cycle is specified as,

$$i_{o\max} = \frac{K_2 \cdot V \cdot \sqrt{2}}{X_s}(1-\cos\theta) \qquad (9)$$

where,
V = rms value of applied alternating voltage
K_2 = correction factor for the peak value

The residual flux density will reduce at the end of the first cycle due to losses in the circuit. It is also a function of damping provided by the transformer losses. The new residual flux density, $B_{r(new)}$, is then presented as,

$$B_{r(new)} = B_{r(old)} - \left[B_{mp} \cdot \frac{K_3 \cdot R}{X_s}(2 \cdot (\sin\theta - \theta\cos\theta)) \right] \qquad (10)$$

where,
R = sum of transformer winding resistance and system resistance
K_3 = correction factor for the decay of inrush

The computations are repeated in order to calculate the peaks of the subsequent cycles. Since the transformers are Delta connected primary, the actual line inrush currents are almost equal to the calculated values.

Two conventional transformers from different manufacturers are put and simulated into the distribution network presented. The computations, based on the previously outlined steps, are carried out for each transformer. The results are shown in Figure 4. Both conventional transformers have the same rated current for HV winding which is represented by Rated I in the figure.

Inrush I1 and Inrush I2 represent the peak inrush currents for the first and second conventional transformers respectively. For the first transformer, the inrush current peak value in the first cycle is about 5 times the rated current of the transformer. It takes about 21 cycles for the current to reduce to the rated value. In the mean time, the inrush current peak value in the first cycle for the second transformer is about 3 times of the rated current. However, the current reaches the rated value after 24 cycles, slightly longer in duration than that of the first transformer.

Figure 5 shows the peak inrush current for the HTS transformer. Inrush I, Rated I and Critical I represent peak inrush current, rated current and critical current respectively. In the first cycle, the peak inrush current is calculated to be only about 2.5 times the rated current of the primary winding. This value is lower than those of the two conventional transformers previously evaluated.

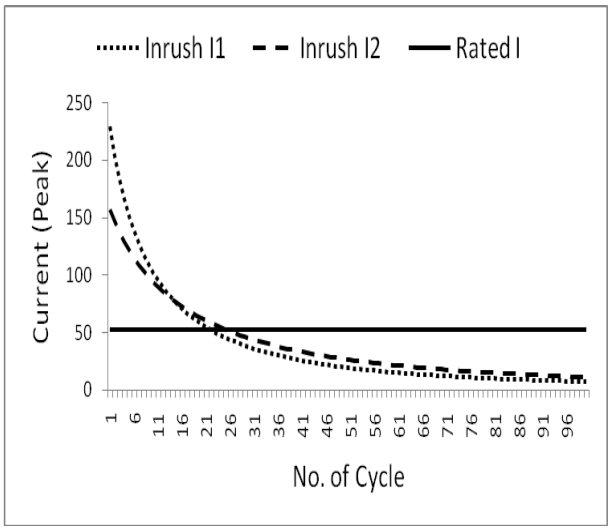

Figure 4: Peak Inrush Currents for Conventional Transformers

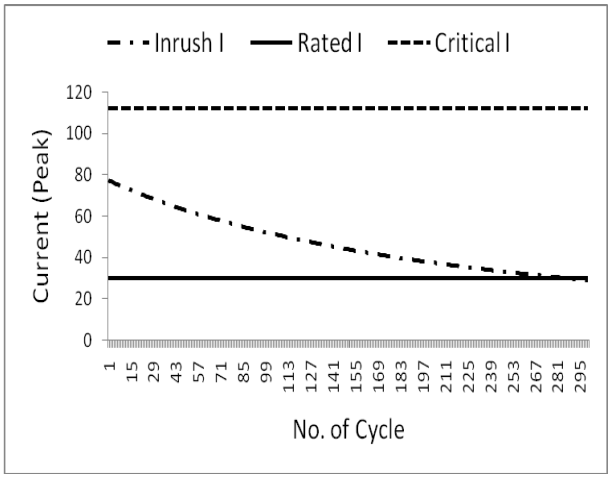

Figure 5: Peak Inrush Currents for HTS Transformer

Also, the peak inrush current values are found to be below the critical current value of the HTS transformer operating at the temperature of 77 K. It is very important to take into account the value of critical current for the primary winding of the HTS transformer. The transformer operates under normal condition at the designated temperature.

Beyond the critical current value, the characteristics of the HTS transformer will change and this includes the superconducting properties of the primary winding. Moreover, the superconducting winding will quench for a large inrush current [8].

The computations for HTS transformer show that longer time duration is required for the inrush current to reduce to the rated current. Figure 5 shows the peak inrush current reaching the rated current only after 280 cycles which is very much higher compared to those of conventional transformers.

5 OBSERVATION

Applying the phase frame calculation method for the short circuit computation gave eminently satisfactory results. The three-phase impedance and admittance matrices are very useful for the study. The method of solution appears to be accurate and efficient. This validates the technique for more advanced and complicated circuit designs.

The sample network with HTS transformer was simulated with different types of short circuit conditions. The calculation provides the fault currents and voltages to be expected on the transformer for each fault classification. Since each utility has its own electrical network characteristics, the computed short-circuit current and voltage values should fall within the specification set by the utility concerns.

Several factors are found to affect the magnitude of inrush currents. The source impedance between the transformer and the source of sustained voltage acts to reduce the magnitude of the peak inrush current. Generally, there will be some external impedance which will reduce the inrush current below the maximum. When the transformer is small compared to the system, which is normally the case, relatively high inrush currents may be obtained.

For maximum inrush current, there is a linear relation between the maximum peak inrush current and the applied voltage. The linear relationship is explained by the fact that under the conditions of residual flux and switching angle, which produce the maximum inrush condition, the iron is completely saturated. The maximum inrush current can also be obtained when the transformer is energized at zero point on the voltage wave. The crest inrush current is reduced as the switching angle varies in either direction from a voltage zero.

The transient inrush currents decay at a rate determined by the resistance of the transformers themselves. Transformers having relatively high losses will in general have faster rates of decay than those which are more efficient. Resistance in the circuit, *i.e.*, between the transformer terminals and the source of sustained voltage not only reduces the maximum initial inrush current but also expedites its rate of decay and assists in restoring normal voltage wave shape more quickly.

6 CONCLUSION

An analysis was carried out to determine what is to be expected and experienced by the HTS transformer windings from short circuit and inrush current phenomena. The outcomes on the application of different type of short circuits toward HTS transformer were displayed. Also, the results on the application of inrush forces toward the transformer were compared with that of conventional transformers. The main purpose is to demonstrate that the HTS transformer with the set up parameters should be performing well in a normal distribution network.

The study exhibits the reliability of HTS transformer to deal with the short circuit and inrush forces. The calculations show how the forces can be withstood by the designs of the transformer and the characteristics of the network. However, the transformer must be designed to withstand mechanical effects of short circuit strong forces. And, even though inrush currents may not be considered to be dangerous, their lengthy existence may unnecessarily cause operation of protective equipment such as relays and fuses.

The findings will establish further investigation on HTS transformer into various distribution network conditions such as the effects of different switching scenarios. It will also be interesting to investigate further on either both the design and connections of the transformer or the characteristics of the electric system that will have more influence on the effect towards the inrush current.

The force patterns for short circuit and inrush are shown to be quite different from each other. The secondary winding will experience the larger short circuit force earlier and is cleared in tens of milliseconds. Meanwhile, the smaller inrush force will be subjected to the energized winding which can last for longer time (few seconds). It will be beneficial to explore further on how these two forces could weaken the HTS windings electrically and mechanically over a period of time.

ACKNOWLEDGEMENT

The research project is supported by Industrial Research Limited, New Zealand, through the Foundation for Research, Science and Technology (FRST) High Temperature Superconductors (HTS) Accelerated Development Transformational Research, Science and Technology (TRST) funding.

REFERENCES

[1] M. A. Abdul Rahman, T. T. Lie, K. Prasad, “Three-Phase Modeling of HTS Transformer in Distribution Networks”, *International Power and Energy Conference*, 2010.

[2] W. H. Kersting and R. C. Dugan, "Recommended Practices for Distribution System Analysis," in *Power Systems Conference and Exposition,* 2006, pp. 499-504.

[3] E. B. Makram, M. A. Bou-Rabee, and A. A. Girgis, "Three-phase modeling of unbalanced distribution systems during open conductors and/or shunt fault conditions using the bus impedance matrix," *Electric Power Systems Research,* vol. 13, pp. 173-183, 1987.

[4] L. F. Blume, G. Camilli, S. B. Farnham, and H. A. Peterson, "Transformer Magnetizing Inrush Currents and Influence on System Operation," *American Institute of Electrical Engineers, Transactions of the,* vol. 63, pp. 366-375, 1944.

[5] N. Glasson, M. Staines, R. Buckley, M. Pannu, and S. Kalsi, "Development of a 1 MVA 3-Phase Superconducting Transformer Using YBCO Roebel Cable," *Applied Superconductivity, IEEE Transactions on,* vol. PP, pp. 1-4, 2010.

[6] W. H. Kersting and W. H. Phillips, "Distribution System Short Circuit Analysis," in *Energy Conversion Engineering Conference, 1990. IECEC-90. Proceedings of the 25th Intersociety*, 1990, pp. 310-315.

[7] T. Ishigohka, K. Uno, and S. Nishimiya, "Experimental Study on Effect of In-Rush Current of Superconducting Transformer," *Applied Superconductivity, IEEE Transactions on,* vol. 16, pp. 1473-1476, 2006.

[8] S. Nishimiya, T. Ishigohka, A. Ninomiya, K. Arai, "Quench Characteristic of Superconducting Transformer by Inrush Current." *Applied Superconductivity, IEEE Transactions on,* vol. 17(2), pp. 1931-1934, 2007.

Appendix A3: Conference paper (ASEMD 2011)

International Conference on Applied Superconductivity and Electromagnetic Devices, Sydney, Australia.

Proceedings of 2011 IEEE International Conference on
Applied Superconductivity and Electromagnetic Devices
Sydney, Australia, December 14-16, 2011

Performance Analysis of HTS Transformer with Fault Current Limiting Properties on Short Circuit Current

Muhammad A. Abdul Rahman, Tek T. Lie, Krishnamachar Prasad
Faculty of Designs and Creative Technologies,
Auckland University of Technology,
Auckland, New Zealand
muhammad.rahman@aut.ac.nz, tek.lie@aut.ac.nz, krishnamachar.prasad@aut.ac.nz

Abstract—**The advent of High Temperature Superconductor (HTS) materials has increased interest in research and development of superconducting transformers with major projects being carried out worldwide. Several benefits were accomplished with the introduction such as lower power loss, smaller size and lighter weight transformer. However, recent development on HTS transformer has focused on its ability to also function as Fault Current Limiter (FCL). This paper will show the performance of a non-FCL HTS transformer on short circuit current and predict how it will behave with HTS-FCL transformer winding conductor architectures.**

Keywords–network modelling; transformer; superconductor; current limiter; short circuit

I. INTRODUCTION

The short circuit capacity design of a transformer is one of the most significant and challenging criteria. Additional generating capacity and interconnections due to the growth of electrical power demand have contributed to an increase in short circuit capacity of power networks. One of the consequences is that the short circuit current handled by transformers becomes severe. The short circuit strength of a transformer should be designed to withstand any fault currents due to external short circuit. Any weakness in the strength may result in a mechanical collapse of windings and deformation of clamping structures. The internal faults initiated by the external short circuits may lead to bushing blowouts, tank bursting, fire hazard, etc.

Superconducting coils for utility power transformers are attractive because they require a comparatively small amount of conductor for the same transformer capacity. In the United States, conventional transformers account for about 25 % of the losses in the power transmission and distribution system and resistive heating is a great portion of these losses [1]. Thus, the use of HTS transformers can result in substantial energy savings and reduce lifetime ownership costs. Other projected benefits include the ability to limit and withstand high currents without the loss of lifetime by thermal damage. They are also able to reduce potential fire and environmental hazards because liquid nitrogen replaces oil which is used for the cooling and insulation in conventional transformers. Furthermore, the weight and volume of HTS transformers are estimated to be about one-half to one - third that of conventional transformers [2]. The authors are currently working on modelling the effects of various distribution network conditions toward a distribution HTS transformer. This paper will analyse the effects of a short circuit current on the HTS transformer winding.

Recent development on HTS transformer has focused on its capability to also operate as a Fault Current Limiter (FCL). A previous study has shown that the use of HTS - FCL devices can effectively reduce short circuit current in power transmission and distribution networks [3]. The HTS - FCL transformer acts as a superconducting transformer under normal operating conditions and as a superconducting fault current limiter under short circuit conditions. The fault current that is limited by the HTS transformer will depend on the characteristics and construction of the winding and the parameters of the HTS wire. The fault current limiting feature in HTS - FCL transformer could provide protection and reduce the wear and tear of other power equipment experiencing the short circuit current. It could also avoid power interruptions and damages to the power grid and equipment. The transformer is also able to improve the transient stability of power system in fault condition. Therefore, efficient and reliable power system can be established if the transformer could produce fault current limiting function only under fault conditions and could reduce impedance under steady state conditions. However, the important concerns of HTS - FCL transformers are the current limiting factor, recovery characteristics and transformer function. This paper will also look into the characteristics and architectural designs of HTS wires adopted for HTS - FCL transformer winding. This information will eventually be used to simulate the analysis and discover the effects of short circuit on HTS - FCL transformer winding.

II. SHORT CIRCUIT ANALYSIS ON HTS TRANSFORMER

An HTS transformer based on a preliminary baseline design the authors are working on [4], as shown in Table I, was modelled in a distribution network [5]. The sample network with HTS transformer is analysed with a short circuit condition. The calculation provides a fault current value to be expected on the transformer winding. The transformer winding is then simulated against the short circuit current. The main objective is to investigate the effects of short circuit current on the transformer winding conductor.

A huge amount of current will be flowing in the transformer windings during the short circuit duration. This situation will result in temperature rise in the winding. Since the duration is very short, typically less than 2 seconds before

The research project is supported by Industrial Research Limited, New Zealand through the Foundation for Research, Science and Technology (FRST) High Temperature Superconductors (HTS) Accelerated Development Transformational Research, Science and Technology (TRST) funding.

interrupted by the protection systems, the temperature rise should not cause any damage to the transformer.

TABLE I. HTS TRANSFORMER DESIGN PARAMETERS

Parameters	Value
Rating (kVA)	1000
Primary Voltage (kV)	11
Secondary Voltage (kV)	0.415
Frequency (Hz)	50
Primary Connection	Delta
Secondary Connection	Wye
HV Rated Current (A)	30
LV Rated Current (A)	1390
HV Winding (no. of turns)	1098
LV Winding (no. of turns)	24
Percent Impedance (%)	5

Calculations of short circuit parameters were carried out to determine the capability to withstand the thermal effects. The thermal effects on the windings resulting from a short circuit event are very critical. The fault currents are significantly higher than the normal load currents. High winding temperatures are to be expected from the event. The temperatures of the windings are calculated using (4) with an assumption that the heat developed during the period is retained in the winding itself, raising its temperature. The heat transfer through the cooling medium is not considered because the thermal time constants of the windings are much longer than the short circuit duration. The heat balance equation is applied during the short circuit and can be expressed in thermal power as

$$P_R = P_C + P_K + P_A \tag{1}$$

where P_R is the power generated from the short circuit, P_C is the power due to the heat capacity, P_K is the power conducted through the conductor and P_A is the power dissipated to the surrounding area. Equation (1) can be expressed as

$$i^2(t) \cdot R(1+\alpha \cdot \Delta T) = mc\frac{d\Delta T}{dt} + 2\lambda A\frac{d\Delta T}{dx} + hS\Delta T \tag{2}$$

where i is the short circuit current, R is the resistance at ambient temperature, α is the temperature coefficient of R, ΔT is the temperature rise, m is the mass, c is the heat specific capacity, λ is the thermal conductivity, A is the cross section area, h is the heat conversion coefficient and S is the external surface.

Since the short circuit will not last long due to interruption by the protection systems, P_K and P_A can be assumed to be negligible. Equation (2) can be rewritten as

$$i^2(t) \cdot R(1+\alpha \cdot \Delta T) = mc\frac{d\Delta T}{dt} \tag{3}$$

and further simplified as

$$In(\Delta T + \frac{1}{\alpha}) = \frac{R\alpha}{mc}\int i^2(t)dt \tag{4}$$

The next step of the analysis is to look into what is happening in the secondary winding of HTS transformer during a short circuit event. However, before going further, the structure of HTS secondary winding needs to be understood. This is crucial in order to envision what the winding is actually undergoing at the time of the period. The structure explained is based on the baseline design the authors are working on.

The HTS conductors are arranged into a continuously transposed cable. These conductors are very thin and fragile tapes. The superconducting layer is a very thin layer of a special ceramic material implanted on a Hastelloy substrate and enclosed by copper plating. The build up is shown in Fig. 1 where the overall thickness is only about 0.1 mm. Any substantial lateral bending cannot be tolerated because it will damage the superconducting layer. Special methods are applied to assemble the conductors and produce the cables.

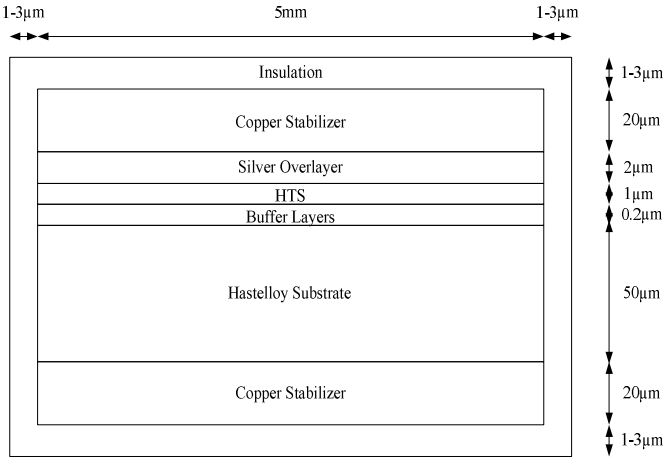

Figure 1. Structure of the HTS conductor.

A huge current will flow through the HTS winding when a short circuit occurs. After a short time, the superconductor will be expected to quench. The quench response time is normally of the order of few milliseconds. The second generation (2 G) superconductor wires will normally quench at currents around 2 - 3 times the critical current [6]. The critical current for this secondary winding at 77 K is 2380 A. It is anticipated that the short circuit current will be transferred to the copper stabilizer layer. Since the copper layer will take over the duty of transmitting short circuit current, the next step is to observe its characteristics in withstanding the situation.

After the quench, the temperature of the conductor is expected to rise due to heat from the excessive current. Particular attention is focused on the specific heat capacity of copper. The specific heat capacity of copper as a function of temperature is shown in Fig. 2 [7,8].

The analysis on HTS transformer begins with the fault current calculation on the secondary winding. The temperature rise and resistance growth of the HTS winding over short circuit duration are shown in Fig. 3 and Fig. 4, respectively. For the calculation, the short circuit is simulated to occur at t = 0 and the superconductor is assumed to quench at the response time of t_o. These are depicted in both Fig. 3 and Fig. 4.

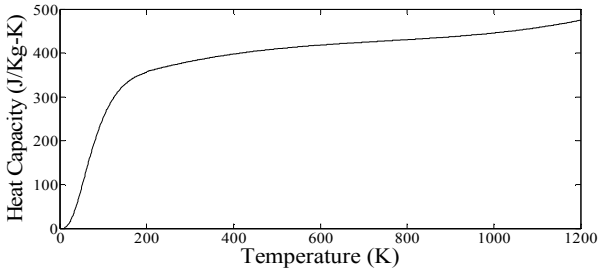

Figure 2. Specific heat capacity of copper vs. temperature.

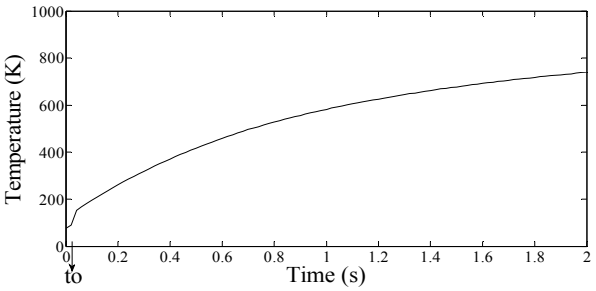

Figure 3. Temperature rise in secondary winding of HTS transformer during short circuit.

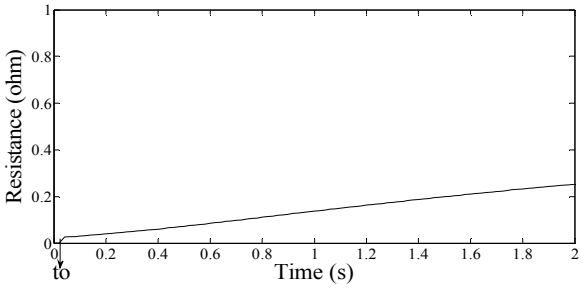

Figure 4. Resistance growth in secondary winding of HTS transformer during short circuit.

The HTS transformer will not withstand the required 2 seconds short circuit condition, as prescribed in IEC 60076 standards [9]. The temperature of the winding will rise beyond the transformer withstand value. Meanwhile, the resistance will also increase with short circuit duration. The fault current will damage the winding if it is permitted to run during the period. Therefore, the HTS transformer, with the present design parameters as shown in Table I, needs to be isolated sooner.

Several alternatives can be considered to address the problem. The first is to limit the fault duration for the HTS transformer to less than 2 seconds withstand time. The set up would require re-coordination of protection system in the power network. Consensus between the relevant parties, especially the users or utilities, must be obtained since the duration is quite short for the distribution system. This option is currently being considered. The other option is to look into the design parameters of the HTS winding conductors. The temperature rise can be reduced by using thicker copper stabilizer or replacing it with stainless steel or high resistance alloy strip. Further analysis needs to be carried out in order to ensure that the size and weight advantage of HTS transformer will not be sacrificed and the losses will be within the acceptable value.

III. HTS Wires for HTS-FCL Transformer

Present studies on HTS - FCL transformer are currently looking into various winding conductor architectures to suppress the fault current and protect the transformer. The transformer will behave as a superconducting transformer in steady state condition and as a superconducting fault current limiter in fault condition. Various conductor designs such as stabilizer free superconductors, superconductors with high resistance alloy strip and hybrid HTS coils are being tested. The superconductor wire designs can be simulated with the HTS transformer to observe the effects from short circuit currents.

The first option employs the second generation superconducting tape which operates with low resistivity in superconducting state and high resistivity in normal state [10]. The stabilizer free wire must provide high resistance - per - length in normal state at 77 K and also high mechanical strength to withstand the short circuit force. This is very important since the superconductor layer is only about 1 % of the total thickness of the wire. The wire design construction is as shown in Fig. 1 but without the copper stabilizer.

For the next alternative, the HTS - FCL tape was put in parallel with a resistive conductor for stability and fault handling [11]. The original design used copper as the parallel conductor to meet the required 2 seconds fault withstands duration. However, the transformer would require the amount of copper nearly as much as a conventional unit. Also, copper produces high eddy current losses. Therefore, high resistance alloys are being considered as the replacement to reduce the fault current and the eddy current losses. The HTS - FCL wire with high resistance alloy strip is developed as in Fig. 5. The design presents robust HTS - FCL wire construction that can be insulated on uncomplicated insulating equipment.

In the other option, a hybrid coil is utilized [12]. The hybrid HTS coil is a combination of limiting and non - limiting coils. The limiting coil is a stabilizer free HTS wire as described in the first alternative. Meanwhile, the non-limiting coil is a surround copper stabilizer HTS wire as applied in the author's preliminary baseline design HTS transformer and shown in Fig. 1. Both of the HTS coils are connected in series. The hybrid structure would allow higher flexibility for both transformer and current limiter design by the variation of the ratio between the coils.

In the previous section, the simplified heat balance equation was applied to calculate the temperature rise in the secondary winding of an HTS transformer. The simulation takes into account the structural design of HTS conductor and assumes the conductor to quench after a short time by the fault current. The calculation also assumed the short circuit current was forced to be diverted from the HTS filaments to the copper stabilizer layers. The fault current generates heat and increases the resistance in the winding. The result shows that the transformer secondary winding can be damaged due to high temperature if the fault current is to be allowed for a period of 2 seconds as specified in IEC 60076 standards [8].

The resistance is also found to increase during the short circuit event.

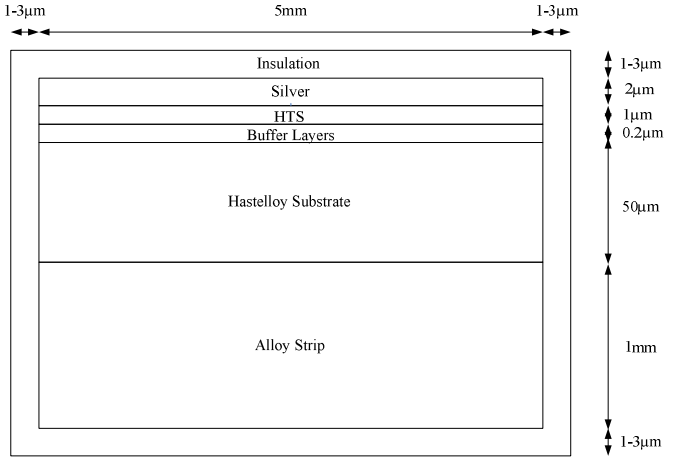

Figure 5. HTS wire with high resistance alloy strip.

Further advancement in the technology enables the research and development of HTS - FCL transformer. Several alternatives for HTS - FCL wire have been introduced. Since the architectural design of the wire has been altered, the previous assumption considered in the calculation must be re-established. During the short circuit duration, the HTS - FCL wire will be transformed from superconducting state into normal or high resistance state. In the superconducting state, the short circuit impedance depends only on the reactance. However, in the normal state, the resistance of the materials will be the dominant factor. The resistance of the wire will be equal to the equivalent resistance of all the parallel layers in the wire. The resistance value will depend on the resistivity, thickness and cross - sectional percentage of each layer material.

The winding resistance will eventually increase the impedance of the transformer. Due to the high resistance of the winding in the normal state, the fault current will be limited below the permissible value. The restricted short circuit current should generate less heat on the winding. Therefore, the temperature rise and the resistance growth on the HTS - FCL wire should also be reduced.

IV. CONCLUSION

An analysis was carried out to determine the effects of short circuit phenomena on an HTS transformer winding. The mathematical model presented enables the estimation of temperature rise developed in the transformer winding during short circuit. Simplifying assumptions made in the computation appear not to significantly affect the model's accuracy.

The calculation on short circuit forces shows the HTS transformer is unable to withstand the duration of 2 seconds as prescribed in the IEC standards. Temperature and resistance of the secondary winding increase tremendously and rise beyond the allowable limit during the period. Therefore, arrangement must be made to isolate the transformer sooner in order to prevent any damage to the transformer and loss of power supply to the customers. The transformer should be limited to fault duration below 2 seconds.

Development of HTS - FCL transformer should be able to improve the obstacles from short circuit current. The fault current will be limited due to high winding resistance in the normal state. The limited fault current will then reduce the increment of heat generated. This circumstance will eventually reduce the growth of the winding resistance. Further studies are currently in progress.

REFERENCES

[1] S. W. Schwenterly, B. W. McConnell, J. A. Demko, A. Fadnek, J. Hsu, F. A. List, M. S. Walker, D. W. Hazelton, F. S. Murray, J. A. Rice, C. M. Trautwein, X. Shi, R. A. Farrell, J. Bascuhan, R. E. Hintz, S. P. Mehta, N. Aversa, J. A. Ebert, B. A. Bednar, D. J. Neder, A. A. McIlheran, P. C. Michel, J. J. Nemce, E. F. Pleva, A. C. Swenton, W. Swets, R. C. Longsworth, R. C. Johsnon, R. H. Jones, J. K. Nelson, R. C. Degeneff, and S. J. Salon, "Performance of a 1 - MVA HTS demonstration transformer," IEEE Transactions on Applied Superconductivity, vol. 9, no. 2, pp. 680-684, June 1999.

[2] B. W. McConnell, "Transformers-a successful application of high temperature superconductors," IEEE Transactions on Applied Superconductivity, vol. 10, no. 1, pp. 716-720, March 2000.

[3] J. X. Jin, S. X. Dou, H. K. Liu, C. Grantham, Z. J. Zeng, Z. Y. Liu, T. R. Blackburn, X. Y. Li, H. L. Liu, and J. Y. Liu, "Electrical application of high T_c superconducting saturable magnetic core fault current limiter," IEEE Transactions on Applied Superconductivity, vol. 7, no. 2, pp. 1009-1012, June 1997.

[4] N. Glasson, M. Staines, R. Buckley, M. Pannu, and S. Kalsi, "Development of a 1 MVA 3-phase superconducting transformer using YBCO roebel cable," IEEE Transactions on Applied Superconductivity, vol. 21, no. 3, pp. 1393-1396, June 2011.

[5] M. A. A. Rahman, T. T. Lie, and K. Prasad, "Three - phase modeling of HTS transformer in distribution networks," in International Power and Energy Conference, pp. 72-77, 2010.

[6] Y. Y. Xie, K. Tekletsadik, D. Hazelton, and V. Selvamanickam, "Second generation high-temperature superconducting wires for fault current limiter applications," IEEE Transactions on Applied Superconductivity, vol. 17, no. 2, pp. 1981-1985, June 2007.

[7] R. Stevens, and J. Boerio - Goates, "Heat capacity of copper on the ITS - 90 temperature scale using adiabatic calorimetry," The Journal of Chemical Thermodynamics, vol. 36, no. 10, pp. 857-863, October 2004.

[8] C. R. Brooks, W. E. Norem, D. E. Hendrix, J. W. Wright, and W. G. Northcutt, "The specific heat of copper from 40 to 920 °C," Journal of Physics and Chemistry of Solids, vol. 29, no. 4, pp. 565-574, April 1968.

[9] Power Transformers - Part 5: Ability to Withstand Short Circuit, IEC Standard 60076-5, 2000.

[10] T. Janowski, B. A. Glowacki, G. Wojtasiewicz, S. Kozak, J. Kozak, B. Kondratowicz-Kucewicz, M. Majka, and M. Wozniak, "Fault current limitation in power network by the superconducting transformers made of 2G HTS," IEEE Transactions on Applied Superconductivity, vol. 21, no. 3, pp. 1413-1416, June 2011.

[11] C. M. Rey, R. C. Duckworth, S. W. Schwenterly, and E. Pleva, "Electrical AC loss measurements on a 2G YBCO coil," IEEE Transactions on Applied Superconductivity, vol. 21, no. 3, pp. 2424-2427, June 2011.

[12] H. Kojima, M. Kotari, T. Kito, N. Hayakawa, M. Hanai, and H. Okubo, "Current limiting and recovery characteristics of 2 MVA class superconducting fault current limiting transformer (SFCLT)," IEEE Transactions on Applied Superconductivity, vol. 21, no. 3, pp. 1401-1404, June 2011.

Appendix A4: Transaction (IEEE – TAS)

IEEE Transactions on Applied Superconductivity.

(Published)

The Effects of Short-Circuit and Inrush Currents on HTS Transformer Windings

M. A. Abdul Rahman, T. T. Lie, *Senior Member, IEEE*, and K. Prasad, *Member, IEEE*

***Abstract*—Rapid changes and developments are being witnessed in the transformer design technologies. The phenomenal growth of power systems has put tremendous responsibilities on the industry to supply reliable and cost-effective transformers. The advent of high-temperature superconductor (HTS) materials has increased interest in research and development of superconducting transformers with major projects being carried out worldwide. The major challenges in the design and development of HTS transformers are the modeling of short-circuit and inrush currents the transformer can withstand. Even though HTS technology is claimed to be more efficient, reliable, and eco-friendly, use of HTS transformers must be appropriately verified through the proper modeling of power system network.**

***Index Terms*—Distribution, inrush, modeling, short circuit, superconductor, transformer.**

I. Introduction

THE SHORT-CIRCUIT capacity design of a transformer is one of the most significant and challenging criteria. Additional generating capacity and interconnections due to the growth of electrical power demand have contributed to an increase in short-circuit capacity of power networks. One of the consequences is that the short-circuit current handled by transformers becomes more severe. The short-circuit strength of a transformer should be designed to withstand any fault currents due to an external short circuit. Any weakness in the strength may result in a mechanical collapse of windings and deformation of clamping structures. The internal faults initiated by the external short circuits may lead to bushing blowouts, tank bursting, fire hazard, etc.

Meanwhile, the inrush current of a transformer can be as high as 7 to 10 times the rated current. Inrush current events are more frequent compared with short circuits. They also last for much longer time compared with short circuits. The users are very anxious about the repeated switching of a transformer. Even though the inrush currents are usually not seriously looked into in the mechanical design considerations, the forces generated due to an extensive number of switchings in a day may weaken the winding over a period of time. The continuous occurrences may lead to loosening of winding and subsequent failure.

Consequently, it is important to develop an understanding of the fundamental high-temperature superconducting (HTS) transformer design issues that can provide guidance for developing practical devices of interest to the electric utility industry. The parameters of an HTS transformer need to be validated before any attempt to carry out to model the behavior of a distribution network under a range of conditions [1]. The predicted performance and reliability of HTS transformers can then be verified through network modeling and analysis. The ultimate purpose is to furnish electric utilities precise information as to which HTS transformers work under various applications with greater technical efficiency and proven reliability.

The modeling is carried out on a three-phase distribution feeder, which is inherently unbalanced [2]. The technical information on the HTS transformer is based on a preliminary baseline design. The results are subsequently compared with the application of typical conventional transformers.

The sample network with an HTS transformer is simulated with different types of short-circuit conditions [3]. The calculations provide the fault currents and voltages to be expected on the transformer for each fault classification. Since each utility has its own electrical network characteristics, the computed short-circuit current and voltage values should fall within the specification set by the utility concerns.

Several factors affecting the inrush phenomena are investigated [4]. The peak values of inrush currents are calculated for every cycle until they reach the primary winding rated current of the transformer to scrutinize the decay pattern. It is believed that the analysis will contribute further by predicting the performance and reliability of the HTS transformer before the installation in a distribution network system.

II. Network Model

A simulation was carried out on a simple distribution feeder. The source voltages are balanced three-phase 11-kV line-to-line. The system involves a short three-wire delta 11-kV tape screened underground cable and four four-wire wye 415-V line-to-line overhead lines with the transformer in between. The network is shown in Fig. 1.

Conventional and HTS distribution transformers are employed in the network study. The electrical characteristics for a typical conventional transformer are based on those used in a distribution system by a utility company. Meanwhile, the technical information on the HTS transformer is based on a

Manuscript received March 22, 2011; revised June 22, 2011; accepted October 17, 2011. Date of publication December 19, 2011; date of current version March 30, 2012. This paper was recommended by Associate Editor P. J. Masson. This work was supported in part by Industrial Research Limited, New Zealand through the Foundation for Research, Science and Technology (FRST) High Temperature Superconductors (HTS) Accelerated Development Transformational Research, Science and Technology (TRST) funding.

The authors are with the Faculty of Designs and Creative Technologies, Auckland University of Technology, Auckland 1142, New Zealand (e-mail: muhammad.rahman@aut.ac.nz; tek.lie@aut.ac.nz; krishnamachar.prasad@aut.ac.nz).

Digital Object Identifier 10.1109/TASC.2011.2173571

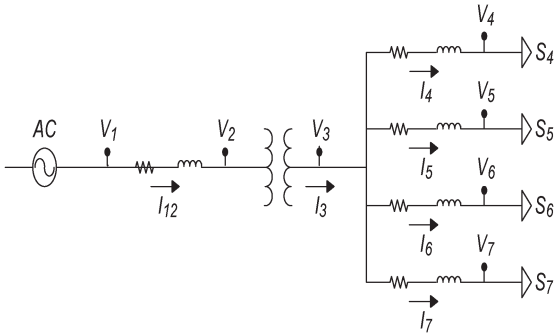

Fig. 1. Network of a simple distribution feeder.

TABLE I
TRANSFORMER DESIGN PARAMETERS

Parameters	Transformer Type	
	HTS	*Conventional*
Rating (kVA)	1000	1000
Primary Voltage (kV)	11	11
Secondary Voltage (kV)	0.415	0.415
Frequency (Hz)	50	50
Primary Connection	Delta	Delta
Secondary Connection	Wye	Wye
HV Rated Current (A)	30	52.5
LV Rated Current (A)	1390	1333
HV Winding (no. of turns)	1098	739
LV Winding (no. of turns)	24	16
Percent Impedance (%)	5	5

preliminary baseline design the authors are working on [5]. The design parameters, as compared with those of a conventional transformer, are shown in Table I.

The underground cable is a 300-mm^2 three-core tape screened cross-linked polyethylene cable, and the overhead line structure uses a 500-kcmil 19 strands all-aluminum conductors, for both the phase and neutral conductors. Each line is short and assumed to be only 0.40 km for the underground cable and 0.10 km for the overhead lines.

III. SHORT-CIRCUIT CURRENT ANALYSIS

The method of applying symmetrical components in the computation of short-circuit currents for unbalanced faults is not suitable for distribution feeders that are inherently unbalanced. The unbalanced mutual coupling between the phases will lead to mutual coupling between the sequence components. In addition, there will be limitation on the phases between which the faults may occur. Therefore, it is important to look into a suitable method for short-circuit analysis of an unbalanced distribution system such as the phase frame method [6].

The model of an unbalanced feeder for short-circuit calculation is presented in Fig. 2. Short circuits can occur at any of the points shown in the model. The short-circuit currents at point 1 are usually acquired from a transmission system short-circuit analysis. The resultant short-circuit MVAs will help to determine the zero and positive sequence impedances of the equivalent system. The short-circuit analysis for points 2, 3, 4, and 5 can then be carried out with the supporting information.

The calculation for short circuits at points 2, 3, 4, and 5 can be carried out using the Thevenin equivalent three-phase circuit

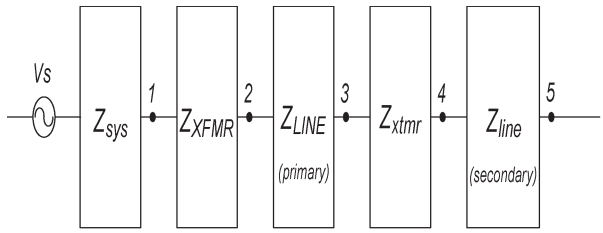

Fig. 2. Model of an unbalanced feeder for short-circuit analysis.

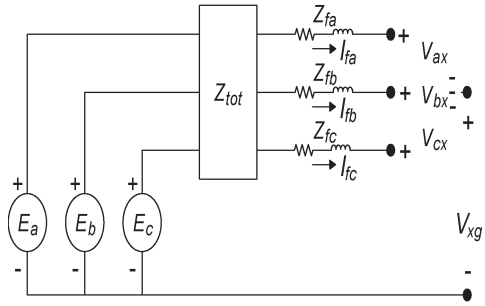

Fig. 3. Thevenin equivalent circuit at the faulted node.

at the short-circuit point. The Thevenin equivalent voltages $(E_{\rm th})$ are the nominal line-to-ground voltages.

Fig. 3 shows the Thevenin equivalent circuit at the faulted node. E_a, E_b, and E_c are the Thevenin equivalent line-to-ground voltages. $[Z_{\rm tot}]$ is the Thevenin equivalent phase impedance matrix at the faulted node. Z_f is the fault impedance. I_{fa}, I_{fb}, and I_{fc} are the fault currents. V_{ax}, V_{bx}, and V_{cx} are the phase voltages (a, b, c) to the point of fault (x). V_{xg} is the voltage from the point of fault (x) to the ground (g).

Applying KVL to the Thevenin equivalent circuit, we obtain the following equation:

$$\begin{bmatrix} E_a \\ E_b \\ E_c \end{bmatrix} = \begin{bmatrix} Z_{aa} & Z_{ab} & Z_{ac} \\ Z_{ba} & Z_{bb} & Z_{bc} \\ Z_{ca} & Z_{cb} & Z_{cc} \end{bmatrix} \cdot \begin{bmatrix} I_{fa} \\ I_{fb} \\ I_{fc} \end{bmatrix} + \begin{bmatrix} Z_f & 0 & 0 \\ 0 & Z_f & 0 \\ 0 & 0 & Z_f \end{bmatrix} \cdot \begin{bmatrix} I_{fa} \\ I_{fb} \\ I_{fc} \end{bmatrix} + \begin{bmatrix} V_{ax} \\ V_{bx} \\ V_{cx} \end{bmatrix} + \begin{bmatrix} V_{xg} \\ V_{xg} \\ V_{xg} \end{bmatrix}. \quad (1)$$

Since we know the values of $[y]$ (from $[Z_{\rm tot}]$ and $[Z_f]$) and $[E_{abc}]$ (from $[E_a]$, $[E_b]$, $[E_c]$), the equivalent injected currents can be obtained from the following equation:

$$\begin{bmatrix} I_{pa} \\ I_{pb} \\ I_{pc} \end{bmatrix} = \begin{bmatrix} I_{fa} \\ I_{fb} \\ I_{fc} \end{bmatrix} + \begin{bmatrix} y_{aa} & y_{ab} & y_{ac} \\ y_{ba} & y_{bb} & y_{bc} \\ y_{ca} & y_{cb} & y_{cc} \end{bmatrix} \cdot \begin{bmatrix} V_{ax} \\ V_{bx} \\ V_{cx} \end{bmatrix} + \begin{bmatrix} y_{sa} \\ y_{sb} \\ y_{sc} \end{bmatrix} \cdot [V_{xg}] \quad (2)$$

where

$$y_{sa} = y_{aa} + y_{ab} + y_{ac} \quad (3)$$

$$y_{sb} = y_{ba} + y_{bb} + y_{bc} \quad (4)$$

$$y_{sc} = y_{ca} + y_{cb} + y_{cc}. \quad (5)$$

These equations can be used to simulate all types of short circuits. The known values are the equivalent injected currents (I_{pa}, I_{pb}, I_{pc}), the equivalent admittances $(y_{aa}, y_{ab}, y_{ac}, y_{ba},$

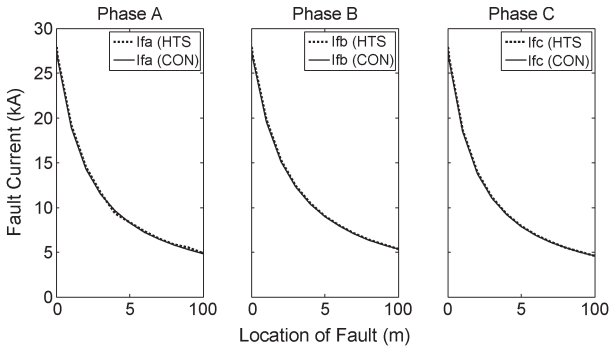

Fig. 4. Three-phase fault currents on conventional and HTS transformers.

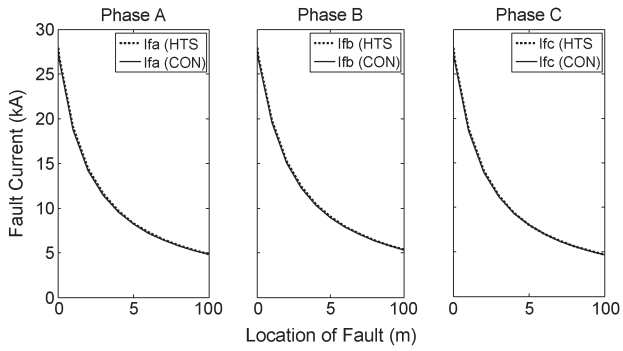

Fig. 5. Three-phase-to-ground fault currents on conventional and HTS transformers.

$y_{bb}, y_{bc}, y_{ca}, y_{cb}, y_{cc}$), and the sum for each row of the admittances (y_{sa}, y_{sb}, y_{sc}). Meanwhile, the unknown values are the fault currents (I_{fa}, I_{fb}, I_{fc}), phase voltages to the point of fault (V_{ax}, V_{bx}, V_{cx}), and the point of fault-to-ground voltage (V_{xg}). Therefore, the equations can be solved by specifying four additional independent equations that will depend on the type of fault being simulated. The seven equations can be presented in the following matrix form:

$$\begin{bmatrix} I_{pa} \\ I_{pb} \\ I_{pc} \\ 0 \\ 0 \\ 0 \\ 0 \end{bmatrix} = \begin{bmatrix} 1 & 0 & 0 & y_{aa} & y_{ab} & y_{ac} & y_{sa} \\ 0 & 1 & 0 & y_{ba} & y_{bb} & y_{bc} & y_{sb} \\ 0 & 0 & 1 & y_{ca} & y_{cb} & y_{cc} & y_{sc} \\ \# & \# & \# & \# & \# & \# & \# \\ \# & \# & \# & \# & \# & \# & \# \\ \# & \# & \# & \# & \# & \# & \# \\ \# & \# & \# & \# & \# & \# & \# \end{bmatrix} \cdot \begin{bmatrix} I_{fa} \\ I_{fb} \\ I_{fc} \\ V_{ax} \\ V_{bx} \\ V_{cx} \\ V_{xg} \end{bmatrix} \tag{6}$$

where # is to be filled up and depends on the type of fault. For example, the conditions for a three-phase fault are

$$I_{fa} + I_{fb} + I_{fc} = 0 \tag{7}$$

$$V_{ax} = 0 \tag{8}$$

$$V_{bx} = 0 \tag{9}$$

$$V_{cx} = 0. \tag{10}$$

Thus, the matrix equations can be expressed as follows:

$$\begin{bmatrix} I_{pa} \\ I_{pb} \\ I_{pc} \\ 0 \\ 0 \\ 0 \\ 0 \end{bmatrix} = \begin{bmatrix} 1 & 0 & 0 & y_{aa} & y_{ab} & y_{ac} & y_{sa} \\ 0 & 1 & 0 & y_{ba} & y_{bb} & y_{bc} & y_{sb} \\ 0 & 0 & 1 & y_{ca} & y_{cb} & y_{cc} & y_{sc} \\ 0 & 0 & 0 & 1 & 0 & 0 & 0 \\ 0 & 0 & 0 & 0 & 1 & 0 & 0 \\ 0 & 0 & 0 & 0 & 0 & 1 & 0 \\ 1 & 1 & 1 & 0 & 0 & 0 & 0 \end{bmatrix} \cdot \begin{bmatrix} I_{fa} \\ I_{fb} \\ I_{fc} \\ V_{ax} \\ V_{bx} \\ V_{cx} \\ V_{xg} \end{bmatrix}. \tag{11}$$

The three-phase fault and three-phase-to-ground fault analyses are carried out on the network with both conventional and HTS transformers. The circuit is shorted at various locations to observe the values of fault current experienced by the transformers. The fault current values for the two types of faults are presented in Figs. 4 and 5, respectively.

Meanwhile, the phase-to-phase and phase-to-ground faults are also analyzed on the same circuit. The shorted locations are the same as those for the three-phase and three-phase-to-ground faults. The fault currents of the transformer experiencing the two faults are shown in Figs. 6 and 7.

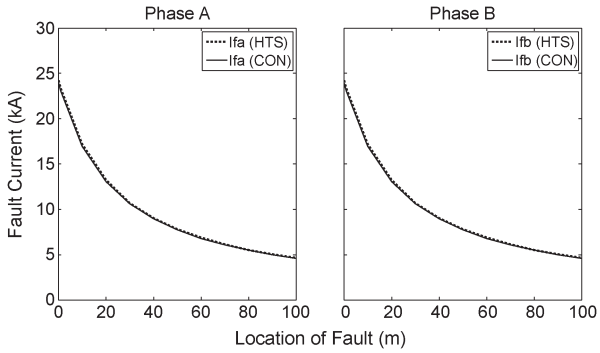

Fig. 6. Phase-to-phase fault currents on conventional and HTS transformers.

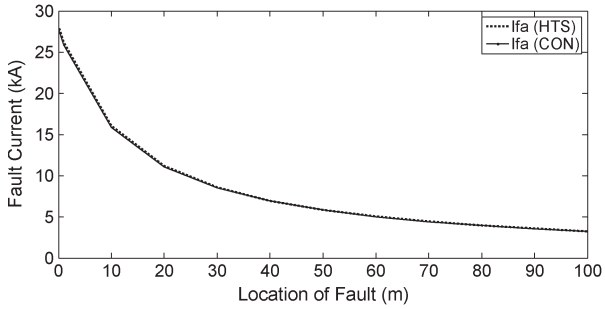

Fig. 7. Phase-to-ground fault currents on conventional and HTS transformers.

Figs. 4–7 show the trends of fault currents experienced by either conventional (CON) or HTS transformers installed in the circuit. The fault currents get higher as the fault locations move nearer to the transformer or the source. Both types of transformers will therefore experience nearly the same kind of fault currents when a short circuit occurs. Each utility has its own electrical network characteristics. For the low voltage distribution network applied in the analysis, certain utilities are specifying their transformers to meet the requirement characteristics of low voltage short-circuit current at 31.5 kA. The short-circuit currents and voltages resulting from the analysis fall within the requirement if the transformer is specified according to the characteristics.

A huge amount of current will be flowing in transformer windings during short-circuit duration. This situation will result in temperature rise in the winding. Since the duration is very

short, typically less than 2 s before interrupted by the protection systems, the temperature rise should not cause any damage to the transformer.

Calculations of the short-circuit parameters for the conventional transformer were carried out to determine the capability of withstanding thermal effects. The thermal effects on the windings resulting from a short-circuit event are critical. The fault currents are significantly higher than the normal load currents. High winding temperatures are to be expected from the event. The temperatures for copper windings are calculated using (15) with an assumption that the heat developed during the period is retained in the winding itself, raising its temperature. The heat transfer through the cooling medium is not considered because the thermal time constants of the windings are much longer than the short-circuit duration.

The heat balance equation is applied during the short circuit and can be expressed in thermal power as

$$P_R = P_C + P_K + P_A \tag{12}$$

where P_R is the power generated from the short circuit, P_C is the power due to the heat capacity, P_K is the power conducted through the conductor, and P_A is the power dissipated to the surrounding area. Equation (12) can be expressed as

$$i^2(t) \cdot R(1 + \alpha \cdot \Delta T) = mc\frac{d\Delta T}{dt} + 2\lambda A\frac{d\Delta T}{dx} + hS\Delta T \tag{13}$$

where i is the short-circuit current, R is the resistance at ambient temperature, α is the temperature coefficient of R, ΔT is the temperature rise, m is the mass, c is the heat specific capacity, λ is the thermal conductivity, A is the cross section area, h is the heat conversion coefficient, and S is the external surface.

Since the short circuit will not last long due to interruption by the protection systems, P_K and P_A can be assumed to be negligible. Thus, (13) can be rewritten as

$$i^2(t) \cdot R(1 + \alpha \cdot \Delta T) = mc\frac{d\Delta T}{dt} \tag{14}$$

and further simplified as

$$In\left(\Delta T + \frac{1}{\alpha}\right) = \frac{R\alpha}{mc}\int i^2(t)dt. \tag{15}$$

The fault is assumed to be a three-phase short circuit and occurring at the end of line (100 m). The fault current is computed from the phase frame calculation and the k-factor of the transformer and line involved. The temperature of the secondary winding will increase as the fault current continues, as shown in Fig. 8.

The result is compared with the computation method proposed in IEC 60076 [7]. The equation applied in the standard is

$$T = T_o + \frac{2(T_o + 235)}{\frac{106000}{J^2 t} - 1} \tag{16}$$

where T_o is the initial temperature in Celsius, J is the short-circuit current density, and t is the duration of short circuit.

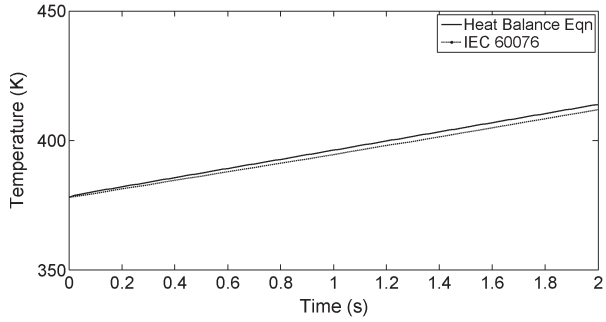

Fig. 8. Temperature rise in secondary winding of a conventional transformer during short circuit.

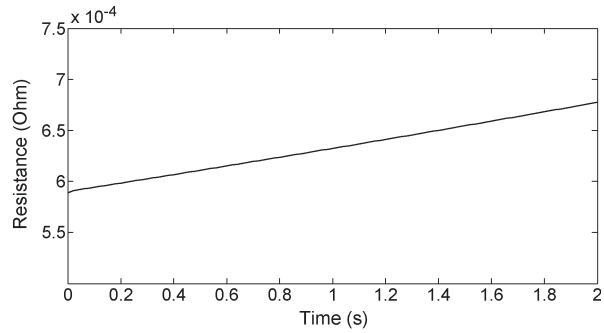

Fig. 9. Resistance growth in secondary winding of a conventional transformer during short circuit.

The calculations for both methods are based on the parameters provided by the supplier of the conventional transformer. The results are almost identical, as shown in Fig. 8, and can be used to justify the computational methods. The values are also well below the permissible 250 °C (523 K) as per IEC 60076 standards [7], which indicates the cross-sectional areas of the windings are sufficient when it comes to the short-circuit condition. Fig. 9 shows the relationship between the resistance growth and the fault duration on the low voltage winding during the short-circuit period using the relation

$$R = \rho(T) \cdot \frac{l}{A} \tag{17}$$

where l is the length of the conductor, and A is the cross-sectional area of the conductor.

The next step in the analysis is to look into what is happening in the secondary winding of the HTS transformer during a short-circuit event. However, before going further, the structure of the HTS secondary winding needs to be understood. This is crucial in order to envision what the winding is actually undergoing at the time of the period. The structure explained is based on the baseline design the authors are working on.

The HTS conductors are arranged into a continuously transposed cable. These conductors are very thin and fragile tapes. The superconducting layer is a very thin layer of a special ceramic material implanted on a Hastelloy substrate and enclosed by copper plating. The build up is shown in Fig. 10, where the overall thickness is only about 0.1 mm. Any substantial lateral bending cannot be tolerated because it will damage the superconducting layer. Special methods are applied to assemble the conductors and produce the cables.

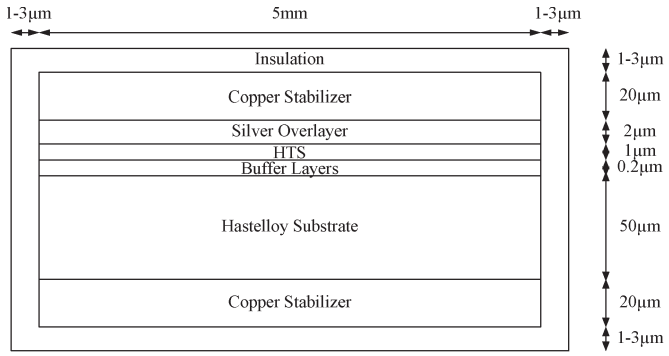

Fig. 10. Structure of the HTS conductors.

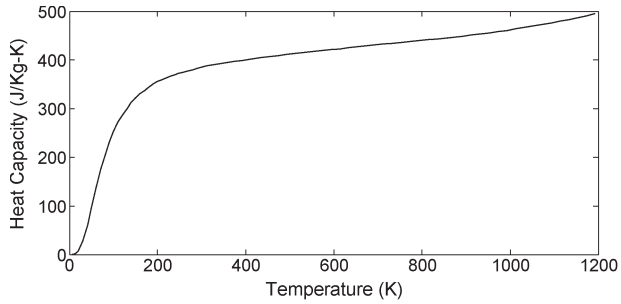

Fig. 11. Specific heat capacity of copper versus temperature.

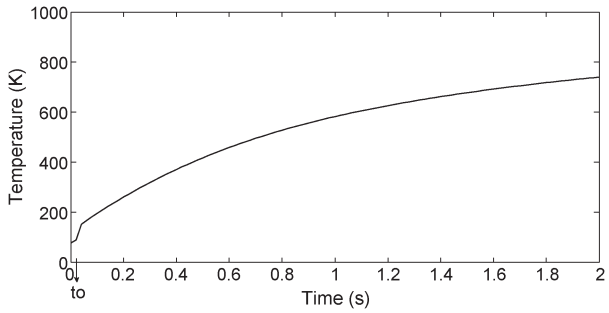

Fig. 12. Temperature rise in secondary winding of an HTS transformer during short circuit.

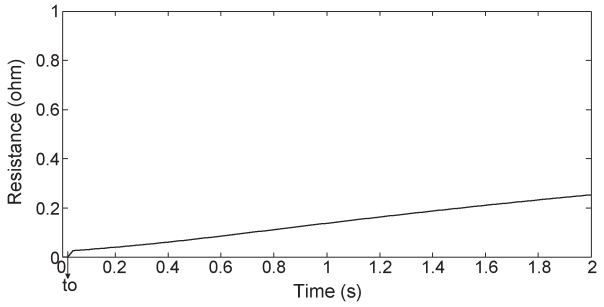

Fig. 13. Resistance growth in secondary winding of an HTS transformer during short circuit.

A huge current will flow through the HTS winding when a short circuit occurs. After a short time, the superconductor will be expected to quench. The quench response time is normally of the order of a few milliseconds. The second-generation (2G) superconductor wires will normally quench at currents around 2–3 times the critical current [8]. The critical current for this secondary winding at 77 K is 2380 A. It is anticipated that the short-circuit current will be transferred to the copper stabilizer layer. Since the copper layer will take over the duty of transmitting the short-circuit current, the next step is to observe its characteristics in withstanding the situation.

After the quench, the temperature of the conductor is expected to rise due to heat from the excessive current. Particular attention is focused on the specific heat capacity of copper. The specific heat capacity of copper as a function of temperature is shown in Fig. 11 [9], [10].

Applying the same computation steps as for the conventional transformer, the analysis on the HTS transformer begins with the fault current calculation on the secondary winding. The temperature rise and resistance growth of the HTS winding over short-circuit duration are shown in Figs. 12 and 13, respectively. For the calculation, the short circuit is simulated to occur at $t = 0$, and the superconductor is assumed to quench at the response time of t_o. These are depicted in both Figs. 12 and 13.

The HTS transformer will not withstand the required 2-s short-circuit condition, as prescribed in IEC 60076 standards [7]. The temperature of the winding will rise beyond the transformer withstand value. Meanwhile, the resistance will also increase with short-circuit duration. The fault current will damage the winding if it is permitted to run during the period. Therefore, the HTS transformer, with the present design parameters as shown in Table I, needs to be isolated sooner.

IV. Inrush Current Analysis

Inrushing of current will not occur if a transformer can be switched on at an instant of a voltage wave that corresponds to the actual flux density in the core at the same particular point of time. Nevertheless, the inrush phenomenon is difficult to prevent because the instance of switching cannot be easily controlled and the instance of switching favorable to one phase is not necessarily favorable to the other two phases.

When a transformer is energized, the magnetizing inrush current will flow for a short period of time. The phenomenon will continue until the normal flux conditions are established. Under most conditions, the phenomenon will produce little consequences. However, in rare cases, it can momentarily impair the proper operation of the system.

The inrush current can be as high as 7 to 10 times the rated current [11]. Inrush transients are more frequent than short circuits, and they last for a few seconds as compared with short circuits that are cleared in tens of milliseconds.

Utilities are very interested in the information on the maximum value and rate of decay of the inrush current. For a three-phase delta connected primary transformer, each phase is independently connected to the network. The inrush phenomenon corresponding to the flux of each phase of this transformer takes place similar to that of a single-phase transformer. The phase inrush current will therefore result in the same value as that of the single-phase transformer. Meanwhile, the line inrush current will be less severe. The line current is $\sqrt{3}$ times the phase current under normal conditions. In an inrush condition,

only one phase that gets switched at the worst will be having large inrush current. Therefore, the line inrush current will be almost equal to the phase inrush current.

In the estimation of inrush current magnitude and decay pattern, operating engineers will be looking on the inrush current peak values for the first few cycles and the time after which the inrush current reduces to a value equal to the rated current. Two assumptions are made in the calculation. The first is that the transformer is energized at voltage equal to zero. The second is that the residual flux is in the same direction as the initial flux change, which gives a maximum possible value of the inrush current.

In the event, after the core saturation, the inrush current is limited by air core reactance, X_s, which can be calculated as

$$X_s = \frac{\mu_\circ \cdot N^2 \cdot A_w}{h_w} \cdot 2 \cdot \pi \cdot f \tag{18}$$

where N is the number of turns of excited winding, A_w is the area inside the mean turn of excited winding, and h_w is the height of energized winding. The angle, θ, at the instance which the core saturates is given by

$$\theta = K_1 \cos^{-1}\left(\frac{B_s \cdot B_{\rm mp} \cdot B_r}{B_{\rm mp}}\right) \tag{19}$$

where B_s is the saturation flux density, B_r is the residual flux density, $B_{\rm mp}$ is the peak value of designed steady-state flux density in the core, and K_1 is the correction factor for saturation angle.

The inrush current peak, $i_{o\max}$, for the first cycle is specified as

$$i_{o\max} = \frac{K_2 \cdot V \cdot \sqrt{2}}{X_s}(1 - \cos\theta) \tag{20}$$

where V is the rms value of applied alternating voltage, and K_2 is the correction factor for the peak value. The residual flux density will reduce at the end of the first cycle due to losses in the circuit. It is also a function of damping provided by the transformer losses. The new residual flux density, $B_{r(\rm new)}$, is then presented as

$$B_{r(\rm new)} = B_{r(\rm old)} - \left[B_{\rm mp} \cdot \frac{K_3 \cdot R}{X_s}\left(2 \cdot (\sin\theta - \theta\cos\theta)\right)\right] \tag{21}$$

where R is the sum of transformer winding resistance and system resistance, and K_3 is the correction factor for the decay of inrush. The computations are repeated in order to calculate the peaks of the subsequent cycles. Since the transformers are delta connected primary, the actual line inrush currents are almost equal to the calculated values.

From the calculations on two conventional transformers from different manufacturers put into the distribution network presented, the inrush current peak values can go up to 3 to 5 times the rated current. Furthermore, they will take between 20 to 30 cycles for the inrush current to reduce to the rated current, as shown in Fig. 14.

Meanwhile, the inrush peak values can go up to 2 to 3 times the rated current for the HTS transformer under study, as shown in Fig. 15. Furthermore, this value is found to be below the critical current value of the primary winding at operating temperature of 77 K. However, it is taking much longer time to reduce to its rated current, i.e., almost 300 cycles.

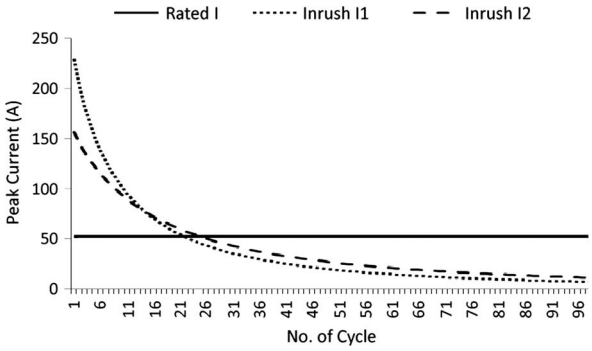

Fig. 14. Peak inrush currents for conventional transformers.

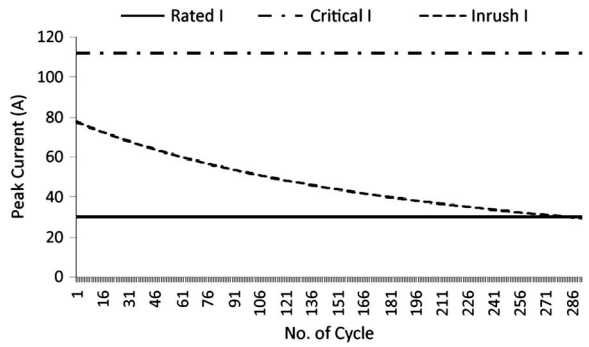

Fig. 15. Peak inrush currents for HTS transformers.

It is very important to take into account the value of the critical current for the primary winding of the HTS transformer. The transformer operates under normal condition at temperature $\leq$ 77 K. Beyond the critical temperature, the characteristics of the HTS transformer will change and this includes the superconducting properties of the primary winding.

V. Discussion

Applying the phase frame calculation method in the network modeling for the short-circuit computation gave eminently satisfactory results. The three-phase impedance and admittance matrices are very useful for the study. The method of solution appears to be accurate and efficient. This validates the technique for more advanced and complicated circuit designs.

The sample network with conventional and HTS transformers are simulated with different types of short-circuit conditions, as shown in Section III. The calculation provides the fault currents for various fault locations to be expected on the transformers for each fault classification. The results are shown in Figs. 4–7. As expected, the three-phase fault provides the highest fault current. In the same section, two computational methods are considered to calculate the temperature rise in secondary winding of the conventional transformer due to the short-circuit current. The results are found to be comparable between the two approaches. The resistance of secondary

winding is worked out from the calculated temperature using the temperature–resistance relationship.

Meanwhile, for the HTS transformer, the heat balance equation is used to calculate the temperature rise in secondary winding. The calculation takes into account the structural design of the HTS conductor and assumes the conductor to quench after a short time by the fault current, forces the current to be diverted from the HTS filaments to the copper stabilizer layers. The fault current generates heat and increases the resistance in the winding. The result shows that the transformer secondary winding can be damaged due to high temperature if the fault current is to be allowed for a period of 2 s, as specified in IEC 60076 standards [7]. The resistance is also found to increase during the short-circuit event.

Several alternatives can be considered to address the problem. The first is to limit the fault duration for the HTS transformer to less than 2-s withstand time. The set up would require recoordination of protection system in the power network. Consensus between the relevant parties, particularly the users or utilities, must be obtained since the duration is quite short for the distribution system. This option is currently being considered. The other option is to look into the design parameters of the HTS winding conductors. The temperature rise can be reduced by using thicker copper stabilizer or replacing it with stainless steel or high resistance alloy strip. Further analysis needs to be carried out in order to ensure that the size and weight advantage of the HTS transformer will not be sacrificed, and the losses will be within the acceptable value.

Present studies on the HTS fault current limiting transformer are currently looking into various winding conductor architectures to suppress the fault current and protect the transformer [12]–[14]. The transformer will behave as a superconducting transformer in steady-state condition and as a superconducting fault current limiter in fault condition. Alternative conductor designs such as superconductors with high resistance alloy strip, stabilizer-free superconductors, and a combination of limiting and nonlimiting coils are being tested. The various superconductor designs can be simulated with this HTS transformer to observe the effects from short-circuit currents.

Section IV describes several factors that are found to affect the magnitude of inrush currents, as shown in (18)–(20). Equation (21) shows how the source impedance between the transformer and the source of sustained voltage acts to reduce the magnitude of the peak inrush current. Generally, there will be some external impedance that will reduce the inrush current below the maximum. When the transformer is small compared with the system, which is normally the case, relatively high inrush currents may be obtained.

For the maximum inrush current, there is a linear relation between the maximum peak inrush current and the applied voltage. The linear relationship is explained by the fact that, under conditions of residual flux and switching angle that produce the maximum inrush condition, the iron core is completely saturated. The maximum inrush current can be obtained when the transformer is energized at zero point on the voltage wave. The crest inrush current is reduced as the switching angle varies in either direction from a voltage zero.

The transient inrush currents decay at a rate determined by the resistance of the transformers themselves. Transformers having relatively high losses will, in general, have faster rates of decay than those which are more efficient, as shown in Figs. 14 and 15. Meanwhile, resistance in the circuit, i.e., between the transformer terminals and the source of sustained voltage, not only reduces the maximum initial inrush current but also expedites its rate of decay and assists in restoring normal voltage wave shape more quickly.

VI. Conclusion

An analysis was carried out to determine the effects of short-circuit and inrush current phenomena on HTS transformer windings. The outcomes on the application of different types of short circuits toward the HTS transformer were studied. In addition, the results on the application of inrush forces toward the transformer were compared with that of conventional transformers.

The force patterns for short circuit and inrush are shown to be quite different from each other. The secondary winding is first to experience the larger short-circuit force, which is cleared in tens of milliseconds. Meanwhile, the smaller inrush force acts on the energized winding and can last for a few seconds. Our study demonstrates the reliability of an HTS transformer to deal with short-circuit and inrush currents.

The mathematical model presented enables the estimation of temperature rise developed in the transformer winding during short circuit. Simplifying assumptions made in the computation appear not to significantly affect the model's accuracy. Comparison of the presented model with the ones provided in the IEC 60076 standards [7] is shown and found to be comparable.

The calculation on short-circuit forces shows the HTS transformer is unable to withstand the duration of 2 s, as prescribed in the IEC standards. Temperature and resistance of the secondary winding tremendously increase and rise beyond the allowable limit during the period. Therefore, arrangement must be made to isolate the transformer sooner in order to prevent any damage to the transformer and loss of power supply to the customers. The transformer should be limited to fault duration below 2 s. Further studies are currently in progress.

Our analysis shows that inrush currents may not be considered dangerous to an HTS transformer. The inrush peak values can go up to several times the rated current value, but as long as they are below the critical current value, the characteristics of HTS winding will not change. However, precautions have to be taken into the network design because their lengthy existence may unnecessarily overwork the protective equipment such as relays and fuses.

References

[1] M. A. A. Rahman, T. T. Lie, and K. Prasad, "Three-phase modeling of HTS transformer in distribution networks," in *Proc. Int. Power Energy Conf.*, 2010, pp. 72–77.

[2] W. H. Kersting and R. C. Dugan, "Recommended practices for distribution system analysis," in *Proc. Power Syst. Conf. Expo.*, 2006, pp. 499–504.

[3] E. B. Makram, M. A. Bou-Rabee, and A. A. Girgis, "Three-phase modeling of unbalanced distribution systems during open conductors

and/or shunt fault conditions using the bus impedance matrix," *Elect. Power Syst. Res.*, vol. 13, no. 3, pp. 173–183, Dec. 1987.

[4] L. F. Blume, G. Camilli, S. B. Farnham, and H. A. Peterson, "Transformer magnetizing inrush currents and influence on system operation," *Trans. Amer. Inst. Elect. Eng.*, vol. 63, no. 6, pp. 366–375, Jun. 1944.

[5] N. Glasson, M. Staines, R. Buckley, M. Pannu, and S. Kalsi, "Development of a 1 MVA 3-phase superconducting transformer using YBCO Roebel cable," *IEEE Trans. Appl. Supercond.*, vol. 21, no. 3, pp. 1393–1396, Jun. 2011.

[6] W. H. Kersting and W. H. Phillips, "Distribution system short circuit analysis," in *Proc. Energy Convers. Eng. Conf.*, 1990, pp. 310–315.

[7] *Power Transformers—Part 5: Ability to Withstand Short Circuit*, IEC Standard 60076-5, 2000.

[8] Y. Y. Xie, K. Tekletsadik, D. Hazelton, and V. Selvamanickam, "Second generation high-temperature superconducting wires for fault current limiter applications," *IEEE Trans. Appl. Supercond.*, vol. 17, no. 2, pp. 1981–1985, Jun. 2007.

[9] R. Stevens and J. Boerio-Goates, "Heat capacity of copper on the ITS-90 temperature scale using adiabatic calorimetry," *J. Chem. Thermodyn.*, vol. 36, no. 10, pp. 857–863, Oct. 2004.

[10] C. R. Brooks, W. E. Norem, D. E. Hendrix, J. W. Wright, and W. G. Northcutt, "The specific heat of copper from 40 to 920 °C*," *J. Phys. Chem. Solids*, vol. 29, no. 4, pp. 565–574, Apr. 1968.

[11] T. Ishigohka, K. Uno, and S. Nishimiya, "Experimental study on effect of in-rush current of superconducting transformer," *IEEE Trans. Appl. Supercond.*, vol. 16, no. 2, pp. 1473–1476, Jun. 2006.

[12] C. M. Rey, R. C. Duckworth, S. W. Schwenterly, and E. Pleva, "Electrical AC loss measurements on a 2G YBCO coil," *IEEE Trans. Appl. Supercond.*, vol. 21, no. 3, pp. 2424–2427, Jun. 2011.

[13] T. Janowski, B. A. Glowacki, G. Wojtasiewicz, S. Kozak, J. Kozak, B. Kondratowicz-Kucewicz, M. Majka, and M. Wozniak, "Fault current limitation in power network by the superconducting transformers made of 2G HTS," *IEEE Trans. Appl. Supercond.*, vol. 21, no. 3, pp. 1413–1416, Jun. 2011.

[14] H. Kojima, M. Kotari, T. Kito, N. Hayakawa, M. Hanai, and H. Okubo, "Current limiting and recovery characteristics of 2 MVA class Superconducting Fault Current Limiting Transformer (SFCLT)," *IEEE Trans. Appl. Supercond.*, vol. 21, no. 3, pp. 1401–1404, Jun. 2011.

M. A. Abdul Rahman received the first degree in electrical engineering from the University of Texas, El Paso, in 1990 and the Master degree in electrical engineering from Universiti Tenaga Nasional, Putrajaya, Malaysia, in 2004. He is currently working toward the Ph.D. degree at Auckland University of Technology, Auckland, New Zealand.

He had served Tenaga Nasional Berhad (TNB), a major power utility company in Malaysia, from 1991. He was a Senior Engineer with the Department of Engineering, Distribution Division, TNB, looking into performance and diagnostic of distribution power equipment. His major interests are power system study, power equipment and accessories performance, condition monitoring and diagnostic, and renewable energy technologies.

T. T. Lie (S'89–M'92–SM'97) received the B.S. degree from Oklahoma State University, Stillwater, in 1986 and the M.S. and Ph.D. degrees from Michigan State University, East Lansing, in 1988 and 1992, respectively.

He had worked in Nanyang Technological University, Singapore. He is now an Associate Professor with the Department of Electrical and Electronic Engineering, Auckland University of Technology, Auckland, New Zealand. His research interests include power system control, deregulated power systems, and renewable energy systems

K. Prasad (M'08) received the B.E. degree from Bangalore University, Bangalore, India, in 1980, the M.Tech. degree in electrical engineering from the Indian Institute of Technology, Madras, India, in 1982, and the Ph.D. degree from the University of Western Australia, Perth, Australia, in 1990.

He is currently a Professor with the Department of Electrical and Electronic Engineering, Auckland University of Technology, Auckland, New Zealand. His research interests include material science, microelectronic devices, and failure analysis and reliability engineering.

Appendix A5: Transaction (DPC – JEPE)

DPC Transactions on Energy and Power Engineering.

(Accepted for publication)

Mth. Year, Volume X, No.X (Serial No.XX)
Journal of Energy and Power Engineering, ISSN XXXX-XXXX, USA

Modelling and Analysis of Distribution Network with HTS Transformer

M. A. Abdul Rahman*, T. T. Lie** and K. Prasad**
School of Engineering, Faculty of Design & Creative Technologies, Auckland University of Technology, Auckland, New Zealand

Received Month Day, Year / Accepted Month Day, Year / Published Month Day, Year.

Abstract: Transformers utilizing high temperature superconductors (HTS) are considered as a timely invention. The number of power transformers age more than 30 years old and nearing retirement is increasing. If this window of opportunity is not grabbed, there would be great reluctance to replace recently installed highly priced capital asset. Major projects of developing HTS transformers are well making progress in the United States, Europe, Japan, Korea and China which indicate the interest. The efforts must have been appropriately verified through the economic interest of the discounted losses. Consequently, it is very important to develop an understanding of the fundamental HTS transformer design issues that can provide guidance for developing practical devices of interest to the electric utility industry. The parameters of HTS transformer need to be validated before any effort is to carry out to model the behaviour of a distribution network under a range of conditions. The predicted performance and reliability of HTS transformers can then be verified through the network modelling and analysis calculation. The ultimate purpose is to furnish electric utilities precise information as to which HTS transformers work under various applications with greater technical efficiency and proven reliability.

Key words: high temperature superconductor; transformer; distribution system; network modelling.

1. Introduction

A Dutch scientist, H. Kamerlingh Onnes, accidentally encountered superconductivity in mercury while observing the relationship between electrical resistance and temperature of the material in 1911. He discovered the resistivity of mercury unexpectedly dropped to zero at a temperature of 4.2 K [1]. Within a couple of years, superconductivity was also detected in lead and tin. As a result, erratic speculation arose from this sensational phenomenon that large field magnets and heavy electric machinery could be operated without power loss. However, this anticipation was met by disappointment and frustration. The superconductivity behaviour of the metals was discovered to disappear above a certain critical temperature. In addition, the characteristic was also observed to be wiped out by relatively small currents and magnetic fields. Onnes had already tested a Ni alloy coated with Pb-rich superconducting solder. Unfortunately, the material lost its superconductivity at magnetic fields less than 50 mT [2].

Numerous superconducting materials were brought to light in the next half century. Extensive research was carried out on electromagnetic properties of these materials. However, moderate accomplishment in terms of critical currents and magnetic fields prevented encouraging follow through in their applications. Nevertheless, Barden, Cooper and Schrieffer [3] disclosed their findings in the BCS theory of superconductivity in 1957, which, among others, provided a description of the microscopic behaviour of

*** Corresponding author:** M.A. Abdul Rahman, doctoral candidate; research fields: power system study, power equipment and accessories performance, condition monitoring and diagnostic. E-mail: muhammad.rahman@aut.ac.nz.

**** Co-authors**: T.T. Lie, Ph.D., associate professor; research fields: power system control, deregulated power systems and renewable energy systems. E-mail: tek.lie@aut.ac.nz. K. Prasad, Ph.D., professor; research fields: material science, microelectronic devices, failure analysis and reliability engineering. E-mail: krishnamachar.prasad@aut.ac.nz.

low temperature superconductors that clarified many ambiguities and uncertainties of the superconductivity nature. During the same period, Kunzler [4] found a new category of superconducting alloy that could withstand very high magnetic fields and large current densities. High performance superconducting wires were commercially available in the mid 1970s from the advancement of these composite wires. The wires were formed by embedding fine superconducting filaments in a normal metal such as aluminium or copper. The invention permitted the building up of high DC and pulsed field magnets. Consequently, the applications on high power AC began to be seriously looked into.

Swiss physicists, Georg Bednorz and Alex Muller, in April 1986, announced the discovery of high temperature superconductor in the perovskite structure Lanthanum-Barium-Copper at 30 K [5]. The discovery opened up interest in research and development for the technology and many superconductors have been found since then [6]-[7]. Several of these superconductors show superconductivity at temperatures higher than liquid-nitrogen temperature (77 K). The most common high temperature superconductors are $Bi_2Sr_2Ca_2Cu_3O_x$ (Bi-2223), $YBa_2Cu_3O_x$ (Y-123 or YBCO) and $Bi_2Sr_2Ca_1Cu_2O_x$ (Bi-2212). These materials have exhibited a superconducting behaviour at temperatures below 110, 92 and 85 K, respectively, which allow them to be operated by cooling them in liquid nitrogen.

However, the research on superconductivity materials at higher temperatures and their material properties is still ongoing [8-12]. The basic advantages of high temperature superconductors (HTS) are (relatively) higher operating temperature and heat capacity. These characteristics allow simple cooling and high stability against disturbances. However, a major shortcoming on high temperature superconductors is the significantly higher material cost. The price of a high temperature superconductor, normally expressed in per metre length per ampere of critical current, is estimated around 10 to 50 times greater than that of copper.

The research work in this paper starts with the review and assessment of the state-of-the-art of HTS transformer designs and technologies. Then, a set of parameters is built up to represent the HTS transformer that can be correlated with existing distribution network designs and modelled accordingly under various network conditions. A real distribution network, which is inherently unbalanced, will be modelled while taking into account the three phase models of all the other relevant network components. The ultimate tasks of the present work are to establish and scrutinize the distribution network model with the application of HTS transformer in relation to power flow and short circuit analysis.

The main objective of this work is to develop an understanding of the fundamental HTS transformer design issues that can provide guidance for developing practical devices of interest to the electric utility industry. At the same time, it will provide transformer manufacturers powerful knowledge of the design technology subject to their customers, who will appreciate the value added services. The study will validate the parameters of HTS transformers and model the behaviour of a distribution network under a range of conditions. The broad understanding of HTS transformer capabilities, which will evolve from this work, will benefit power network designers so that they will be able to refine the network accordingly. The study will then verify the predicted performance and reliability of HTS transformers through a network modelling and analysis calculation. Finally, the study will furnish electric utilities precise information as to which HTS transformers work under various applications with greater technical efficiency and proven reliability.

2. HTS Transformer

The prospects for the applications of the superconductor technology have been recognized in

the early stage of the material development. The ability to transmit electricity without resistance and the associated magnetic characteristics of the superconductors has opened up a new vision, particularly in revolutionizing the electricity supply industry [13]. The applications would offer numerous benefits such as increase in energy efficiency due to low losses and high current carrying capability characteristic of the materials. They would also be able to offer environmental advantages from the production of oil-free equipment and low magnetic field leakage devices [14]. Other potential benefits include reduction in equipment size, deferment in expansion, increase in reliability and flexibility in transmission and distribution of power system [15].

However, all the possible advantages from the superconductor technology development mentioned above require realistic analysis in order to quantify them. The markets are targeted at the power industry. Power utilities and industrial manufacturers are frequently questioned on the adequacy, reliability and cost of the conventional equipment. These factors are able to create ambiguities to assist in the exploitation of superconductor technology. Finally, the ultimate focus for the new technology will be on the lower electricity costs, improved environmental quality and competitive products for global competition [15].

High temperature superconductivity is still an on-going area of research worldwide. The characteristics of higher transition temperature and economical cryogenic cooling have increased the potential for the applications in the electrical power industry. The advancement of high temperature superconducting technologies has spurred on the demonstration of various prototypes such as power cables, transformers, motors and fault current limiters [14]-[19].

Significant acceleration programmes have been carried out in the USA, Europe and Asia in the hope for larger application scales. The US Department of Energy (DOE) and Electricite de France (EDF) lead the programs related to the electric power sector in the USA and France, respectively [20]-[21]. In Japan, several national projects on superconducting apparatus have been conducted by NEDO (New Energy and Industrial Technology Development Organization) since 2000 with the objectives for real applications in the years of 2011-2015 [22]. A 10-year DAPAS (Development of the Advance Power system by Applied Superconductivity technologies) programme in Korea has entered the final phase with several significant development achievements [23]. Meanwhile, the State “863” Program (High Technology Research & Development Program) by the Ministry of Science and Technology of China, Chinese Academy of Sciences (CAS) and the power equipment industries which has supported the power application research of superconductor in China since the year 2000, has successfully made, tested and demonstrated several superconducting power equipment on the field [24]. Amongst the critical factors that are being looked into for full commercialization of the application are stability and reliability, robustness, energy efficiency and cost-effectiveness of the superconductors [14]-[15].

Strong international interest in the development and commercialization of the HTS transformer can be observed [23]-[28]. Some have estimated that in the year 2020, up to 80% of new power transformers will be using high temperature superconductors instead of copper [11]. The expectations seem rather high in the power engineering sector. Several studies have been carried out to compare conventional and high temperature superconducting power transformers [29]-[30]. The viability of a superconducting transformer is dealt not only with technical points of view but also economical aspects. The conventional copper transformers have been produced for almost a century and have reached their physical and technological limits in many aspects. The crucial expectation will be of what cost-effective conditions the overall efficiency of a high temperature

superconducting transformer can be made higher than that of a conventional copper transformer.

3. Distribution Network Modelling

More and more people have worked on the development of modelling and analysis on distribution network. Previously, most advancement was devoted to large transmission networks and synchronous generators. Various tools are now available for distribution engineers to run power flow studies and simulate loading conditions on the network. Such progression on the analysis tools allows for in-depth studies in power flow, losses, short circuit, *etc*. This paper is looking into transformer as well as overhead and underground lines in the modelling and analysis.

3.1 Transformer

The research study focuses on three-phase step down distribution transformer models with delta-grounded wye connection. This is a popular connection to serve a four-wire feeder system and to provide service to loads which are primarily single phase [31]. The transformer models are generalized for the connection with other series components of the network such as line segments and voltage regulators. The matrix equations to calculate the voltages and currents at the input point as a function of the voltages and currents at the output point are,

$$[VLN_{abc}]_{in} = [a] \cdot [VLN_{abc}]_{out} + [b] \cdot [I_{abc}]_{out} \quad (1)$$

$$[I_{abc}]_{in} = [c] \cdot [VLN_{abc}]_{out} + [d] \cdot [I_{abc}]_{out} \quad (2)$$

The equation for the voltages at the output point as a function of voltages at the input point and the currents at the output point is also required,

$$[VLN_{abc}]_{out} = [A] \cdot [VLN_{abc}]_{in} + [B] \cdot [I_{abc}]_{out} \quad (3)$$

Several electrical characteristics such as voltage and capacity ratings, impedance, load and no load loss of the distribution transformers are required to develop the model. These parameters are significant, especially to observe the operational differences between the conventional transformers and the HTS transformers. The parameters will be used to calculate the generalized matrices for the modelling of the transformers.

3.2 Line

The line models are generalized for the connection with other series components of the distribution network. The matrix equations are basically the same as equations (1) - (3). The major parameters for modelling of lines segments will be the series impedance and shunt admittance. The accurate measurements are significant prior to carrying out the analysis of a distribution feeder [32]-[33]. The actual phasing of each conductor needs to be clarified and the correct spacing between each conductor needs to be confirmed.

In 1926, John Carson developed a set of equations to calculate the self and mutual impedances of power lines which took the ground as the return path of the currents [34]. At this stage, several unknown values such as resistance and Geometric Mean Radius (GMR) of dirt and distances from conductors to dirt have been identified. The equations utilize conductor images. Every conductor above ground has an image conductor with the same distance below ground. The Carson's equations were then modified to solve the problem regarding the identified unknown values.

3.2.1 Overhead

The modified Carson's equations are used to compute the primitive self and mutual impedances of overhead lines.

Fig. 1 shows a typical bare overhead line structure where D_{ab}, D_{ac} and D_{bc} are the distances between phases. Meanwhile D_{nax}, D_{nbx} and D_{ncx} are the horizontal distances between the neutral and the phases, respectively, and D_{ny} is the vertical distance between the neutral and the phases. The distance between the neutral and the ground is labelled as D_{ng}. For the phase frame analytical method, the primitive impedance matrix needs to be converted to a 3×3 phase impedance

matrix for connection with other components. Kron reduction method can be applied to achieve the required matrix size [35].

On the other hand, the shunt admittance calculation will include the conductance and capacitive susceptance of the line. However, the conductance is normally very small and can be ignored. The general application applied in Carson's equations is also employed in the calculation of the shunt capacitance.

3.2.2 Underground

The study focuses on the tape screened type for the underground cables which are very popular and common at the moment. The cable consists of a phase conductor covered by a semiconducting layer which is bonded to the insulation. The insulating material is covered by another semiconducting layer. The copper tape screen is applied helically around the second semiconducting layer. The final layer is the insulating jacket which encircles the tape screen.

The modified Carson's equations are also used to compute the primitive self and mutual impedances of the phase conductor and the tape screen for the underground cables. Since the tape screens for all the phases touch each other and become common neutral, the three-wire underground cables will result in a 4x4 primitive impedance matrix.

However, as for the overhead lines, the matrix can also be partitioned. For the phase frame analytical method, the primitive impedance matrix needs to be reduced to a 3×3 phase impedance matrix for connection with other components. Fig. 2 shows a three-wire line segment.

The tape screen is grounded so that it has the same potential at any position. Because of the screening, the electric field is assumed to be created by the charge of the phase conductor which will be confined to the surrounding tape screen. The general voltage drop equation can be applied to calculate the capacitance between the phase conductor and the tape screen.

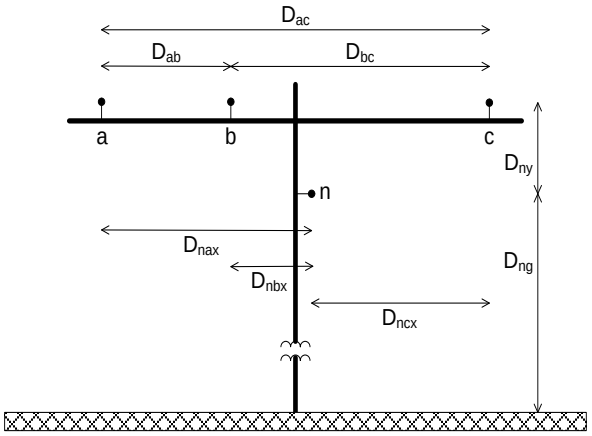

Fig. 1 Typical Three Phase Overhead Line Structure

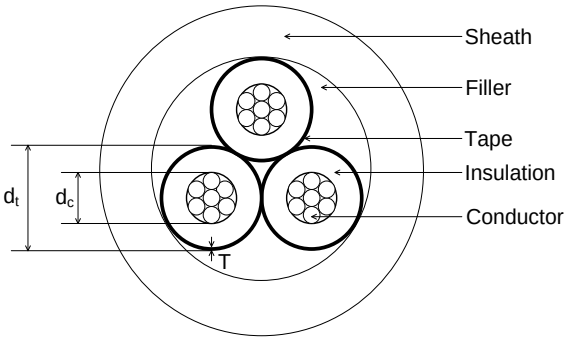

Fig. 2 Three Core Tape-Screen Cable

3.2.3 Generalised Matrices

Fig. 3 shows the three phase distribution overhead and underground line models. The generalized matrices for the line are developed from the model of the phase impedance matrices and the phase admittance matrices.

The critical steps in the analysis are to determine the actual phasing of the lines and the correct spacing between conductors. Several parameters such as voltage rating, insulation type, conductor size, phase connection, conductors spacing, *etc*., of the conductors are significant in the calculation for the modelling of overhead lines and underground cables. These parameters are used to calculate the generalized matrices for the modelling of the line segments.

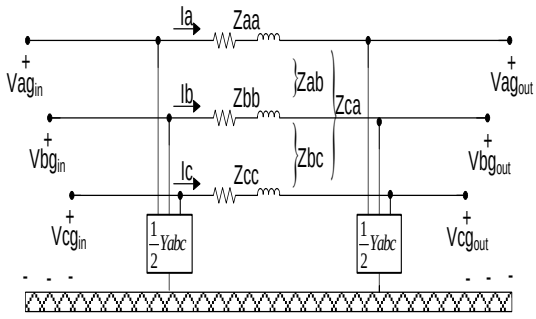

Fig. 3 Three-Phase Distribution Line Segment

4. Analysis Technique

The evaluation of distribution power network can be well distinguished from that of transmission for its unbalanced loading characteristic. The main contributing features for the analysis are the unequal single-phase loads and the non-equilateral conductor spacing either for overhead lines or underground cables. The conventional power flow and short circuit programs which are implemented in the transmission network studies would not be adequate. Those programs are based on balanced network where the single-phase equivalent system is employed. For the distribution network assessment, three-phase modelling for the major power components must be applied. In the analysis, the electrical characteristics of all the major components will have to be acquired for the network evaluation.

4.1 Power Flow Analysis

The power flow analysis is applied to determine the normal steady-state operating condition of the network under study. Various outputs can be obtained from the analysis such as voltage magnitudes and angles at all nodes in the network, power flow and power loss in each line segment and total network power input and power losses. However, information such as three-phase voltages at the substation and complex power of all the loads and the load models should be made available prior to conducting the analysis. Ladder iterative technique is employed for the analysis. Kirchhoff's Voltage Law (KVL) and Kirchhoff's Current Law (KCL) are utilized to determine the node voltages and the line currents respectively. Nevertheless, the technique has to be adjusted to suit the radial system characteristic and nonlinear feature of the distribution network. The load currents are instead calculated by dividing the conjugates of complex power loads by the node voltages. The forward and backward sweep or the iteration will be continued until the difference between the calculated and the specified voltages at the source meet the acceptable tolerance.

The unbalanced three-phase distribution network can be divided into series components and shunt components. The series components are transformers, overhead lines, underground cables and voltage regulators. The components are connected in terms of generalized matrices through the input and output voltages and currents as defined in general equations (1) - (3). Meanwhile, the shunt components are spot loads, distributed loads and capacitor banks.

4.2 Short Circuit Analysis

The method of applying symmetrical components in the computation of short circuit currents for unbalanced faults is not suitable for distribution feeders that are inherently unbalanced. The unbalanced mutual coupling between the phases will lead to mutual coupling between the sequence components. Also, there will be limitation on the phases between which the faults may occur. Therefore, it is important to look into a suitable method for short circuit analysis of an unbalanced distribution system using the phase frame method.

The model of an unbalanced feeder for short circuit calculation is presented in Fig. 4. Short circuits can occur at any of the points shown in the model. The short circuit currents at point 1 are usually acquired from a transmission system short circuit analysis. The resultant short circuit MVAs will help to determine the zero and positive sequence impedances of the equivalent system. The short circuit analysis for points

2, 3, 4 and 5 can then be carried out with the supporting information.

The calculation for short circuits at points 2, 3, 4 and 5 can be carried out using the Thevenin equivalent three-phase circuit at the short circuit point. The Thevenin equivalent voltages (E_{th}) are the nominal line-to-ground voltages.

Fig. 5 shows the Thevenin equivalent circuit at the faulted node. E_a, E_b and E_c are the Thevenin equivalent line-to-ground voltages. $[Z_{tot}]$ is the Thevenin equivalent phase impedance matrix at the faulty node. Z_f is the fault impedance. I_{fa}, I_{fb} and I_{fc} are the fault currents. V_{ax}, V_{bx} and V_{cx} are the phase voltages (a, b, c) to the point of fault (x). V_{xg} is the voltage from the point of fault (x) to the ground (g).

5. Case Study

5.1 Network Characteristics

A simulation was carried out on a simple distribution feeder. The source voltages are balanced three-phase 11 kV line-to-line. The system involves a short three-wire delta 11 kV tape screened underground cable and four four-wire wye 415 V line-to-line overhead lines with the transformer in-between. The network is shown in Fig. 6.

Conventional and HTS distribution transformers are employed in the network study. The technical information on the HTS transformer is based on a preliminary baseline design the authors are working on. The electrical characteristics for a typical conventional transformer and the under study HTS transformer are shown in Table 1.

Meanwhile, the underground cable is a 300 mm^2 three-core tape screened XLPE cable as shown in Fig. 2 and the overhead line structure is as per Fig. 1 using 500 kcmil 19 strands AAC for both the phase and neutral conductors. Each line is short and assumed to be only 0.40 km for the underground cable and 0.10 km for the overhead lines. The loads for each phase a, b and c for each low voltage feeders are assumed to be 40 kVA at 0.85, 0.90 and 0.95 lagging power factors, respectively, which means the total loads for the circuit are 480 kVA.

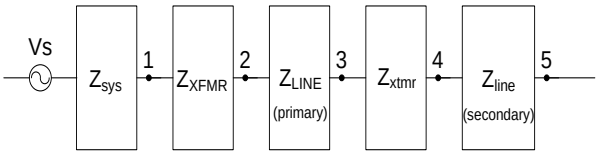

Fig. 4 Model of an Unbalanced Feeder for Short Circuit Analysis

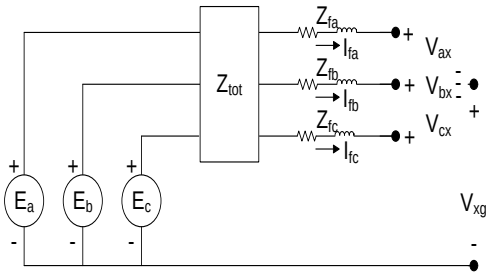

Fig. 5 Thevenin Equivalent Circuit at The Faulty Node

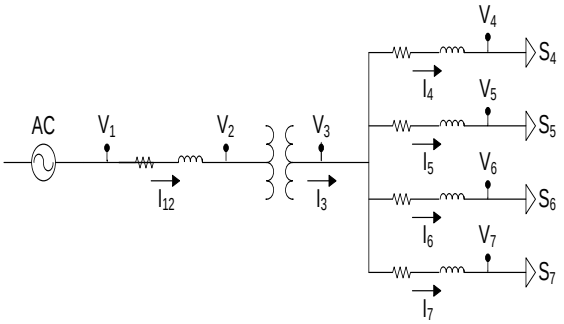

Fig. 6 Network of a Simple Distribution Feeder

Table 1 Typical Electrical Characteristic of Transformers

Transformer Types	Electrical Characteristics	
	Conventional	***HTS***
VA Rating (kVA)	1000	1000
Voltage Rating (kV)	11/0.415	11/0.415
Load Loss (W)	7000	1250
No Load Loss (W)	1400	800
Impedance (%)	5	5
Connection	Δ-Y	Δ-Y

5.2 Results

Power flow analysis was carried out on the circuit. After four iterations, the magnitudes of voltage errors are less than the acceptable tolerance of 0.001 per-units. The values of voltages and currents at the respective nodes for both transformers are shown in Table 2 and Table 3, respectively.

The line-to-neutral voltages at each node are within the acceptable range for the system voltages of 11 kV and 415 V line-to-line voltages. The currents are dependent on the loads and they are within the 350 A rating of the line segments.

Table 2 Voltages At The Respective Nodes

Node Voltage	Phase	Transformer	
		Conventional	*HTS*
V_1	a	$6350.85\angle 30^0$	$6350.85\angle 30^0$
	b	$6350.85\angle -90^0$	$6350.85\angle -90^0$
	c	$6350.85\angle 150^0$	$6350.85\angle 150^0$
V_2	a	$6349.50\angle 0^0$	$6349.50\angle 0°$
	b	$6349.60\angle -120^0$	$6349.60\angle -120^0$
	c	$6349.40\angle 120^0$	$6349.40\angle 120^0$
V_3	a	$236.00\angle -31^0$	$236.59\angle -31^0$
	b	$236.49\angle -151^0$	$237.10\angle -151^0$
	c	$237.16\angle 89^0$	$237.81\angle 89^0$
V_4	a	$229.22\angle -32^0$	$229.85\angle -32^0$
	b	$231.93\angle -153^0$	$232.56\angle -153^0$
	c	$233.83\angle 87^0$	$234.49\angle 87^0$

Table 3 Currents At The Respective Nodes

Line Current	Phase	Transformer	
		Conventional	*HTS*
I_{12}	a	$25.49\angle -31^0$	$25.42\angle -31^0$
	b	$24.94\angle -145^0$	$24.86\angle -145^0$
	c	$27.64\angle 93^0$	$27.57\angle 93^0$
I_3	a	$698.04\angle -64^0$	$696.20\angle -64^0$
	b	$689.85\angle -178^0$	$687.99\angle -178^0$
	c	$684.18\angle 69^0$	$682.26\angle 69^0$
$I_4= I_5= I_6= I_7$	a	$174.52\angle -64^0$	$174.06\angle 64^0$
	b	$172.47\angle -178^0$	$172.00\angle -178^0$
	c	$171.05\angle 69^0$	$170.57\angle 69^0$

The results show that the voltage and current values for HTS and conventional transformers are very close, with less than 1% difference. Power loss calculation can also be carried out in the analysis. The losses are calculated at each network segment. Figs. 7, 8 and 9 show the losses at different load conditions for line segments, transformer segment and total network, respectively.

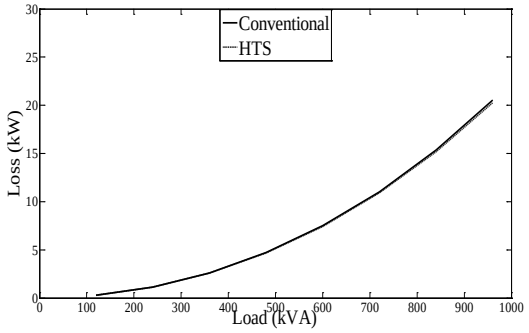

Fig. 7 Line Segments Losses at Various Load Conditions

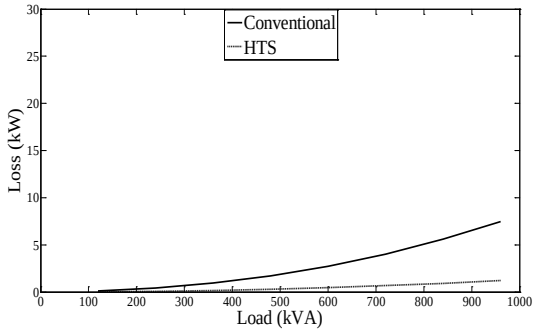

Fig. 8 Transformer Segment Losses at Various Load Conditions

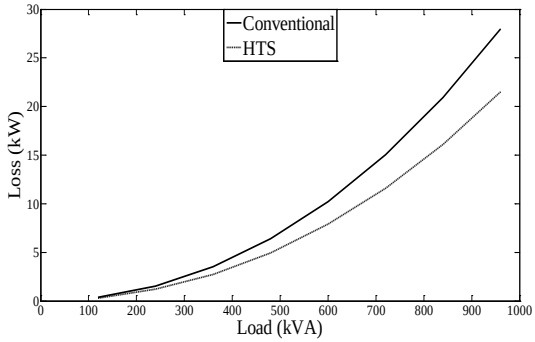

Fig. 9 Total Segment Losses at Various Load Conditions

Power losses for the line segments are the correct values for all the three phases. Applying both types of transformers would provide minor differences in the loss values, particularly at low and medium load conditions. For the transformer segment, the values are not the actual transformer losses. These values are without the winding losses under no-load condition. No-load losses from hysteresis loss and eddy currents are also not included in the loss values. However, the variations between both transformers particularly under high load conditions are very significant to indicate the improvement in energy efficiency.

The three-phase fault, three-phase-to-ground fault, phase-to-phase fault and phase-to-ground fault analysis are carried out on the network with HTS transformer. The circuit is shorted at the far end of the low voltage line segment, *i.e.*, 100 m and at the near end, *i.e*., 0.1 m from the transformer. The fault current and voltage values are presented in Tables 4 and 5, respectively. The fault currents and voltages will be experienced by the HTS transformer if the fault occurred.

Each utility has its own electrical network characteristics. For the low voltage distribution network applied in the analysis, certain utilities are specifying their transformers to meet the requirement characteristics of maximum service voltage at 1.1 kV_{rms} and low voltage short-circuit current at 31.5 kA. The short-circuit currents and voltages resulting from the analysis fall within these requirements.

6. Conclusion

An analysis was carried out to validate the parameters of a typical HTS transformer design in a simple distribution feeder and compared with that of a conventional transformer to demonstrate that HTS transformer with the set up parameters should be performing as well as a conventional transformer in a normal distribution network.

Applying the phase frame calculation method gave eminently satisfactory results. The three-phase impedance and admittance matrices were very useful for the study. The method of solution appeared to be accurate and efficient. This validates the technique for more advanced and complicated circuit designs.

Load flow and system losses calculation were carried out on the network with the application of both conventional and HTS transformers. The computation provides the actual losses on the line segments. Even though the actual transformer losses would not be available through network modelling, the load loss fraction of the losses can be employed as part of the comparison for the performance of the two transformers. The advantage of using HTS transformer can be observed through the reduction of real power requirement, especially on heavy loading networks.

The sample network with HTS transformer was simulated with different types of short-circuits conditions. The calculation provides the fault currents and voltages to be expected on the transformer for each fault classification. Since each utility will have its own electrical network characteristics, the computed short-circuit current and voltage values should fall within the specification set by the utility concerns.

The findings from this work will lead to further investigation on HTS transformer into various distribution network conditions such as the effects of different switching scenarios. These analyses will contribute further in predicting the performance and reliability of HTS transformer before the installation in a distribution network system.

Acknowledgments

The research project is supported by Industrial Research Limited, New Zealand through the Foundation for Research, Science and Technology (FRST) High Temperature Superconductors (HTS) Accelerated Development Transformational Research, Science and Technology (TRST) funding.

Table 4 Currents and Voltages for Three Phase Faults

Short Circuit Values	3-Phase Fault		3-Phase to Ground Fault	
	Far End	Near End	Far End	Near End
I_{fa} (kA)	4.88∟-99°	27.93∟-118°	4.62∟-73°	24.2∟-88°
I_{fb} (kA)	5.37∟134°	27.94∟122°	4.62∟107°	24.2∟92°
I_{fc} (kA)	4.61∟12°	27.92∟2°	0	0
V_{ax} (V)	0	0	0	0
V_{bx} (V)	0	0	0	0
V_{cx} (V)	0	0	365∟88°	360∟90°
V_{xg} (V)	8.58∟102°	0.05∟92°	122∟-92°	120∟-90°

Table 5 Currents and Voltages for One or Two Phase Faults

Short Circuit Values	Phase-a to Phase-b Fault		Phase-a to Ground Fault	
	Far End	Near End	Far End	Near End
I_{fa} (kA)	4.62∟-73°	24.2∟-88°	3.27∟-106°	27.91∟-118°
I_{fb} (kA)	4.62∟107°	24.2∟92°	0	0
I_{fc} (kA)	0	0	0	0
V_{ax} (V)	0	0	0	0
V_{bx} (V)	0	0	299∟-164°	241∟-150°
V_{cx} (V)	365∟88°	360∟90°	279∟102°	240∟90°
V_{xg} (V)	122∟-92°	120∟-90°	0	0

References

[1] J.K. Sykulski, Modelling electromagnetic fields and power losses in high temperature superconductors, IEE Colloquium on Computer Methods for Material Modelling in Elecgtromagnetics 1997, pp. 2/1-2/6.

[2] D. Larbalestier, A. Gurevich, D.M. Feldmann, A. Polyanski, High-Tc superconducting materials for electric power applications, Nature 414 (6861) (2001) 368.

[3] J. Bardeen, L.N. Cooper, J.R. Schrieffer, Theory of superconductivity, Physical Review 108 (5) (1957) 1175.

[4] J.E. Kunzler, Superconductivity in high magnetic fields at high current densities, Reviews of Modern Physics 33 (4) (1961) 501.

[5] J.G. Bednorz, K.A. Müller, Possible high-Tc superconductivity in the Ba-La-Cu-O system, Zeitschrift für Physik B Condensed Matter 64 (2) (1986) 5.

[6] M.P. Oomen, AC loss in superconducting tapes and cables, PhD, University of Twente, 2000.

[7] S.H. Pan, E.W. Hudson, K.M. Lang, H. Eisaki, S. Uchida, J.C. Davis, Imaging the effects of individual zinc impurity atoms on superconductivity in Bi2Sr2CaCu2O8+[delta], Nature 403 (6771) (2000) 746.

[8] D. Djurek, Z. Medunić, A. Tonejc, M. Paljević, PbCO3·2PbO+Ag2O and PbCO3·PbO+Ag2O (PACO) systems: route for novel superconductors, Physica C: Superconductivity 351 (1) (2001) 4.

[9] B. Seeber, Handbook of Applied Superconductivity, Institute of Physics Publishing Bristol UK, 1998.

[10] T.P. Sheahen, Introduction to High-Temperature Superconductivity, Plenum Press, New York, 1994.

[11] T.P. Sheahen, B.W. McConnell, J.W. Mulholland, Method for estimating future markets for high-temperature superconducting power devices, IEEE Transactions on Applied Superconductivity 12 (2) (2002) 1784-1789.

[12] R. Wesche, High-Temperature Superconductors: Materials, Properties, and Applications, Kluwer Academic Publishers, Boston/Dordrecht/London, 1998.

[13] F. McGowan, New developments in superconducting materials : Implications for the electricity supply industry, Energy Policy 16 (5) (1988) 506-513.

[14] M. Chen, L. Donzel, M. Lakner, W. Paul, High temperature superconductors for power applications, Journal of the European Ceramic Society 24 (6) (2004) 1815-1822.

[15] W.G. Garlick, Power system applications of high temperature superconductors, Cryogenics 37 (10) (1997) 649-652.

[16] A.D. Appleton, Near term engineering applications of high Tc superconductors, Cryogenics 34 (Supplement 1) (1994) 31-38.

[17] R.F. Giese, T.P. Sheahen, A.M. Wolsky, D.K. Sharma, High-temperature superconductors: their potential for utility applications, IEEE Transactions on Energy Conversion 7 (3) (1992) 589-597.

[18] S.P. Hornfeldt, HTS in electric power applications, transformers, Physica C: Superconductivity 341-348 (Part 4) (2000) 2531-2533.

[19] H. Jones, Superconductors in the transmission of electricity and networks, Energy Policy 36 (12) (2008) 4342-4345.

[20] R.A. Hawsey, D.K. Christen, Progress in research, development, and pre-commercial deployment of second generation HTS wires in the USA, Physica C: Superconductivity 445-448 (2006) 488-495.

[21] P. Manuel, F.X. Camescasse, M. Coevoet, V. Leitloff, F. Lesur, E. Serres, P. Suau, J.A. Muraz, Prospects for application of high temperature superconductors to electric power networks, Physica C: Superconductivity 372-376 (Part 3) (2002) 1591-1597.

[22] O. Tsukamoto, S. Akita, Overview of R&D activities on applications of superconductivity to power apparatuses in Japan, Cryogenics 42 (6-7) (2002) 337-344.

[23] P. Minwon, J. Young-Sik, R. Kang-Sik, Recent activities of HTS power application in Korea, International Journal of Applied Ceramic Technology 4 (3) (2007) 217-224.

[24] X. Liye, L. Liangzhen, Recent progress of power application of superconductor in China, IEEE Transactions on Applied Superconductivity 17 (2) (2007) 2355-2360.

[25] G. Donnier-Valentin, P. Tixador, E. Vinot, Considerations about HTS superconducting transformers, IEEE Transactions on Applied Superconductivity 11 (1) (2001) 1498-1501.

[26] A. Formisano, F. Marignetti, R. Martone, G. Masullo, A. Matrone, R. Quarantiello, M. Scarano, Performance evaluation for a HTS transformer, IEEE Transactions on Applied Superconductivity 16 (2) (2006) 1501-1504.

[27] K. Funaki, M. Iwakuma, K. Kajikawa, M. Hara, J. Suchiro, T. Ito, Y. Takata, T. Bohno, S.I. Nose, M. Konno, Y. Yagi, H. Maruyama, T. Ogata, S. Yoshida, K. Ohashi, H. Kimura, K. Tsutsumi, Development of a 22 kV/6.9 kV single-phase model for a 3 MVA HTS power transformer, IEEE Transactions on Applied Superconductivity 11 (1) (2001) 1578-1581.

[28] E. Sissimatos, G. Harms, B.R. Oswald, Optimization of high-temperature superconducting power transformers, IEEE Transactions on Applied Superconductivity 11 (1) (2001) 1574-1577.

[29] B.W. McConnell, S.P. Mehta, M.S. Walker, HTS transformers, Power Engineering Review, IEEE 20 (6) (2000) 7-11.

[30] T. Nagasawa, M. Yamaguchi, S. Fukui, Design study of a high-temperature superconducting transformer, Electrical Engineering in Japan 142 (1) (2003) 25-31.

[31] W.H. Kersting, Transformer model test system, IEEE PES Transmission and Distribution Conference and Exposition, Vol. 3, 2003, pp. 1022-1026.

[32] W.H. Kersting, W.H. Phillips, Distribution feeder line models, IEEE Transactions on Industry Applications 31 (4) (1995) 715-720.

[33] R.M. Ciric, A.P. Feltrin, L.F. Ochoa, Power flow in four-wire distribution networks-general approach, IEEE Transactions on Power Systems 18 (4) (2003) 1283-1290.

[34] J.R. Carson, Wave propagation in overhead wires with ground return, Bell System Technical Journal (1926).

[35] E.B. Makram, M.A. Bou-Rabee, A.A. Girgis, Three-phase modeling of unbalanced distribution systems during open conductors and/or shunt fault conditions using the bus impedance matrix, Electric Power Systems Research 13 (3) (1987) 173-183.

Appendix A6: Transaction (IEEE – TAS)

IEEE Transactions on Applied Superconductivity.

(Accepted for publication)

Computation of the Thermal Effects of Short Circuit Currents on HTS Transformer Windings

M. A. Abdul Rahman, T. T. Lie, Senior Member IEEE, K. Prasad, Senior Member IEEE

***Abstract* -- The active development of High Temperature Superconductor (HTS) materials has led to extensive research and development studies of superconducting transformers worldwide. Considerable benefits have been accomplished with the introduction of HTS transformer such as reduced power loss, size and transformer weight. However, recent advancement in the design technology has focused on the HTS transformer's ability to also perform as Fault Current Limiter (FCL). This study presents the computation of the thermal effects of short circuit currents on a non-FCL HTS transformer and demonstrates how it will behave with a HTS-FCL winding conductor.**

Index Terms – Transformer, Superconductor, Current Limiter, Short Circuit, Thermal Effect.

I. INTRODUCTION

The expansion of generating capacity and the extension of interconnections due to the increase of electrical power requirement have contributed to the growth of short circuit capacity in power networks. Subsequently, the short circuit current the transformers have to cope with becomes more severe [1]. The short circuit capacity of a transformer should be tailored to withstand any fault current incidence due to external short circuit. Any shortcoming in the strength may contribute to mechanical collapse of the windings and deformation of the clamping structures. The short circuit fault that occurs in the power system outside the transformer will generate defects inside the transformer. The internal defects initiated by the external short circuit current may lead to bushing blowouts, tank bursting, fire hazard, *etc*.

HTS winding applications for power transformers are captivating because they require a comparatively smaller amount of conductor for the same transformer capacity. In the United States, conventional transformers account for about 25% of the losses in the power transmission and distribution system and resistive heating is acknowledged to contribute a great portion of these losses [2]. Therefore, the use of HTS transformers is able to bring about substantial energy savings and economized lifetime ownership costs. Other projected benefits include the capability to limit and withstand high currents and consequently minimize the loss of lifetime by thermal damage. They are also able to reduce potential fire and environmental hazards with the use of liquid nitrogen as a substitute to oil for cooling and insulation of the transformers. Last but not least, the weight and volume of HTS transformers are estimated to be about one-half to one-third that of conventional transformers [3]. This study focuses on modelling the effects of various distribution network conditions towards a distribution HTS transformer and looks comprehensively into the thermal effects of short circuit current on various architectural designs and fault current limiting properties of HTS transformer winding conductor.

Recent developments on HTS transformer have focused on its capability to also operate as a Fault Current Limiter (FCL). A previous study [4] has shown that the use of HTS-FCL devices can effectively reduce short circuit current in power transmission and distribution networks. The HTS-FCL transformer acts as a superconducting transformer under normal operating conditions and as a superconducting fault current limiter under short circuit conditions. The fault current that is limited by the HTS transformer will depend on the characteristics and construction of the winding and the parameters of the HTS wire. Several investigations [5-8] were carried out to study the behaviour of HTS-FCL conductors for the implementation in a number of power equipment.

The fault current limiting feature in HTS-FCL transformer could provide protection and reduce the wear and tear of other power equipment experiencing the short circuit current. It could also avoid power interruptions and damages to the power grid and equipment. The transformer is also able to improve the transient stability of power system in fault condition. Therefore, efficient and reliable power system can be established if the transformer could produce fault current limiting function only under fault conditions and could reduce the impedance under steady state conditions. However, the important concerns of HTS-FCL transformers are the current limiting factor, recovery characteristics and transformer function. This work scrutinizes the properties and characteristics of the materials adopted for the HTS-FCL transformer winding conductors. This information will eventually be used to carry out the analysis and determine the thermal effects of short circuit current on the HTS-FCL transformer windings.

The basic parameters of the conventional and the HTS transformers are presented in TABLE I. The transformers are applied for distribution power network.

Manuscript received March 09, 2012. This work was supported in part by Industrial Research Limited, New Zealand through the Foundation for Research, Science and Technology (FRST) High Temperature Superconductors (HTS) Accelerated Development Transformational Research, Science and Technology (TRST) funding. The FRST is now acknowledged as the Ministry of Science and Innovation (MSI).

M. A. Abdul Rahman, T. T. Lie and K. Prasad are with the Faculty of Designs & Creative Technologies, Auckland University of Technology, Auckland, New Zealand (email:muhammad.rahman@aut.ac.nz, tek.lie@aut.ac.nz, krishnamachar.prasad@aut.ac.nz)

TABLE I: BASIC PARAMETERS FOR THE TRANSFORMERS

Parameters	Value
Rating (kVA)	1000
Primary Voltage (kV)	11
Secondary Voltage (kV)	0.415
Frequency (Hz)	50
Primary Connection	Delta
Secondary Connection	Wye

II. ANALYZING APPROACH

The analysis looked into a couple of computational approaches to evaluate the thermal effect on the transformer secondary winding due to short circuit current. The investigation started with a standard calculation approach that was well established for evaluating conventional transformers. Another approach to determine the thermal effect was by the application of heat balance equation on a conventional transformer experiencing a short circuit condition. The calculated results from the two approaches were compared and observed for any significant variation.

A possible high and low short circuit current values were employed in the calculation and scrutinized on how they will affect the analysis. Since the fault current values may vary depending on the conditions, the analysis also looked for another value which can be considered as a highly probable fault current to occur in the transformers. Finally, the analysis looked into the dynamics of alternative current electrical system by determining the asymmetrical short circuit current values from the symmetrical fault current magnitude and the X/R ratio of transformer winding coil. These fault current values were utilized to observe the thermal effect expected on the low voltage conductor.

A. *Standard calculation*

The ability to sustain without damage the thermal effect on the winding of a transformer from an external short circuit event is very important. The fault current which will run through the transformer winding is significantly higher than the normal operating current. This event will eventually contribute to the increase in the transformer winding temperature. However, the heat transfer through the cooling arrangement of the transformer winding should not be considered because the thermal time constant of the winding is usually several minutes and this is very much longer than the fault duration which is normally within 2 seconds before being interrupted by the protection system. International Electrotechnical Commission (IEC) has introduced a standard approach to exhibit the ability to withstand the thermal effect from the short circuit current in a conventional transformer [9]. The standard shows the calculation procedures to determine and demonstrate the transformer capability to endure the thermal and dynamic effects of the fault conditions. The formulation will provide the highest average temperature to be experienced by the winding conductor after a short circuit.

The equation applied in the standard for the average temperature (T) in the copper winding conductor of a conventional transformer after the short circuit is

$$T = T_o + \frac{2(T_o + 235)}{\frac{106000}{J^2 t} - 1} \quad (1)$$

where T_o is the initial winding temperature in Celsius (°C), J is the short circuit current density in Amperes per square millimetre (A/mm^2) and t is the duration of the short circuit in seconds (s).

Meanwhile, equation (2) shows the relationship between the resistance growth and the resistivity at various temperatures on the low voltage winding during the short circuit period

$$R(T) = \rho(T) \cdot \frac{l}{A} \quad (2)$$

where l is the length of the conductor and A is the cross sectional area of the conductor. The resistivity values of copper at various temperatures are shown in Figure 1. The data was acquired from cryogenic and room temperature sources [10-12].

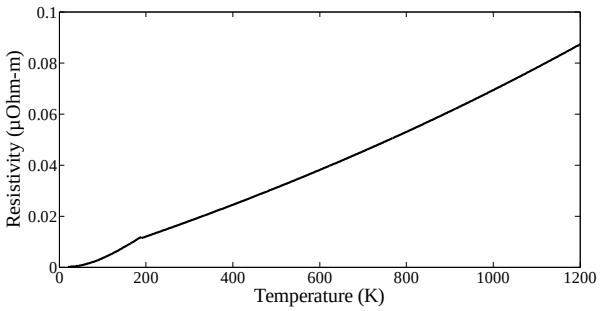

Figure 1: Resistivity of copper at various temperatures

Further information on the parameters of the conventional transformer would be required for the calculation. The data are presented in TABLE II.

TABLE II: PARAMETERS FOR THE CONVENTIONAL TRANSFORMER

Parameters for Low Voltage Winding	Conventional Transformer
Rated Current (I_r), A	1333
Cross Sectional Area (A), mm^2	430.00 × 1.30
Length (l), m	45
Copper Density (d), kg/m^3	8960
Resistance per phase at ambient (R), Ω	5.64×10^{-4}
Short Circuit Impedance (Z_{sc}), %	4.75
Overall Rated Current Density (J_r), A/mm^2	2.3846

B. *Heat balance equation*

Computations of the transformer short circuit parameters should be undertaken to determine the transformer capability to withstand the thermal effects. The thermal effects on the windings due to a short circuit event are very critical. The fault currents are significantly larger than the normal load currents.

High winding temperatures are to be expected from the incident. Another alternative to calculate the temperature rise in the transformer winding is by applying the heat balance equation.

$$C(T)\cdot m\cdot\frac{\Delta T}{\Delta t}=k(T)\cdot A\cdot\frac{\Delta T}{l}+\rho(T)\cdot J_{sc}^{2}\cdot v \tag{3}$$

where $C(T)$ is the specific heat capacity, m is the mass of the winding, ΔT is the change in temperature, Δt is the time duration, $k(T)$ is the thermal conductivity, A is the cross-sectional area of the winding, l is the length of the winding, $\rho(T)$ is the resistivity, J_{sc} is the short circuit current density and v is the volume of the winding. The temperature of the winding was calculated with an assumption that the heat developed during the event was retained in the winding itself, raising its temperature. For a conventional transformer, the heat transfer through the cooling medium was not taken into account because the thermal time constant of the winding is much larger than that of the short circuit current. Meanwhile, for an HTS transformer, the thermal time constant for the tape is small. However, the thermal power dissipated through the cooling medium when the applied current is much higher than the critical current is also small and hence neglected when the temperature difference between the winding and liquid nitrogen becomes more than 13 K.

The thermal power conducted through the conductors was very small compared to the thermal power due to the heat capacity and the resistivity. The heat balance equation applied during the short circuit duration was rewritten and the change in temperature was presented as

$$\Delta T=\frac{\rho(T)\cdot J_{sc}^{2}\cdot v}{\dfrac{C(T)\cdot m}{\Delta t}-\dfrac{k(T)\cdot A}{l}} \tag{4}$$

The resistivity and specific heat capacity values are dependent on the temperature. The resistivity variation with temperature for copper was presented in Figure 1. Meanwhile, the specific heat capacities for copper, as a function of temperature, are shown in Figure 2. The specific heat data was based on published sources [10, 13, 14].

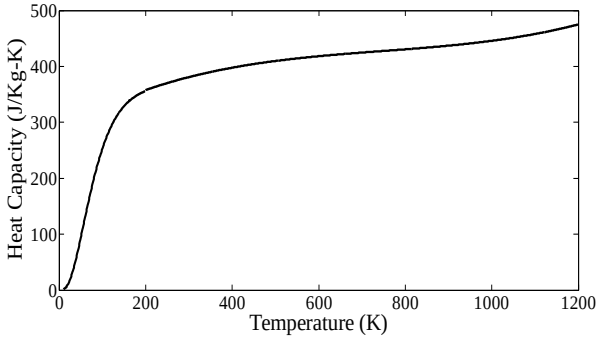

Figure 2: Specific heat capacity of copper at various temperatures

The information given in TABLE II was gathered and substituted into equation (4). The resistivity and heat capacity values at various temperatures were provided in Figure 1 and Figure 2, respectively. The short circuit current density for the secondary winding of the transformer (J_{sc}) is equal to the overall rated current density (J_r) or the rated current over the cross sectional area of the winding (I_r /A), divided by the short circuit percent impedance (%Z_{sc}), *i.e.*,

$$J_{sc}=\frac{I_r/A}{\%Z_{sc}}=\frac{J_r}{\%Z_{sc}} \tag{5}$$

Meanwhile, the first initial winding temperature is chosen as 105 °C (378 K) which corresponds to the sum of the maximum permissible ambient temperature and the temperature rise allowed for the winding insulation system of the transformer [9]. The calculation was done in steps with the fault duration (t) taken at 0.1 second interval until it reached the maximum allowable period of 2 seconds.

C. Comparison with a conventional transformer

The calculations for both methods were based on the parameters provided by the supplier of the conventional transformer. The results were almost identical and the percentage error or variation is very small as shown in Figure 3. The outcomes were utilized to justify the computational methods. The short circuit temperature values for the two approaches after the 2 seconds period were also well below the permissible 250°C (523 K) as described in the standard [9]. The calculated values of 411.95 K for the IEC approach and 412.07 K for the Heat Balance approach indicated that the cross sectional area of the winding was sufficient when it comes to the short circuit condition.

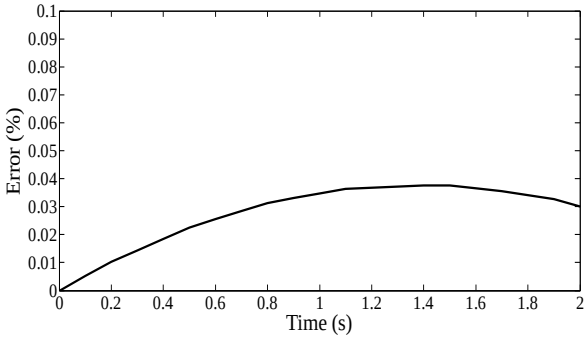

Figure 3: Comparison of the calculated temperature rise in the secondary winding

The resistance growth for the affected phase of the secondary copper winding can be developed through the calculation from equation (2). The temperature-resistance relationship for the second calculation method of the conventional transformer is pictured in Figure 4.

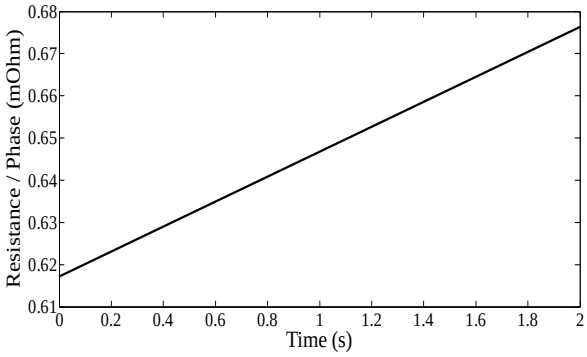

Figure 4: Resistance growth in the secondary winding during short circuit

The graph shows that the resistance of the copper winding will increase when the temperature increases. In this case, the temperature of the winding increased because of the application of the short circuit current. The temperature can also rise due to other circumstances such as an increase in the network loading. However, the increase in the resistance of the winding will be much smaller compared to the increase due to short circuit current.

D. Application of the calculated fault current values

The short circuit current density was calculated using equation (5). The equation requires the values of the rated current of the winding (I_r), the short circuit impedance (Z_{sc}), and the cross-sectional area of the winding (A). The first two parameters can normally be acquired from the transformer name plate. However, the cross-sectional area of the low voltage winding would require further advice from the manufacturer.

Another alternative to compute the short circuit current density is by acquiring the short circuit current to be experienced by the transformer and then dividing the value with the cross sectional area of the transformer winding. Various types of faults in the same conventional transformer have previously been discussed [15]. The fault currents based on the type of faults at different fault locations were calculated and presented. Since the three phase fault will normally produce the highest short circuit currents, the values from the three phase fault were utilized for this analysis. The high and low fault currents for the conventional transformer, *i.e.,* 27.51 kA and 5.64 kA, respectively, were used and compared to observe the thermal effect in the winding conductor. The temperature rises for the two seconds period were calculated using equation (4).

The calculated data shows that a greater short circuit current will contribute to a higher temperature rise in the winding conductor. The graphical comparison between the two fault currents applied to the transformer using the heat balance equation and the highest average temperature attained by the winding through the standard calculation in IEC60076 with the short circuit current of 28.06 kA is shown in Figure 5.

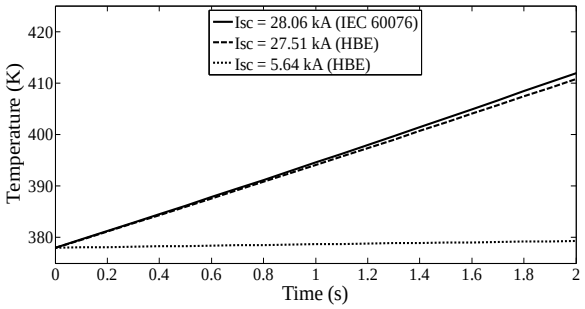

Figure 5: Comparison of the temperature rise at the two fault current conditions

Figure 5 shows that the higher fault current provided a significant increase in the winding temperature. The temperature rise was almost close to the highest average temperature calculated using the IEC standard. Meanwhile, for the lower fault current, the temperature rise was not as significant compared to the higher fault current.

E. Application of the dynamic asymmetrical fault current values

The Ohm's Law stated that if the voltage remains constant, when the impedance increases, the fault current decreases. However, this does not take into account the dynamics of alternative current (AC) electrical system. A fault occurs in an electrical system is a sudden event. The system will take some time to adapt and its response will change with time until reaching the steady state. This transient response of the electrical system is very short.

The impedance in AC electrical system has two components: the resistance (R) and the reactance (X). The resistance is a measure on how hard it is for the current to flow through the material. Under normal operating conditions, the current will flow through a material having resistance and the heat will be transferred from the material to the surrounding. Meanwhile, the reactance depends on two components, *i.e.*, inductance and system frequency. The inductance is a reflection on how hard it is to change the current. All conducting materials have some inductance, but a good example is a coil of wire. The system frequency around the world is fixed at either 50 or 60 Hz. Therefore, the reactance is basically dependent only upon the inductance.

The voltage and current in a linear AC electrical system are sine waves. A pure resistive system will have both the voltage and the current in phase. Meanwhile, a pure reactive system will have the voltage to lead the current by 90^0. When a fault occurs, the current waveform is no longer a sinusoidal waveform. Instead, the waveform is now the sum of a symmetrical sinusoidal waveform and a decaying exponential. The summation value will cause the current to have a much larger value than the sinusoidal waveforme alone. The waveform is called the asymmetrical current because it does not have symmetry above and below the time axis.

The actual waveform of the asymmetrical short circuit current is not easy to predict because it depends on the actual time in the voltage cycle waveform when the fault occurs. However, the largest fault current value can be acquired when the fault occurs at the point when the voltage is zero. Therefore, the asymmetrical fault current will depend solely on the X/R ratio and the magnitude of the symmetrical fault current. The peak asymmetrical short circuit current can be calculated using the following equation.

$$I_{sc(peak-asymmetrial)} = k \cdot I_{sc(symmetrical)} \tag{6}$$

The peak asymmetrical short circuit current can be converted to the rms value by dividing it with $\sqrt{2}$. The k factor is also called the asymmetry factor and is given by the following equations.

$$k = \sqrt{2} \cdot \left\{ 1 + \exp\left[-\left(\theta + \frac{\pi}{2} \right) \cdot \frac{r}{x} \right] \cdot \sin\theta \right\} \tag{7}$$

$$\theta = \tan^{-1}\left(\frac{x}{r} \right) \tag{8}$$

where R is the resistance, X is the reactance, and θ is in radians. The thermal effect on the secondary winding can be observed by applying the dynamic short circuit current, resistivity, and heat capacity values into the heat balance equation. The temperature rises of the secondary winding due to the two short circuit conditions compared to the standard IEC calculation are depicted in Figure 6. The values are expected to increase at the first few cycles and decrease at a later stage when compared to the result shown in Figure 5.

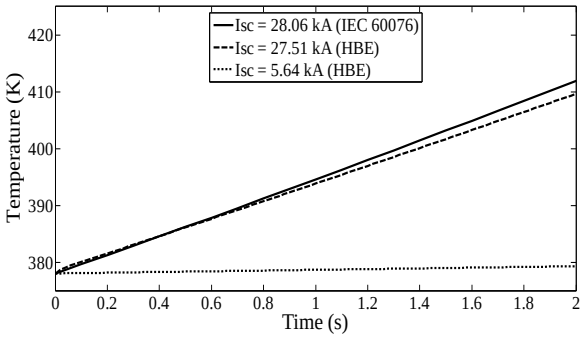

Figure 6: Dynamic temperature rise for the two fault conditions

The consideration of the X/R ratio is very important in performing the short circuit current calculation. The higher the ratio, the higher is the asymmetrical fault current. The application in this part of the analysis would be utilized in the investigation on the thermal effect of the winding conductor due to the short circuit current on the HTS transformer winding.

III. Analysis on HTS Transformer Winding

The following step of the analysis is to investigate the thermal effects in the secondary winding of the HTS transformer during a short circuit event. However, the structure of the HTS secondary winding conductor needs to be understood prior to going further into the analysis. This is significant in order to anticipate what the winding conductor will be actually undergoing during the period. The structure for the HTS winding conductor to be explained is based on a baseline design this study is working on [16].

A. Architectural design

The HTS conductors are built into a continuously transposed cable. These conductors are very thin and fragile tapes. The superconducting layer is a very thin layer of a special ceramic material implanted on a Hastelloy substrate and enclosed by copper plating. The architectural structure is shown in Figure 7 where the overall thickness is only about 0.1 mm. Any substantial lateral bending cannot be tolerated because it will damage the superconducting layer. Special methods are employed to assemble the conductor and produce the cable.

In this part of the study, it was assumed that the short circuit current would be shifted to the copper stabilizer layer after the occurrence of the fault. Since the copper layer would take over the duty of transmitting the short circuit current, the next step was to observe its characteristics in withstanding the situation.

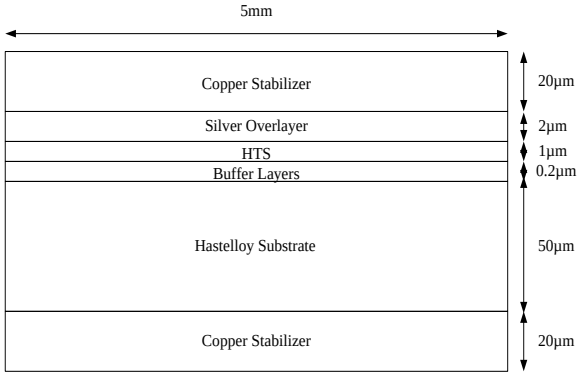

Figure 7: Structure of the HTS Winding Conductor

B. Thermal effects on the existing design

After the short circuit, the temperature of the conductor was expected to rise due to heat from the excessive current. Particular attention was focused on the specific heat capacity of copper. The specific heat capacity of copper as a function of temperature was presented in Figure 2 and the resistivity of copper with respect to temperature was provided previously in Figure 1.

Applying the same computation steps in the heat balance equations in (3) and (4), the analysis on the HTS transformer was carried out. The reactance value for the HTS transformer was acquired through per unit (p.u.) calculation method, as shown in TABLE III, in which the winding was limited by the 0.05 p.u. leakage reactance. Meanwhile, the resistance was based on that of copper stabilizer layer.

TABLE III: Reactance Value as Per Unit Calculation

Parameters	Calculation & Values
Power, S_{base}	1000000 VA
Voltage, V_{base}	415 V
Current, I_{base}	$\frac{S_{base}}{V_{base}} = 2410\,A$
Impedance, Z_{base}	$\frac{V_{base}^2}{S_{base}} = 0.1722\,\Omega$
Per Unit Leakage Reactance, $X_{p.u.}$	0.05
Low Voltage Reactance, X_{LV}	$Z_{base} \cdot X_{p.u.} = 0.0086\,\Omega$

The heat balance equation (4) was applied with all the parameters acquired to calculate the temperature rise during the fault condition. These parameters are presented in TABLE IV. The transformer was not expected to be able to withstand the required 2 seconds period as per IEC standard. Therefore, instead of the 2 seconds duration, the observation for the HTS transformer was only focused on the first 1-second period. The temperature was expected to grow faster compared to that of conventional transformer due to the significantly smaller cross sectional area of the copper stabilizer, which should contribute to higher resistance value for the fault current to flow through.

TABLE IV: PARAMETERS OF THE HTS TRANSFORMER

Parameters for Low Voltage Winding	Value
Cross Sectional Area per strand (A), mm^2	5.00 × 0.04
Number of Strands	17
Length (l), m	23
Copper Density (d), kg/m^3	8960
Short Circuit Impedance (Z_{sc}), %	5.00

A huge current will run through the HTS winding conductor when a short circuit occurs. After a short moment, the superconductor will be expected to quench. The superconductor quenches at current just higher than the critical current. Under AC supply, the HTS-FCL superconductor would require currents at 2-3 times the critical current to heat it over the critical temperature, before the fault current reaches its first maximum [17]. However, the non HTS-FCL superconductor with copper stabilizer would need much higher current for the same objective.

The quench response time is assumed to be of the order of few milliseconds. However, some researchers calculate it to be in the range of few picoseconds. For the calculation, the short circuit was simulated to occur at t = 0 and the superconductor winding was assumed to quench at the response time of t_o. These situations are depicted in Figures 8, 9 and 12.

The temperature rises for the copper stabilizer of the HTS winding over short circuit duration are shown in Figure 8. Three values of short circuit current were employed in the calculations. Two of them were the high fault current (27.55 kA) and the low fault current (5.67 kA) which were based on the calculations presented in a previous work [15]. The other value was a predicted peak current in the LV winding (14.30 kA) based on 0.14 p.u. fault impedance [18].

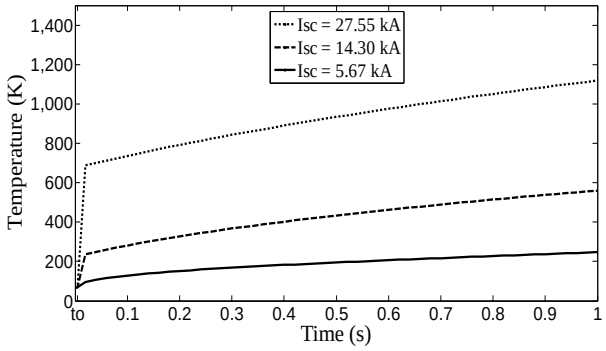

Figure 8: Temperature rise in the copper stabilizer of the HTS secondary winding

From Figure 8, it can be observed that the HTS transformer would not be able to withstand the required 2 seconds short circuit condition, as prescribed in IEC 60076 standards [9]. The temperature of the copper layer in the winding would rise beyond its withstand value. The fault current would damage the winding if it was permitted to run during the period. Therefore, the HTS transformer, with the present design parameters as shown in TABLE IV, needs to be isolated sooner.

However, the amount of short circuit current entering the transformer would be the determining factor for the withstand capability. The low fault current of 5.67 kA would let the transformer to experience a temperature lower than room temperature even after 1 second compared to the medium fault current of 14.30 kA, which would experience the rise to the room temperature only after 0.1 second. Any higher fault current value would bring about a potentially damaging temperature to the transformer winding.

Several alternatives can be considered to address the problem. The first is to limit the fault duration for the HTS transformer to less than 2 seconds withstand time. The set up would require re-coordination of protection system in the power network. Consensus between the relevant parties, especially the users or utilities, must be obtained since the duration is quite short for the distribution system. This option is currently being considered. The other option is to look into the design parameters of the HTS winding conductors. The temperature rise can be reduced by using thicker copper stabilizer or replacing it with stainless steel or high resistance alloy strip. Further analysis needs to be carried out in order to ensure that the size and weight advantage of HTS transformer will not be sacrificed and the losses will be within the acceptable value.

C. Thermal effects on various stabilizer thicknesses

Further investigation was carried out for the HTS winding conductor with various copper stabilizer thicknesses. A previous study [19] has looked at thermal stability of the same winding conductor architecture as the operating current approaches the critical current. The present work, meanwhile, explored the effects on the conductor due to short circuit current which would first rise beyond the critical current but will then subside throughout the fault duration.

Three different copper stabilizer thicknesses, *i.e.*, the original 40 µm, and the alternative 60 and 80 µm, were employed in the analysis. The stabilizer thicknesses were the total thickness of copper in the structure. This means that the 80 µm thickness was made up of a 40 µm copper layer on each side. The analysis was looking into the temperature rise of the secondary winding for the various copper layer thicknesses during the fault duration. The predicted fault current of 14.30 kA was applied in the computation. The results are shown in Figure 9.

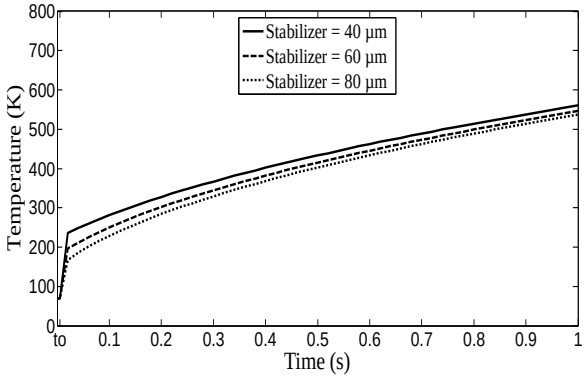

Figure 9: Temperature rise for various copper stabilizer thicknesses

Figure 9 shows the temperature rise in the secondary winding due to the short circuit current. The increase was larger with thinner copper stabilizer. However, each conductor would still experience the temperatures much higher than the room temperature if allowed to operate until the end of the one second period.

D. Effects on stabilizer free with thicker silver overlayer

A study was conducted previously [20] on superconducting Yttrium Barium Copper Oxide (YBCO) tapes with Ion Beam Assisted Deposition (IBAD) substrate. Parts of the analysis were to investigate short circuit effects on stabilizer free conductors. The construction of the tapes was the same as in Figure 7 but without the copper stabilizer. However, various thicknesses of silver over layer, which would dominate the resistance, were applied. In this study, another analysis was carried out on the stabilizer free superconducting wires with silver protective layer of 10, 20 and 30 µm thicknesses instead of the normal 2 µm.

The resistivity and heat capacity of silver at various temperatures are presented in Figure 10 and Figure 11, respectively. The resistivity data were acquired from cryogenic and room temperature sources [10-12]. Meanwhile, the heat capacity tabulated data were gathered also from cryogenic and room temperature sources [10, 13].

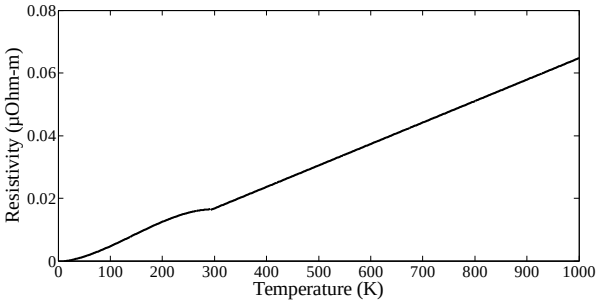

Figure 10: Resistivity of silver at various temperatures

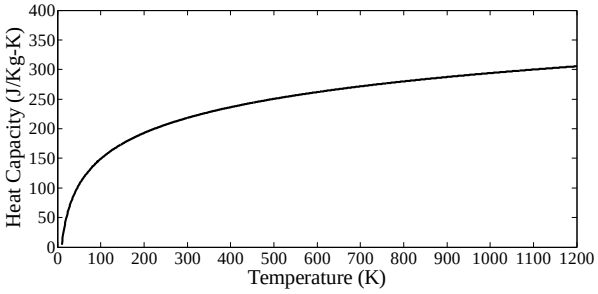

Figure 11: Specific heat capacity of silver at various temperatures

The values of the temperature rise for the first 1 second duration are shown in Figure 12. The high temperature rises show that the conductor would not withstand the required 2 seconds period. The values seemed not to improve much even with thicker silver protective layer.

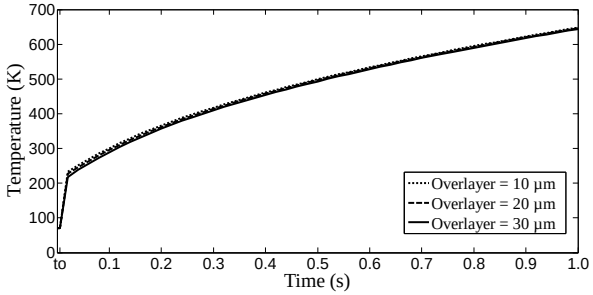

Figure 12: Temperature rise for various stabilizer free silver overlayer thicknesses

IV. ANALYSIS ON HTS-FCL TRANSFORMER WINDING

Present studies on HTS-FCL transformer are investigating varieties of winding conductor architecture to suppress the fault current and protect the transformer. The transformer will operate as a superconducting transformer in steady state condition and as a superconducting fault current limiter in fault condition. Various HTS conductor designs such as superconductors with high resistance alloy strip, stabilizer free superconductors and hybrid HTS coils are being evaluated. The superconductor wire designs can be simulated with the HTS transformer to observe the thermal effects from short circuit currents.

A. Options for HTS-FCL winding construction

For the first option, the HTS tape was put in parallel with a resistive conductor for stability and fault handling [21]. The original design used copper as the parallel conductor to meet the required fault withstands duration. However, the transformer would require an amount of copper nearly as much as a conventional unit in order to meet the standard requirement of 2 seconds duration. Also, copper produces high eddy current losses. Therefore, high resistance alloys are being considered as the replacement to reduce the fault current and eddy current losses. The HTS-FCL wire with high resistance alloy strip is developed as shown in Figure 13. The design presents a robust HTS-FCL wire construction that can be insulated on uncomplicated insulating equipment.

The second alternative employs the second generation superconducting tape which operates with low resistivity in superconducting state and high resistivity in normal state [22]. The stabilizer free wire must provide high resistance-per-length in normal state at 77 K and also high mechanical strength to withstand the short circuit force. This is very important since the superconductor layer is only about 1 percent of the total thickness of the wire. The wire design construction is identical to the one shown in Figure 7 but without the copper stabilizer.

In the third option, a hybrid coil is utilized [23]. The hybrid HTS coil is a combination of limiting and non-limiting coils. The limiting coil is a stabilizer free HTS wire as described in the second alternative. Meanwhile, the non-limiting coil is a surround copper stabilizer HTS wire as applied to our preliminary baseline design HTS transformer, shown in Figure 7. Both the HTS coils are connected in series. The hybrid structure would allow higher flexibility for both transformer and current limiter design by the variation of the ratio between the coils.

This investigation focused on the first FCL-HTS wire architectural design mentioned in this subsection. Several previous studies have worked on this design [6, 24, 25]. They were carried out on certain high resistance alloy strips at various thicknesses. The effectiveness of current limiting characteristics in a combination of YBCO tape and Cupronickel (C71500) tape was verified [24]. The AC over-current tests beyond the critical current in which the test current was damped with time were conducted. The study was looking into the possibility of stabilizing the power system by improving the function of fault current limiting.

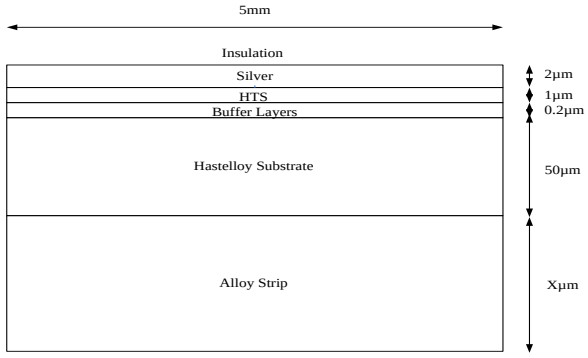

Figure 13: HTS wire with high resistance alloy strip

In addition to the first high resistance alloy, stainless steel (SS316L) was also considered for the coated conductor. Over-current characteristics of HTS wire with stainless steel as the stabilizer material were investigated [6]. Among the commercialized HTS conductor, the wire was considered at that time by the investigation to be more proper than others for HTS-FCL function. Another study on HTS wire with stainless steel stabilizer [25] was also conducted by applying a fault current and observing the resistance increase trends. This study indicated that the HTS wire with stainless steel stabilizing layers can have positive effects on the performance of the current-limiting elements.

B. Analytical approach for conductor with stainless steel stabilizer

In Section III, the heat balance equation was applied to calculate the temperature rise in the copper stabilizer of the secondary winding conductor of an HTS transformer. The simulation took into account the structural design of HTS conductor and assumed the conductor to quench after a short time by the fault current. The calculation also assumed the short circuit current was forced to be diverted from the HTS filaments to the copper stabilizer layers. The fault current generates heat and increases the resistance in the winding. The result shows that the transformer secondary winding conductor can be damaged due to the thermal effect if the fault current is to be allowed for a period of 2 seconds as specified in IEC 60076 standards.

This study investigated a high resistance alloy, stainless steel (SS316L), which has very high resistivity and can be used as a stabilizing metal. Fundamental data for the material such as resistivity and specific heat capacity were gathered for computation in the analysis. The resistivity and heat capacity values for the alloy with respect to temperature are presented in Figure 14 and Figure 15, respectively. The architectural design of the HTS wire was based on Figure 13. Three different short circuit current values were considered in the investigation to observe the performance of the high resistance alloy. The same simulation as for the HTS transformer with copper stabilizer was carried out taking into account the assumed fault current values.

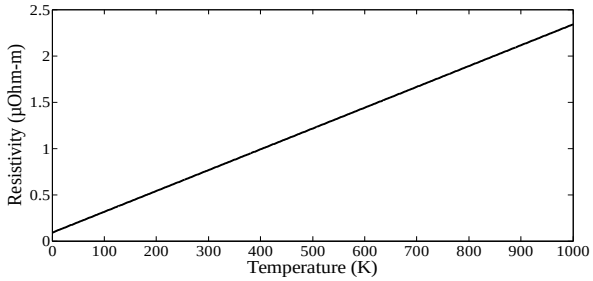

Figure 14: Resistivity of stainless steel at various temperatures

The resistivity value of stainless steel at 293 K was used as the reference. At this temperature, the resistivity is 0.7496 µΩ-m [26] and the temperature coefficient for resistivity is assumed to be $0.003/^{0}C$ [27]. The resistivity values of the material at other temperatures are calculated based on this reference value. The actual resistivity value decreases very little below the room temperature. In addition, it changes very little even at liquid nitrogen temperature. However, the variation between the assumed and the actual values is very small and would not affect the result on the calculation for temperature increase in the stainless steel layer. Meanwhile, the values for heat capacity are from several sources [28-30].

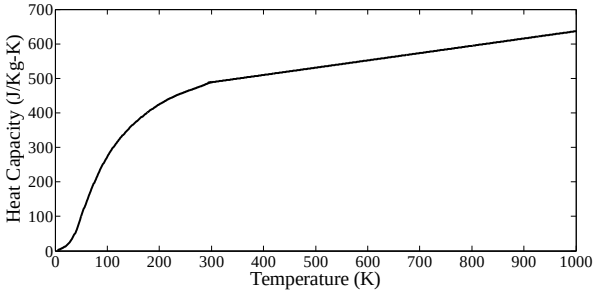

Figure 15: Heat capacity of stainless steel at various temperatures

C. Thermal effects on the stainless steel stabilizer

The results from the calculation of the temperature rise on the winding conductor with stainless steel stabilizer are shown in Figure 16. The thickness of the stainless steel stabilizer was the same as the copper stabilizer, *i.e.*, 40 µm.

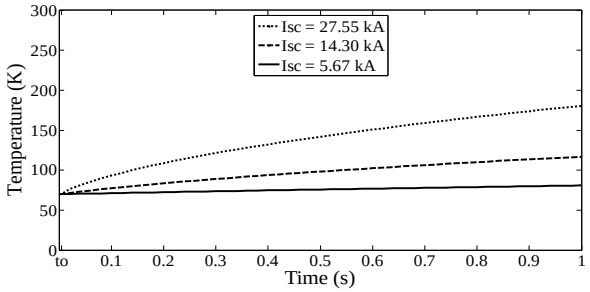

Figure 16: Temperature rise in stainless steel stabilizer from the fault currents

The temperature rises for all the applied short circuit currents were very much lower compared to the conductor with copper stabilizer. The temperature values have not reached the room temperature even after the 1 second period. The results clearly show that the HTS-FCL winding conductor was able to withstand the thermal effects of the short circuit currents.

The conductor was also simulated with different stabilizer thicknesses. The range of thicknesses investigated was the same as for the copper stabilizer, *i.e.*, 40, 60 and 80 µm. The applied fault current was 14.30 kA, also the same as the previous simulation. The results are presented in Figure 17. The temperature rises were found to be identical for all the three stabilizer thicknesses. There would not be significant differences in terms of thermal effect by using the stainless steel stabilizer within the thickness range.

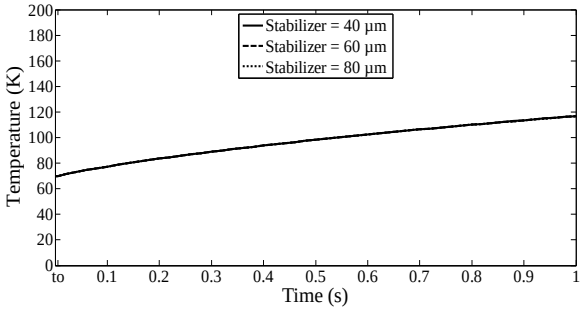

Figure 17: Temperature rise for various stainless steel stabilizer thicknesses

D. Comparison on the performance of the HTS and HTS-FCL conductors

The analysis on copper stabilizer has shown its inability to withstand high fault currents for the duration required by the normal standard. The transformer has to be protected by the protection system sooner in order to avoid any damage to the equipment. Meanwhile, the investigation on stainless steel stabilizer has demonstrated that it was able to endure the thermal effect better than copper. Figure 18 shows the temperature rise in both stabilizers when the 14.30 kA fault current was applied on to the transformer. The current in the stainless steel layer was considered to quickly drop below the initial fault current because of the much higher transformer impedance that exists when the superconductor quenches under constant supply voltage.

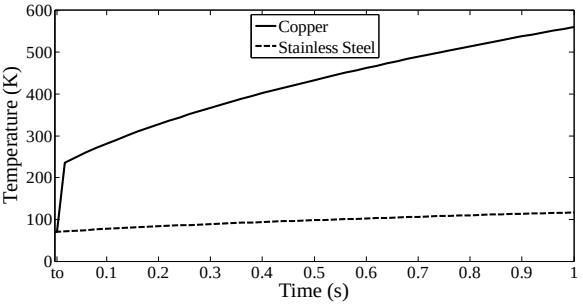

Figure 18: Temperature rise in copper and stainless steel stabilizers due to the fault current

While the temperature for copper went up higher than the room temperature just after 0.1 second, the temperature for stainless steel was still very much lower than the room temperature even after reaching the one second period. The high resistance alloy would be able to provide the HTS-FCL winding conductor the capability to perform as superconducting transformer under normal operating condition and superconducting fault current limiter under short circuit condition.

V. DISCUSSION

Thermal effects of short circuit phenomena on an HTS transformer winding are analysed. The mathematical model presented enables the estimation of temperature developed in the transformer winding during short circuit. The investigation was conducted on HTS wires with various specified copper stabilizer thicknesses and stabilizer free HTS conductors with various specified silver protective layer thicknesses. Further analysis was carried out to investigate the HTS-FCL superconductor winding design.

The fault current values used in the calculation were based on the possible short circuit currents to be experienced by the transformer. The fault current computation included the reactance of the relevant HTS conductor coil of the secondary winding and the resistance of the materials expected to carry the fault current. The heat balance equation was then utilized to calculate the temperature rise in secondary winding. The calculation took into account the structural design of HTS conductor and assumed the conductor to quench after a short time by the fault current, forced the current to be diverted from the HTS filaments to the stabilizer layers. The fault current generated heat and increased the resistance in the winding. The resistance increase was determined by the temperature-resistance relationship. The specified thicknesses for the relevant conductor layers selected for each analysis in this study were referred to several previously mentioned studies.

The investigation on HTS wire with various copper stabilizer thicknesses showed that the fault current would not be sufficiently suppressed. Thicker stabilizer would allow higher fault current to pass through the winding and this would reduce the temperature rise. The conductor configuration would not permit the HTS transformer to operate as a good fault current limiter. Meanwhile, the results from the heat balance equation calculation showed that the transformer secondary winding with any of the three copper stabilizer thicknesses could still be damaged due to the thermal effect if the fault current was to be allowed for a period of 2 seconds as specified in the IEC 60076 standards. Therefore, the protection system would have to be coordinated so that the system would trip in less than 2 seconds. The set up would depend on the transformer withstand temperature and the consensus between the relevant parties.

A short circuit analysis on stabilizer free conductors with various specified silver protective layer thicknesses also led to the same outcomes. As per analysis on copper stabilizer conductor, the short circuit current was assumed to be diverted to the silver layer which dominates the resistance. Any thickness beneath the specified values would result in better fault current suppression, but the silver layer would not be able to withstand the thermal effect. Moreover, the superconducting wire design configuration without any metal stabilizer would

not be easy to handle. The fabrication of a conductor coil from this conductor would be very complicated to prevent any chemical or mechanical damage.

Further advancement in the technology enables the research and development of HTS-FCL transformer. Several alternatives for HTS-FCL wire have been introduced. Since the architectural design of the wire has been altered, the previous assumptions considered in the calculation must be re-established. During the short circuit duration, the HTS-FCL wire will be transformed from superconducting state into normal or high resistance state. In the superconducting state, the short circuit impedance depends only on the reactance. Meanwhile, in the normal state, the resistance of the materials will be the dominant factor. The resistance of the wire will be equal to the equivalent resistance of all the parallel layers in the wire. The resistance value will depend on the resistivity, thickness and cross-sectional percentage of each layer material. However, the analysis of this study focused only on the dominant layer of the conductor.

The winding resistance will eventually increase the impedance of the transformer. Due to the high resistance of the winding in the normal state, the fault current can be suppressed below the permissible value, *i.e.*, the critical current of the superconductor. The restricted short circuit current should generate less heat on the winding. Therefore, the temperature rise and the resistance growth on the HTS-FCL wire should also be reduced. The temperature rises for the stainless steel stabilizer at three different thicknesses throughout the one second short circuit period were presented.

The overall performance based on the analysis carried out showed that stainless steel was a good stabilizer or high resistance alloy strip for the HTS-FCL conductor. However, other factors should also be considered when deciding the optimum selection. One of them should be the suitability for the application. This study focused on the utilization of HTS-FCL conductor on the secondary winding of a distribution power transformer. Therefore, the design of the winding coil and the transformer itself must be taken into consideration in the selection of the type and thickness of the stabilizer. Different applications such as switchgear and fault current limiter should have different considerations for the selection. Another major factor should be the cost of the alloys and the manufacturing process. The economy factor is very critical since the HTS-FCL transformer will not only be compared with the conventional transformer but also with the normal HTS transformer.

VI. CONCLUSION

The calculation on short circuit forces even with various copper stabilizer thicknesses shows the normal HTS transformer is unable to withstand the duration of 2 seconds as prescribed in the IEC standards. The fault current is very much above the critical current and the drop will depend on the stabilizer thickness. The temperature of the secondary winding increases tremendously and rises beyond the allowable limit during the period. Therefore, arrangement must be made to isolate the transformer sooner in order to prevent any damage to the transformer and loss of power supply to the customers. Analysis on superconductor without metal stabilizer with specified silver protective layer thicknesses also provided the same findings. However, stabilizer free conductor would not be easy to fabricate into a coil.

Development of HTS-FCL transformer should be able to minimize the obstacles due to short circuit current. The fault current will be limited because of high winding resistance in the normal state. The limited fault current will then reduce the increase in heat generated. This circumstance will eventually reduce the growth of the winding resistance. An analysis on high resistance alloys of cupronickel and stainless steel as the stabilizer metal for HTS-FCL conductor was also carried out. The results show that the alloys are able to suppress the fault current to the designated level with the right thickness. The alloys are also capable to restrain the temperature rise of the superconductor. However, further research needs to be done to determine the optimum selection of stabilizer metal where other factors such as the application of the HTS-FCL conductor and the economy of the implementation have to be considered.

REFERENCES

[1] S. V. Kulkarni and S. A. Khaparde, *Transformer Engineering: Design and Practice*. New York, NY: Marcel Dekker, Inc., 2004.

[2] S. W. Schwenterly, B. W. McConnell, J. A. Demko, A. Fadnek, J. Hsu, F. A. List, M. S. Walker, D. W. Hazelton, F. S. Murray, J. A. Rice, C. M. Trautwein, X. Shi, R. A. Farrell, J. Bascuhan, R. E. Hintz, S. P. Mehta, N. Aversa, J. A. Ebert, B. A. Bednar, D. J. Neder, A. A. McIlheran, P. C. Michel, J. J. Nemce, E. F. Pleva, A. C. Swenton, W. Swets, R. C. Longsworth, R. C. Johsnon, R. H. Jones, J. K. Nelson, R. C. Degeneff, and S. J. Salon, "Performance of a 1-MVA HTS demonstration transformer," *IEEE Transactions on Applied Superconductivity*, vol. 9, no. 2, pp. 680-684, June 1999. doi: 10.1109/77.783387

[3] B. W. McConnell, "Transformers - a successful application of high temperature superconductors," *IEEE Transactions on Applied Superconductivity*, vol. 10, no. 1, pp. 716-720, March 2000. doi: 10.1109/77.828332

[4] J. X. Jin, S. X. Dou, H. K. Liu, C. Grantham, Z. J. Zeng, Z. Y. Liu, T. R. Blackburn, X. Y. Li, H. L. Liu, and J. Y. Liu, "Electrical application of high T_c superconducting saturable magnetic core fault current limiter," *IEEE Transactions on Applied Superconductivity*, vol. 7, no. 2, pp. 1009-1012, June 1997. doi: 10.1109/77.614678

[5] T. Janowski, S. Kozak, B. Kondratowicz-Kucewicz, G. Wojtasiewicz, and J. Kozak, "Analysis of transformer type superconducting fault current limiters," *IEEE Transactions on Applied Superconductivity*, vol. 17, no. 2, pp. 1788-1790, June 2007. doi: 10.1109/TASC.2007.898134

[6] M. C. Ahn, D. K. Park, S. E. Yang, M. J. Kim, H. M. Kim, H. Kang, K. Nam, B.-Y. Seok, J.-W. Park, and T. K. Ko, "A Study on the design of the stabilizer of coated conductor for applying to SFCL," *IEEE Transactions on Applied Superconductivity*, vol. 17, no. 2, pp. 1855-1858, June 2007. doi: 10.1109/TASC.2007.898130

[7] Y. J. Kim, D. K. Park, S. E. Yang, W. C. Kim, M. C. Ahn, Y. S. Yoon, N. Y. Kwon, H. Lee, and T. K. Ko, "Analytical design method of high-T_c coated conductor for a resistive superconducting fault current limiter using finite element method," *IEEE Transactions on Applied Superconductivity*,

vol. 20, no. 3, pp. 1172-1176, June 2010. doi: 10.1109/TASC.2010.2040385
[8] W. Schmidt, H. P. Kraemer, H. W. Neumueller, U. Schoop, D. Verebelyi, and A. P. Malozemoff, "Investigation of YBCO coated conductors for fault current limiter applications," *IEEE Transactions on Applied Superconductivity*, vol. 17, no. 2, pp. 3471-3474, June 2007. doi: 10.1109/TASC.2007.899709
[9] *Power Transformers - Part 5: Ability to Withstand Short Circuit*, IEC60076-5:2000, 2000.
[10] J. E. Jankowski, "Convective heat transfer model for determining quench recovery of high temperature superconducting YBCO in liquid nitrogen," MSc Thesis, Dept. Mech. Eng., Massachusetts Institute of Technology, Cambridge, MA, 2004.
[11] D. R. Lide, *CRC Handbook of Chemistry and Physics*, 84th ed. Boca Raton, FL: CRC Press, 2003.
[12] Y. Iwasa, *Case Studies in Superconducting Magnets*. New York, NY: Plenum Press, 1994.
[13] A. F. Mills, *Heat Transfer*, 2nd ed. Upper Saddle River, NJ: Prentice Hall, 1999.
[14] C. A. Thompson, W. M. Manganaro, and F. R. Fickett, *Cryogenic Properties of Copper*. Boulder, CO: National Institute of Standards and Technology, 1990.
[15] M. A. Abdul Rahman, T. T. Lie, and K. Prasad, "The Effects of Short-Circuit and Inrush Currents on HTS Transformer Windings," *IEEE Transactions on Applied Superconductivity*, vol. PP, pp. 1-8, 2011. doi: 10.1109/TASC.2011.2173571
[16] S. Kalsi, "HTS transformer development utilizing IRL's continuously transposed cable (CTC)," Kalsi Green Power System, LLC 2008.
[17] Y. Y. Xie, K. Tekletsadik, D. Hazelton, and V. Selvamanickam, "Second generation high-temperature superconducting wires for fault current limiter applications," *IEEE Transactions on Applied Superconductivity*, vol. 17, no. 2, pp. 1981-1985, June 2007. doi: 10.1109/TASC.2007.898186
[18] M. Staines, N. Glasson, M. Pannu, K. P. Thakur, R. Badcock, N. Allpress, P. D'Souza, and E. Talantsev, "The development of a roebel cable based 1 MVA HTS transformer," *Superconductor Science and Technology*, vol. 25, no. 1, p. 014002, January 2012. doi: 10.1088/0953-2048/25/1/014002
[19] J. H. Bae, H. Y. Park, B. Y. Eom, K. C. Seong, and S. K. Baik, "Thermal stability of YBCO coated conductor with different Cu stabilizer thickness," *Physica C: Superconductivity*, vol. 470, no. 20, pp. 1880-1882, November 2010. doi: 10.1016/j.physc.2010.05.227
[20] T. Yazawa, K. Koyanagi, M. Takahashi, M. Ono, K. Toba, H. Takigami, M. Urata, Y. Iijima, T. Saito, N. Ameniya, and Y. Shiohara, "Superconducting fault current limiter using high-resistive YBCO tapes," *Physica C: Superconductivity*, vol. 468, no. 15-20, pp. 2046-2049, September 2008. doi: 10.1016/j.physc.2008.05.123
[21] C. M. Rey, R. C. Duckworth, S. W. Schwenterly, and E. Pleva, "Electrical AC loss measurements on a 2G YBCO coil," *IEEE Transactions on Applied Superconductivity*, vol. 21, no. 3, pp. 2424-2427, June 2011. doi: 10.1109/TASC.2011.2112324
[22] T. Janowski, B. A. Glowacki, G. Wojtasiewicz, S. Kozak, J. Kozak, B. Kondratowicz-Kucewicz, M. Majka, and M. Wozniak, "Fault current limitation in power network by the superconducting transformers made of 2G HTS," *IEEE Transactions on Applied Superconductivity*, vol. 21, no. 3, pp. 1413 - 1416, June 2011. doi: 10.1109/TASC.2011.2112325
[23] H. Kojima, M. Kotari, T. Kito, N. Hayakawa, M. Hanai, and H. Okubo, "Current limiting and recovery characteristics of 2 MVA class superconducting fault current limiting transformer (SFCLT)," *IEEE Transactions on Applied Superconductivity*, vol. 21, no. 3, pp. 1401 – 1404, June 2011. doi: 10.1109/TASC.2010.2089413
[24] A. Tomioka, T. Otonari, T. Ogata, M. Iwakuma, H. Okamoto, H. Hayashi, Y. Iijima, T. Saito, Y. Gosho, K. Tanabe, T. Izumi, and Y. Shiohara, "AC over-current test results of YBCO conductor for YBCO power transformer with fault current limiting function," *Physica C: Superconductivity*, vol. 471, no. 21-22, pp. 1367-1373, November 2011. doi: 10.1016/j.physc.2011.05.196
[25] H. I. Du, M. J. Kim, Y. J. Kim, D. H. Lee, B. S. Han, and S. S. Song, "Study on resistance characteristics and operating conditions of YBCO thin-film wire for current limitation considering insulation layer," *Physica C: Superconductivity*, vol. 470, no. 20, pp. 1666-1670, November 2010. doi: 10.1016/j.physc.2010.05.184
[26] U. Ugur, "Resistivity of steel," in *The Physics Factbook*., G. Elert, Ed., 2006.
[27] T. R. Kuphaldt, "Temperature coefficient of resistance," n.d.
[28] D. Mann, "LNG materials and fluids," 1st ed Boulder, CO: National Bureau of Standards, 1977.
[29] Y. S. Touloukian and C. Y. Ho, "Thermophysical properties of selected aerospace materials. Part II: Thermophysical properties of seven materials," West Lafayette, IN: Thermophysical and Electronic Properties Information Center, CINDAS, Purdue University, 1976, pp. 39-46.
[30] A. A. Tavassoli, "Assessment of austenitic stainless steels," *Fusion Engineering and Design*, vol. 29, pp. 371-390, March 1995. doi: 10.1016/0920-3796(95)80044-X

BIBLIOGRAPHY

M. A. Abdul Rahman obtained his first degree in Electrical Engineering from University of Texas (El Paso), USA in 1990. He had served Tenaga Nasional Berhad (TNB), a major power utility company in Malaysia, from 1991. In 2004, he graduated with a Master in Electrical Engineering from University Tenaga Nasional, Malaysia. He was a Senior Engineer with Department of Engineering, Distribution Division, TNB looking into performance and diagnostic of distribution power equipment. He is currently pursuing his Ph.D. degree at Auckland University of Technology, New Zealand. His major interests are power system study, power equipment and accessories performance, condition monitoring and diagnostic.

T. T. Lie (S'89-M'92-SM'97) received his B.S. degree from Oklahoma State University, USA in 1986. He then obtained his M.S. and Ph.D. degrees from Michigan State University, USA in 1988 and 1992, respectively. He had worked in Nanyang Technological University, Singapore. Dr. Lie is now a Professor in the Dept. of Electrical and Electronic Engineering, Auckland University of Technology, New Zealand. His research interests include power system control, deregulated power systems and renewable energy systems

K. Prasad (M'2008-SM'2012) received his B.E. degree from Bangalore University, India, in 1980, M. Tech. in Electrical Engineering from the Indian Institute of Technology, Madras, India, in 1982 and Ph.D. from the University of Western Australia, Perth, Australia, in 1990. He is currently a Professor in the Department of Electrical and Electronic Engineering, Auckland University of Technology, New Zealand. His research interests include Material Science, Microelectronic Devices, Failure Analysis and Reliability Engineering.

Appendix B: Derivation for generalised matrices

Appendix B1 – Generalized matrices (transformer): Derivation for delta–grounded wye connection

Appendix B2 – Generalized matrices (line segment): Derivation for overhead line and underground cable

Appendix B1: Generalized matrices (transformer)

Derivation for delta – grounded wye connection

The actual winding turn ratio (n_t) from Figure 3.1 is

$$n_t = \frac{V(line-to-line)_{rated\,HV}}{V(line-to-neutral)_{rated\,LV}}. \tag{B1.1}$$

Meanwhile, the transformer ratio (a_t) is

$$a_t = \frac{n_t}{\sqrt{3}} = \frac{V(line-to-line)_{rated\,HV}}{V(line-to-line)_{rated\,LV}}. \tag{B1.2}$$

Figure 3.1 also shows that the primary line-to-line voltages as a function of the ideal secondary voltages can be defined as

$$V_{AB} = -n_t \cdot V_{tb} \tag{B1.3}$$

$$V_{BC} = -n_t \cdot V_{tc} \tag{B1.4}$$

$$V_{CA} = -n_t \cdot V_{ta}. \tag{B1.5}$$

The three equations can be transformed into a matrix form as

$$\begin{bmatrix} V_{AB} \\ V_{BC} \\ V_{CA} \end{bmatrix} = \begin{bmatrix} 0 & -n_t & 0 \\ 0 & 0 & -n_t \\ -n_t & 0 & 0 \end{bmatrix} \cdot \begin{bmatrix} V_{ta} \\ V_{tb} \\ V_{tc} \end{bmatrix}. \tag{B1.6}$$

From the theory of symmetrical components (Kersting, 2002), the line-to-line and line-to-neutral voltages are related to their line-to-line and line-to-neutral sequence voltages respectively by

$$\begin{bmatrix} V_{AB} \\ V_{BC} \\ V_{CA} \end{bmatrix} = \begin{bmatrix} 1 & 1 & 1 \\ 1 & a_s^2 & a_s \\ 1 & a_s & a_s^2 \end{bmatrix} \cdot \begin{bmatrix} VLL_0 \\ VLL_1 \\ VLL_2 \end{bmatrix} \tag{B1.7}$$

and

$$\begin{bmatrix} V_{AN} \\ V_{BN} \\ V_{CN} \end{bmatrix} = \begin{bmatrix} 1 & 1 & 1 \\ 1 & a_s^2 & a_s \\ 1 & a_s & a_s^2 \end{bmatrix} \cdot \begin{bmatrix} VLN_0 \\ VLN_1 \\ VLN_2 \end{bmatrix} \tag{B1.8}$$

where

$$a_s = 1.0 \angle 120° = -0.5000 + j0.8660 . \tag{B1.9}$$

Meanwhile, the relation between line-to-line and line-to-neutral for the sequence voltages are given by

$$\begin{bmatrix} VLN_0 \\ VLN_1 \\ VLN_2 \end{bmatrix} = \begin{bmatrix} 1 & 0 & 0 \\ 0 & t_s^* & 0 \\ 0 & 0 & t_s \end{bmatrix} \cdot \begin{bmatrix} VLL_0 \\ VLL_1 \\ VLL_2 \end{bmatrix} \tag{B1.10}$$

where

$$t_s = \frac{1}{\sqrt{3}} \angle 30° = 0.5000 + j0.2887 \tag{B1.11}$$

$$t_s^* = \frac{1}{\sqrt{3}} \angle -30° = 0.5000 - j0.2887 . \tag{B1.12}$$

Substituting the above equations (B1.7), (B1.8), and (B1.10), the following equation is obtained.

$$\begin{bmatrix} V_{AN} \\ V_{BN} \\ V_{CN} \end{bmatrix} = \begin{bmatrix} 1 & 1 & 1 \\ 1 & a_s^2 & a_s \\ 1 & a_s & a_s^2 \end{bmatrix} \cdot \begin{bmatrix} VLN_0 \\ VLN_1 \\ VLN_2 \end{bmatrix}$$

$$\begin{bmatrix} V_{AN} \\ V_{BN} \\ V_{CN} \end{bmatrix} = \begin{bmatrix} 1 & 1 & 1 \\ 1 & a_s^2 & a_s \\ 1 & a_s & a_s^2 \end{bmatrix} \cdot \begin{bmatrix} 1 & 0 & 0 \\ 0 & t_s^* & 0 \\ 0 & 0 & t_s \end{bmatrix} \cdot \begin{bmatrix} VLL_0 \\ VLL_1 \\ VLL_2 \end{bmatrix}$$

$$\begin{bmatrix} V_{AN} \\ V_{BN} \\ V_{CN} \end{bmatrix} = \begin{bmatrix} 1 & 1 & 1 \\ 1 & a_s^2 & a_s \\ 1 & a_s & a_s^2 \end{bmatrix} \cdot \begin{bmatrix} 1 & 0 & 0 \\ 0 & t_s^* & 0 \\ 0 & 0 & t_s \end{bmatrix} \cdot \begin{bmatrix} 1 & 1 & 1 \\ 1 & a_s^2 & a_s \\ 1 & a_s & a_s^2 \end{bmatrix}^{-1} \cdot \begin{bmatrix} V_{AB} \\ V_{BC} \\ V_{CA} \end{bmatrix}$$

$$\begin{bmatrix} V_{AN} \\ V_{BN} \\ V_{CN} \end{bmatrix} = \begin{bmatrix} 1 & 1 & 1 \\ 1 & a_s^2 & a_s \\ 1 & a_s & a_s^2 \end{bmatrix} \cdot \begin{bmatrix} 1 & 0 & 0 \\ 0 & t_s^* & 0 \\ 0 & 0 & t_s \end{bmatrix} \cdot \begin{bmatrix} 1 & 1 & 1 \\ 1 & a_s^2 & a_s \\ 1 & a_s & a_s^2 \end{bmatrix}^{-1} \cdot \begin{bmatrix} 0 & -n_t & 0 \\ 0 & 0 & -n_t \\ -n_t & 0 & 0 \end{bmatrix} \cdot \begin{bmatrix} V_{ta} \\ V_{tb} \\ V_{tc} \end{bmatrix}$$

which can be presented in a condensed form as

$$[VLN_{ABC}] = [a_t] \cdot [V_{tabc}] \tag{B1.13}$$

where

$$[a_t] = \begin{bmatrix} 1 & 1 & 1 \\ 1 & a_s^2 & a_s \\ 1 & a_s & a_s^2 \end{bmatrix} \cdot \begin{bmatrix} 1 & 0 & 0 \\ 0 & t_s^* & 0 \\ 0 & 0 & t_s \end{bmatrix} \cdot \begin{bmatrix} 1 & 1 & 1 \\ 1 & a_s^2 & a_s \\ 1 & a_s & a_s^2 \end{bmatrix}^{-1} \cdot \begin{bmatrix} 0 & -n_t & 0 \\ 0 & 0 & -n_t \\ -n_t & 0 & 0 \end{bmatrix}$$

$$[a_t] = \frac{-n_t}{3} \begin{bmatrix} 0 & 2 & 1 \\ 1 & 0 & 2 \\ 2 & 1 & 0 \end{bmatrix}.$$

Meanwhile, the ideal secondary voltages in Figure 3.1 are given by

$$V_{ta} = V_{an} + (Z_{ta} \cdot I_a) \tag{B1.14}$$

$$V_{tb} = V_{bn} + (Z_{tb} \cdot I_b) \tag{B1.15}$$

$$V_{tc} = V_{cn} + (Z_{tc} \cdot I_c). \tag{B1.16}$$

The three equations (B1.14), (B1.15) and (B1.16) can be transformed into a matrix form as

$$\begin{bmatrix} V_{ta} \\ V_{tb} \\ V_{tc} \end{bmatrix} = \begin{bmatrix} V_{an} \\ V_{bn} \\ V_{cn} \end{bmatrix} + \begin{bmatrix} Z_{ta} & 0 & 0 \\ 0 & Z_{tb} & 0 \\ 0 & 0 & Z_{tc} \end{bmatrix} \cdot \begin{bmatrix} I_a \\ I_b \\ I_c \end{bmatrix}. \tag{B1.17}$$

Substituting (B1.13) into a condensed form of the equivalent line-to-neutral voltages, it becomes

$$[VLN_{ABC}] = [a_t] \cdot ([VLN_{abc}] + [Z_{tabc}] \cdot [I_{abc}])$$

$$[VLN_{ABC}] = [a_t] \cdot [VLN_{abc}] + [a_t] \cdot [Z_{tabc}] \cdot [I_{abc}]$$

$$[VLN_{ABC}] = [a_t] \cdot [VLN_{abc}] + [b_t] \cdot [I_{abc}]$$

where

$$[b_t] = [a_t] \cdot [Z_{tabc}]$$

$$[b_t] = \frac{-n_t}{3} \begin{bmatrix} 0 & 2 & 1 \\ 1 & 0 & 2 \\ 2 & 1 & 0 \end{bmatrix} \cdot \begin{bmatrix} Z_{ta} & 0 & 0 \\ 0 & Z_{tb} & 0 \\ 0 & 0 & Z_{tc} \end{bmatrix}$$

$$[b_t] = \frac{-n_t}{3} \begin{bmatrix} 0 & 2Z_{tb} & Z_{tc} \\ Z_{ta} & 0 & 2Z_{tc} \\ 2Z_{ta} & Z_{tb} & 0 \end{bmatrix}.$$

The primary line-to-line voltages as a function of the equivalent line-to-neutral voltages can be defined from Figure 3.1 as

$$V_{AB} = V_{AN} - V_{BN} \tag{B1.18}$$

$$V_{BC} = V_{BN} - V_{CN} \tag{B1.19}$$

$$V_{CA} = V_{CN} - V_{AN}\,. \tag{B1.20}$$

In a matrix form for the three equations (B1.18), (B1.19) and (B1.20) is

$$\begin{bmatrix} V_{AB} \\ V_{BC} \\ V_{CA} \end{bmatrix} = \begin{bmatrix} 1 & -1 & 0 \\ 0 & 1 & -1 \\ -1 & 0 & 1 \end{bmatrix} \cdot \begin{bmatrix} V_{AN} \\ V_{BN} \\ V_{CN} \end{bmatrix}. \tag{B1.21}$$

From (B1.6) and (B1.21), it becomes

$$\begin{bmatrix} V_{ta} \\ V_{tb} \\ V_{tc} \end{bmatrix} = \begin{bmatrix} 0 & -n_t & 0 \\ 0 & 0 & -n_t \\ -n_t & 0 & 0 \end{bmatrix}^{-1} \cdot \begin{bmatrix} 1 & -1 & 0 \\ 0 & 1 & -1 \\ -1 & 0 & 1 \end{bmatrix} \cdot \begin{bmatrix} V_{AN} \\ V_{BN} \\ V_{CN} \end{bmatrix}. \tag{B1.22}$$

In a condensed form, the equation can be rewritten as

$$[V_{tabc}] = [A_t] \cdot [VLN_{ABC}] \tag{B1.23}$$

where

$$[A_t] = \begin{bmatrix} 0 & -n_t & 0 \\ 0 & 0 & -n_t \\ -n_t & 0 & 0 \end{bmatrix}^{-1} \cdot \begin{bmatrix} 1 & -1 & 0 \\ 0 & 1 & -1 \\ -1 & 0 & 1 \end{bmatrix}$$

$$[A_t] = \frac{1}{n_t} \begin{bmatrix} 1 & 0 & -1 \\ -1 & 1 & 0 \\ 0 & -1 & 1 \end{bmatrix}.$$

Also, from Figure 3.1, the ideal secondary voltages are given by

$$V_{ta} = V_{an} + \left(Z_{ta} \cdot I_a\right) \tag{B1.24}$$

$$V_{tb} = V_{bn} + \left(Z_{tb} \cdot I_b\right) \tag{B1.25}$$

$$V_{tc} = V_{cn} + \left(Z_{tc} \cdot I_c\right). \tag{B1.26}$$

The three equations (B1.24), (B1.25) and (B1.26) can be transformed into a matrix form as

$$\begin{bmatrix} V_{ta} \\ V_{tb} \\ V_{tc} \end{bmatrix} = \begin{bmatrix} V_{an} \\ V_{bn} \\ V_{cn} \end{bmatrix} + \begin{bmatrix} Z_{ta} & 0 & 0 \\ 0 & Z_{tb} & 0 \\ 0 & 0 & Z_{tc} \end{bmatrix} \cdot \begin{bmatrix} I_a \\ I_b \\ I_c \end{bmatrix} \tag{B1.27}$$

which can be condensed as

$$[V_{tabc}] = [VLN_{abc}] + [Z_{tabc}] \cdot [I_{abc}]. \tag{B1.28}$$

Combining (B1.23) and (B1.28), it becomes

$$[A_t] \cdot [VLN_{ABC}] = [VLN_{abc}] + [Z_{tabc}] \cdot [I_{abc}]$$

$$[VLN_{abc}] = [A_t] \cdot [VLN_{ABC}] - [Z_{tabc}] \cdot [I_{abc}]$$

$$[VLN_{abc}] = [A_t] \cdot [VLN_{ABC}] - [B_t] \cdot [I_{abc}]$$

where

$$[B_t] = [Z_{tabc}]$$

$$[B_t] = \begin{bmatrix} Z_{ta} & 0 & 0 \\ 0 & Z_{tb} & 0 \\ 0 & 0 & Z_{tc} \end{bmatrix}.$$

By applying KCL into Figure 3.2, the line currents as functions of the delta currents are

$$I_A = I_{AC} - I_{BA} \tag{B1.29}$$

$$I_B = I_{BA} - I_{CB} \tag{B1.30}$$

$$I_C = I_{CB} - I_{AC}. \tag{B1.31}$$

The three equations (B1.29), (B1.30) and (B1.31) can be transformed into a matrix form as

$$\begin{bmatrix} I_A \\ I_B \\ I_C \end{bmatrix} = \begin{bmatrix} 1 & -1 & 0 \\ 0 & 1 & -1 \\ -1 & 0 & 1 \end{bmatrix} \cdot \begin{bmatrix} I_{AC} \\ I_{BA} \\ I_{CB} \end{bmatrix}. \tag{B1.32}$$

Meanwhile, the delta primary currents in relation to the secondary line currents are

$$I_{AC} = \frac{1}{n_t} I_a \tag{B1.33}$$

$$I_{BA} = \frac{1}{n_t} I_b \tag{B1.34}$$

$$I_{CB} = \frac{1}{n_t} I_c. \tag{B1.35}$$

Converting the three equations (B1.33), (B1.34) and (B1.35) into a matrix form, the following equation is obtained.

$$\begin{bmatrix} I_{AC} \\ I_{BA} \\ I_{CB} \end{bmatrix} = \frac{1}{n_t} \begin{bmatrix} 1 & 0 & 0 \\ 0 & 1 & 0 \\ 0 & 0 & 1 \end{bmatrix} \cdot \begin{bmatrix} I_a \\ I_b \\ I_c \end{bmatrix}. \tag{B1.36}$$

From the two above matrix equations (B1.32) and (B1.36), it becomes

$$\begin{bmatrix} I_{AC} \\ I_{BA} \\ I_{CB} \end{bmatrix} = \begin{bmatrix} 1 & -1 & 0 \\ 0 & 1 & -1 \\ -1 & 0 & 1 \end{bmatrix} \cdot \frac{1}{n_t} \begin{bmatrix} 1 & 0 & 0 \\ 0 & 1 & 0 \\ 0 & 0 & 1 \end{bmatrix} \cdot \begin{bmatrix} I_a \\ I_b \\ I_c \end{bmatrix}. \quad \text{(B1.37)}$$

In a condensed form, the equation can therefore be rewritten as

$$[I_{ABC}] = [c_t] \cdot [VLN_{abc}] + [d_t] \cdot [I_{abc}] \quad \text{(B1.38)}$$

where

$$[c_t] = \begin{bmatrix} 0 & 0 & 0 \\ 0 & 0 & 0 \\ 0 & 0 & 0 \end{bmatrix}$$

and

$$[d_t] = \begin{bmatrix} 1 & -1 & 0 \\ 0 & 1 & -1 \\ -1 & 0 & 1 \end{bmatrix} \cdot \frac{1}{n_t} \begin{bmatrix} 1 & 0 & 0 \\ 0 & 1 & 0 \\ 0 & 0 & 1 \end{bmatrix}$$

$$[d_t] = \frac{1}{n_t} \begin{bmatrix} 1 & -1 & 0 \\ 0 & 1 & -1 \\ -1 & 0 & 1 \end{bmatrix}.$$

Appendix B2: Generalized matrices (line segment)

Derivation for overhead line and underground cable

Applying KCL at the output and KVL to the model in Figure 3.7, three condensed equations are obtained.

$$[I_{abc}]_{input} = [I_{abc}]_{line} + \frac{1}{2}[y_{abc}] \cdot [V_{abc}]_{input} \tag{B2.1}$$

$$[I_{abc}]_{line} = [I_{abc}]_{output} + \frac{1}{2}[y_{abc}] \cdot [V_{abc}]_{output} \tag{B2.2}$$

$$[V_{abc}]_{input} = [V_{abc}]_{output} + [z_{abc}] \cdot [I_{abc}]_{line}. \tag{B2.3}$$

Substituting (B2.2) into (B2.3), the following equation is obtained.

$$[V_{abc}]_{input} = [V_{abc}]_{output} + [z_{abc}] \cdot \left([I_{abc}]_{output} + \frac{1}{2}[y_{abc}] \cdot [V_{abc}]_{output} \right)$$

$$[V_{abc}]_{input} = \left([U] + \frac{1}{2}[z_{abc}] \cdot [y_{abc}] \right) [V_{abc}]_{output} + [z_{abc}] \cdot [I_{abc}]_{output}$$

$$[V_{abc}]_{input} = [a] \cdot [V_{abc}]_{output} + [b] \cdot [I_{abc}]_{output}$$

where

$$[a] = [U] + \frac{1}{2}[z_{abc}] \cdot [y_{abc}]$$

$$[b] = [z_{abc}].$$

Also substituting (B2.2) and (B2.3) into (B2.1), the following equation is obtained.

$$[I_{abc}]_{input} = [I_{abc}]_{line} + \frac{1}{2}[y_{abc}] \cdot \left([V_{abc}]_{output} + [z_{abc}] \cdot [I_{abc}]_{line} \right)$$

$$[I_{abc}]_{input} = \left([I_{abc}]_{output} + \frac{1}{2}[y_{abc}] \cdot [V_{abc}]_{output} \right)$$

$$+\frac{1}{2}[y_{abc}]\cdot\left([V_{abc}]_{output}+[z_{abc}]\cdot\left([I_{abc}]_{output}+\frac{1}{2}[y_{abc}]\cdot[V_{abc}]_{output}\right)\right)$$

$$[I_{abc}]_{input}=\left([y_{abc}]+\frac{1}{4}[y_{abc}]\cdot[z_{abc}]\cdot[y_{abc}]\right)[V_{abc}]_{output}+\left([U]+\frac{1}{2}[y_{abc}]\cdot[z_{abc}]\right)[I_{abc}]_{output}$$

$$[I_{abc}]_{input}=[c]\cdot[V_{abc}]_{output}+[d]\cdot[I_{abc}]_{output}$$

where

$$[c]=[y_{abc}]+\frac{1}{4}[y_{abc}]\cdot[z_{abc}]\cdot[y_{abc}]$$

$$[d]=[U]+\frac{1}{2}[y_{abc}]\cdot[z_{abc}].$$

The matrix equation in partition matrix form from (3.5) and (3.6) in chapter 3 is

$$\begin{bmatrix}[V_{abc}]_{input}\\ [I_{abc}]_{input}\end{bmatrix}=\begin{bmatrix}[a] & [b]\\ [c] & [d]\end{bmatrix}\cdot\begin{bmatrix}[V_{abc}]_{output}\\ [I_{abc}]_{output}\end{bmatrix}.$$

The matrix equation for voltages and currents at the output as functions of voltages and currents at the input is given by

$$\begin{bmatrix}[V_{abc}]_{output}\\ [I_{abc}]_{output}\end{bmatrix}=\begin{bmatrix}[a] & [b]\\ [c] & [d]\end{bmatrix}^{-1}\cdot\begin{bmatrix}[V_{abc}]_{input}\\ [I_{abc}]_{input}\end{bmatrix}$$

$$\begin{bmatrix}[V_{abc}]_{output}\\ [I_{abc}]_{output}\end{bmatrix}=\begin{bmatrix}[d] & -[b]\\ -[c] & [a]\end{bmatrix}\cdot\begin{bmatrix}[V_{abc}]_{input}\\ [I_{abc}]_{input}\end{bmatrix}.$$

Since $[a]=[d]$,

$$\begin{bmatrix}[V_{abc}]_{output}\\ [I_{abc}]_{output}\end{bmatrix}=\begin{bmatrix}[a] & -[b]\\ -[c] & [d]\end{bmatrix}\cdot\begin{bmatrix}[V_{abc}]_{input}\\ [I_{abc}]_{input}\end{bmatrix}$$

or

$$[V_{abc}]_{output}=[a]\cdot[V_{abc}]_{input}-[b]\cdot[I_{abc}]_{input}$$

$$[I_{abc}]_{output}=-[c]\cdot[V_{abc}]_{input}+[d]\cdot[I_{abc}]_{input}.$$

Meanwhile, the matrix equation for voltages at the output as functions of voltages at input and currents at output is given by

$$[V_{abc}]_{input}=[a]\cdot[V_{abc}]_{output}+[b]\cdot[I_{abc}]_{output}$$

$$[V_{abc}]_{output}=[a]^{-1}\cdot\left([V_{abc}]_{input}-[b]\cdot[I_{abc}]_{output}\right)$$

$$[V_{abc}]_{output}=[a]^{-1}\cdot[V_{abc}]_{input}-[a]^{-1}\cdot[b]\cdot[I_{abc}]_{output}$$

$$[V_{abc}]_{output}=[A]\cdot[V_{abc}]_{input}-[B]\cdot[I_{abc}]_{output}$$

where

$$[A]=[a]^{-1}$$

$$[B]=[a]^{-1}\cdot[b].$$